MOLECULAR MECHANISMS THAT GOVERN STEM CELL DIFFERENTIATION AND THEIR IMPLICATIONS IN CANCER

by

Lama Abdullah AlAbdi

A Dissertation

Submitted to the Faculty of Purdue University

In Partial Fulfillment of the Requirements for the degree of

Doctor of Philosophy

Department of Biochemistry

West Lafayette, Indiana

August 2019

THE PURDUE UNIVERSITY GRADUATE SCHOOL
STATEMENT OF COMMITTEE APPROVAL

Dr. Humaira Gowher, Chair
Department of Biochemistry
Dr. Scott D. Briggs
Department of Biochemistry
Dr. Damon R. Lisch
Botany and Plant Pathology
Dr. Stanton B. Gelvin
Department of Biological Sciences

Approved by:
Dr. Andrew Mesecar
Head of the Graduate Program

This is dedicated to my mother, father, brothers, mentors, and friends.
Without you, I would not have come this far.

ACKNOWLEDGMENTS

I would like to acknowledge all of those who have helped me develop as a scholar and a scientist over my years as a graduate student:

My family for their sacrifices, love and support,

My friends for understanding the commitments attached to being in research,

Dr. Humaira Gowher for being a great mentor and friend,

Thesis Committee members, Drs. Scott Briggs, Damon Lisch, and Stanton Gelvin for constructive feedback, valuable advice, and helping me grow as an independent researcher,

Current and past lab members Drs., Christopher Petell, Qianyi Yang, Ming He, Debapriya Saha, Mohd Saleem Dar, and graduate students, Allison Norvil Isaiah Mensah, and Sarah McGovern for their support and for the useful discussions.

I would also like to thank several undergraduates who helped me grow as a mentor and significantly contributed to my work- Stephen McCune, Brice, H. Spears, James A. Breedlove, and Nicole Adkins.

I also would like to extend my gratitude to Drs. Nadia Lanman, Sagar Utturkar, and Putu Ayu Sudyanti for analyzing our genome-wide data,

And my colleagues who were always very supportive and helpful in our scientific discussions as well as experimental execution.

Lastly, I would like to thank several funding resources:

King Saud University for the graduate fellowship that supported me for the duration of my study.

Department of Biochemistry, College of Agriculture, Purdue University, for providing the infrastructure, optimal environment, and financial support through Bird Stair fellowship that

facilitated the completion of this work. Purdue Center for Cancer Research (PCCR) for travel and shared resource grants.

TABLE OF CONTENTS

LIST OF TABLES

LIST OF FIGURES

ABSTRACT

Author: AlAbdi, Lama A. PhD
Institution: Purdue University
Degree Received: August 2019
Title: Molecular Mechanisms that Govern Cellular Differentiation Using Stem Cell Models
Committee Chair: Humaira Gowher

Mammalian development is orchestrated by global transcriptional changes, which drive cellular differentiation, giving rise to diverse cell types. The mechanisms that mediate the temporal control of early differentiation can be studied using embryonic stem cell (ESCs) and embryonal carcinoma cells (ECCs) as model systems. In these stem cells, differentiation signals induce transcriptional repression of genes that maintain pluripotency (PpG) and activation of genes required for lineage specification. Expression of PpGs is controlled by these genes' proximal and distal regulatory elements, promoters and enhancers, respectively. Previously published work from our laboratory showed that during differentiation of ESCs, the repression of PpGs is accompanied by enhancer silencing mediated by the Lsd1/Mi2-NuRD-Dnmt3a complex. The enzymes in this complex catalyze histone H3K27Ac deacetylation and H3K4me1/2 demethylation followed by a gain of DNA methylation mediated by the DNA methyltransferase, Dnmt3a. The absence of these chromatin changes at PpG enhancers during ESC differentiation leads to their incomplete repression. In cancer, abnormal expression of PpG is commonly observed. Our studies show that in differentiating F9 embryonal carcinoma cells (F9 ECCs), PpG maintain substantial expression concomitant with an absence of Lsd1-mediated H3K4me1 demethylation at their respective enhancers. The continued presence of H3K4me1 blocks the downstream activity of Dnmt3a, leading to the absence of DNA methylation at these sites. The absence of Lsd1 activity at PpG enhancers establishes a "primed" chromatin state distinguished by the absence of DNA methylation and the presence of H3K4me1. We further established that the activity of Lsd1 in these cells was inhibited by Oct3/4, which was partially repressed post-differentiation. Our data reveal that sustained expression of the pioneer pluripotency factor Oct3/4 disrupts the enhancer silencing mechanism. This generates an aberrant "primed" enhancer state, which is susceptible to activation and supports tumorigenicity.

As differentiation proceeds and multiple layers of cells are produced in the early embryo, the inner cells are depleted of O_2, which triggers endothelial cell differentiation. These cells form vascular structures that allow transport of O_2 and nutrients to cells. Using ESC differentiation to endothelial cells as a model system, studies covered in this thesis work elucidated a mechanism by which the transcription factor Vascular endothelial zinc finger 1 (Vezf1) regulates endothelial differentiation and formation of vascular structures. Our data show that Vezf1-deficient ESCs fail to upregulate the expression of pro-angiogenic genes in response to endothelial differentiation induction. This defect was shown to be the result of the elevated expression of the stemness factor Cbp/p300-interacting transactivator 2 (Cited2) at the onset of differentiation. The improper expression of Cited2 sequesters histone acetyltransferase p300 from depositing active histone modifications at the regulatory elements of angiogenesis-specific genes that, in turn, impedes their activation.

Besides the discovery of epigenetic mechanisms that regulate gene expression during differentiation, our studies also include development of a sensitive method to identify activities of a specific DNA methyltransferase at genomic regions. In mammals, DNA methylation occurs at the C5 position of cytosine bases. The addition of this chemical modification is catalyzed by a family of enzymes called DNA methyltransferases (Dnmts). Current methodologies, which determine the distribution of Dnmts or DNA methylation levels in genomes, show the combined activity of multiple Dnmts at their target sites. To determine the activity of a particular Dnmt in response to an external stimulus, we developed a method, Transition State Covalent Crosslinking DNA Immunoprecipitation (TSCC-DIP), which traps catalytically active Dnmts at their transition state with the DNA substrate. Our goal is to produce a strategy that would enable the determination of the direct genomic targets of specific Dnmts, creating a valuable tool for studying the dynamic changes in DNA methylation in any biological process.

CHAPTER 1. INTRODUCTION

1.1 Mammalian development

1.1.1 Embryogenesis

The peri-implantation stage of embryonic development is conserved across many organisms (1). It starts with fertilization of the oocyte by the sperm, followed by multiple steps of cell fate decisions that end in the formation of blastocyst. The blastocyst consists of three cell types: the trophectoderm, the extraembryonic primitive endoderm, and the embryonic epiblast (1-5). Studies have shown that pluripotency as a property arises from the epiblast (6). Newly emerging epiblast cells are thought to differentiate into all somatic and germ line cells that constitute an organism (7). The dynamic process of differentiation is orchestrated by meticulous and complex mechanisms of regulation that control different layers of organization.

Owing to its complexity and transient nature, coupled with the inaccessibility of the embryonic sample for analysis, it is challenging to dissect the molecular mechanisms governing embryonic development. The development of stem cell models provided a breakthrough in our understanding of embryogenesis. These cell models retain the same pluripotent properties observed in the epiblast as they can differentiate to any lineage under similar environmental conditions (6). This was supported by *in vivo* experiments showing that these pluripotent cells contribute to normal development when injected into the early embryo (8, 9). Using these model cell lines, our understanding of early developmental stages as well as mechanisms regulating cell fate decisions and commitments has evolved.

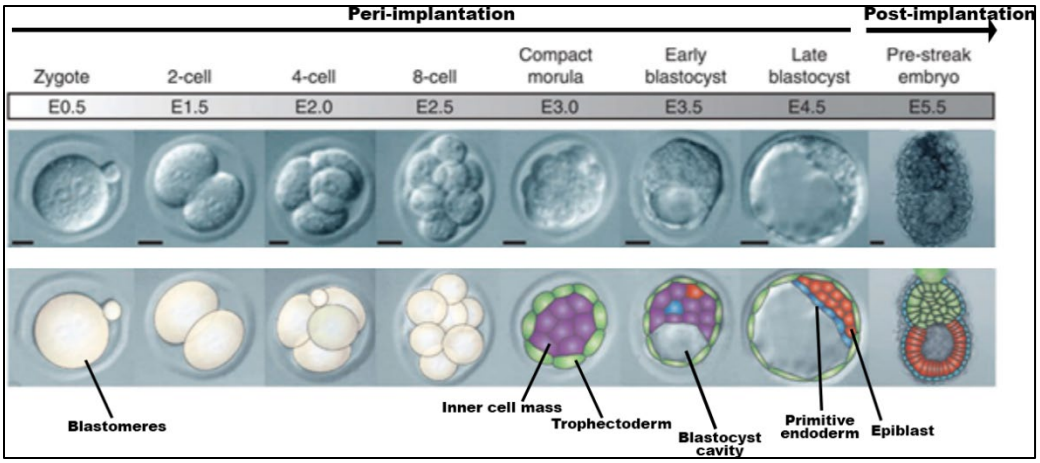

Figure 1.1 Early stages of the mammalian embryonic development.

The zygote is generated from the fertilization of the oocyte by the sperm. Two cell-fate decisions take place prior to implantation stage (E4.5). First, is the specification of the trophectoderm and inner cell mass. The second is when the primitive endoderm and the embryonic epiblast emerge from the inner cell mass. E: Embryonic day post-fertilization. The scale bars are 50 µm. Figure adapted from (10).

1.1.2 Embryonic stem cell models

In an effort to study development, several cell lines were generated or derived from different stages of embryonic development. Teratocarcinoma were the first to be identified as pluripotent stem cells in culture (11). They are a highly aggressive germ line tumor with a heterogeneous population of cells, which include the pluripotent embryonal carcinoma cells (ECCs) (12). The hypothesis whether these cells had embryonic origin was tested by transplanting embryos into the testes of adult mice. Tumors derived from these transplantations were isolated and clonally expanded, giving rise to embryonal carcinoma cell lines (13). The stemness of these cell lines, including the murine F9 and P19 ECCs, was evident in their differentiation potential and their ability to contribute to normal embryonic development when injected back into a developing embryo (8, 11). These cell lines were used to investigate early developmental stages and mechanisms regulating differentiation prior to the isolation of embryonic stem cells (ESCs).

In 1981, ESCs with full capacity of self-renewal and differentiation were derived from mouse embryos at the blastocyst-stage (14, 15). The isolation of these cells revolutionized our understanding of the molecular mechanisms that mediate maintenance of pluripotency and induction of differentiation. Experiments using ESCs supported their role as a model to study embryogenesis by demonstrating how they mimic early developmental stages and the transcriptional changes driving cell fate specifications (9).

1.1.3 Endothelial cell differentiation and angiogenesis

During embryonic development, primordial endothelial cells and blood vessels emerge from the extraembryonic yolk sac soon after gastrulation (16). This process is initiated by the recruitment of epiblast cells to the primitive streak where they undergo epithelial-mesenchymal transition. When these migratory cells reach the yolk sac, they form either mesoderm or definitive endoderm (17). The mesoderm layer then undergoes differentiation to form the first differentiated cell types in the embryo: primitive endothelial and hematopoietic cells. Together, these cells develop to generate a primitive network of tubules. Remodeling and maturation of these tubules give rise to the circulatory network. Concurrent with maturation of the vasculature is the induction

of hematopoiesis: the production of circulating blood cells. The key regulatory protein which controls vascular formation is vascular endothelial growth factor (VEGF) (18).

During embryogenesis, the cardiovascular system is the first functional organ to develop (19). This occurs as early as Embryonic day (E) 7.5 when hypoxic cues are detected. Vascular structures form following the induction of hypoxia-inducible factor 1 (HIF1-α), which binds to the regulatory elements of VEGF, activating its transcription (20, 21). Induced VEGF, in turn generates a signaling gradient directing the migration of endothelial cells and thus the orientation of vascular growth (21). Methods using VEGF signaling have been developed to induce differentiation of ESCs to endothelial cells and their remodeling to form vascular structures in tissue culture (22, 23). These experimental systems serve as a model to study mechanisms regulating endothelial cell differentiation and angiogenesis *in vitro*.

1.2 Gene transcription

In living cells, genetic information is stored in the DNA with genes being the basic structural units (24, 25). The expression of genetic information, initiated by gene transcription, is regulated by genomic regions identified as: 1) Proximal regulatory elements, known as promoters, 2) Distal regulatory elements, or enhancers, and 3) Insulator elements.

Whereas a promoter is proximal to its gene and functions as the site where the transcriptional machinery initially binds to generate a new transcript, enhancers can be remotely located relative to their target gene. Enhancers mediate the spatial and temporal control of gene expression in a tissue specific manner. (26, 27). They communicate with promoters by forming enhancer-promoter loops (28). Insulators can block the formation of these loops, hence protecting genes from inappropriate environmental signals (29). The formation of these loops creates another layer of gene expression regulation as well as higher-order chromatin structures.

Gene expression starts by the transcription of DNA to its messenger molecule: RNA. This is initiated by the presence of DNA binding proteins, called transcription factors, which bind to their specific DNA sequences located at the enhancer and promoter regions (30). When transcription factors bind, they recruit the transcriptional machinery comprised of RNA polymerase II (RNA pol II) and its associated factors; this forms the transcriptional initiation complex that is localized to the promoter (31). The phosphorylation patterns on the C-terminal repeat domain (CTD) of RNA pol II determines which factors are bound as well as the

transcriptional function of the polymerase: paused, elongating, or terminating (32). In order to fine-tune and ensure proper gene transcription, there needs to be concerted regulation between transcription factor binding and epigenetic regulation (33).

1.3 Transcription factors

Transcription factors (TFs) are proteins that regulate transcription by directly binding to DNA in a sequence specific manner. Therefore, they are considered to be the first interpreters of the genomic code (34). Many of these proteins serve as “master regulators” or “pioneer factors” governing complex processes that control cell type specification, fate determination, and developmental patterning (35). In cell culture experiments, several reports demonstrated the power of TFs in driving differentiation, de-differentiation, and trans-differentiation (36). TF sequences, binding sites, and regulatory roles are highly conserved between organisms, indicating a conservation in functions (37). This conservation is supported by the observations that mutations in these analogous sequences are found in many diseases (38). Furthermore, aberrant expression of TFs has been noted in many cancers (39, 40). These observations highlight the critical physiological roles these proteins play in the spatiotemporal control of gene expression.

Many studies demonstrated how TFs function as activators or repressors of gene transcription (41, 42). Upon their binding at regulatory elements, they can recruit coactivator or repressor complexes, including chromatin modifiers, to exert their catalytic functions on target genes. Studies have reported TFs, through their effector domains, directly binding to RNA pol II (43-45). Other mechanisms have been delineated where TFs, lacking an effector domain, function through sterically blocking the binding of other proteins to a genomic site (46). With most of the genomic sequence now annotated with regulatory functions, tremendous effort is currently employed to decode TFs functional interactions and their roles in modulating gene expression.

1.4 Epigenetic regulation

Epigenetics is defined as heritable, and reversible changes to gene expression without altering the DNA sequence (47). Epigenetic regulation takes place via chemical modifications on DNA or histones, non-coding RNA expression, and chromatin structural changes (48-52). In mammals, DNA methylation occurs by the deposition of a methylation mark on the fifth carbon

of cytosine, predominantly in a CpG context (53). DNA methylation at the regulatory elements is associated with stable gene repression as it prevents the binding of TFs and recruits methyl-binding proteins that help in chromatin condensation (54-57). The enzymes catalyzing this reaction are known as DNA methyltransferases (Dnmts). Histones can also alter gene expression by changes in their localization and compactness at regulatory elements (50, 52). Additionally, chemical changes to the histone tails create a code that recruits or averts the binding of epigenetic modifiers or readers (47, 51). This, in turn, marks a gene as active, primed, poised, or repressed (58). Epigenetic regulation also occurs via non-coding RNA in a cis- or trans- manner (49, 59). Several non-coding RNAs act as repressors or activators of transcription by binding to their target DNA or acting as a scaffold to recruit proteins to a particular site (60). Finally, the spatial organization of the genome in the nucleus through enhancer-promoter looping, topologically associated domains (TADs), and lamina associated domains (LADs) functions to isolate certain loci that are active or repressed (61-63). This segregation helps in the rapid activation and recruitment of RNA pol II to a core promoter leading to the activation of a subset of genes in a tissue-specific manner (64).

1.5 ATP-dependent chromatin remodeling

Chromatin remodeling refers to the use of ATP hydrolysis as a source of energy to alter, evict, or restructure nucleosomes to modulate gene expression (65). This occurs by regulating the access of TFs to their cognate DNA binding motifs (66). Chromatin remodeling complexes contain a single ATPase subunit, which binds and hydrolyzes ATP for energy, and multiple regulatory subunits. These regulatory subunits modulate the catalytic activity of the ATPase and give rise to functional specificity (67). The combinatorial effect of the assembly of multiple tissue-specific regulatory subunits together with a different core ATPase subunit results in unique complexes of particular functional properties. The resulting complexes collaborate with TFs for tailored recruitment to regulatory regions of the genome and the control of gene expression (68).

1.6 Post-translational modifications on histones

Histones are highly conserved proteins that package the DNA into nucleosomes. DNA is wrapped around the C-terminal globular domain of histones; thus mediating the interactions

between the different subunits, which then forms the nucleosome core (25). The N-terminal region forms a flexible tail which, together with some residues of the globular domain, can carry post-translational modifications. These modifications influence DNA-histone interactions between and within nucleosomes, therefore affecting chromatin structure (69). These covalent modifications include: methylation, acetylation, phosphorylation, ubiquitination, sumoylation, and ADP ribosylation, all of which collaborate to alter transcription, cell cycle flow, DNA replication and repair (51). These modifications are either deposited by writers, removed by erasers, or identified by readers.

1.6.1 Histone acetylation

Histone acetylation is the transfer of an acetyl group from Acetyl-coenzyme A to specific lysine residues in histones (70). The addition of an acetyl group neutralizes the positive charge of lysine. It is speculated that this neutralization weakens DNA-histone interactions, allowing for an open chromatin state (71). Consequently, histone acetyltransferase (HAT) activity is typically observed in transcriptional coactivator complexes: Gcn5/PCAF and CBP/P300 as examples (72).

Histone deacetylases (HDACs) are part of transcriptional corepressor complexes such as CoREST and NuRD/Mi-2 (73). HDACs catalyze the removal of the acetyl group, presenting an enzymatic regulatory network that modulates the acetylation levels, and therefore the transcriptional activity, at genomic loci (74). Histone deacetylation usually serves as the first enzymatic activity in a sequence of events that lead to the repression of enhancers and promoters (75). By removing acetyl groups from histone lysines, HDACs not only alter transcription, but also trigger other epigenetic activities that alter the chromatin state, such as methylation, ubiquitination, and sumoylation (75-79). Because it serves as an epigenetic switch for further enzymatic activity leading to transcriptional repression, HDAC activity is systematically controlled by many molecular mechanisms, which include protein–protein interactions and posttranslational modifications (80, 81)

1.6.2 Histone methylation

Histone methylation is the methylation on lysine or arginine residues (69). Lysine residues can be mono-, di-, or tri-methylated by SET-domain containing enzymes (82). In mammals, different methyltransferases may share the same substrate histones H3 and H4 lysine targets.

However, it is speculated that enzyme specificity lies in the genes they regulate and the biological processes that targets them to different regions of the genome (83). For example, H3K9 at the promoters of repressed genes is methylated by Suv39h1, G9A, and ESET. H3K27 is methylated by Ezh2 of the PRC2 repressive complex. Methylation can also be an active mark. The MLL family of enzymes catalyzes the methylation of H3K4 at the enhancers and promoters of active genes. Set2 methylates H3K36 at the bodies of actively transcribed genes (83, 84). H3K36me3 serves as a mark that recruits Dnmt3b to methylate gene bodies, preventing cryptic transcription from occurring (85). Histones H3- and H4-arginine residues are mono- and di-methylated by the coactivator arginine methyltransferase (CARM1) and protein arginine N-methyltransferase 1 (PRMT1) (86).

Histone methylation can be reversed by the activities of two families of demethylation enzymes: Lsd1, which mainly demethylates di- and mono- H3K4 and H3K9 marks, and JmjC family of enzymes which prefers trimethylated lysine and arginine residues as substrates (87). Lsd1 activity on its histone substrates is often regulated by its binding partners. For example, the CoREST complex positively regulates Lsd1 activity by promoting its stability *in vivo* as well as by providing a hypo-acetylated nucleosome, the preferred substrate for Lsd1 to act upon. Another Lsd1 interacting partner, BHC80, dampens Lsd1 activity by the physical interaction of its SNAG domain with the catalytic domain of Lsd1 (79, 88, 89). Additionally, Lsd1 is known to interact with a magnitude of TFs that either help with recruitment or regulate its activity (90-92). These findings suggest that the dynamic regulation of Lsd1 histone demethylation activity at the promoters and enhancers of genes is modulated by signaling pathways, which dictate Lsd1 binding partners.

1.7 DNA methylation

DNA methylation is the covalent addition of a methyl group to the fifth carbon position of cytosine (93). In the mammalian genome, this predominantly occurs in the palindromic CpG where the majority (~80%) are methylated (94, 95). Evaluation of DNA methylation distribution throughout the genome is indispensable for our interpretation of 5mC functions. When deposited at regulatory elements, DNA methylation is strongly associated with repression of transcription (96). Using genome-wide methylation profiling, methylation levels in somatic cells were identified across many genomic elements, with retroviral sequences and transposable elements showing the

highest methylation (97). Enigmatically, CpG islands (CGI) exhibit reduced methylation levels (94). CGI are often associated with promoter and enhancer regions where levels of 5mC range from 10% to 50%, respectively (57). Furthermore, whereas changes in CGI methylation are rarely observed in healthy tissue, aberrant CGI hyper-methylation is a hallmark of cancers (96). Genome-wide methylome profiling studies illustrated that under physiological conditions, there is a 15 to 21% change in the methylation status of CpGs, with sites either gaining or losing DNA methylation (98, 99). Interestingly, these tissue-specific differentially methylated regions (DMRs) are mainly found at enhancers or super enhancers (44, 99, 100). Depletion of 5mC is influenced by chromatin state. This is exemplified by the presence of methylated H3K4 at the promoters and enhancers, which inhibits the deposition of a methyl mark at these regulatory sites (101, 102). The binding of TFs or CXXC zinc finger-containing proteins protect CpGs from methylation (53). Moreover, the presence of pioneer TFs may cause epigenetic remodeling and depletion of DNA methylation at specific sites (103).

DNA methylation can also occur at intragenic regions. Specifically, the presence of the histone mark H3K36me3, a predominant modification at gene bodies, recruits DNA methyltransferases to these sites (104, 105). Although 5mC is negatively correlated with transcription, in this context, this epigenetic mark has been demonstrated to function differently. Genes that are highly transcribed have abundant intragenic 5mC (96, 106). Correlation studies have demonstrated that the presence of 5mC at gene bodies functions to antagonize the activity of polycomb repressive complex (PRC2), hence, promoting transcription (107). Furthermore, it has been postulated that intragenic 5mC is required for the regulation of promoter use and alternative splicing events as well as precluding cryptic transcription initiation (96, 108, 109).

1.7.1 DNA methyltransferases

DNA methylation is an epigenetic modification catalyzed by two families of DNA methyltransferases (Dnmts): 1) maintenance DNA methyltransferase: Dnmt1, which has high affinity for hemimethylated DNA (110, 111). Dnmt1 associates with the replication fork to copy methylation patterns from the template strand to the newly synthesized strand, thus preserving methylation patterns throughout cellular division (112, 113). 2) *De novo* DNA methyltransferases: Dnmt3a and Dnmt3b establish new patterns of methylation. Dnmt1, however, does not exclusively maintain DNA methylation; rather, the activities of Dnmt3s are also required for maintenance of

established methylation (96, 114). In mammals, Dnmt1 and Dnmt3 enzymes methylate largely at CpG dinucleotides (115). Given the low sequence specificity of these enzymes, it is important to understand the mechanism(s) that regulate and recruit Dnmts to specific sites in the genome.

1.7.2 Mechanisms regulating DNA methylation

Post-fertilization, an epigenetic ground state is formed concomitantly with genome-wide erasure of methylation marks inherited from parental gametes (116-119). Erasure of 5mC marks is known to occur by active or passive mechanisms. Passive dilution of 5mC marks results from DNA replication and cell division. Active demethylation occurs by the enzymatic oxidation of 5mC to 5-hydroxymethylcytosine (5hmC) catalyzed by the TET family of enzymes (120). 5hmC is the most abundant derivative of 5mC and is thought to carry its own regulatory roles. TETs are reported to be enriched at regulatory elements and are associated with TFs (121), indicating a role of TETs in modulating 5mC dynamics concurrent with TF binding. DNA demethylation is complete when TET oxidative activity is accompanied by base-excision repair following thymine DNA glycosylation (121).

1.8 Epigenetic dysregulation in cancer

1.8.1 Mechanisms of epigenetic dysregulation in cancer

Numerous studies have provided evidence showing that epigenetic dysregulation is a common mechanism in cancer. This includes deregulation of DNA methylation (122-124), histone modifications, and chromatin remodeling machinery (125). Notably, epigenetic events are intercorrelated; a change in an epigenetic mark may influence the deposition or erasure of another. The interdependence between histone demethylation and gain of DNA methylation is an example (102, 126). Mutations in epigenetic factors are not the only drivers of cancer; dysregulation of their expression, activity, or recruitment may also contribute to the initiation or progression of the disease.

1.8.2 Cancer stem cells

Tumors are composed of a heterogeneous population of cells. It is speculated that this heterogeneity rises from phenotypic and epigenetic plasticity (70). The phenotypic plasticity theory posits that tumor heterogeneity results from the divergence and expansion of tumor

initiating clones (71). The more popular hypothesis of epigenetic stemness is supported by many studies demonstrating the aberrant expression of pluripotency factors within the tumor environment as well as the resemblance of cancer biology to development (70, 72). This has given rise to the concept of cancer stem cells (CSCs). CSCs are a subpopulation of cancer cells that are defined by an enhanced tumorigenicity and expression of PpG, making them resemble embryonic stem cells (73, 74). These cancer cells express genes critical for stemness and embryonic development. Moreover, when exposed to differentiation signals, they are able to differentiate to the corresponding cell types. These features further highlight the similarities between cancer and pluripotency (75-77). Importantly, CSCs have been identified and isolated from different types of cancers (78).

1.9 Methods in DNA methylation

1.9.1 Probing for DNA methylation

Several methods have been developed and improved for the detection of DNA methylation. These detection methods can be segregated into two categories: A) Genome-wide profiling of DNA methylation, which include: HPLC-UV, LC-MS/MS, ELISA-based methods, methylation-sensitive restriction digestion, or bisulfite conversion followed by sequencing, and luminometric methylation assay (LUMA), all of which vary in sensitivity, accessibility, and quantity/quality of sample required (127-131). B) Site-specific evaluation of DNA methylation state. These assays are not limited to chemical conversion of cytosine such as bisulfite conversion followed by PCR, pyrosequencing, bead array, or methylation-specific PCR, but also methylation sensitive digestion followed by PCR or qPCR, electrochemical biosensors, and optical biosensing strategies (127, 132-134).

1.9.2 Probing for Dnmts

Dnmt activity has been extensively studied *in vitro* and *in vivo*. *In vitro* studies involve the use of recombinant enzymes where their activities and specificities are interrogated in the presence of DNA or nucleosomal substrates (135). The effect of pathological mutations on the enzymes' stability, activity, and substrate preference has also been evaluated (136). The activities of Dnmts have been investigated *in vivo* using knockout mice and cell lines, luciferase reporter-based assays, and approaches utilizing small molecule inhibitors (137-143). Mechanisms that recruit Dnmts to

their target sites have been resolved by co-immunoprecipitation (Co-IP) experiments and chromatin immunoprecipitation assays (ChIP) (144, 145). These experiments also elucidated the redundancy and specificity of these enzymes to discrete genomic sites (146-148).

1.9.3 Single-cell approaches

In order to distinguish specific and distinct cellular epigenetic signatures from bulk populations of cells, single-cell high-resolution methylome assays were developed. Single-cell reduced representation bisulfite sequencing (scRRBS) and single-cell bisulfite sequencing (scBS-seq) were among the first techniques to evolve (149). Since then, technological improvements were implemented to increase yield, resolution, and throughput. These include incorporation of multifaceted analyses of methylome, transcriptome, and chromatin accessibility (150-153). Several databases designated for single-cell datasets have been generated for many organisms and cell states (154).

1.9.4 Manipulation of DNA methylation

The discoveries made in the DNA methylation field have been tested and supported by genome-wide manipulations using genetic- and pharmacological-based methods (56, 95). Non-targeted perturbation of this mark is unavoidably accompanied by pleiotropic effects that could lead to misinterpretation of the results. Due to the development and creative evolution of genome-editing strategies, guided alteration of the 5mC state is feasible. Targeted methylation or demethylation of genomic DNA involves the use of Dnmt or TET proteins fused with a DNA binding domain, such as zinc fingers, transcription activator–like effectors (TALEs), and catalytically-dead Cas9 (dCas9) (155-157). These fusion remodelers have specific 5mC remodeling capacity (158). One of the potential pitfalls of the targeted approach is the presence of spurious off-target activity (155). To mitigate this issue, multiple molecules of the modulator proteins are tethered to a genomic locus. This is achieved by increasing the local concentration of the epigenetic regulator via SunTag or RNA scaffolding strategies (159, 160).

1.10 Summary

1.10.1 Loss of Lsd1 regulation in carcinoma cells

Our studies in differentiating F9 ECCs show that several PpG, including the pioneer transcription factor Oct3/4, maintain substantial levels of expression. We demonstrated that the enhancers of these PpG are not silenced by a gain of DNA methylation due to the retention of H3K4me1 post-differentiation. Interestingly, similar studies in differentiating P19 ECCs showed that the expression of Oct3/4 and Nanog were reduced by over 90%. We further observed histone H3K4me1 demethylation as well as a gain of DNA methylation at PpG enhancers in differentiating P19 ECCs but not F9 ECCs. Based on these observations and previously reported interactions between Lsd1 and Oct3/4 (161, 162), we investigated the effect of Lsd1-Oct3/4 interaction on Lsd1 catalytic activity. Using *in vitro* histone demethylation assays and recombinant proteins, our data show that in the presence of Oct3/4, the catalytic activity of Lsd1 is significantly reduced. These data suggest a mechanistic model that elucidates the regulation of Lsd1 activity by its interaction with Oct3/4 at PpG enhancers. In undifferentiated ESCs and ECCs, Lsd1-Oct3/4 interaction at active PpG enhancers leads to Lsd1 inhibition, which is relieved post-ESC and P19 ECC differentiation by the rapid downregulation of Oct3/4. However, in differentiating F9 ECCs, partial repression of Oct3/4 retains Lsd1 in an inhibited state. At regulatory sites, where H3K27Ac is deacetylated while the H3K4me1 mark is retained together with the absence of DNA methylation, creates a "primed" enhancer state. Therefore, our data suggest that aberrant expression of the pioneer pluripotency factor Oct3/4 in cancer cells could disrupt epigenetic regulation of enhancer silencing and induce a chromatin state that renders enhancers susceptible to reactivation.

1.10.2 Trapping Dnmt3a and identifying its direct targets.

The current methodologies employed to investigate the activity of DNA methyltransferases (Dnmts) using genome-wide profiles of DNA methylation or binding of Dnmts by chromatin immunoprecipitation experiments, provide limited information about the temporal activity of these enzymes. This is because Dnmts stay bound to chromatin irrespective of their need to be catalytically active at their binding sites (101). Identifying the spatiotemporal response of Dnmts under various stimuli will help unravel the dynamic regulation of DNA methylation and its role in controlling gene expression. Additionally, specific targets of multiple Dnmts can be identified,

thus classifying the individual contributions of these enzymes in setting patterns of DNA methylation across the genome. We aimed at developing a method that would facilitate the determination of the direct genomic targets undergoing active methylation via the catalytic activities of Dnmts. We implemented a catalysis-specific chemical crosslinking strategy that enabled the formation of stable Dnmt-DNA adducts. This was done by repurposing the suicide-inhibitor drug 5-Aza-2′-deoxycytidine (5-Aza-dC), a 2′-deoxycytidine analog that is incorporated into the genome during replication. When a Dnmt is recruited to methylate a site where 5-Aza-dC is incorporated, the enzyme will not be able to release an intermediate of the reaction and it will remain in a locked position (163). Our data showed that this adduct can be immunoprecipitated and sequenced. Given that Dnmt3a is the principal Dnmt for PpG enhancer methylation in differentiating ESCs (102), we sought to standardize a protocol for ESC differentiation as a monolayer that would support 5-Aza-dC treatments (164). We were efficiently able to differentiate ESCs to a neuronal lineage where pluripotency genes are repressed and their enhancers are silenced by DNA methylation. Our data further illustrated 5-Aza-dC incorporation during differentiation, evident by Dnmt3a capture in dot blot assays. We aim at using the immunoprecipitated material from this differentiation as a proof of principle showing Dnmt3a captured at the enhancers of PpG. This technique will provide a valuable tool for studying the dynamic changes in DNA methylation in any biological or diseased state.

1.10.3 Significance

Considering the complexity of cancer biology, there has been an astonishing evolution in our understanding of cancer development and progression. Recent hypotheses in the field favor the concept of “Cancer Stem Cells” (CSCs); a rare population within the tumor environment that can proliferate indefinitely and give rise to different cell types constituting the heterogeneous populations found in cancers (165). Cancer reoccurrence and therapeutic resistance have been attributed to the existence of CSCs, which makes them an attractive target in our pursuit of the development of cancer therapeutics. Therefore, understanding the biology of these cells, and how they emerge, is paramount for our understanding of cancer biology. Because CSCs have many characteristics common with ESCs (166), comparing the molecular mechanisms of proliferation and differentiation will shed light into how these cells fail to repress (or how they re-activate) their pluripotency program. Our studies using F9 ECCs as a CSC model facilitated our understanding

of a mechanism underlying their defect in proper differentiation. Understanding how CSCs differentiate and dedifferentiate is crucial for the development of differentiation-inducing therapeutics which, in conjunction with other drugs, can be used for the permanent eradication of cancer. Furthermore, as aberrant regulation of DNA methyltransferases is widely reported in the cancers epigenetic landscape, we developed a method for the capture of Dnmts during catalysis. This technique will provide sensitive and precise reports of Dnmt activities in many biological contexts. As a valuable approach, this method will enable the dissection of the distinct biological functions of Dnmt3a and Dnmt3b, their enzymatic mechanisms, and the effect of disease-relevant mutations on their activity. Moreover, tracking the specific activities of Dnmts and comparing them to the dynamic changes in chromatin signatures and TFs binding profiles, could predict potential new mechanisms that regulate Dnmt activities during ESC differentiation. These mechanisms, conceivably, control distinct developmental programs during differentiation and embryogenesis, thus opening new prospects for future studies.

CHAPTER 2. OCT3/4-MEDIATED INHIBITION OF LSD1 ACTIVITY PROMOTES THE ACTIVE AND PRIMED STATE OF PLURIPOTENCY ENHANCERS

Lama AlAbdi, Debapriya Saha, Ming He, Mohd Saleem Dar, Sagar M. Utturkar, Putu Ayu Sudyanti, Stephen McCune, Brice, H. Spears, James A. Breedlove, Nadia A. Lanman, Humaira Gowher.

2.1 Declaration of collaborative work

Dr. Humaira Gowher and Lama AlAbdi wrote the manuscript and designed experiments.

Lama AlAbdi, Debapriya Saha, Ming He, Mohd Saleem Dar, Stephen McCune, Brice, H. Spears, and James A. Breedlove performed experiments.

Debapriya Saha performed MethylRAD sequencing experiments.

Ming He performed the Lsd1 Western blot comparing ESCs and ECCs.

Mohd Saleem Dar performed the H3K4me1 ChIP-qPCR for Lsd1 overexpressing ECCs.

Stephen McCune, Brice, H. Spears, and James A. Breedlove performed qPCR replicates for ChIP-qPCR and RT-qPCR experiments.

Sagar M. Utturkar performed bioinformatic analysis for H3K4me1 ChIP-seq

Putu Ayu Sudyanti and Nadia A. Lanman performed bioinformatic analysis for MethylRAD sequencing.

All other experiments were performed by Lama AlAbdi.

2.2 Abstract

Enhancer reactivation and pluripotency gene (PpG) expression were recently shown to induce stemness and enhance tumorigenicity in cancer stem cells. Silencing of PpG enhancers during embryonic stem cell differentiation involves changes in chromatin state, facilitated by the activity of Lsd1/Mi2-NuRD-Dnmt3a complex. In this study, we observed a widespread retention of H3K4me1 at PpG enhancers and only partial repression of PpGs in F9 embryonal carcinoma cells (ECCs) post-differentiation. The absence of H3K4me1 demethylation could not be rescued by Lsd1 overexpression. Based on the observation that H3K4me1 demethylation is accompanied by strong Oct3/4 repression in P19 ECCs, we tested if Lsd1-Oct3/4 interaction modulates Lsd1

activity. Our data show a dose-dependent inhibition of Lsd1 by Oct3/4 *in vitro* and retention of H3K4me1 at PpG enhancers post-differentiation in Oct3/4 overexpressing P19 ECCs. These data reinforce the idea that Lsd1-Oct3/4 interaction in cancer stem cells may establish a primed enhancer state that is susceptible to reactivation.

2.3 Introduction

Cell type specific gene expression is regulated by chromatin conformation, which facilitates the interaction of distally placed enhancer elements with the specific gene promoter (167-170). Enhancers house the majority of transcription factor binding sites and amplify basal transcription, thus playing a critical role in signal dependent transcriptional responses [summarized in (171)]. Epigenome profiling combined with the transcriptional activity in various cell types led to the identification of potential enhancers, which are annotated as silent, primed, or active based on their epigenetic features. These epigenetic features include histone modifications, DNA methylation, and enhancer-associated RNA (eRNA) (58, 172, 173). Whereas histone H3K4me1 (monomethylation) and H3K4me2 (dimethylation) is present at both active and primed enhancers, active enhancers invariantly are marked by histone H3K27Ac (acetylation) and are transcribed to produce short read eRNA (174-178).

During embryonic stem cell (ESC) differentiation, pluripotency gene (PpG) specific enhancers are silenced via changes in histone modifications and a gain of DNA methylation (102, 179, 180). In response to the differentiation signal, the coactivator complex (Oct3/4, Sox2, Nanog, and Mediator complex) dissociates from the PpG enhancers followed by the activation of pre-bound Lsd1-Mi2/NuRD enzymes. The histone demethylase Lsd1 demethylates H3K4me1, and the HDAC activity of the NuRD complex deacetylates H3K27Ac (179). Our previous studies have shown that the histone demethylation event is critical for the activation of DNA methyltransferase Dnmt3a, which interacts with the demethylated histone H3 tails through its chromatin-interacting ADD (ATRX-Dnmt3a-Dnmt3L) domain, allowing site-specific methylation at pluripotency gene enhancers (PpGe) (102). These studies also suggest that aberrant inhibition of Lsd1 activity could cause a failure to gain DNA methylation, leading to incomplete repression of PpGs.

Several studies have reported on potential mechanisms that control site specific targeting and catalytic activity of Lsd1. Whereas Lsd1 interaction with CoREST ([co]repressor for element-1-silencing transcription factor) activates the enzyme, BHC80 inhibits Lsd1 demethylation activity

(79). The substrate specificity of Lsd1 is regulated by its interaction with androgen receptor and estrogen related receptor α, or by alternative splicing which adds four or eight amino acids to the Lsd1 enzyme (181-185). Lsd1 is targeted to various genomic regions through its interaction with SNAG domain containing TFs, such as Snail and GFI1B (92, 186). The SNAG domain binds to the Lsd1 active site by mimicking the histone H3 tail and could potentially inhibit its activity (89). Interaction of the p53 C-terminal domain with the Lsd1 active site inhibits Lsd1 enzymatic activity (91). Lsd1 was also shown to be present in the Oct3/4 interaction network, and therefore could be targeted to Oct3/4-bound regulatory elements, which largely control pluripotency and stemness (161, 162).

Studies by the Cancer Genome Anatomy Project (CGAP) show that one out of three cancers expresses PpGs, suggesting their role in dysregulated proliferation during tumorigenesis (187, 188). Further, expression of PpGs, Oct3/4, Sox2, and Nanog potentiates self-renewal of putative cancer stem cells (CSCs) (189-197). CSCs proliferate as well as differentiate to give rise to cancer cells of various lineages (165). However, in order to retain the ability to proliferate, many cancer cells maintain expression of PpGs (198, 199). This has led to the development of terminal differentiation therapy, which aims to limit the proliferating cancer cell population (200). Embryonal Carcinoma cells (ECCs) have been used as a model cell line to study CSCs. ECCs were derived from developing mouse embryos at E6-7.5 and share regulatory characteristics with ESCs, including their ability to differentiate into various somatic lineages (166, 201-203). To understand the mechanism by which cancer cells retain PpG expression, we investigated the mechanism of enhancer-mediated regulation of PpG expression in ECCs. Our data showed that in differentiating F9 ECCs, the PpGs are only partially repressed. This was concomitant with H3K27 deacetylation, but with an absence of Lsd1-mediated H3K4me1 demethylation at PpGe. The presence of H3K4me1 prevented Dnmt3a from methylating the DNA at these sites, potentially abrogating PpGe silencing. Drug-mediated inhibition as well as overexpression of Lsd1 had little or no effect on enhancer silencing and PpG repression, confirming a loss of Lsd1 dependence in differentiating F9 ECCs. Given that Oct3/4 was expressed at substantial levels in F9 ECCs post-differentiation, we investigated the effect of Lsd1-Oct3/4 interaction on Lsd1 catalytic activity. Using *in vitro* histone demethylation assays, we discovered that Lsd1-Oct3/4 interaction inhibits Lsd1 activity, potentially causing retention of H3K4me1 at PpGe in F9 ECCs. We tested this prediction in P19 ECCs in which we observed H3K4me1 demethylation at PpGe, accompanied by loss of Oct3/4

expression post-differentiation. Overexpression of Oct3/4 in differentiating P19 ECCs led to retention of H3K4me1 at PpGe, confirming the role of Oct3/4-mediated Lsd1 inhibition at these sites. Taken together our data show that inhibition of Lsd1 and Dnmt3a activities leads to the establishment of a "primed" enhancer state, which is open for coactivator binding and prone to reactivation. We speculate that aberrant expression of Oct3/4 in CSCs facilitates the establishment of "primed" enhancers, reactivation of which support tumorigenicity.

2.4 Materials and Methods

2.4.1 Cell culture and differentiation

F9 embryonal carcinoma cells (F9 ECCs), P19 embryonal carcinoma cells (P19 ECCs), and E14Tg2A Embryonic stem cells (ESCs) were cultured and maintained in gelatin-coated tissue culture plates. Differentiation of ECCs was induced by plating $20X10^6$ cells in low attachment 15 cm petri dishes and the addition of 1μM Retinoic acid (RA). ESCs were differentiated by the same method with a concurrent withdrawal of leukemia inhibitory factor (LIF). The medium was replenished every two days and samples were collected on Days 4 and 8 post-differentiation.

Plasmids expressing Myc-Dnmt3a2 and FLAG-Lsd1 WT were transfected into F9 ECCs using Lipofectamine 2000. One day post-transfection, an undifferentiated (UD) sample was collected (D0) and transfected cells were induced to differentiate on gelatinized plates by the addition of RA. The next day, differentiated cells were trypsinized and plated on low adherence petri dishes. Samples were collected on Days 4 and 8 post-differentiation. Lsd1 inhibitor treatment was performed 6 hr prior to induction of differentiation as previously described (102).

P19 ECCs were transfected with pCAG-Myc-Oct3/4 (Addgene 13460) (204) using Lipofectamine 2000 per the manufacturer's instructions. Transfected cells were clonally propagated, and Myc-Oct3/4 expression was determined by Western blots with anti-cMyc antibody (Millipore, MABE282).

2.4.2 Bisulfite sequencing

Bisulfite conversion was performed using an EpiTect Fast Bisulfite Conversion Kit (Qiagen, 59802) according to the manufacturer's protocol. PCR conditions for outer and inner amplifications were performed (102). The pooled samples were sequenced using NGS on a Wide-Seq platform. The reads were assembled and analyzed by Bismark and Bowtie2. Methylated and

unmethylated CpGs for each target were quantified, averaged, and presented as percent CpG methylation. Data are represented as average of at least two biological replicates. The number of CpGs for regions tested is listed in Table 2.1. The total number of reads used to calculate percent CpG methylation are listed in Tables 2.2 and 2.3. Primer sequences can be found in Table 2.4.

2.4.3 MethylRAD sequencing

Genomic DNA was isolated using a standard phenol:chloroform extraction, followed by ethanol precipitation. DNA from various samples was digested with *Fsp*EI for 4hr at 37°C and subjected to electrophoresis through a 2% agarose gel. The generated 30 base pair fragments were cut out, purified, and adaptors were ligated at 4°C overnight (129). The ligated DNA was PCR amplified with index primers and sequenced using a NovaSeq 6000 platform. The primers used for PCR amplification are listed in Table 2.4.

2.4.4 MethylRAD sequencing: Alignment and Quality Control

A total of 258,987,008 single end 1x150 sequencing was performed sing a NovaSeq 6000 platform for undifferentiated (UD) and day 4 post-differentiation (D4) F9 ECC samples. The program FastQC v. 0.11.7 was used to check data quality pre- and post-quality trimming/adapter removal (205). Adapters were removed from reads using Trimmomatic v. 0.36 (206). Trimmomatic is a program that removes adapter sequences and trims short Illumina reads based on quality. Cutadapt version 2.2 was used to trim reads further, removing the first two and last two bases of each read (207). Reads containing greater than 0 N's were discarded. After trimming, a total of 112,289,569 reads remained in the UD and D4 samples. Reads, which do not have *Fsp*E1 sites present anywhere in the read, were removed using 'grep', leaving a total of 71,730,977 reads. Finally, Bowtie2 version 2.3.3 was used to map reads to the ENSEMBL *Mus musculus* reference genome version GRCm38.93 (208, 209). A maximum of 1 mismatch was allowed in read mapping. The mapping rate of reads was 89%, with 64% of the reads mapped to the genome exactly 1 time and included in further analyses.

2.4.5 MethylRAD sequencing: Data preprocessing

Methylated sites were catalogued by iterating through all read sequences to find a matched pattern of methylation (i.e. CCGG, CCAGG, and CCTGG) and recording its location in the genome. The number of reads mapping to each methylated site was recorded and adjusted for

substitution, deletion, and insertion accordingly. Sites were also matched with the reference genome for verification. Sites that had less than 5 reads were removed from downstream analysis; counts from duplicate sites between patterns were summed as one site. Python and R scripts used in this analysis are included at www.github.com/natallah.

2.4.6 MethylRAD sequencing: Annotation to LSD1 Enhancers

Sites annotated as LSD1-bound enhancers in (179) were modified to include 1 kb up- and downstream of the identified start site. Both the UD and D4 differentiated F9 ECC samples were annotated to the modified LSD1 regions using BEDTools intersect. The total amount of methylation in a region was determined by combining the read counts of all sites in that region. Upper and lower quartiles were used in thresholding regions as gaining or losing methylation. Specifically, all regions with at least 22 counts more in undifferentiated than in day 4 differentiated samples were identified as losing DNA methylation as differentiation occurred. All regions with at least 30 counts more in D4 samples than in UD samples were identified as gaining DNA methylation.

2.4.7 MethylRAD sequencing: Quantifying methylated regions

The union of enhancers found in both the UD and D4 differentiated F9 ECC samples was determined. The difference in methylation for each combined enhancer regions were computed by subtracting the total methylation in D4 differentiated F9 ECC samples to that of the undifferentiated sample. Comparative figures were produced from these final data.

2.4.8 MethylRAD sequencing: Determining methylation level of enhancers

DNA sequences of all known enhancers for the ESC_J1 strain of mouse were downloaded from EnhancerAtlas V2.0 (210). Overlaps between MethylRAD sites and enhancers were found using BEDTools intersect. Reads that overlapped the enhancer for the same gene were then summed together. Raw counts were normalized for length. The average length of enhancers in the EnhancerAtlas database was computed for each gene. If different studies in the database reported variable lengths for enhancers, the average length of the enhancer was computed. Counts for each sample were then divided by the length of the enhancer and subsequently multiplied by 1000 (to enhance readability). The 25th and 75th percentiles were computed for all enhancers separately for UD and D4 samples and were used as cutoffs for low and intermediate methylation. Thus, for

UD samples, enhancers annotated as having low methylation have normalized counts between (0, 24.57], intermediate methylation are between (24.57, 243.68], and high methylation have greater than 243.58 normalized counts. Enhancers in D4 samples are annotated as highly methylated if normalized counts are observed to be between (0, 24.06], intermediate counts are between (24.06, 256.56], and high counts have greater than 256.56 normalized counts.

2.4.9 Chromatin Immunoprecipitation and ChIP-Seq

ChIP was performed as described (102). Chromatin was sheared by sonication using a Covaris E210 device, according to the manufacturer's protocol. A total of 8 µg of sheared cross-linked chromatin was incubated with 8 µg of antibody pre-loaded on a 1:1 ratio of protein A and protein G magnetic beads (Life Technologies, 10002D and 10004D, respectively). After washing the beads, the samples were eluted using 1% SDS, 10 mM EDTA, 50 mM Tris-HCl, pH 8.0. Crosslinking was reversed by incubation at 65°C for 30 min with shaking. Samples were treated with RNase (Roche, 11119915001) for 2 h at 37°C, and subsequently treated with Proteinase K (Worthington, LS004222) for 2 h at 55°C. DNA was purified by phenol:chloroform extraction followed by ethanol precipitation and quantified using PicoGreen (Life Technologies, P11495) and NanoDrop 3300 fluorospectrometer. qPCR was then performed using equal amounts of IN and IP samples. Fold enrichment was calculated as: $2^{(C_t(IN)-C_t(IP))}$. Table 2.4 lists sequences of primers used.

2.4.10 ChIP-Seq: Quality Control and Mapping

Sequencing was performed using a NovaSeq 6000 to generate > 80 million paired-end (2x50) reads (>80 million) UD and D4 F9 ECC samples. Sequence data quality was determined using FastQC software and quality based trimming and filtering (minimum quality score 30 and minimum read-length 20) was performed through TrimGalore tool (205, 211) . Greater than 95% of the reads from all samples were retained after quality control and were used for the mapping. Mapping was performed against the mouse reference genome (GRCm38) using Bowtie2 with a maximum of 1 mismatch (209). The overall mapping rate was >97% for all samples. Bowtie2 derived BAM files were further filtered to retain the reads with minimum MAPping Quality (MAPQ) 10.

2.4.11 ChIP-Seq: Peak-calling

Peak calling was performed using epic2 for each Input-ChIP pair using the mouse reference genome (GRCm38) (212). The tool was run with MAPQ10 filtered BAM files and the default parameters (--falsediscovery-rate-cutoff 0.05, --binsize 200).

2.4.12 ChIP-Seq: Peak-annotation

Peak-annotation and visualization was performed with R-package ChIPseeker (213). Annotations were performed for all epic2 peaks called with default parameters.

2.4.13 Pathway Analysis

IPA (Ingenuity Pathway Analysis), (IPA, QIAGEN Redwood City, www.qiagen.com/ingenuity), was used in the annotation of genes and in performing the pathway analyses.

2.4.14 Gene expression analysis

RNA was isolated by using the TRIzol reagent (Invitrogen, 15596026) according to the manufacturer's protocol. Samples were treated with DNAse (Roche, 04716728001) at 37°C, and then purified using a Quick-RNA^{TM} MiniPrep Plus Kit (ZymoReseach, R1057). Reverse-transcription quantitative PCR was performed by using Verso One-Step RT-qPCR kits (Thermo Scientific, AB-4104A) with 1 µg of purified RNA. Gene expression was calculated as ΔC_t which is C_t(Gene)- C_t(*Gapdh*). Change in gene expression is reported as fold change relative to that in undifferentiated cells, which was set to 1. Data were reported as average ± SEM (standard error of the mean) of at least two biological replicates. See Table 2.4 for primers used.

2.4.15 Co-immunoprecipitation

Co-immunoprecipitation experiments were performed as described (179). Briefly, undifferentiated F9 ECCs and ESCs were washed and harvested in cold 1XPBS. Cellular proteins were extracted using TNEN250 lysis buffer (50 mM Tris pH 7.5, 5 mM EDTA, 250 mM NaCl, 0.1% NP-40) complemented with protease inhibitors at 4°C with rotation for 30 min. Complexes were then immunoprecipitated overnight at 4°C with rotation by incubating the supernatant solution supplemented with two volumes of TNENG (50 mM Tris pH 7.5, 5 mM EDTA, 100 mM NaCl, 0.1% NP-40, 10% glycerol) with Dynabeads® M280 (Life Technologies, 11203D) bound

to 5 µg of antibody. Beads were washed with TNEN125 (50 mM Tris pH 7.5, 5 mM EDTA, 125 mM NaCl, 0.1% NP-40) and samples were eluted by boiling for 10 min in Laemmli's loading buffer containing 100 mM DTT. Western blots were performed with NuPAGE 4-12% Tris-Bis gels. Antibodies used included: Lsd1 (abcam, ab17721), HDAC1 (abcam, ab7028), Mi-2b (abcam, ab72418).

2.4.16 Microscopy

Bright field images of Embryoid bodies (EBs) were obtained with a Zeiss microscope using a 10X objective. Alkaline phosphatase staining was performed using solutions supplied by an alkaline phosphatase staining kit (Sigma, AB0300). Cells were cross-linked with 1% formaldehyde for 5 min, followed by quenching with a final concentration of 150 mM glycine. Cells were washed twice with 1XPBS, then twice with combined staining solution (BCIP and NBT). The stain was developed in the dark for 5 min, and then washed three times with 1XPBS. SSEA-1 immunofluorescence was performed using the following antibodies: anti-SSEA-1 (Millipore, MAB430) and AlexaFluor 555 nm (Life Technologies, A21422). SSEA-1 and Alkaline phosphatase staining were imaged using 20X objectives under Nikon Ts and Zeiss microscopes, respectively.

2.4.17 *In vitro* Lsd1 demethylase activity assay

An *in vitro* fluorometric assay was used to detect Lsd1 demethylase activity using an Epigenase^{TM} kit (Epigentek, P-0379) according to the manufacturer's protocol. A total of 0.25 µM of Lsd1 (Sigma, SRP0122) was used together with 0.5 µM (or as indicated) of Oct3/4 (abcam, ab134876 and ab169842) or BSA (Sigma, A3059) or the catalytic domain of Dnmt3a (purified in-house) or 0.1 mM of the Lsd1 inhibitor Tranylcypromine (TCP). Signals were measured using a CLARIOstar plate reader and analyzed using MARs software as described by the manufacturer.

2.4.18 Histone demethylation assay

Lsd1 histone demethylation assays were performed as described (214). A total of 30 µg of bulk histones (Sigma, H9250) in a histone demethylation buffer (50 mM Tris pH 8.5, 50 mM KCl, 5 mM MgCl, 0.5% BSA, and 5% glycerol) were incubated with 0.25 µM of Lsd1 (Sigma, SRP0122) alone, or increasing concentrations (0.125 µM, 0.25 µM, 0.5 µM, 1 µM) of Oct3/4 (abcam, ab134876 and ab169842), or 0.1 µM TCP for 4 hr at 37°C. Lsd1 activity was monitored by

Western blot using anti-H3K4me2 antibody (abcam, ab32356). The membrane was stained by Ponceau S to determine equal loading of the reaction mix.

2.4.19 Western blots

Western blot analysis was performed using the standard method and the following antibodies and dilutions: anti-Dnmt3a, 1:1000 (Active Motif, 39206), Anti-Lsd1, 1:1000 (abcam, ab17721) and anti-β Actin, 1:1000 (Santa Cruz, sc8628), and anti-Rabbit, 1:10,000 (Jackson Immunoresearch, 111-035-003) or anti-Mouse, 1:10,000 (Jackson Immunoresearch, 115-035-003). Chemiluminescence was performed according to the manufacturer's protocol (Thermo-Fisher Scientific, 34580).

Table 2.1 Number of CpGs at each site used for Bis-Seq DNA methylation analysis.

Genomic element		***No. of CpGs***
Enhancer	Lefty1	4
	Lefty2	6
	Sall4	4
	Sox2	10
	Trim28	6
	Esrrb	6
	Oct3/4	4
Promoter	Lefty1	6
	Lefty2	9
	Sall4	10
	Sox2	18
	Trim28	19
	Esrrb	29
Imprinted region	H19	11

The number of CpG sites used to compute percent methylation within the H19 imprinted region, PpG enhancers, and promoters.

Table 2.2 Number of reads for each enhancer used for Bis-Seq analysis.

Sample	***Lefty1***	***Lefty2***	***Sall4***	***Sox2***	***Trim28***	***Esrrb***	***Oct3/4***	***Total***
ESCs UD	28465	21981	2861	5826	17973	6034	1902	**85042**
ESCs D4	401	275	216	881	269	5381	6322	**13745**
F9 ECCs UD	57536	49939	27259	40357	14261	22395	6322	**232670**
F9 ECCs D4	62876	38534	29204	32570	13304	21569	8865	**214866**
F9 ECCs D6	62185	38590	30187	28239	10163	13059	6980	**182422**
F9 ECCs+Myc-Dnmt3a UD	3733	2692	1308	2612	1249	24671	311	**38969**
F9 ECCs+Myc-Dnmt3a D8	2734	1637	1135	2665	1097	4316	350	**24705**
F9 ECCs+FLAG-Lsd1 UD	2513	2267	816	4204	820	24412	1791	**43102**
F9 ECCs+FLAG-Lsd1 D8	2819	1950	1946	4530	1169	21576	1601	**42022**
P19 ECCs UD	26651	18427	10541	31377	9437	46154	7044	**175098**
P19 ECCs D4	40376	30470	18198	27196	11267	56736	14506	**241010**
P19 ECCs D8	4713	8696	5880	28944	6475	24128	4498	**96640**
P19 ECCs+Myc-Oct3/4 UD	23029	11988	11538	9324	7735	28746	7510	**130029**
P19 ECCs+Myc-Oct3/4 D4	35014	20519	14300	18022	13227	43559	14989	**210333**
Total	**353045**	**247965**	**156838**	**236746**	**108446**	**342735**	**76669**	**1522445**

The total number of reads from Wide-Seq runs that were used for data presented in this study. The number of reads was calculated for each sample and enhancer, along with the overall total number of reads.

Table 2.3 Number of reads for promoters and imprinted regions used for Bis-Seq analysis.

Sample	***Lefty1***	***Lefty2***	***Sall4***	***Sox2***	***Trim28***	***Esrrb***	***H19***	***Total***
F9 ECCs UD	51	726	486	9556	7575	4191	11062	**33647**
F9 ECCs D4	99	1590	1400	17431	16307	13865	9376	**60068**
Total	**150**	**2316**	**1886**	**26987**	**23882**	**18056**	**20438**	**93715**

The total number of reads from Wide-Seq runs that were used in this study. The number of reads was calculated for each sample, promoter site, and imprinted locus, as well as the overall total number of reads.

Table 2.4 Primers used in this study.

For Bisulfite PCR (enhancers):	***Primer sequence***
Trim28 out HSO3 F	ATGGATGTTTATGGAAGTAGTAGAAATA
Trim28 out HSO3 R	ACATCTAAATACTACCCAAAACCATTAC
Trim28 in HSO3 F	AATAGTTTAGGTTTTATTTTTTTTAAGATT
Trim28 in HSO3 R	AAACCATTACTTCAAAATAACTTTAAATTA
Sall4 out HSO3 F	AGGGATTATAATTTTTTGAGTTTTAGTTTATA
Sall4 out HSO3 R	AAAACCTCTAAAAAAACAATCAATACTCTTAA
Sall4 in HSO3 F	TATATAGAGAGGTTTAAATAAAGGGTTTTT
Sall4 in HSO3 R	TTTAAAACCACTAAACATATTAAAACATAA
Sox2 out HSO3 F	AGAAAATTGAGTTATTAAGGTAGTAATTATTT
Sox2 out HSO3 R	AAACCAAAAACCTTAACTACCAAACATAA
Sox2 in HS03 F	TAAAATTTTTATAGTTTTAATTGTTAAATA
Sox2 in HSO3 R	TATTATATCTAAAACCAACTAACAATATTAT
Lefty2 out HSO3 F	TTAGAAGTTTTTGGGGGAGAGGTTTGATTTA
Lefty2 out HSO3 R	TCAAAAATCATAACTCTTCCCACACCTCAAA
Lefty2 in HSO3 F	ATAATATGAGGGAGAGGTTTAGTTTTT
Lefty2 in HSO3 R	CACCTCAAACTCTATCTACTACTAACTTTA
Esrrb out HSO3 F	TTTGGAGAGGAAATATGTTAATTTTGAATA
Esrrb out HSO3 R	AAATCAACACACAAAATTCACTAAAAAAACA
Esrrb in HSO3 F	AATAGGGATTTTTTTTGGGATAGAAAT
Esrrb in HSO3 R	ATTCACTAAAAAAAAAAAAAAATCTCAAA
Lefty1 out HSO3 F	AAATAAGGAGGTAGGGGTAGAGAATATTTGA
Lefty1 out HSO3 R	AAAAAACAATCTCCCTCCCACCTAACA
Lefty1 in HSO3 F	TTTAGAGGAGAAGTTAAGTTTAGTATAGAGAATA
Lefty1 in HSO3 R	ACACCTAATCAAACCCATTATACAAAAT
Oct3/4 out HSO3 F	TAATGGGATTTTTAGATTGGGTTTAGAAAA
Oct3/4 out HSO3 R	TAACCCTAAACAAATACTCAACCCTTAAAT
Oct3/4 in HSO3 F	TTTGAGGGTTATTTTTTTGTAAAGATAA
Oct3/4 in HSO3 R	AAAAAAAATATCTAACTTCAAATTCAAA
H19 out HSO3 F	GAGTATTTAGGAGGTATAAGAATT
H19 out HSO3 R	ATCAAAAACTAACATAAACCCT
H19 in HSO3 F	GTAAGGAGATTATGTTTATTTTTGG
H19 in HSO3 R	CCTCATTAATCCCATAACTAT

Table 2.4 continued

For Bisulfite PCR (promoters):	***Primer sequence***
Sox2 out HSO3 F	AAGGTTTTTTTTGAAATTGTTATTATTAAA
Sox2 out HSO3 R	AATATTAACTCTCTCTTAAATACATAA
Sox2 in HS03 F	AAAAATTTTTTTGTGTTAGGGTTGGGAGTTA
Sox2 in HSO3 R	ACTATCCAACTAATATTTCAAAAAACTAACAAA
Esrrb out HSO3 F	AATTTGTAAAAGATAGGGTTTTTGATTTGAAGTTTA
Esrrb out HSO3 R	TATAAACCAAAACCCCCACCCAAAACCTAAAT
Esrrb in HSO3 F	AATTTAAAGTTTTTTAGAATTTTGAAGT
Esrrb in HSO3 R	AATCCTCCATAATACCACTAATACAATCCT
Trim28 out HSO3 F	TTTATTTTGTTTTTGTGTTTTTGGTATTTTAAAG
Trim28 out HSO3 R	TCTAATCTAAAATAAAAAATAACAAAATCAAAT
Trim28 in HSO3 F	ATTATATTTTTTTTTTTTGAGGTAGGAAGT
Trim28 in HSO3 R	TTTCATCTCAAAAACAAAATCAATAT
Lefty1 out HSO3 F	ATAATAAAGGGTGGTTTTGTTGGAGAGTTAGGGAATA
Lefty1 out HSO3 R	TATCCTTTCCCTTTCTTACTATAAAAAAATT
Lefty1 in HSO3 F	TTTTATAATTTATTATGGTTTTTTTATTTAT
Lefty1 in HSO3 R	AAATCTACCCCATCCCAATCTCTAAACCAAAATACA
Lefty2 out HSO3 F	ATTTATTAAGTATTAAGATTTAGTTGTTGTAAA
Lefty2 out HSO3 R	AACTACAACTATATATCACTATACCAAACCTATTTAA
Lefty2 in HSO3 F	AGATTTGGTTTTTGGATGGTTTTTGTTTTTAA
Lefty2 in HSO3 R	ATTCTCCATAAACCAATAAAAATCTAAATTT
Sall4 out HSO3 F	TAAAGGAATAGAATTATATTATATAATGTTTTTTTTAA
Sall4 out HSO3 R	ATCTTTCTACTTTACATTTTCTTAATTAACTATTT
Sall4 in HSO3 F	TTTTTTGAGTTGTAAATTGTATATTTTTTTAGATTT
Sall4 in HSO3 R	AATAAATCAACTAAACCACAAATTTAATAT

Table 2.4 continued

For RT-qPCR:	***Primer sequence***
Oct3/4 F	TCTTTCCACCAGGCCCCCGGCTC
Oct3/4 R	TGCGGGCGGACATGGGGAGATCC
Sox2 F	ATGATGGAGACGGAGCTGAA
Sox2 R	TTGCTGATCTCCGAGTTGTG
Esrrb F	CCTCATCAACTGGGCCAAGC
Esrrb R	TACACGATGCCCAAGATGAGAATCT
Nanog F	ACCTGAGCTATAAGCAGGTTAAGAC
Nanog F	GTGCTGAGCCCTTCTGAATCAGAC
Trim28 F	GAGATGGAGAGCGAACAGTCTAC
Trim28 R	TGTCACAGCTCTCACAGAACAG
Prdm14 F	ACAGCCAAGCAATTTGCACTAC
Prdm14 R	TTACCTGGCATTTTCATTGCTC
Lefty1 F	CTACAACACAGCCATGCCAG
Lefty1 R	CTCCATTCCGAACACTAGCAGGT
Lefty2 F	GCAAGAGGTTCAGCCAGAATTT
Lefty2 R	GCTGCTCCATTCCGAACACTA
Olig2 F	CGCAGCGAGCACCTCAAATCTAA
Olig2 R	CCCAGGGATGATCTAAGCTCTCGAA
Foxa2 F	CTCTTCCGTGAGCAACATGA
Foxa2 R	GCGCCCACATAGGATGAC
Gata6 F	CTTGCGGGCTCTATATGAAACTCCAT
Gata6 R	TAGAAGAAGAGGAAGTAGGAGTCATAGGGACA
Gata4 F	CTCTATCACAAGATGAACGGCATCAAC
Gata4 R	TCTGGCAGTTGGCACAGGAGAG
Cxc4 F	GAAGTGGGGTCTGGAGACTAT
Cxcr4 R	TTGCCGACTATGCCAGTCAAG
Fgf5 F	GAAAAGACAGGCCGAGAGTG
Fgf5 R	GAAGTGGGTGGAGACGTGTT
Sall4 F	GTGCTCCAGTGAACTCCCC
Sall4 R	ACAGCATTTGTTGCAGATGTGA
Dnmt3l F	ATGGACAATCTGCTGCTGACTG
Dnmt3l R	CGCATAGCATTCTGGTAGTCTCTG
Dnmt3a F	GTCACACAGAAGCATATCCAGGAG
Dnmt3a R	GTTGACAATGGAGAGGTCATTGC
Lsd1 F	GATGGGATTTGGCAACCTTAACAAG
Lsd1 R	AAACAAATTGACACTTGGGTCCC
Gapdh F	CAAAATGGTGAAGGTCGGTGTGAA
Gapdh R	CAACAATCTCCACTTTGCCACTG

Table 2.4 continued

For ChIP-qPCR:	***Primer sequence***
Sox2 F	TGGCGAGTGGTTAAACAGAG
Sox2 R	TAGCGAGAACTAGCCAAGCA
Esrrb F	CGAGCTTCAGCTGGCTATTT
Esrrb R	GAGCTCCAGATCCCCTACAC
Trim28 F	GGTCTGCAATTGAAGGAAGG
Trim28 R	TTAAACAGCAGGGGGTAAGG
Lefty1 F	GTAGCCAGCAGACAGGACAA
Lefty1 R	ATCCCCAATCCACATTCACT
Lefty2 F	AGGCCTAGCTTTTGCATCAC
Lefty2 R	TCTCCCAGAGTCGATCTTCC
Sall4 F	GAAATAAACATCTGGGAGAAGGA
Sall4 R	GGAAACCCCAGATTGAGAGA
Oct3/4 F	TATAGGTGTGGCATTCCGCATC
Oct3/4 R	TGCCACAAACCACCTGTATTTTAG
Ctrl F	ACCTAAACCTCATAAAGACACAACA
Ctrl R	TGACGTGTTCTTGGATTCAGT

Table 2.4 continued

MethylRAD-adaptor and index primers	***Primer sequence***
Adaptor-1 sense	ACACTCTTTCCCTACACGACGCTCTTCCGATCT
Adaptor-1 antisense	NNNNAGATCGGAAGAGC(AminoC6)
Adaptor-2 sense	GTGACTGGAGTTCAGACGTGTGCTCTTCCGATCT
Adaptor-2 antisense	NNNNAGATCGGAAGAGC(AminoC6)
P1	ACACTCTTTCCCTACACGACGCT
P2	GTGACTGGAGTTCAGACGTGTGCT
i5- UDA5073	AATGATACGGCGACCACCGAGATCTACACGATAACAAGTACACTCTTTCC CTACACGACGCT
i5- UDA5074	AATGATACGGCGACCACCGAGATCTACACAGCGGTGGACACACTCTTTCC CTACACGACGCT
i5- UDA5075	AATGATACGGCGACCACCGAGATCTACACGGTTATGCTAACACTCTTTCC CTACACGACGCT
i5- UDA5076	AATGATACGGCGACCACCGAGATCTACACAACCGCATCGACACTCTTTCC CTACACGACGCT
i7- UDA7120	CAAGCAGAAGACGGCATACGAGATGAACTTCCTTGTGACTGGAGTTCAG ACGTGT
i7- UDA7119	CAAGCAGAAGACGGCATACGAGATAGGTCCTTCCGTGACTGGAGTTCAG ACGTGT
i7- UDA7118	CAAGCAGAAGACGGCATACGAGATTATGGAGATTGTGACTGGAGTTCAG ACGTGT
i7- UDA7117	CAAGCAGAAGACGGCATACGAGATCGCAAGAGCCGTGACTGGAGTTCAG ACGTGT

A list of all PCR primers used in this study (5' to 3'), separated by technique. The presence of an (AminoC6) modification at the 3' end of the antisense oligonucleotide of each adaptor is used to block extension.

2.5 Results

2.5.1 PpGs are partially repressed in differentiating F9 ECCs

ECCs share many characteristics with ESCs, including mechanisms governing regulation of gene expression and differentiation (201). Based on the observation that aberrant PpG expression is commonly found in cancers (187, 188), we compared the magnitude of PpG repression in F9 ECCs with that in ESCs pre- and post-differentiation. F9 ECCs and ESCs were induced to differentiate with retinoic acid (RA) and expression of eight PpGs at 4 and 8 days (D4 and D8) post-induction was measured by RT-qPCR. The data show that in differentiating F9 ECCs, several PpGs were incompletely repressed, of which genes encoding the pioneer factors Oct3/4 and Nanog showed only 50% loss of expression at D8 post-differentiation. In ESCs, the expression of most PpGs was reduced by more than 80% at D4 post-differentiation (Figures 2.1A and B). The expression of Sox2 and Trim28 was maintained post-differentiation as an anticipated response to RA signaling guiding ESCs towards neural lineage. A substantial increase in the expression of the genes *Lefty1* and *Lefty2* in F9 ECCs suggests potential activation of germ cell and testis developmental programs (215). Continued expression of PpGs in F9 ECCs was also evident by positive alkaline phosphatase staining and SSEA-1 immunofluorescence in differentiating F9 ECCs that is completely lost in ESCs post-differentiation (Figures 2.1C and D). We asked if failure to exit pluripotency in F9 ECCs was caused by an inability to activate lineage-specific genes. Our data showed a 10 to 50-fold increase in expression of the lineage specific genes *Gata4*, *FoxA2*, *Olig2*, *Gata6*, *Cxcr4,* and *Fgf5* (Figure 2.1E), reflecting a standard response to signal of differentiation. Given that previous studies in ESCs have established a critical role of enhancer silencing in complete PpG repression, we next investigated if PpGe were fully decommissioned in F9 ECCs post-differentiation.

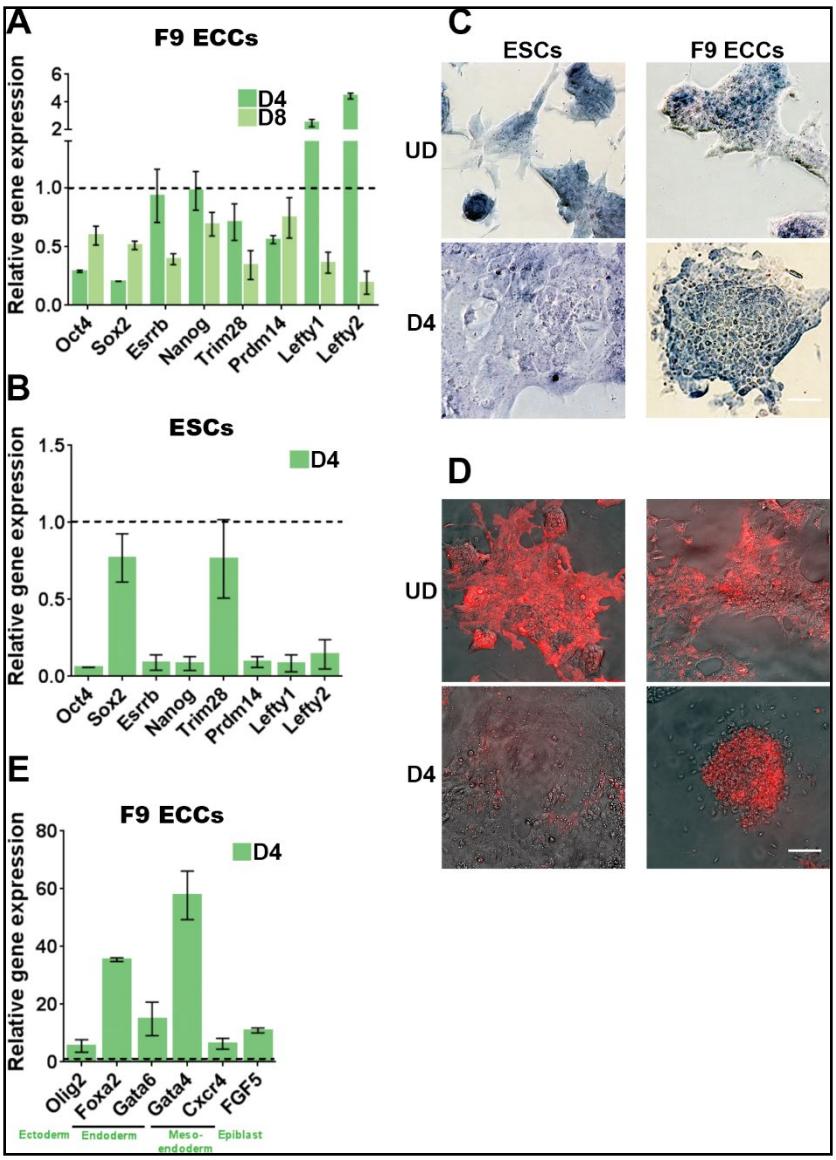

Figure 2.1 Pluripotency genes are partially repressed in F9 embryonal carcinoma cells.

UD: undifferentiated; D4, D8: Days post-induction of differentiation; ESCs: embryonic stem cells and F9 ECCs: F9 embryonal carcinoma cells, PpGs: pluripotency genes. (A, B, and E) Gene expression analysis by RT-qPCR of PpGs in (A) F9 ECCs, (B) ESCs (E) lineage specific genes in F9 ECCs. The Ct values for each gene were normalized to Gapdh and expression is shown relative to that in undifferentiated cells (dotted line). In F9 ECCs, the lineage specific genes show a 40 to 60-fold induction of gene expression (E) whereas the expression of PpGs is on average reduced to about 50% post-differentiation. (B) Average and SEM of two biological replicates are shown for each gene. (C) Alkaline phosphatase staining and (D) SSEA-1 immunofluorescence of ESCs and F9 ECCs pre- and post-differentiation. Positive signal indicates pluripotency that is lost post-differentiation in ESCs. The scale bar is a 100 µm.

2.5.2 DNA methylation is not established at PpGe during F9 ECC differentiation

We have previously reported that in differentiating ESCs, PpGe decommissioning involves gain of DNA methylation, which is required for complete PpG repression (102). We used bisulfite sequencing (Bis-Seq) (Tables 2.1 and 2.2) to compare DNA methylation changes at a subset of PpGe in F9 ECCs to that in ESCs post-differentiation. Whereas DNA methylation was significantly gained in ESCs within 4 days post-differentiation, the PpGe remained hypomethylated in F9 ECCs at 4 and 6 days post-differentiation (Figures 2.2A, B, and 2.3A). A similar hypomethylated state persisted at PpG promoters in F9 ECCs except the highly methylated *Lefty2* promoter, where DNA methylation was partially lost post-differentiation (Figure 2.3B). This result is consistent with the observed partial repression of most PpGs and an induction of *Lefty2* expression in these cells (Figure 2.1A).

We confirmed that absence of DNA methylation at PpGe was not due to the low expression of Dnmt3a in F9 ECCs post-differentiation (Figures 2.3C and D). Based on the previous observations in cancers, that overexpression of DNA methyltransferases leads to DNA hypermethylation (115, 216-219); we tested if overexpression of Dnmt3a could rescue DNA methylation at PpGe. F9 ECCs were transfected with Myc-Dnmt3a and differentiated at 24 hr post-transfection to ensure expression of recombinant Dnmt3a during differentiation (Figure 2.3E). However, we observed no gain in DNA methylation at PpGe and no additional decrease in the expression of PpGs when compared to untransfected cells at D8 post-differentiation (Figures 2.2C and D). These data indicate that the over-expression of Dnmt3a does not rescue the differentiation defects observed in F9 ECCs.

We next assayed DNA methylation genome-wide using MethylRAD sequencing to analyze changes at all PpGe in F9 ECCs pre- and post-differentiation (129). Similar to methylation dependent restriction assays, this method uses *Fsp*EI enzyme, which cuts DNA bidirectionally from mC to create 31-32 bp fragments (220, 221). The restriction fragments were isolated for library preparation and high throughput sequencing. Using this method, we captured DNA methylation at 1,370,254 cytosines genome-wide, with a required minimum read support of five reads. The reads were distributed among all chromosomes representing all annotated genomic elements (Figure 2.4A). DNA methylation levels at enhancers (low-intermediate-high) were calculated based on highest (75th percentile) and lowest (25th percentile) number of reads at all annotated enhancers in the genome, which were obtained from the EnhancerAtlas 2.0. We filtered

the data to focus our analysis on DNA methylation changes at 3840 PpGe previously annotated in ESCs as Lsd1 bound regions (179). Our method identified 1,865 PpGe in F9 ECCs. Compared to methylation levels at all other known enhancers, the PpGe cluster into the low/intermediate methylation group (Figure 2.4B). The difference in methylation for each PpGe region was computed by subtracting the DNA methylation level in D4 differentiated from that in undifferentiated F9 ECCs. The data show 1488 (82%) regions fail to gain DNA methylation post-differentiation of F9 ECCs (no change in DNA methylation; NCDM PpGe) (Figure 2.2E). To determine the function of genes associated with NCDM PpGe, we performed Ingenuity pathway analysis (IPA) (www.qiagen.com/ingenuity), which showed a significant enrichment of Oct3/4- and Nanog-regulated mammalian embryonic stem cell and molecular mechanisms of cancer pathways (Figure 2.2F).

Given that DNA methylation by Dnmt3a at PpGe requires H3K27 deacetylation and H3K4 demethylation by Lsd1/Mi2NurD complex (179), we anticipate a potential impediment in this process causing a widespread failure to acquire DNA methylation at PpGe.

Figure 2.2 Pluripotency gene enhancers do not gain DNA methylation in differentiating F9 embryonal carcinoma cells.

UD: undifferentiated; D4, D8: Days post-induction of differentiation; D8 UT: untransfected F9 ECCs differentiated for 8 days; D8+Myc-Dnmt3a: F9 ECCs overexpressing Myc-Dnmt3a and differentiated for 8 days; ESCs: embryonic stem cells and F9 ECCs: F9 embryonal carcinoma cells; PpGe: pluripotency gene enhancers.

(A, B, and C) DNA methylation analysis using Bis-Seq. Genomic DNA was treated with bisulfite and PpGe regions were amplified by PCR. The amplicons were sequenced on a high throughput-sequencing platform (Wide-Seq) and the data were analyzed using Bismark software. DNA methylation of PpGe in (A) ESCs (B) F9 ECCs pre- and post-differentiation. Less than 10% DNA methylation was recorded in F9 ECCs whereas the H19 imprinted region, used as a control, showed DNA methylation at 80%. At the same regions, DNA methylation increased up to 30% in ESCs. See also Figure S1A.

(C) DNA methylation of PpGe in F9 ECCs overexpressing Myc-Dnmt3a. (D) Gene expression analysis by RT-qPCR PpGs in F9 ECCs overexpressing Myc-Dnmt3a pre- and post-differentiation. (C, D) show no significant increase in DNA methylation or gene repression 8 days post-differentiation The C_t values for each gene were normalized to Gapdh and expression is shown relative to that in undifferentiated cells (dotted line). Data for A, B, C and D are the average and SEM of two biological replicates.

(E) Genome-wide DNA methylation analysis by MethylRAD sequencing. Genomic DNA was digested with the restriction enzyme *Fsp*EI that cuts methylated DNA into 31-32 bp fragments. The fragments were sequenced and mapped on mm10 mouse genome. The number of reads per region were used as a measure for extent of DNA methylation and compared between undifferentiated and D4 differentiated F9 ECCs. The waterfall plot shows DNA methylation changes at PpGe computed by subtracting normalized counts in D4 samples from normalized counts in undifferentiated samples. Upper and lower quartiles were used in thresholding regions as gaining or losing methylation. The pie chart shows fractions of PpGe with increase, decrease or no change in DNA methylation (NCDM). See also Figure S2B.

(F) Top ten statistically significant enriched canonical pathways amongst the genes associated with the NCDM enhancers, which showed no change. The x-axis shows the log10 (adjusted p-value), with the p-value adjusted for multiple testing using the Benjamini-Hochberg method.

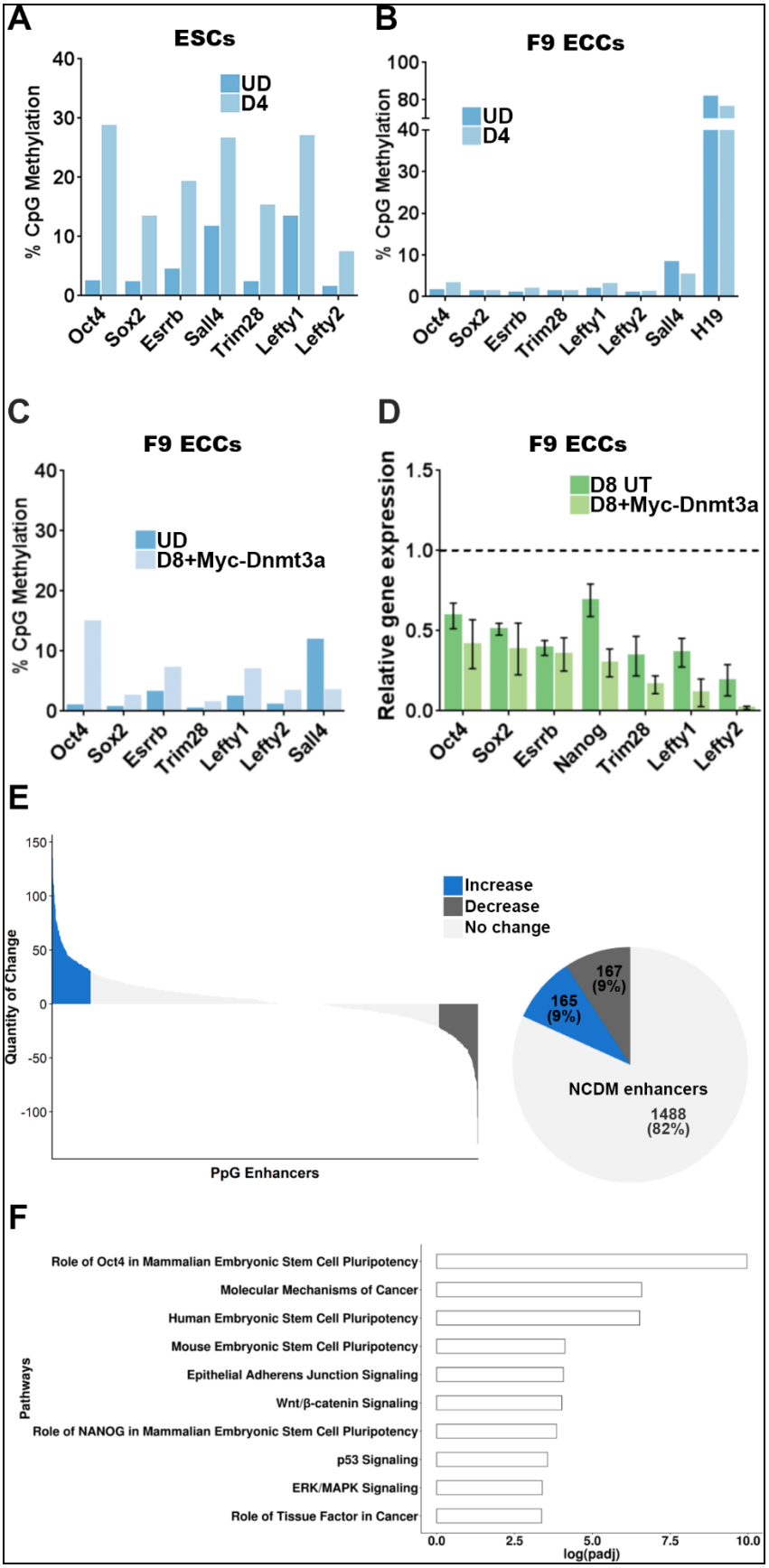
A
ESCs
% CpG Methylation
UD
D4
Oct4
Sox2
Esrrb
Sall4
Trim28
Lefty1
Lefty2
B
F9 ECCs
% CpG Methylation
UD
D4
Oct4
Sox2
Esrrb
Trim28
Lefty1
Lefty2
Sall4
H19
C
F9 ECCs
% CpG Methylation
UD
D8+Myc-Dnmt3a
Oct4
Sox2
Esrrb
Trim28
Lefty1
Lefty2
Sall4
D
F9 ECCs
Relative gene expression
D8 UT
D8+Myc-Dnmt3a
Oct4
Sox2
Esrrb
Nanog
Trim28
Lefty1
Lefty2
E
Quantity of Change
Increase
Decrease
No change
PpG Enhancers
167
(9%)
165
(9%)
NCDM enhancers
1488
(82%)
F
Pathways
Role of Oct4 in Mammalian Embryonic Stem Cell Pluripotency
Molecular Mechanisms of Cancer
Human Embryonic Stem Cell Pluripotency
Mouse Embryonic Stem Cell Pluripotency
Epithelial Adherens Junction Signaling
Wnt/β-catenin Signaling
Role of NANOG in Mammalian Embryonic Stem Cell Pluripotency
p53 Signaling
ERK/MAPK Signaling
Role of Tissue Factor in Cancer
log(padj)

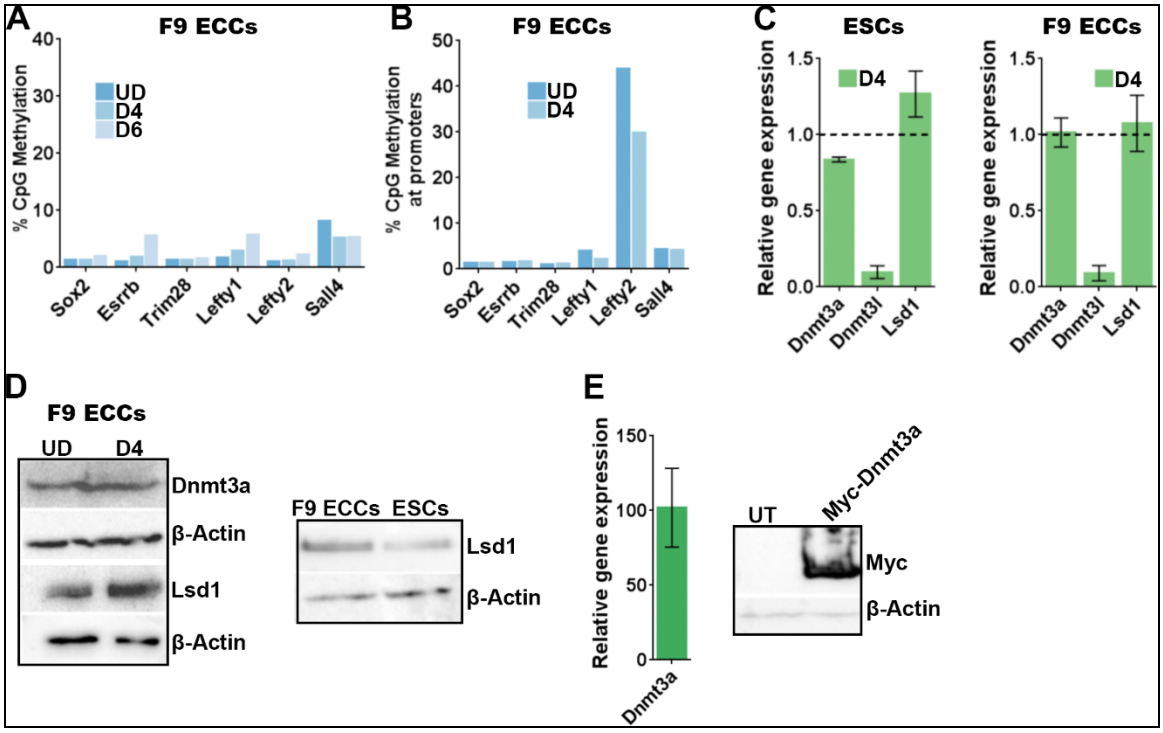

Figure 2.3 Expression of epigenetic effectors in F9 ECCs.

UD: undifferentiated. D4: Days post-differentiation. ESCs: embryonic stem cells and F9 ECCs: F9 embryonal carcinoma cells; PpGe: pluripotency gene enhancers.

(A and B) Bis-Seq analysis of DNA methylation at PpG (A) enhancers and (B) promoters in F9 ECCs pre- and post-differentiation. The DNA methylation at PpGe remained under 10% even at 6 days post-differentiation. DNA methylation at PpG promoters is also low except Lefty2, which shows very high methylation in the UD state that is reduced post-differentiation.

(C) RT-qPCR comparing the changes in expression of DNA methyltransferase Dnmt3a and histone demethylase Lsd1 in ESCs with that in F9 ECCs pre- and post-differentiation. The C_t values are normalized to *Gapdh* and represented relative to expression in undifferentiated cells (dotted line). In both ESCs and ECCs, Lsd1 and Dnmt3a expression is maintained post-differentiation.

(D) Western blot. A total of 50 µg of total protein from undifferentiated and differentiated cells was loaded in each well. Left panel confirms comparable expression of Dnmt3a and Lsd1 pre- and post-differentiation in F9 ECCs. Right panel compares Lsd1 expression in F9 ECCs with ESCs showing very similar levels in these cells. β-Actin is the loading control.

(E) Gene expression analysis by RT-qPCR and Western blot confirming recombinant Myc-Dnmt3a overexpression in F9 ECCs 24 hr post-differentiation (48 hr post-transfection). The data are normalized to a *Gapdh* control and shown relative to untransfected that is set to 1. β-Actin is used as loading control for Western blot.

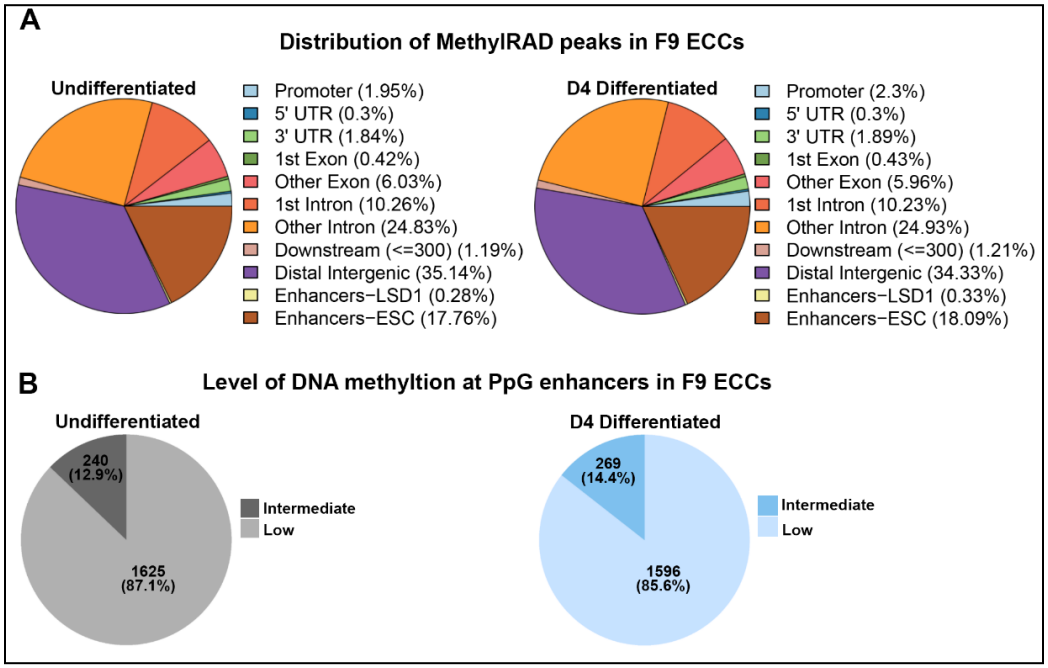

Figure 2.4 Distribution of MethylRAD peaks.

(A) Fractional distribution of MethylRAD peaks in undifferentiated and differentiated F9 ECCs across regulatory regions of the genome.

(B) Pie charts show the level of methylation at PpGe in undifferentiated (grey) and D4 differentiated (blue) samples. Most PpGe had low levels of methylation or to a lesser extent, intermediate levels of methylation, with none having high CpG methylation.

2.5.3 A "primed" PpGe state is established during F9 ECC differentiation

We asked if the chromatin state at PpGe in F9 ECCs is impermissible to DNA methylation. Using chromatin immunoprecipitation followed by qPCR (ChIP-qPCR) we examined histone H3K27 deacetylation and our data showed a decrease in H3K27Ac at PpGe in F9 ECCs post-differentiation. This result suggests that, similar to ESCs, PpGe are active in undifferentiated F9 ECCs and initiate the decommissioning process post-differentiation (Figures 2.5A and 2.6A). Furthermore, deacetylation at *Lefty1* and *Lefty2* enhancers suggests enhancer-switching involving the potential use of germline-specific enhancers post-differentiation, leading to an observed increase in *Lefty1* and *Lefty2* expression (Figure 2.1A). Numerous studies have proposed that deacetylation of H3K27Ac followed by H3K27 methylation by the PRC2 enzyme complex establishes a silenced state (222-224). Our data showed no increase of H3K27me3 at the PpGe in both ESCs as well as F9 ECCs post-differentiation, suggesting that PRC2 activity is nonessential for PpGe silencing (Figures 2.6B and C).

We next monitored H3K4me1 demethylation by Lsd1 at PpGe during F9 ECC differentiation. Surprisingly, we observed a retention or an increase in H3K4me1 at five out of seven tested PpGe post-differentiation (Figure 2.5B), suggesting a potential disruption of Lsd1 activity. We verified similar expression levels of Lsd1 in F9 ECCs compared to ESCs (Figures 2.2C and D). To examine if Lsd1 interacts with the Mi2/NuRD complex in F9 ECCs, we performed co-immunoprecipitation (Co-IP) experiments using whole cell extracts. Antibodies against Lsd1 and HDAC1 were used for reciprocal Co-IP. The data show the presence of Chd4, HDAC1 and Lsd1 and no significant difference in protein complexes between ESCs and F9 ECCs (Figure 2.6D). To test its recruitment to PpGe, ChIP-qPCR showed similar enrichment of Lsd1 in F9 ECCs and ESCs at four tested enhancers (Figure 2.5C). These data suggest that retention of H3K4me1 at PpGe is not caused by the absence of the enzyme but rather due to lack of Lsd1 activity in F9 ECCs post-differentiation.

To confirm the above conclusion, we next tested the effect of Lsd1 overexpression or inhibition on PpGe silencing and PpG repression in differentiating F9 ECCs. F9 ECCs were transfected with a FLAG-Lsd1 overexpressing plasmid and differentiated at 24 hr post-transfection (Figure 2.7A). We observed no change in H3K4me1 at PpGs post-differentiation. Rather, we saw a small increase at some enhancers, suggesting an inhibitory mechanism which affects Lsd1

irrespective of the source of expression (Figure 2.5D). An increase in H3K4me1 post-differentiation could result from partial activity of Lsd1 by which it demethylates H3K4me2 to H3K4me1 at these sites. Additionally, Lsd1 overexpression had no effect on PpG repression or DNA methylation at PpGe post-differentiation (Figures 2.7B and C).

Previous studies in ESCs have shown that treatment with the Lsd1 inhibitors pargyline and TCP (tranylcypromine) at the onset of differentiation results in H3K4me1 retention at PpGe and incomplete repression of PpGs (179). F9 ECCs were treated with pargyline and TCP 6 hr prior to induction of differentiation. In contrast to 70-80% cell death caused by the Lsd1 inhibitor in ESCs, F9 ECCs remained largely viable upon treatment (Figure 2.7D). Expression analysis of PpGs showed a slight relief of PpG repression in treated cells, suggesting a partial Lsd1 activity at PpGe (Figure 2.7E). Interestingly, pargyline treatment affected the H3K4me1 enrichment gained post-differentiation in untreated cells (WT and Lsd1 overexpressing), confirming the partial activity of Lsd1 at these sites (Figure 2.5E). To test if Lsd1 activity contributed to the generation of H3K4me1 in the undifferentiated state, we transiently overexpressed Lsd1 in F9 ECCs and allowed cells to grow for 72 hr. ChIP-qPCR analysis showed no increase in H3K4me1 levels in Lsd1 overexpressing cells (Figure 2.7F). This result suggests that, similar to our observation in ESCs, the deposition of H3K4me1 in the undifferentiated F9 ECCs is largely accomplished by MLL3/4 histone methyltransferases, and Lsd1 activity at these sites is initiated only in response to a differentiation signal (196, 225).

Taken together, these observations suggest that the restricted activity of Lsd1 at PpGe leads to retention of H3K4me1 post-differentiation. Moreover, following the deacetylation of H3K27, the absence of DNA methylation and the presence of H3K4me1 converts these enhancers to a “primed” state, prone to reactivation in the presence of a coactivator.

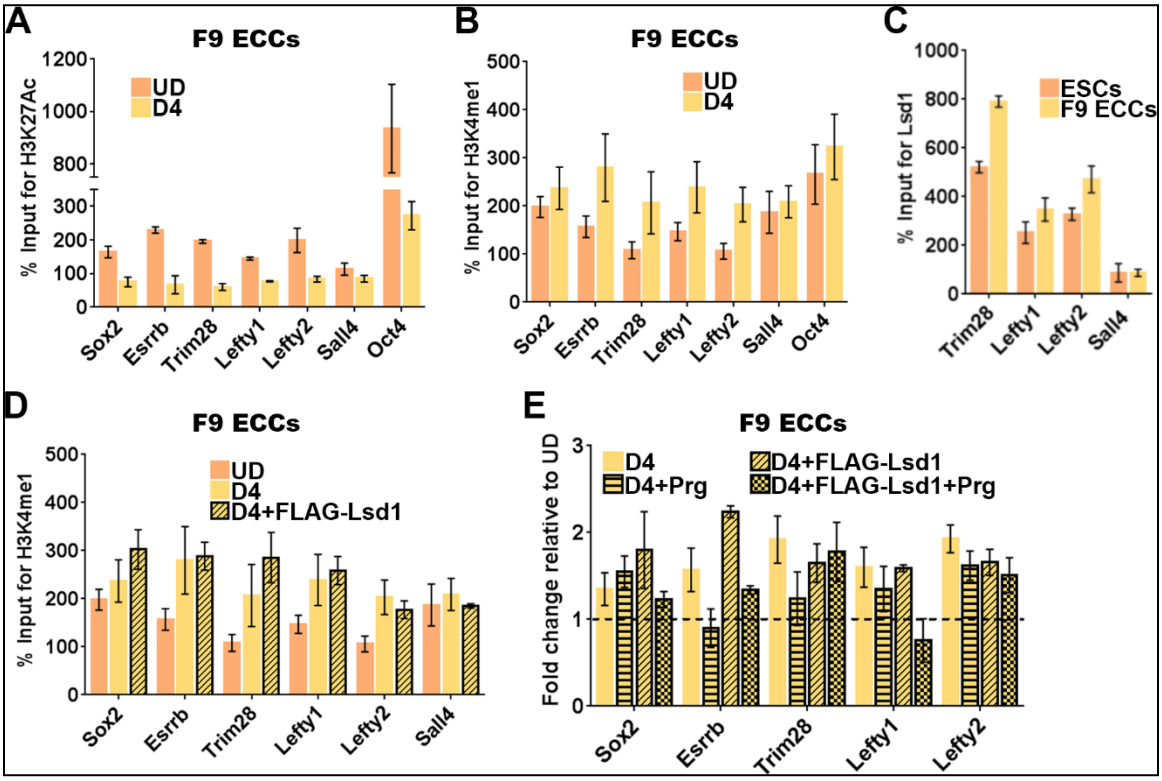

Figure 2.5 Changes in chromatin modifications establish a "primed" state at pluripotency gene enhancers in F9 embryonal carcinoma cells.

UD: undifferentiated; D4: Days post-induction of differentiation; D4+FLAG-Lsd1: F9 ECCs overexpressing FLAG-Lsd1 and differentiated for 4 days; Prg: Pargyline; ESCs: embryonic stem cells and F9 ECCs: F9 embryonal carcinoma cells; PpGe: pluripotency gene enhancers.

(A-E) Chromatin immunoprecipitation (ChIP)-qPCR assays showing percent enrichment over input. Histone modifications at PpGe (A) H3K27Ac and (B) H3K4me1 in F9 ECCs pre- and D4 post-differentiation. Whereas deacetylation of PpGe is observed as a decrease in the H3K27Ac signal, histone H3K4me1 is retained post-differentiation.

(C) Similar Lsd1 occupancy in undifferentiated ESCs and F9 ECCs.

(D) Enrichment of H3K4me1 in F9 ECCs expressing recombinant FLAG-Lsd1 compared to untransfected cells at D4 post-differentiation. There is a slight increase in H3K4me1 at some PpGe.

(E) Fold change in enrichment of H3K4me1 at PpGe in pargyline treated and untreated, WT, and FLAG-Lsd1 overexpressing F9 ECCs, at D4 post-differentiation. Fold change is represented as relative to enrichment in the undifferentiated state (dotted line).

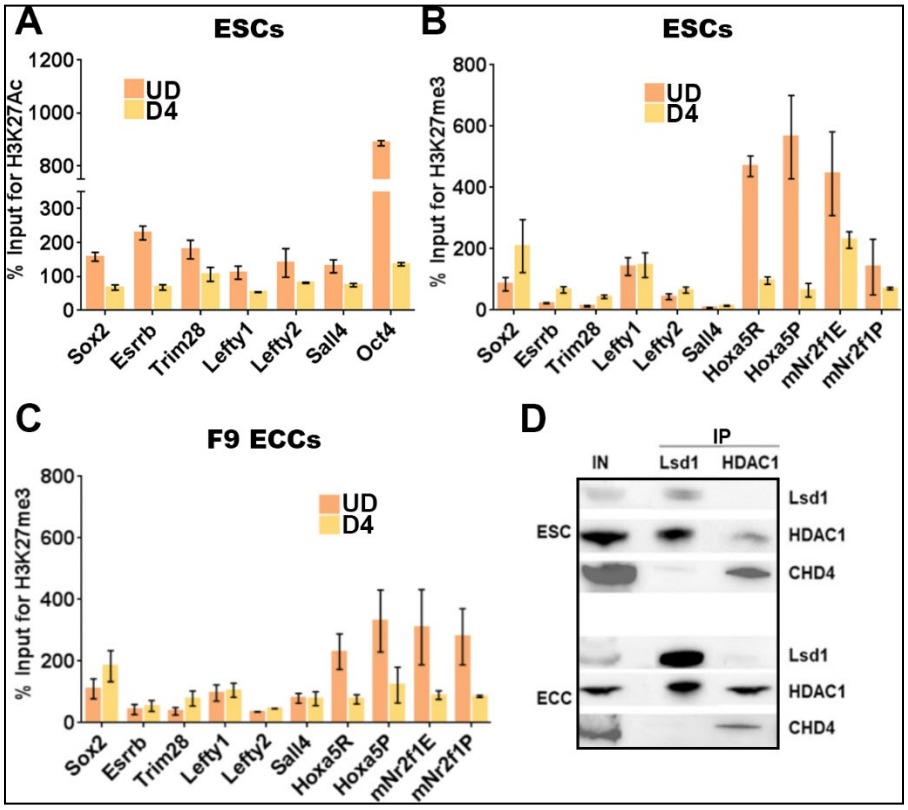

Figure 2.6 H3K27 modification of PpGe in ESCs and F9 ECCs.

UD: undifferentiated; D4: Days post-induction of differentiation; IP: immunoprecipitation

(A, B, and C) ChIP-qPCR was used to determine the percent enrichment of histone modifications at PpGe. (A) H3K27Ac in ESCs (B) H3K27me3 in ESCs and (C) H3K27me3 in F9 ECCs pre- and post-differentiation. Whereas deacetylation of PpGe is observed as a decrease in H3K27Ac signal post-differentiation in ESCs, there is no gain of H3K27me3 at these sites, neither in ESCs nor in F9 ECCs. As previously reported, we observed a decrease in H3K27me3 at the enhancers and promoters of *Hoxa5* and *mNr2f1* genes, consistent with their transcriptional activation in response to differentiation (226).

(D) Co-IP was performed with anti-Lsd1 or anti-HDAC1 using whole cell extracts from undifferentiated ESCs and F9 ECCs. 20% of the input and eluate from Co-IP were probed for Lsd1-Mi2/NuRD subunits (Lsd1, HDAC1, and CHD4) on Western blot.

Figure 2.7 Overexpression or inhibition of Lsd1 has little to no effect on differentiation and PpGe silencing in F9 ECCs.

UD: undifferentiated; D8: Days post-induction of differentiation; Prg: pargyline; TCP: Tranylcypromine.

(A) Gene expression analysis by RT-qPCR and Western blot examining the expression of recombinant FLAG-Lsd1 in F9 ECCs 24 hr post-differentiation (48 hr post-transfection). The C_t values are normalized to *Gapdh* and represented relative to expression in untransfected cells (set to 1). β-Actin is used as loading control for Western blot

(B) Gene expression analysis by RT-qPCR of PpGs in F9 ECCs expressing FLAG-Lsd1. Similar to the situation with untransfected WT F9 ECCs, PpGs are partially repressed in these cells, showing no effect of recombinant Lsd1 on PpG repression.

(C) Bis-Seq analysis of DNA methylation at PpGe in F9 ECCs expressing recombinant FLAG-Lsd1 showed no gain, corresponding to no loss of H3K4me1 at these sites. Data are an average and SEM of two biological replicates.

(D) Bright field microscopy of ESCs and ECCs differentiated for 4 days in the presence of the Lsd1 inhibitors Prg or TCP. 80-90% cell death is observed in ESCs. Lsd1 inhibitors have no effect on F9 ECC differentiation as shown by a normal morphology of embryoid bodies. Scale bar is 100 μm.

(E) Gene expression analysis of PpGs by RT-qPCR in differentiating F9 ECCs untreated or treated with Prg and TCP. A slight derepression of PpGs was observed in inhibitor treated cells post-differentiation. Gene expression was normalized to *Gapdh* and represented as relative change to gene expression in undifferentiated (dotted line). (F) Undifferentiated F9 ECCs were transfected with FLAG-Lsd1 and cultured for 72 hr. H3K4me1 enrichment was determined using ChIP-qPCR. No change in H3K4me1 levels was observed compared to nontransfected (UT) cells.

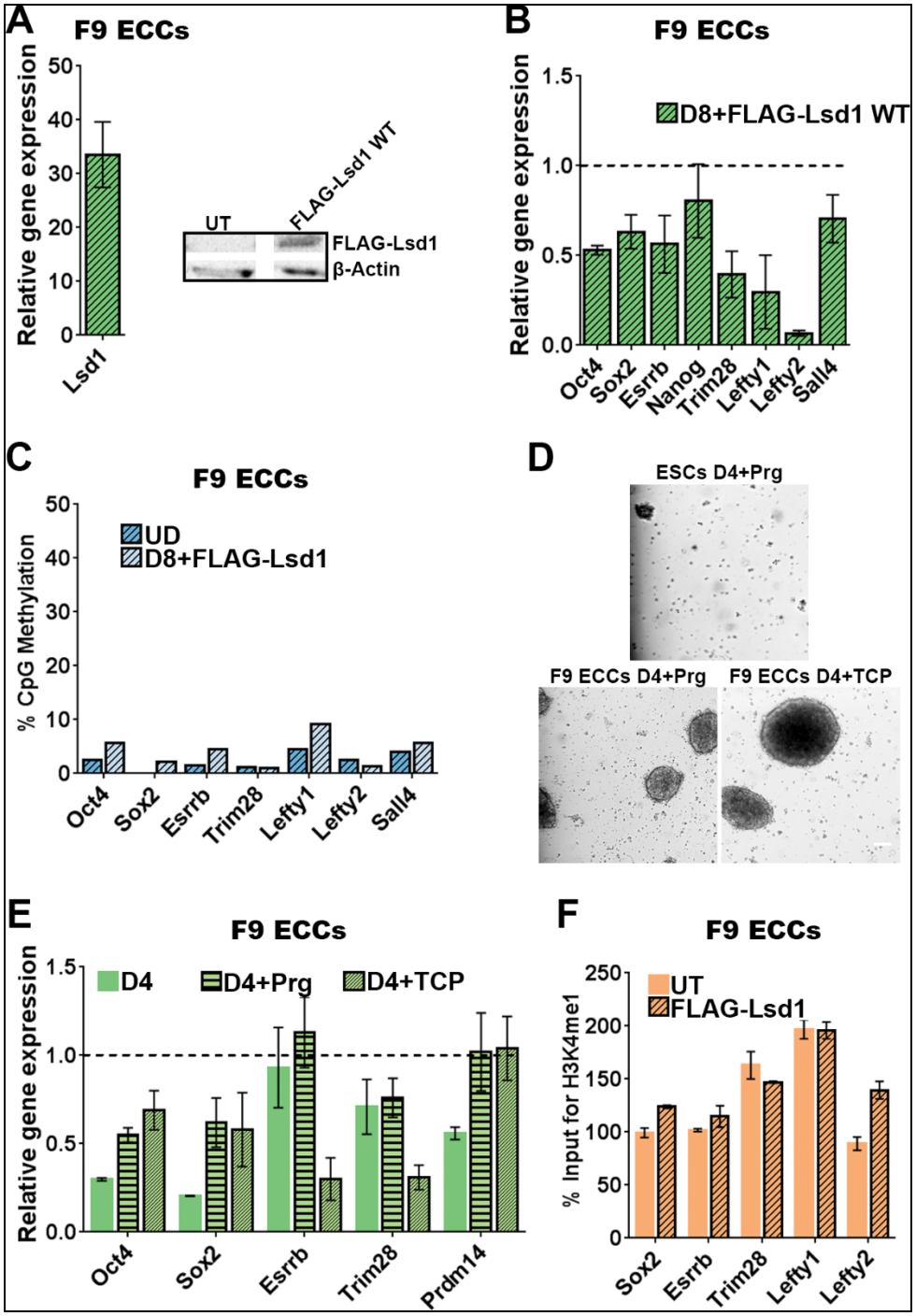
A
F9 ECCs
Relative gene expression
50
40
30
20
10
0
Lsd1
UT
FLAG-Lsd1 WT
FLAG-Lsd1
β-Actin
B
F9 ECCs
Relative gene expression
1.5
1.0
0.5
0.0
D8+FLAG-Lsd1 WT
Oct4
Sox2
Esrrb
Nanog
Trim28
Lefty1
Lefty2
Sall4
C
F9 ECCs
% CpG Methylation
50
40
30
20
10
0
UD
D8+FLAG-Lsd1
Oct4
Sox2
Esrrb
Trim28
Lefty1
Lefty2
Sall4
D
ESCs D4+Prg
F9 ECCs D4+Prg
F9 ECCs D4+TCP
E
F9 ECCs
Relative gene expression
1.5
1.0
0.5
0.0
D4
D4+Prg
D4+TCP
Oct4
Sox2
Esrrb
Trim28
Prdm14
F
F9 ECCs
% Input for H3K4me1
250
200
150
100
50
0
UT
FLAG-Lsd1
Sox2
Esrrb
Trim28
Lefty1
Lefty2

2.5.4 High throughput analysis of changes in H3K4me1 at PpGe

To identify and enumerate PpGe with aberrant retention of H3K4me1 post-differentiation, we performed ChIP-Seq analysis of H3K4me1 genome-wide in undifferentiated and D4 differentiated F9 ECCs. Peak calling was performed using Epic2 for each input-ChIP pair and the list was filtered to calculate the number of peaks with cut off (FDR<=0.05 and Log2FC>=2) (Figure 2.9A). We analyzed the distribution of H3K4me1 peaks at the regulatory elements across the genome (Figure 2.9B). For further analysis, we identified 1425 H3K4me1 peaks found within 1 kbp of PpGe previously annotated in ESCs (179). The difference in peak enrichment (i.e. log2FoldChange) between differentiated and undifferentiated was calculated to score for changes in H3K4me1 post-differentiation. The data showed no change, increase, or decrease in 733, 510, and 182 PpGe, respectively. Therefore, 87% of PpGe showed no significant decrease in H3K4me1 (no decrease in histone methylation; NDHM PpGe) (Figure 2.8A). We next computed the correlation between the three PpGe sub-groups and the 1792 PpGe that undergo H3K4me1 demethylation in differentiating ESCs (179). The data showed that a significant fraction of NDHM PpGe, which exhibit an increase (74%) or no change (69%) in H3K4me1 in F9 ECCs, overlap with PpGe that are H3K4me1 demethylated in ESCs (Figures 2.8B, C, and 2.9C). These observations strongly support our previous conclusion that in F9 ECCs, Lsd1 activity is inhibited leading to retention of H3K4me1 at PpGe. IPA of NDHM PpGe–associated genes showed highest enrichment for Oct3/4-regulated and stem cell pathways. Comparatively, genes associated with PpGe that undergo H3K4me1 demethylation, show enrichment for signaling pathways (Figures 2.8D and 2.9D). A correlation between NCDM and NCHM PpGe showed that 65% of the NDHM PpGe fail to acquire DNA methylation, underpinning the role of histone demethylation in the regulation of DNA methylation at PpGe (Figure 2.8E) (102).

Figure 2.8 Retention of H3K4me1 at most pluripotency gene enhancers in F9 ECCs post-differentiation.

ESCs: embryonic stem cells and F9 ECCs: F9 embryonal carcinoma cells; PpGe: pluripotency gene enhancers; D4: Days post-induction of differentiation

Genome-wide H3K4me1 levels in F9 ECCs pre- and post-differentiation were measured by ChIP-Seq. Peak calling was performed using Epic2 for each input-ChIP pair. 1425 H3K4me1 peaks were identified in F9 ECCs within 1 kbp of previously annotated PpGe in ESCs (179). See also Figure S5A. Histone demethylation activity of Lsd1 was surmised by calculating the change in H3K4me1 peak enrichment at PpGe between D4 differentiated and undifferentiated samples.

(A) Waterfall plot represents changes in H3K4me1, which were calculated as the difference between log2FC of D4 and undifferentiated samples, and transformed to Z-score. Z-score thresholds of +1 and -1 were used to define the fractions showing increase, no change, or decrease in H3K4me1 shown in the pie chart. Taken together, 87% PpGe show an increase or no change (NDCM) in H3K4me1 enrichment.

(B, C) Venn diagram showing an overlap between PpGe that show (B) an increase, or (C) no change in peak enrichment in F9 ECCs but undergo histone H3K4me1 demethylation in ESCs post-differentiation (179).

(D) Top ten statistically significant enriched canonical pathways amongst the genes associated with increase and no change in F9 ECCs. The x-axis shows the log10 (adjusted p-value), with the p-value adjusted for multiple testing using the Benjamini-Hochberg method.

(E) Overlap between the PpGe showing no change in DNA methylation (NDHM) and PpGe that show no decrease in H3K4me1 *(NCDM).*

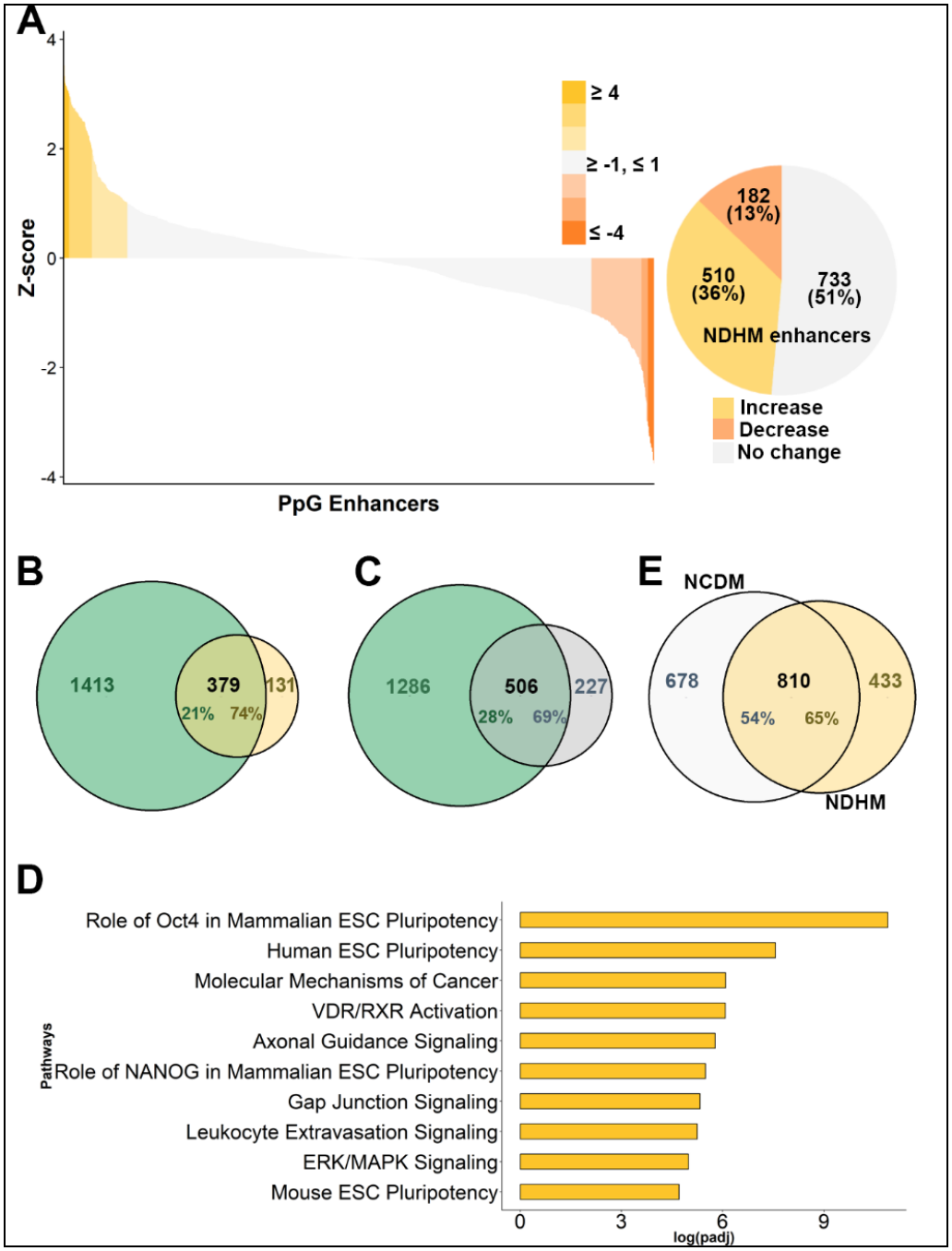
A
4
2
0
-2
-4
Z-score
PpG Enhancers
≥ 4
≥ -1, ≤ 1
≤ -4
182
(13%)
510
(36%)
733
(51%)
NDHM enhancers
Increase
Decrease
No change
B
1413
379
131
21%
74%
C
1286
506
227
28%
69%
E
NCDM
678
810
433
54%
65%
NDHM
D
Role of Oct4 in Mammalian ESC Pluripotency
Human ESC Pluripotency
Molecular Mechanisms of Cancer
VDR/RXR Activation
Axonal Guidance Signaling
Role of NANOG in Mammalian ESC Pluripotency
Gap Junction Signaling
Leukocyte Extravasation Signaling
ERK/MAPK Signaling
Mouse ESC Pluripotency
Pathways
0
3
6
9
log(padj)

Figure 2.9 Distribution of H3K4me1 ChIP-Seq peaks.

(A) Summary of the overlapping LSD1 bound sites between H3K4me1 peaks in F9 ECCs and ESCs (179). To determine correct overlap, Whyte et al. peak coordinates were converted from mm8 to mm10 using CrossMap tool (227).

(B) Fractional distribution of H3K4me1 peaks in undifferentiated and differentiated F9 ECCs throughout the genome.

(C) Overlap of the sites that show decrease in H3K4me1 post-differentiation in ESCs (179), and F9 ECCs.

(D) Top ten most statistically significant enriched canonical pathways amongst the genes associated with decrease in F9 ECCs.

A

With mm10 converted coordinates			
Sample	Epic2_peaks	LSD1 Bound	
		Single peak nearest to the gene	Within 1KB of Whyte et al Peaks
F9-undifferentiated-H3K4me1	25,382	1,837	965
F9-D4 differentiated-H3K4me1	44,237	2,002	1,103

B

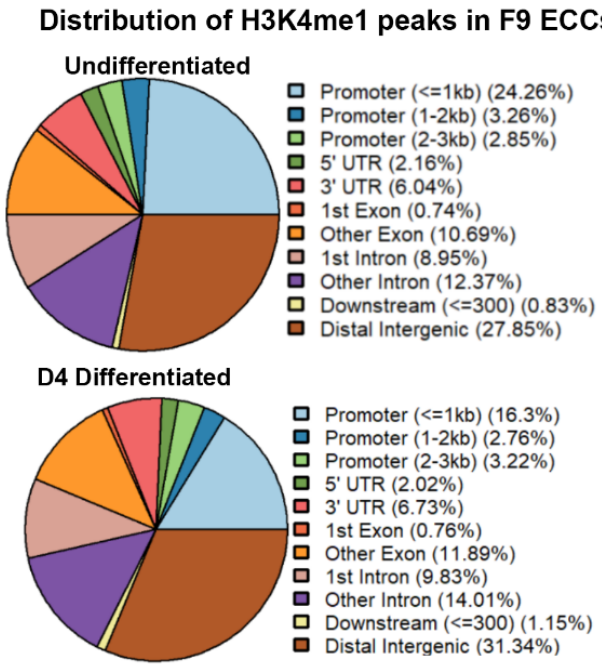

C

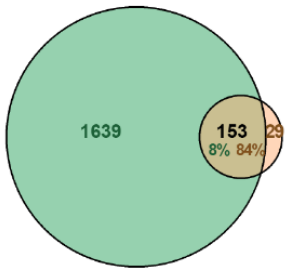

D

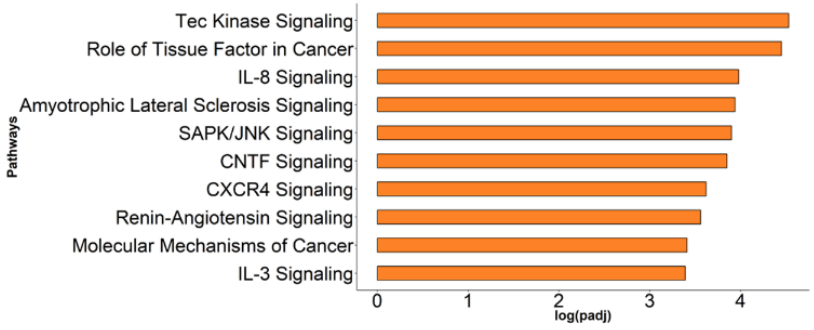

2.5.5 Lsd1 activity at PpGe is inhibited by its interaction with Oct3/4

Next, we sought to determine the mechanism that inhibits Lsd1 activity. Due to its continued expression in F9 ECCs post-differentiation, we assumed that Oct3/4 remains associated with PpGe, preventing the demethylation of H3K4me1. We tested this hypothesis in P19 ECCs in which Oct3/4 expression was reported to be strongly repressed post-differentiation (228). After confirming a 90% reduction in Oct3/4 expression (Figure 2.10A), we probed H3K4me1 demethylation at PpGe during P19 ECC differentiation. Indeed, our data show decreased enrichment of H3K4me1 at PpGe 4 days post-differentiation (Figure 2.10B). Similar to ESCs, we also observed a massive cell death when P19 ECCs were exposed to the Lsd1 inhibitor during differentiation (Figure 2.12A). The change in the chromatin state was accompanied by a 40% gain of DNA methylation at these sites (Figure 2.10C).

This observation, together with the IPA showing enrichment of Oct3/4-regulated genes in NCHM and NCDM enhancers, suggested that Oct3/4 might regulate the demethylase activity of Lsd1 at PpGe. Co-precipitation experiments using recombinant proteins, GST-Lsd1 and Oct3/4, confirmed a direct interaction between Oct3/4 and Lsd1 (Figure 2.11A). This report is concurrent with previous ones suggesting that Oct3/4 interacts with Lsd1 and the Mi2/NuRD complex in ESCs (161, 162). To test the effect of Oct3/4 interaction on Lsd1 catalytic activity, we performed *in vitro* Lsd1 demethylation assays using H3K4me2 peptide as a substrate. Our data showed that in the presence of Oct3/4, Lsd1 activity was reduced by 60-70% in a dose dependent manner. This reduction in activity was not observed in the presence of recombinant Dnmt3a protein (Figures 2.11B and C). We also performed Lsd1 demethylation assays using purified histones as a substrate and detected H3K4me2 demethylation on a Western blot. The data clearly show reduced H3K4me2 signal in presence of Lsd1, which was rescued in the presence of 0.1 mM TCP. An accumulation of H3K4me2 signal with an increase in Oct3/4 concentration in the reaction mix clearly showed increased inhibition of Lsd1 activity by Oct3/4 (Figure 2.11D). These data suggest that in F9 ECCs, due to its continued expression post-differentiation, Oct3/4 remains bound at PpGe and inhibit Lsd1. We tested this prediction directly by stably expressing recombinant Oct3/4 in P19 ECCs (Figure 2.12B). Following differentiation of Oct3/4-expressing P19 cells, examination of H3K4me1 showed retention of this mark at PpGe, indicating the inhibition of Lsd1 by recombinant Oct3/4 (Figure 2.11E). This inhibition was accompanied by derepression of

several PpGs and reduced gain in DNA methylation at their respective enhancers (Figures 2.11F and G).

Taken together we propose the following model to explain the regulation of Lsd1 activity at PpGe. At the active PpGe, Lsd1 activity is inhibited by its interaction with bound Oct3/4. Post-differentiation, this inhibition is relieved by dissociation of Oct3/4 from its binding sites. However, in cancer cells where Oct3/4 expression is maintained, Lsd1 is held in its inhibited state, leading to incomplete demethylation. Retention of H3K4me1 in turn blocks the activation of Dnmt3a from its autoinhibited state, resulting in an absence of DNA methylation at PpGe. The absence of DNA methylation and the presence of H3K4me1 convert these enhancers to a "primed" state, prone to activation in the presence of a coactivator (Figure 2.13). Based on previous reports that Oct3/4 as well as Lsd1 are aberrantly expressed in several cancers (229-235), Oct3/4-Lsd1 interaction could mistarget Lsd1 activity, leading to aberrant gene expression.

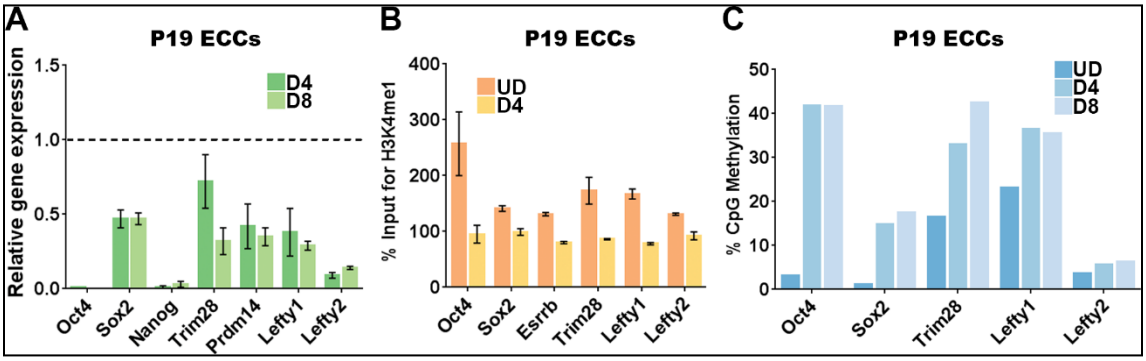

Figure 2.10 PpGe are decommissioned in differentiating P19 ECCs.

UD: undifferentiated; D4, D8: Days post-induction of differentiation; P19 ECCs: P19 embryonal carcinoma cells, PpGs: pluripotency genes; PpGe: Pluripotency gene enhancers.

(A) Gene expression analysis by RT-qPCR of PpGs in P19 ECCs: The C_t values for each gene were normalized to *Gapdh* and expression is shown relative to that in undifferentiated cells (dotted line). Similar to the repression of PpGs in ESCs (Figure 1A), PpGs, especially *Oct3*/4 and *Nanog*, show more than 90% reduction in expression.

(B) ChIP-qPCR showing H3K4me1 enrichment in UD and D4 differentiated P19 ECCs. A decrease in H3K4me1 was observed at all PpGe post-differentiation, showing histone demethylation activity.

(C) DNA methylation analysis of PpGe using Bis-Seq in UD, D4, and D8 differentiated P19 ECCs. A 40% increase in DNA methylation level was observed at PpGe post-differentiation. Average and SEM of two biological replicates are shown for each gene.

Figure 2.11 Oct3/4 directly interacts with Lsd1 and inhibits its catalytic activity.

TCP: tranylcypromine; ECCs: embryonal carcinoma cells; PpGe: pluripotency gene enhancers D4: Days post-induction of differentiation.

(A) GST-pull down experiment showing direct interaction between Lsd1 and Oct3/4. Recombinant GST-Lsd1 was incubated with Oct3/4 at about 1:2 molar ratio and precipitated using GST-Sepharose. The co-precipitated Oct3/4 is detected using anti-Oct3/4 antibody.

(B) Lsd1 demethylase assay was performed using 0.25μM of Lsd1 and H3K4me2 peptide as substrate. Lsd1 demethylation activity was completely inhibited by 0.1 mM TCP (tranylcypromine) in the reaction. To test the effect of Oct3/4 on Lsd1 activity, demethylation assays were performed in the presence of 0.5 μM Oct3/4 at 1:2 (Lsd1:Oct3/4) molar ratio. The catalytic domain of Dnmt3a at the same molar ratio was used as a control.

(C) Dose dependent inhibition assays were performed using increasing concentrations of Oct3/4 in the following molar ratios of Lsd1:Oct3/4, (1:0.5), (1:1), (1:2), (1:3), (1:4). Data are an average and SD of at least 5 experimental replicates.

(D) Lsd1 demethylation assays were performed using 0.25 μM of Lsd1 and 30 μg bulk histones as substrate with increasing concentrations of Oct3/4 in the reaction. Upper Panel: Histone demethylation was detected by using anti H3K4me2 on Western blot showing a retention of signal in presence of increasing concentration of Oct3/4. Lower panels: Amount of Lsd1 enzyme and increasing amounts of Oct3/4 in the histone demethylation reaction. Ponceau S stain of bulk histones shows equal loading on the gel.

(E) ChIP-qPCR showing percent enrichment of H3K4me1 at PpGe in P19 ECCs stably expressing recombinant Myc-Oct3/4 pre- and post-differentiation. The data show retention of H3K4me1 post-differentiation.

(F) Gene expression analysis by RT-qPCR of PpGs in P19 ECCs expressing recombinant Myc-Oct3/4. The C_t values were normalized to Gapdh and expression is shown relative to that in undifferentiated cells (dotted line).

(G) DNA methylation analysis of PpGe using Bis-Seq in UD and D4 differentiated P19 ECCs WT and expressing recombinant Myc-Oct3/4. Oct3/4 expressing cells show failure to gain DNA methylation at PpGe post-differentiation compared to untransfected WT. Average and SEM of two biological replicates are shown.

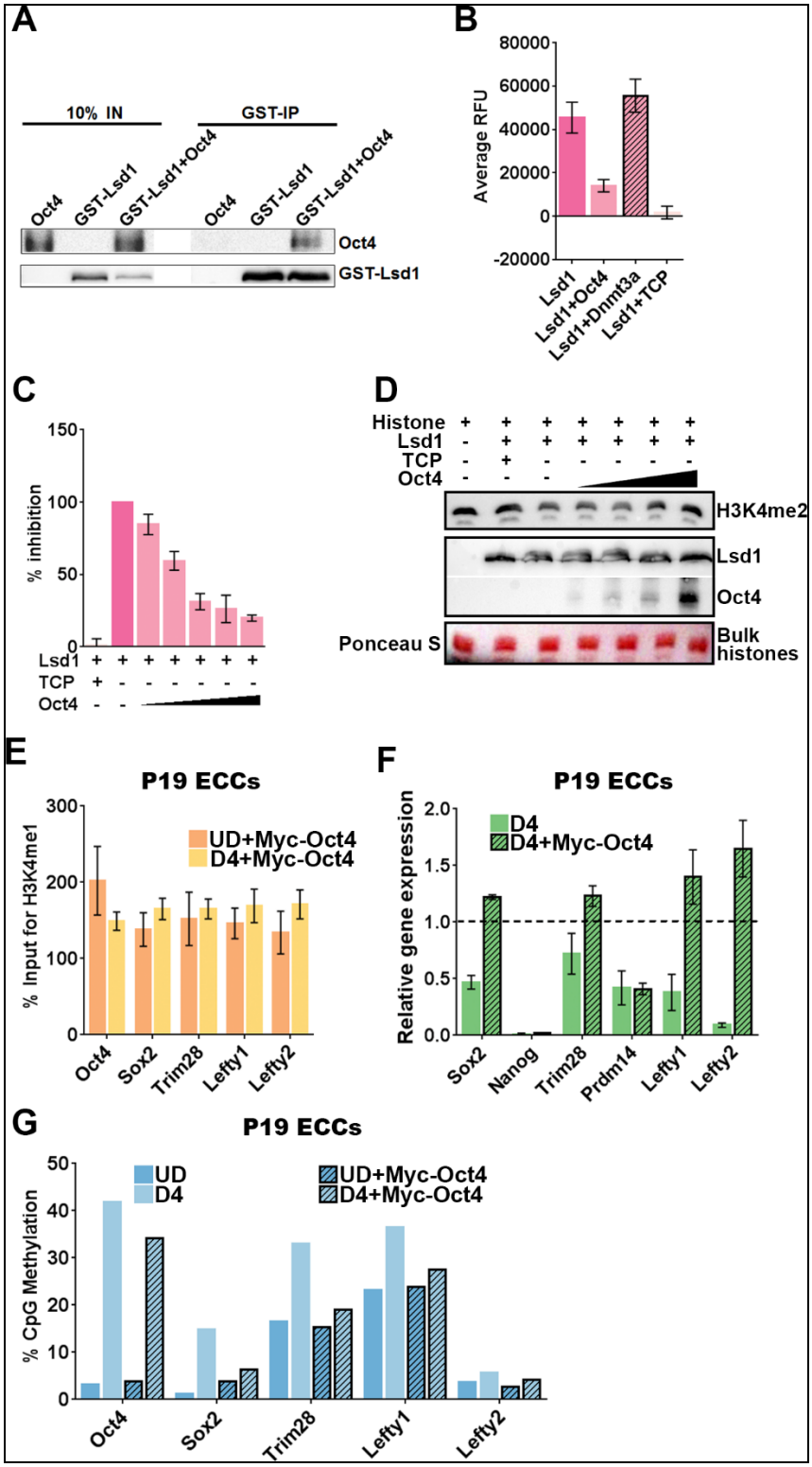
A
10% IN
GST-IP
Oct4
GST-Lsd1
GST-Lsd1+Oct4
Oct4
GST-Lsd1
GST-Lsd1+Oct4
Oct4
GST-Lsd1
B
Average RFU
80000
60000
40000
20000
0
-20000
Lsd1
Lsd1+Oct4
Lsd1+Dnmt3a
Lsd1+TCP
C
% inhibition
150
100
50
0
Lsd1 + + + + + + +
TCP + - - - - - -
Oct4 - - ▲
D
Histone + + + + + + +
Lsd1 - + + + + + +
TCP - + - - - - -
Oct4 - - - ▲
H3K4me2
Lsd1
Oct4
Ponceau S
Bulk histones
E
P19 ECCs
% Input for H3K4me1
300
200
100
0
UD+Myc-Oct4
D4+Myc-Oct4
Oct4
Sox2
Trim28
Lefty1
Lefty2
F
P19 ECCs
Relative gene expression
2.0
1.5
1.0
0.5
0.0
D4
D4+Myc-Oct4
Sox2
Nanog
Trim28
Prdm14
Lefty1
Lefty2
G
P19 ECCs
% CpG Methylation
50
40
30
20
10
0
UD
D4
UD+Myc-Oct4
D4+Myc-Oct4
Oct4
Sox2
Trim28
Lefty1
Lefty2

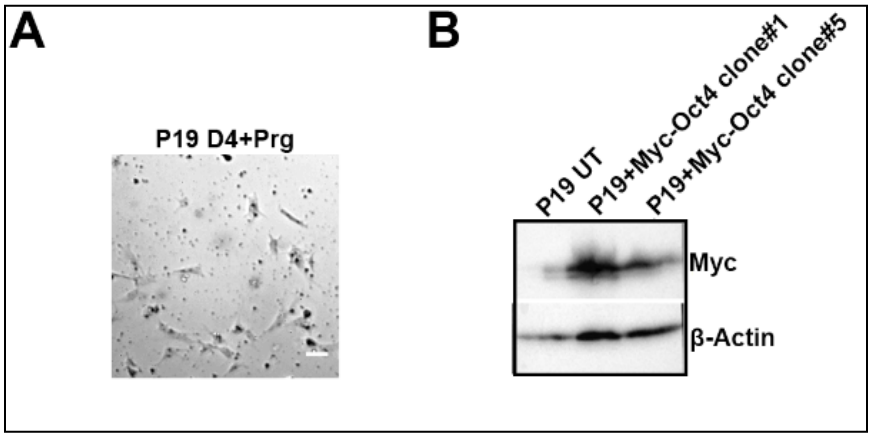

Figure 2.12 P19 ECCs are sensitive to Lsd1 inhibitor.

D4: Days post-induction of differentiation; Prg: pargyline; UT: untransfected control.

(A) Bright field microscopy of P19 ECCs differentiated for 4 days in presence of Lsd1 inhibitor, Prg. 80-90% cell death is observed in P19 ECCs indicating that Lsd1 activity at PpGe is required for differentiation. Scale bar is 100 μm.

(C) Expression analysis by Western blot confirming recombinant Myc-Oct3/4 overexpression in two independent clones of P19 ECCs. β-Actin is used as loading control for Western blot. Oct3/4 directly interacts with Lsd1 and inhibits its catalytic activity.

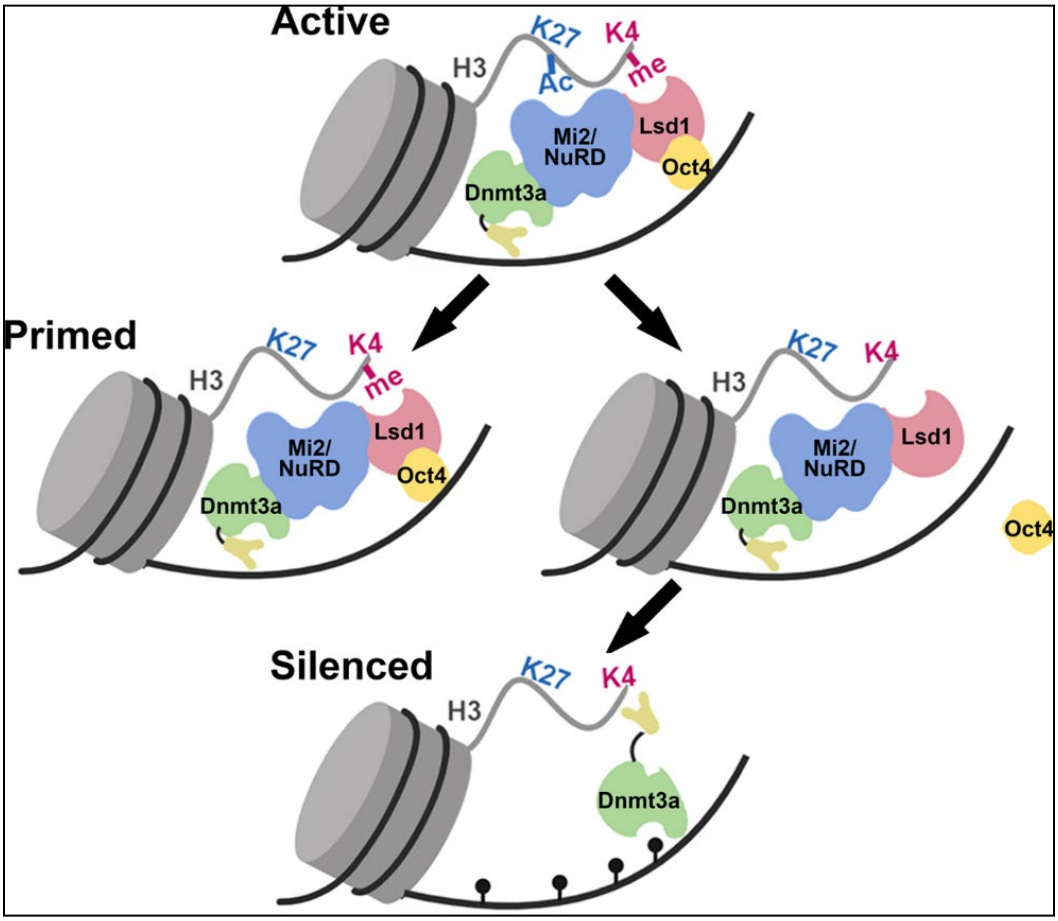

Figure 2.13 Model of epigenetic state at PpGe in F9 ECCs during differentiation.

In an undifferentiated state, the PpGe are active, bound by the coactivator complex and containing chromatin modifications including H3K4m2/1 and H3K27Ac. In response to signal of differentiation, the dissociation of the coactivator complex including Oct3/4 is followed by the activity of the Lsd1-Mi2/NuRD complex, which facilitates enhancer silencing. The histone deacetylase (HDAC) removes H3K27Ac at PpGe, and Lsd1 demethylates H3K4me1, followed by DNA methylation by Dnmt3a. However, in F9 ECCs, Lsd1 activity is inhibited in the presence of Oct3/4, causing retention of H3K4me1. The ADD domain of Dnmt3a cannot interact with H3K4 methylated histone tail and will potentially remain in the autoinhibited state, thus preventing DNA methylation at these sites. Consequently, PpGe instead of being silenced acquire a “primed” state. Black pins represent methylated CpGs.

2.6 Discussion

The preservation of the epigenetic state of enhancers in various cell types indicates that aberrant changes could promote tumorigenesis, which is supported by recent studies revealing a crucial role for enhancer-mediated activation of oncogenes (236-240). Changes in H3K4me1 levels and DNA accessibility at various enhancers have been reported to many cancers (241). Some studies also propose a role for changes in enhancer states in therapy resistance of cancer cells. These studies showed loss or gain of H3K4me1/2 at the enhancers in resistant breast cancer cells and loss of H3K27 acetylation at enhancers in T cell acute lymphoblastic leukemia (T-ALL) (242, 243). In addition, DNA hypermethylation concomitant with overexpression of DNA methyltransferases is a hallmark of many cancers (115, 218). Changes in DNA methylation at enhancers occur in breast, lung, prostate, and cervical cancers (225, 244-246). These studies suggest that the chromatin state of enhancers can be used as a diagnostic to predict aberrant expression of tissue-specific genes in cancer. Our data showing a congruous response of PpGe to signals of differentiation in ESCs supports this prediction. During ESC differentiation, all tested PpGe undergo histone deacetylation and a gain of DNA methylation, irrespective of the transcriptional status of the associated gene. This observation is exemplified by H3K27Ac deacetylation and gain of DNA methylation at Sox2 and Trim28 enhancers despite the maintained expression of these genes.

Our study reveals a mechanism by which developmental enhancers could acquire aberrant histone modification and DNA methylation states that affect gene expression. We show in F9 ECCs compromised activity of the histone demethylase, Lsd1, results in the retention of H3K4me1 and the absence of DNA methylation at the PpGe, leading to a primed state of enhancers. Unlike the silenced state, the “primed” enhancer state grants accessibility for coactivator binding which renders cells highly vulnerable to a small increase in the expression of oncogenic coactivators or master transcription factors (58, 247).

We discovered that Lsd1 activity is inhibited by its interaction with the pioneer transcription factor Oct3/4, which is expressed at a substantial level in F9 ECCs post-differentiation. Recently, a similar observation was reported from flow-cytometric analysis showing that compared to ESCs, a significantly higher number of F9 ECCs have persistent Oct3/4 expression post-differentiation (248). Aberrant expression of Oct3/4, Sox2, and Nanog is

associated with tumor transformation, metastasis, and drug resistance (190, 249). We speculate that during differentiation of cancer stem cells, inhibition of Lsd1 by Oct3/4 leads to PpGe priming/reactivation, which enhances PpG expression. Our studies further highlight the versatility of Lsd1 binding and activity, which can be fine-tuned by its interaction with numerous factors, allowing the enzyme to function in various cellular processes including differentiation and disease.

CHAPTER 3. TRANSITION STATE COVALENT CROSSLINKING OF DNMT3A TO IDENTIFY ITS DIRECT TARGETS GENOME-WIDE

Lama AlAbdi, Nicole Adkins, James Breedlove, and Humaira Gowher

3.1 Declaration of collaborative work

Dr. Humaira Gowher and Lama AlAbdi designed experiments.
Lama AlAbdi, Nicole Adkins, and James A. Breedlove performed experiments.
Nicole Adkins performed screening experiments for FLAG-Dnmt3a expressing cell lines.
James A. Breedlove developed Dot blots and prepared buffers.
All other experiments were performed by Lama AlAbdi.

3.2 Abstract

DNA methylation is an epigenetic modification necessary for stable gene repression. In mammals, it is catalyzed by DNA methyltransferases Dnmt1, Dnmt3a, and Dnmt3b. Current methodologies, which determine the distribution of DNA methylation in genomes, show the results of combined activities of multiple Dnmts at their target sites. To examine the activity of a particular Dnmt in response to an external stimulus, we developed a method, Transition State Covalent Crosslinking DNA Immunoprecipitation (TSCC-DIP), which traps catalytically active Dnmts in their transition state with the DNA substrate. The strength of our method lies in its ability to determine the direct genomic targets of specific Dnmts. Once fully developed, TSCC-DIP will be a valuable tool for studying the specific functions of Dnmts in establishing and maintaining the dynamic changes in DNA methylation during static or kinetic biological states.

3.3 Introduction

In mammals, DNA methylation involves the covalent deposition of a methyl group at the C5 position of cytosine bases. This chemical reaction is catalyzed by a group of enzymes called DNA methyltransferases (Dnmts) (118, 250-252). These enzymes are subdivided into two families based on their substrate preference: Dnmt1 is a maintenance methyltransferase with high affinity for hemi-methylated DNA. Dnmt1 is responsible for conserving methylation patterns during DNA

replication and untimely demethylation events (253). The *de novo* DNA methyltransferases Dnmt3a and Dnmt3b, together with their inactive homolog Dnmt3l, establish the genomic methylation patterns during early embryogenesis and cell fate decisions (252). As DNA methylation at regulatory elements is strongly associated with gene repression, deposition of this epigenetic mark is necessary for fine-tuning gene expression, especially in early developmental stages (96). Numerous studies have reported observations of altered DNA methylation patterns in many cancers (244, 245), suggesting a critical role in tumor initiation and/or progression.

Functional redundancy among the different Dnmts is reflected by their high sequence similarities (254). However, specific targets for Dnmts have also been reported (104, 255). The activity of Dnmts is regulated via posttranslational modifications or interactions with other proteins (256). The active *de novo* DNA methyltransferases, Dnmt3a and Dnmt3b, have been reported to associate with TFs and epigenetic effectors that modulate their activities. For example, Dnmt3a can be targeted to specific genomic loci by interacting with TFs such as c-Myc, p53, and RP58 (257-259). Dnmt3s can also be recruited through interacting with epigenetic modifiers such as HP1, G9a, Suv39h1, and HDACs to promote a repressive chromatin environment (260-266). Furthermore, Dnmts have specialized domains that direct these enzymes to certain genomic regions via histone-Dnmt interactions (104, 126, 267-269). Many studies have also reported on the mechanisms regulating Dnmt3 catalytic activity. Such mechanisms include auto-inhibition and enhanced activation by homo- or hetero-dimerization/-oligomerization (101, 126, 267, 268, 270).

Given the complexity of Dnmt regulation and biological functions, there is a need to understand the relationship between mechanisms regulating gene expression and the dynamic changes in DNA methylation in the context of a static or kinetic cellular state(s). To answer some of the questions addressing the functional relationship between DNA methylation and transcriptional regulation, it is important to tackle some technical limitations associated with the strategies used to address them. The gold standard assays in the field rely on either conventional (nonspecific) chemical crosslinking or harsh chemical conversion. To examine Dnmt occupancy profiles, chemical crosslinking and chromatin immunoprecipitation are usually the methods of choice (271). However, these approaches often lead to epitope masking as well as nonspecific association of Dnmts to genomic regions due to protein-protein interactions. These techniques usually suffer from high noise to signal ratio and false positive associations (272). Bisulfite conversion followed by sequencing is usually used to analyze DNA methylation levels (273). In

determining DNA methylation patterns, valuable information is lost because this approach sums the total methylation outcome of all Dnmts expressed in the biological sample analyzed.

We developed a new method to investigate DNA methylation that relies on capturing a Dnmt in its transition state by covalently crosslinking it to DNA during catalysis. This method, termed Transition State Covalent Crosslinking followed by DNA Immunoprecipitation (TSCC-DIP), will provide single-base resolution of specific genomic targets of Dnmts captured during their activity. Our approach is built on previous protocols such as the Rapid Assay of the DNA Adduct Response (RADAR), in which transient intermediates are trapped by drug treatments (274). We used a drug that specifically inhibited active Dnmts. These enzymes are trapped in the intermediate state and thus selectively chemically cross-linked. To capture Dnmts, we treated the cells with 5-Aza-2′-deoxycytidine (5-Aza-dC). This suicide-inhibitor is a 2′-deoxycytidine analog which undergoes random incorporation into the genome during replication (275). When a Dnmt is recruited to methylate 5-Aza-dC at a genomic locus, a stable transient intermediate is formed (163, 276). Proteins that are part of the DNA-Dnmt adducts are then immunoprecipitated and the DNA sequenced to identify the sites subjected to Dnmt catalysis.

To this end, we chose embryonic stem cells (ESCs) that express FLAG-Dnmt3a as a proof of concept model. The cells were treated with 50 μM 5-Aza-dC for 8 hr before collection. Next, gDNA was isolated using a RADAR lysis buffer, which preserves DNA-protein adducts while removing unbound Dnmts, thus ensuring specificity and sensitivity. Using dot blot assays, our data showed that we were able to enrich for Dnmt3a-DNA adducts in the 5-Aza-dC treated samples. We further demonstrated that this adduct can be immunoprecipitated and sequenced. To examine specific Dnmt functions in a dynamic state as the cells are undergoing fate decisions in response to stimuli, we standardized a protocol to differentiate ESCs as a monolayer. Our data provided evidence for the robustness of our differentiation protocol and demonstrated that PpG enhancers gained DNA methylation concomitant with their transcriptional repression. Dot blot assays provided evidence for 5-Aza-dC incorporation and Dnmt3a capture during the different stages of differentiation. Once completely developed, this method will provide a valuable tool for studying the dynamic changes in DNA methylation in any biological process.

3.4 Materials and Methods

3.4.1 Cell culture and drug treatments

E14tg2a embryonic stem cells (ESCs) grown on gelatinized dishes in the presence of leukemia inhibitory factor (LIF) as previously described, were co-transfected with pCAG-3XFLAG-Dnmt3a-GFP and HSC1-GiP (Addgene 58254) (102). Clonal expansions were screened using anti-FLAG antibody and the transgenic cell line with the highest expression of FLAG-Dnmt3a was selected. A sister cell line with puromycin (puro) resistance but lacking FLAG-Dnmt3a expression was used as a control. Cells were grown to 80% confluency and treated with 50 μM 5-Aza-2′-deoxycytidine (Millipore, 189825) for 8 hr (or as indicated) at 37^{o}C and 5% CO_2.

3.4.2 Genomic DNA purification

Cells were washed on the plate twice with 1XPBS and then lysed with RADAR assay buffer (1% Sacosyl, 2% IGEPAL, 10 mg/mL DTT, 20 mM EDTA, 20 mM Tris-HCl pH 8, 0.1M NaOAc, 2.5 M GTC, 4 M LiCl) (72). Genomic DNA (gDNA) was precipitated with isopropanol and resuspended in 8 mM NaOH. Samples were diluted with 1XTBS pH 7.4 and sheared using a probe sonicator with one second on and one second off for a total of five seconds at 30% amplitude.

3.4.3 Dot blot assay

Equal amounts of samples were applied to a nitrocellulose membrane under vacuum suction and washed with 1XTBST. The blot was probed with anti-FLAG 1:1000 (Sigma, F3165), anti-Dnmt3a, 1:1000 (Active Motif, 39206), anti-Dnmt1, 1:1000 (abcam, ab13537), followed by anti-Rabbit, 1:10,000 (Jackson Immunoresearch, 111-035-003) or anti-Mouse, 1:10,000 (Jackson Immunoresearch, 115-035-003 antisera). Chemiluminescence was performed according to the manufacturer's protocol (Thermo-Fisher Scientific, 34580).

3.4.4 Immunoprecipitation and sequencing

Equal amounts of sheared gDNA were incubated with Anti-FLAG G1 affinity resin (GenScript, L00432) overnight at 4^{o}C with rotation. Complexes were eluted with FLAG peptide. Samples were incubated with Proteinase K, and the DNA was purified using a standard phenol:chloroform purification followed by ethanol precipitation. Yield was quantified using a nanodrop spectrophotometer. Samples were sequenced using NGS on a Wide-Seq platform. The

reads were assembled and visualized by IGV. Bedtools was used to remove any reads that overlapped between 5-Aza-2′-deoxycytidine treated and untreated samples. Mapped reads were compared to publically available Dnmt3a ChIP-seq performed using ESCs (104) (GSM1382257_MmES).

3.4.5 Neuronal differentiation and drug treatments

E14Tg2A ESCs expressing FLAG-Dnmt3a-Puro or Puro-only cells were maintained in media containing LIF and induced to differentiate to neuronal progenitors in a monolayer culture as described (164). Briefly, 10,500 cells per cm^2 were plated in a 10 cm gelatinized plate containing N2B27 differentiation media comprised of (1:1 ratio of DMEM/F12: Neurobasal media supplemented with insulin (12.5 µg/mL), apo-transferrin (50 µg/mL), progesternone (1 ng/mL), putrescine (50 µM), sodium selenite (15 nM), bovine serum albumin (0.0025 %), 5 ml of B27 supplement, 0.2 mM L-glutamine, and 0.1 mM 2-mercaptoethanol). The medium was changed every 24 hr and cells were treated with 50 µM 5-Aza-dC for 12 hr prior to collection.

3.4.6 Expression analysis

Cell pellets collected during differentiation were resuspended in TRIzol reagent (Invitrogen, 15596026) and RNA was isolated according to the manufacturer's protocol. Samples were treated with DNAse (Roche, 04716728001) at 37°C, and then purified using Quick-RNA™ MiniPrep Plus Kit (ZymoReseach, R1057). Complementary DNA (cDNA) was synthesized using Tetro Reverse Transcriptase (Bioline, BIO-65050) with gene specific primers and 1 µg of purified RNA as per the manufacturer's instructions. Reverse-transcription quantitative PCR (RT-qPCR) was performed using the qPCR master mix EvaGreen following the manufacturer's conditions (MidSci, BEQPCR-S). Gene expression was calculated as ΔC_t which is C_t(Gene)-C_t(*β-Actin*). The change in gene expression is reported as fold change relative to that in undifferentiated cells, which was set to 1. See Table 3.1 for primers used.

3.4.7 Bisulfite conversion

Bisulfite sequencing was performed to detect changes in DNA methylation levels between undifferentiated and differentiated cells (UD, D1, D2, D3, and D4). Following bisulfite treatment using the EpiTect Fast Bisulfite Conversion Kit (Qiagen, 59802) and 1 µg of DNA as per the

manufacturer's protocol, bisulfite-converted DNA was amplified using nested primers as reported (102). Inner PCR products of each sample were purified, pooled, and sequenced using a Wide-Seq platform. The reads were mapped by Bowtie2 and analyzed by Bismark for percent DNA methylation. Percent methylation for each enhancer was computed by taking the total average of percent methylation reported for each CpG within the region. See Table 3.1 for primers used for bisulfite sequencing, and Table 3.2 for the number of reads for each sample.

3.4.8 Methylation-dependent PCR (MD-PCR)

Genomic DNA was isolated using the conventional phenol:chloroform extraction protocol followed by isopropanol precipitation. MD-PCR was performed as described in (277). gDNA was digested with *Pvu*II (for the analysis of β-globin, Pgk2, and Igf2r) or *Hind*III (for the analysis of ApoA1, and H19) either alone (denoted as Uncut) or with *Hpa*II restriction enzyme (denoted as *Hpa*II). Primers flanking the *Hpa*II cut site were used to PCR amplify 20 ng of the digested gDNA. See Table 3.1 for primers used. PCR products were then resolved on 16% TBE-PAGE gels and visualized after ethidium bromide staining.

3.4.9 Western blots

Western blotting was performed using the standard method and the following antibodies and dilutions: anti-FLAG 1:1000 (Sigma, F3165), and anti-β Actin, 1:1000 (Santa Cruz, sc8628), followed by anti-Mouse, 1:10,000 (Jackson Immunoresearch, 115-035-003). Chemiluminescence was performed according to the manufacturer's protocol (Thermo-Fisher Scientific, 34580).

Table 3.1 Primers used in this study.

For RT-qPCR:	***Primer sequence (5' to 3')***
Oct3/4 F	TCTTTCCACCAGGCCCCCGGCTC
Oct3/4 R	TGCGGGCGGACATGGGGAGATCC
Sox1 F	GCGATGCCAACTTTTGTATG
Sox1 R	AGAGGGGATTGCGGTATAAA
Sox2 F	ATGATGGAGACGGAGCTGAA
Sox2 R	TTGCTGATCTCCGAGTTGTG
B-Actin F	CTATTGGCAACGAGCGGTTC
B-Actin R	GCAGCTCAGTAACAGTCCGC
For Bis-Seq:	**Primer sequence (5' to 3')**
Sox2 out HSO3 F	AGAAAATTGAGTTATTAAGGTAGTAATTATTT
Sox2 out HSO3 R	AAACCAAAAACCTTAACTACCAAACATAA
Sox2 in HS03 F	TAAAATTTTTATAGTTTTAATTGTTAAATA
Sox2 in HSO3 R	TATTATATCTAAAACCAACTAACAATATTAT
Lefty2 out HSO3 F	TTAGAAGTTTTTGGGGGAGAGGTTTGATTTA
Lefty2 out HSO3 R	TCAAAAATCATAACTCTTCCCACACCTCAAA
Lefty2 in HSO3 F	ATAATATGAGGGAGAGGTTTAGTTTTT
Lefty2 in HSO3 R	CACCTCAAACTCTATCTACTACTAACTTTA
Esrrb out HSO3 F	TTTGGAGAGGAAATATGTTAATTTTGAATA
Esrrb out HSO3 R	AAATCAACACACAAAATTCACTAAAAAAACA
Esrrb in HSO3 F	AATAGGGATTTTTTTTGGGATAGAAAT
Esrrb in HSO3 R	ATTCACTAAAAAAAAAAAAAATCTCAAA
Lefty1 out HSO3 F	AAATAAGGAGGTAGGGGTAGAGAATATTTGA
Lefty1 out HSO3 R	AAAAAACAATCTCCCTCCCACCTAACA
Lefty1 in HSO3 F	TTTAGAGGAGAAGTTAAGTTTAGTATAGAGAATA
Lefty1 in HSO3 R	ACACCTAATCAAACCCATTATACAAAAT
Oct3/4 out HSO3 F	TAATGGGATTTTTAGATTGGGTTTAGAAAA
Oct3/4 out HSO3 R	TAACCCTAAACAAATACTCAACCCTTAAAT
Oct3/4 in HSO3 F	TTTGAGGGTTATTTTTTTGTAAAGATAA
Oct3/4 in HSO3 R	AAAAAAAATATCTAACTTCAAATTCAAA

Table 3.1 continued

For MD-PCR:	**Primer sequence (5' to 3')**
β globin F	CTTGGCAAGGATTTCACCCCCGCTGCAC
β globin R	ATAAAATGTAATCATAATGTAGTGTGTA
Pgk2 F	GGTGTAAAGATAGT
Pgk2 R	ATTTTACCTTCCAGAAGCTC
Igf2r F	AATCGCATTAAACCCTCCGAACCT
Igf2r R	TAGCACAACTCCAATTGTGCTGCG
H19 F	ATCCAGGAGGCATAAGAATTCTGCAAGG
H19 R	GGCTGTGTAGGGATGAGTCAAGTTCTC
ApoAI F	GATGGTGCAACTGCCTTA
ApoAI R	ATTCTGTTCTCTGTGCCC
Snrpn F	CCCTCTCCCACATAGTAAAAATCTGT
Snrpn R	CGTCCCAGGCAATGGCTGC

List of all gene expression, bisulfite sequencing, and MD-PCR primers used in this study separated by technique.

Table 3.2 Wide-Seq reads reported for each sample and enhancer.

Sample	*Lefty1*	*Lefty2*	*Sox2*	*Esrrb*	*Oct3/4*	***Total***
FLAG-Dnmt3a UD	12855	11779	7151	15112	4586	**51483**
FLAG-Dnmt3a D1	21179	18341	10939	14516	6598	**71573**
FLAG-Dnmt3a D2	16294	13967	8509	12492	4550	**55812**
FLAG-Dnmt3a D3	15076	13214	7466	13395	4679	**53830**
FLAG-Dnmt3a D4	16020	14984	8400	12607	4462	**56473**
Total	**81424**	**72285**	**42465**	**68122**	**24875**	**289171**

The total number of reads from a Wide-Seq run used for data presented in this study. In this table, the number of reads is presented with respect to sample as well as enhancer. The total number of reads per sample and site are also shown, as well as the total number of reads.

3.5 Results

3.5.1 Crosslinking active Dnmts during catalysis

Once transported inside the cells, 5-Aza-dC is first activated to 5-Aza-2′-deoxycytidine-triphosphate. The activated form is then randomly incorporated into the genome as a substitute for cytosine by the replication machinery (278). 5-Aza-dC, in the Aza-guanine dinucleotide pair, is flipped into the enzyme's active site as it is recognized by Dnmts as a substrate (279, 280). The acting enzyme will commence the methylation reaction by establishing a covalent bond between its catalytic cysteine residue and the C6 atom of the cytosine ring (281, 282). The covalent bond, which is normally resolved during cytosine methylation reactions, remains in place in Dnmt-Aza intermediates. This is due to the substitution of C5 by a nitrogen atom in 5-Aza-dC (Figure 3.1A). Hence, the methylation reaction is impeded and the Dnmt remains covalently linked to DNA, forming Dnmt-DNA adduct (Figure 3.1B). Due to the stability of the covalent intermediate, we sought to test the feasibility of immunoprecipitating these adducts by targeting specific Dnmts and sequencing the immunoprecipitated product (Figure 3.1C)

It is important to note that under prolonged 5-Aza-dC treatment conditions, the formed adduct obstructs DNA functionality, which in turn triggers DNA damage signaling and base-excision DNA repair. Stress induced accumulation of Dnmt-DNA adducts would then likely lead to cell death and apoptosis (283, 284).

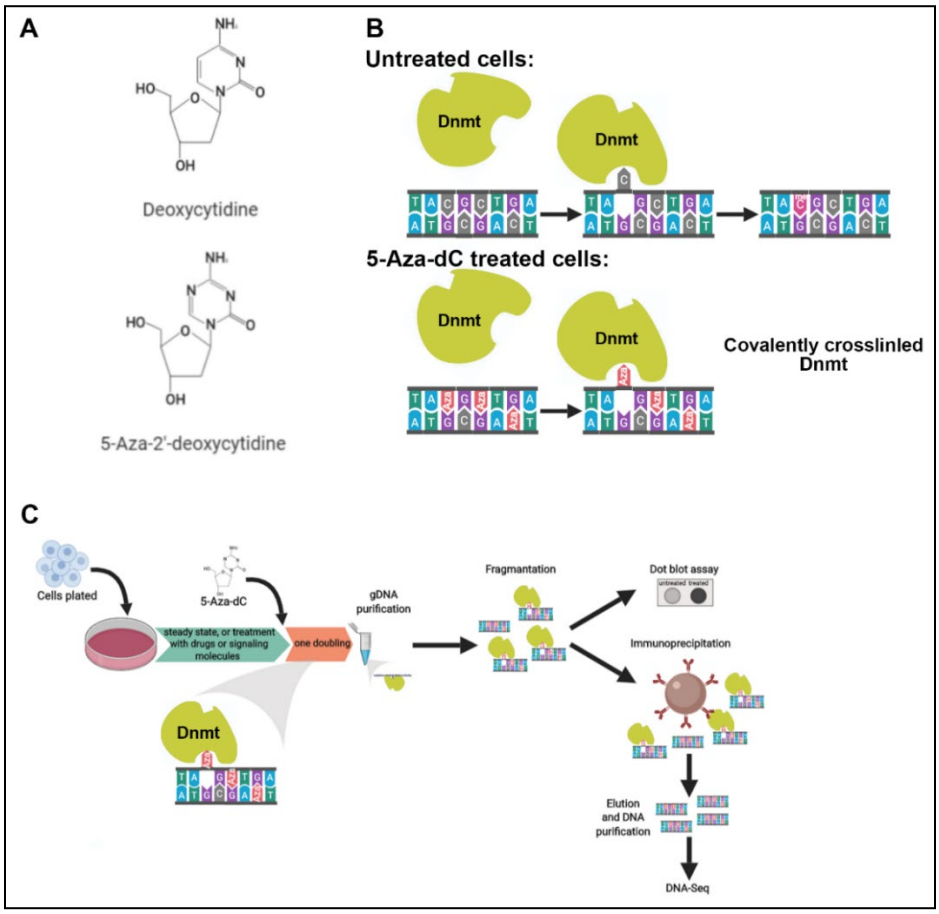

Figure 3.1 Conceptual theory behind TSCC-DIP.

(A) Comparison between the chemical structures of deoxycytidine (top) and 5-Aza-dC (bottom). The inhibitor drug 5-Aza-dC contains a nitrogen atom in place of C5 in deoxycytidine. (B) Model for adduct formation: When a Dnmt recognizes a cytosine substrate, the base is flipped into the active site making a transition intermediate. Upon the deposition of a methyl group to the C5 position of the cytosine, the product is formed following the enzyme-product release. In the case of 5-Aza-dC, the enzyme cannot complete the reaction and is fixed in the intermediate transition state. (C) Illustration detailing TSCC-DIP experimental design: plated cells are treated with a standardized amount of 5-Aza-dC. After they undergo at least one doubling, genomic DNA is harvested and extracted using RADAR lysis buffer. After gDNA fragmentation and validation of Dnmt trapping via dot blot, the Dnmt-DNA adduct can be immunoprecipitated with a Dnmt-specific antibody. A library is then constructed for the eluate to be sequenced and mapped.

3.5.2 Optimization of 5-Aza-dC treatment

In order to assess the fidelity of our strategy, we first demonstrated that stable DNA-Dnmt adducts created by treatment with 5-Aza-dC can be isolated and detected by immunoblotting. To test this hypothesis, we performed a time-course treatement with 5-Aza-dC (Figure 3.2A). We argued that this would also assist in optimizing the treatment conditions, for each Dnmt, to get maximum Dnmt capture without compromising the cells' viability due to prolonged exposure to the cytotoxic drug. Our data showed an increase in Dnmt1 and Dnmt3a enrichment over time as evaluated by dot blot assay. The highest signal was observed at 24 hr post-treatment (Figure 3.2B and C). However, when taking into account cellular morphology and viability, we observed that starting 12 hr post-treatment there is consedrable cell death (Figure 3.2D). In order to elimintate background contributions from autophagus cells, all future experiments were performed at 8 hr after 5-Aza-dC treatement. The difference in the observed crosslinking effeciency and enrichments between Dnmt1 and Dnmt3a is potentially due to differences in their expression and/or activity in these cells.

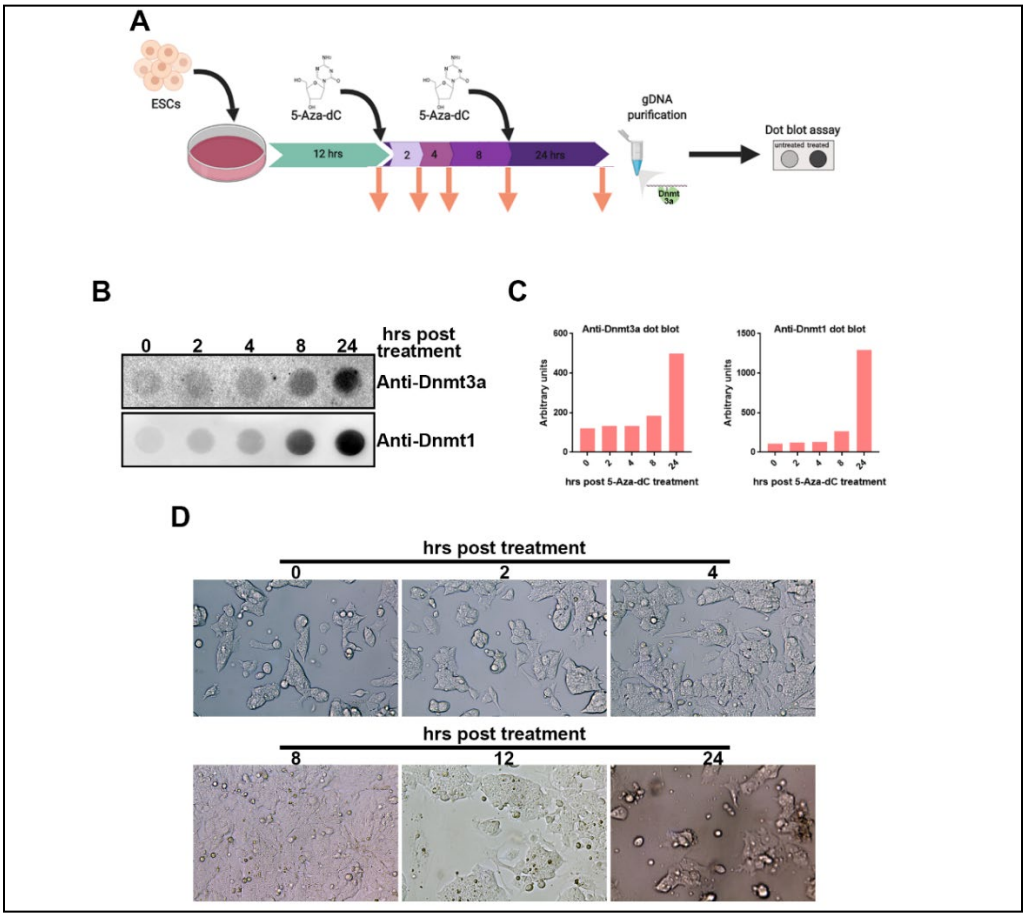

Figure 3.2 Time-course experiment for TSCC-DIP optimization.

(A) Schematic representation of the experimental design: ESCs were plated for 12 hr followed by 5-Aza-dC treatment. Genomic DNA samples were collected at different times (2, 4, 8, and 24 hr) after lysing the cells using the RADAR lysis buffer. Equal amounts of gDNA were blotted using dot blot assays and probed with anti-Dnmt1 and anti-Dnmt3a antibodies to test for Dnmt trapping by 5-Aza-dC treatment compared to untreated control (0 hr). (B) Dot blot assays showing increase in Dnmt1 and Dnmt3a signal as a function of time (2, 4, 8, and 24 hr) after 5-Aza-dC treatment compared to an untreated control (0 hr). (C) Quantification of the signal for each time-point normalized to that of background. The highest signal observed was at 24 hr post-treatment. Analysis was performed using ImageJ. (D) Bright-field microscopy images of cells at different times post-5-Aza-dC treatment compared to untreated (0 hr) control. There is significant cell death observed at 12 and 24 hr post-treatment.

3.5.3 Dnmt3a-DNA adducts map to known Dnmt3a loci

To increase the robustness of our assay, we used two transgenic cell lines: ESCs expressing FLAG-Dnmt3a (FLAG-Dnmt3a) as well as a vector only control (EV) (Figure 3.3A). We argued that the use of a tagged Dnmt3a would increase the enrichment and effeciency of immunoprecipitated material after 5-Aza-dC treatment. To validate that FLAG-Dnmt3a expression had no effect on methylation patterns compared to the EV control, we used methylation-dependednt PCR analysis (MD-PCR). Examination of DNA methylation status at the regulatory elements of tissue specific genes (β-globin and Pgk2), imprinted regions (H19, Igf2R, and Snrpn), and the house keeping gene (ApoA1) showed no difference in methylation status between the two cell lines (Figure 3.3B). These data suggest that the overall methylation is not perturbed due to the expression of FLAG-Dnmt3a, thus enabling the direct comparision of the two cell lines.

We treated both cell lines with 5-Aza-dC for 8 hr, then blotted equal amounts of gDNA onto a nitrocellulose membrane. After probing with anti-Dnmt1 and anti-FLAG antibodies, we observed a signal enrichment for Dnmt1 and FLAG-Dnmt3a in the 5-Aza-dC treated sample compared to untreated control (Figure 3.4A and B). To assess the specificity of our assay we also blotted gDNA from EV control cells treated or untreated with 5-Aza-dC. Our data showed no signal for FLAG-Dnmt3a in the control EV cell line. These data further support our conclusion that the signal observed resulted from FLAG-Dnmt3a-DNA adducts. Because gDNA was sonicated prior to blotting, these observations also indicated that gDNA fragmentation did not disrupt the cross-linked Dnmt-DNA adducts (Figure 3.4C).

After establishing that Dnmt3a-DNA adducts were stable for immunoblotting, we asked if they were stable for immunoprecipitation. Equal amounts of sonicated DNA, from 5-Aza-dC treated and untreated samples, were incubated with anti-FLAG Sepharose resin for immunoprecipitation. After quantifying the eluates, we noted a significant enrichment in DNA amounts in the treated sample compared to the untreated control (Figure 3.4D). Eluates were sequenced using a Wide-Seq platform, which generated a total number of 3,736 reads for the untreated sample, 3,388 of which mapped to the mouse genome (mm9), and 7,460 reads from 5-Aza-dC treated eluate, where 6,779 mapped to the reference genome. To determine the sites of Dnmt3a activity, we subtracted the number of reads in the untreated control from the treated

sample for each site. A site was marked as occupied by active FLAG-Dnmt3a if the number of reads after substration were more than 1.

We next compared our data to those of a previously published Dnmt3a ChIP-seq dataset performed in ESCs (104) (GSM1382257_MmES). Not only did we note a significant overlap between the two datasets, there was also higher signal/noise ratio using our capture method when compared to the conventional approach (ChIP-seq) (Figure 3.4E). Regions where Dnmt3a was detected in the ChIP-seq dataset but was either not represented in our "sites of Dnmt3a activity" or only found in our untreated control sample were annotated as sites of inactive Dnmt3a occupancy. Identifying sites of inactivity contribute to our understanding of how Dnmts are regulated by deciphering if they associate with these regions because they are primed for activity or as part of other chromatin modifying complexes (if not both).

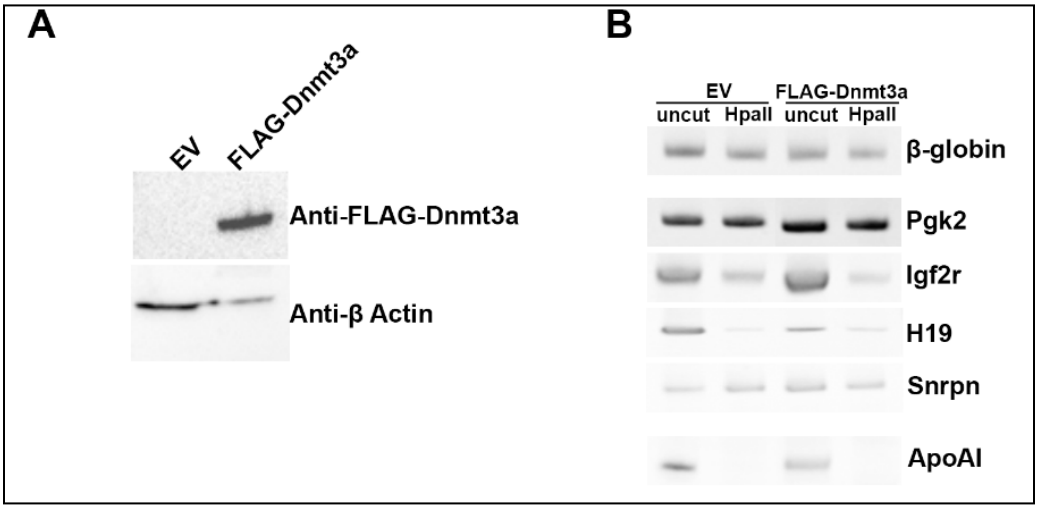

Figure 3.3 Methylome analysis of the FLAG-Dnmt3a transgenic cell line and the EV control.

(A) Western blot showing FLAG-Dnmt3a expression in the transgenic cell line. Empty vector (EV) was used as a negative control. β Actin is the loading control. (B) Methylome analysis of selected sites in ESCs expressing FLAG-Dnmt3a. Genomic DNA was digested with *Pvu*II or *Hind*III alone (uncut) or together with *Hpa*II (*Hpa*II). PCR product from amplified cleaved gDNA samples collected from FLAG-Dnmt3a and EV transgenic cell lines were loaded onto 16% TBE-PAGE gels and were stained with ethidium bromide. There is no difference in the methylation status between EV and FLAG-Dnmt3a in the regulatory elements of β-globin and Pgk2 (Tissue-specific genes), Igf2r, H19, and Snrpn (Imprinted genes), nor ApoA1 (Housekeeping gene).

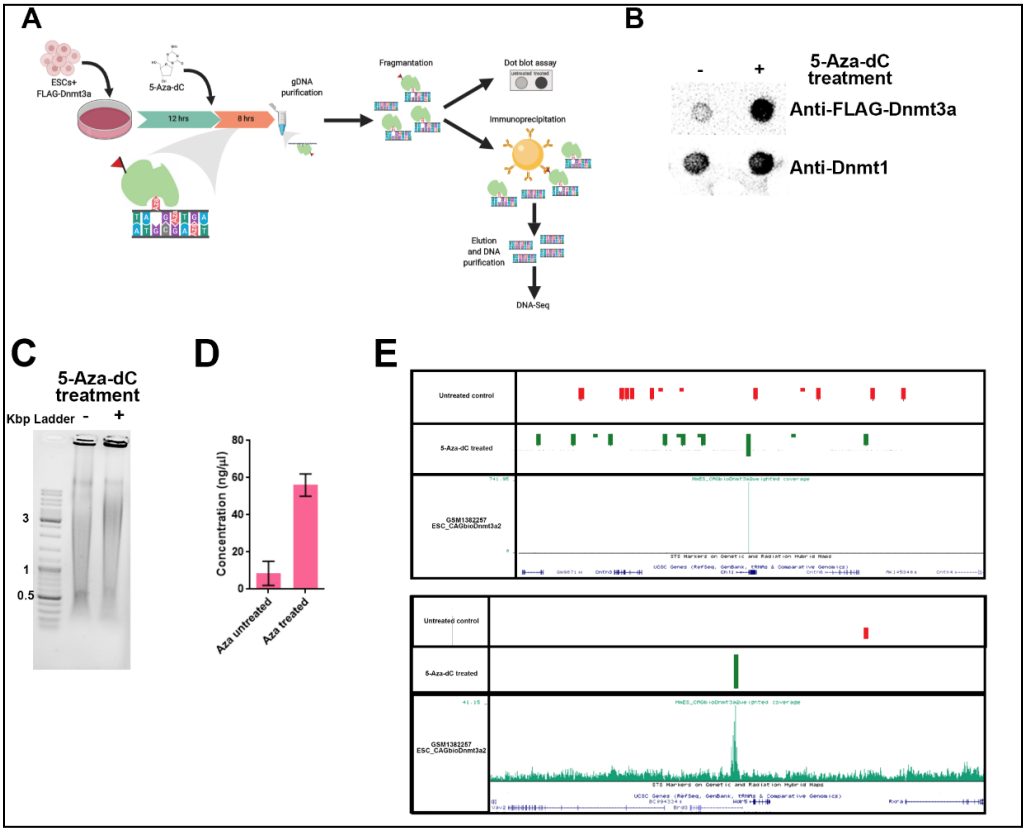

Figure 3.4 Mapping trapped FLAG-Dnmt3a sites using TSCC-DIP.

(A) Cartoon representation of TSCC-DIP protocol: FLAG-Dnmt3a and EV were plated for 12 hr followed by 5-Aza-dC treatment for 8 hr. gDNA was collected and precipitated. Equal amounts of fragmented gDNA were blotted using a dot blot assays and probed with anti-Dnmt1 and anti-FLAG antibodies to test for Dnmt trapping by 5-Aza-dC treatment compared to untreated control. Then, FLAG-Dnmt3a-DNA adducts were immunoprecipitated, quantified, and sequenced. (B) Dot blot assay showing increase in Dnmt1 and FLAG-Dnmt3a signal in 5-Aza-dC treated sample compared to untreated control. (C) 1% agarose gel showing comparable shearing patterns of fragmented gDNA from sample and control. (D) Eluate quantification by nanodrop spectrophotometer demonstrating enrichment in the DNA amount in 5-Aza-dC treated sample compared to control. (E) IGV and UCSC screen shots showing overlap between the mapped Wide-seq reads from the 5-Aza-dC treated sample and published Dnmt3a ChIP-seq.

3.5.4 Dnmt3a-DNA adducts during neuronal differentiation

To provide further support for our proposed method, we sought to test if we could capture Dnmt3a during methylation deposition at previously identified sites in response to environmental signals. Our previous studies identified Dnmt3a as the principal Dnmt methylating and silencing pluripotency gene enhancers in ESCs induced to differentiate to the neuronal lineage in the presence of Retinoic acid (102). To test this hypothesis, we optimized a neuronal differentiation protocol that enabled the efficient differentiaiton of ESCs to neuronal prognitors in a monolayer culture (164). We reasoned that a monolayer culture would be more permissiple to 5-Aza-dC incorporation than are embryoid bodies (Figure 3.5A).

To confirm the profiency of our differentiation, we analyzed the expression of pluripotency factors and neuronal markers pre- and post-differentiation by RT-qPCR. Our data showed complete repression of the pioneer pluripotency gene Oct3/4 and an induction of the neuronal markers Sox1 and Sox2 in both the FLAG-Dnmt3a expressing sample and in the EV control (Figure 3.5B). These results indicat that FLAG-Dnmt3a expression does not have an effect on differention and pluripotency gene repression.

Next, we examined if the enhancers of pluripotency genes gain DNA methylation post-differentiation using this differention method. Evaluation of five pluripotency gene enhancers by bisulfite conversion followed by sequencing (Bis-seq), showed a gradual increase in DNA methylation levels duing differentiation (Figure 3.5C). This result is in agreement with previous reports showing gain of DNA methylation at these enhancers by the enzymatic activity of Dnmt3a in response to a differentition signal (102).

Dot blot assays probing for FLAG-Dnmt3a-DNA adducts in samples treated and untreated with 5-Aza-dC during the course of differentiation showed enrichment in FLAG-Dnmt3a signal only in the treated samples (Figure 3.5D). This result suggests that 5-Aza-dC was incorporated during differntiation and that these adducts can be detected by immunoblotting. Furthermore, 5-Aza-dC did not seem to have a discernable effect on the differentiaiton process, as determined by examination of cellular morphology and viability during differentiation (Figure 3.5E).

Figure 3.5 Trapping FLAG-Dnmt3a during neuronal differentiation.

(A) Schematic representation of the experimental design: ESCs were plated for 12 hr followed by 5-Aza-dC treatment. gDNA samples were collected after lysing the cells using a RADAR lysis buffer at different times post-differentiation. Equal amounts of gDNA were blotted using a dot blot apparatus and probed with anti-FLAG antibody to test for FLAG-Dnmt3a trapping by 5-Aza-dC treatment compared to an untreated control. (B) Gene expression analysis by RT-qPCR of pluripotency genes and neuronal markers in FLAG-Dnmt3a and EV ESCs induced to differentiate to neuronal lineage. The C_t values for each gene were normalized to *β-actin* and expression is shown relative to that of the corresponding untreated-undifferentiated (UD) cells, which is set to one. In both cell lines, we observed repression of *Oct3/4* and induction of neuronal genes, attesting to the efficacy of the differentiation protocol. (C) gDNA from FLAG-Dnmt3a samples UD-untreated and D1-D4 treated samples were treated with bisulfite and pluripotency gene enhancers were amplified by nested PCR. The amplicons were sequenced on a Wide-Seq platform and the data were analyzed using Bismark software. There is gain in DNA methylation post-differentiation induction compared to the untreated UD sample. No signal was observed from EV samples (D) Dot blot assay showing increase in FLAG-Dnmt3a signal during differentiation compared to untreated UD samples (E) Bright-field microscopy images of cells during differentiation and 5-Aza-dC treatments. There is no significant cell death cause by 5-Aza-dC treatment compared to the untreated control. Images were taken at 20X magnification.

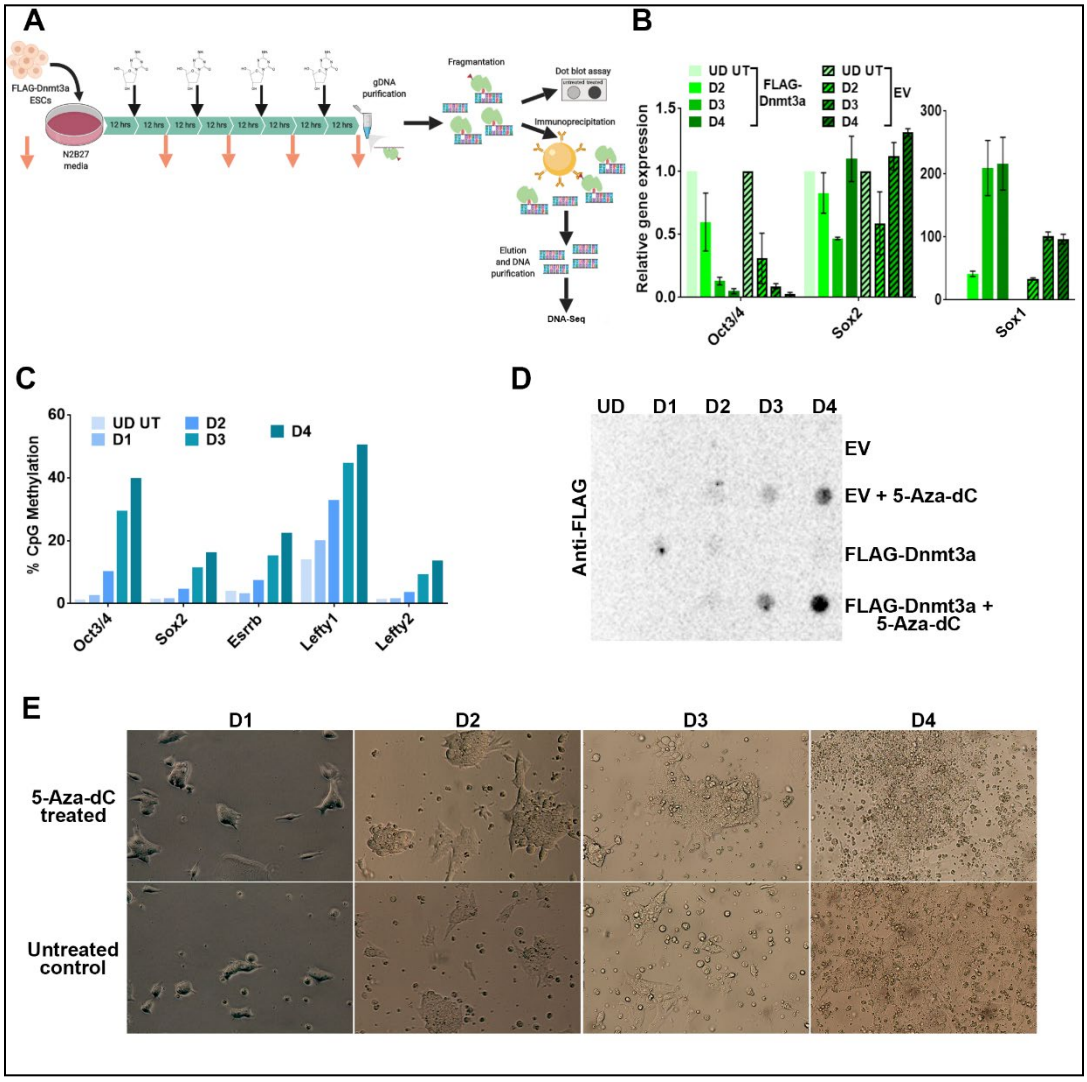
A
FLAG-Dnmt3a ESCs
N2B27 media
12 hrs
gDNA purification
Fragmantation
Dot blot assay
Immunoprecipitation
Elution and DNA purification
DNA-Seq
B
UD UT
D2
D3
D4
FLAG-Dnmt3a
EV
Relative gene expression
Oct3/4
Sox2
Sox1
C
% CpG Methylation
Oct3/4
Sox2
Esrrb
Lefty1
Lefty2
D
UD
D1
D2
D3
D4
Anti-FLAG
EV
EV + 5-Aza-dC
FLAG-Dnmt3a
FLAG-Dnmt3a + 5-Aza-dC
E
5-Aza-dC treated
Untreated control

3.6 Discussion

DNA methylation is a versatile epigenetic mark; it is associated with stable gene repression when deposited at regulatory elements and active transcription when present at gene bodies (96, 106). Alterations in the DNA methylation landscape are associated with cancers and many developmental diseases (244, 245, 285). These abnormal changes in DNA methylation patterns could be attributed to genetic mutations in Dnmts or due to a disruption in mechanisms regulating their activities (147, 258). Therefore, the development of detection techniques, which allow for a robust and specific examination of the distinct, as well as redundant, activities of Dnmts could help in unravelling the biology of the diseased state.

In the past, specific genomic targets of Dnmts were mapped using experiments that relied on their depletion followed by analysis of the regions that were affected by their loss (286). However, we argue that such studies cannot exclude the possibility of functional dependence and regulation by other Dnmts. For example, Dnmt3a can be the principal Dnmt methylating certain CpGs within a region. In its absence, Dnmt3b could compensate. Conversely, if Dnmt3b were required to be in a complex with Dnmt3a in order to be active at a specific site, depletion of Dnmt3a would likely demolish Dnmt3b-specific sites.

Despite the numerous methods developed to detect Dnmt occupancy and their product of catalysis, the spatiotemporal information about their activities is often lost. Here, we show that TSCC-DIP enables the detection of Dnmts during their catalysis via locking the active enzyme with its substrate in the transition intermediate state. This method is simple to implement, inexpensive, and timesaving. However, this approach depends on the incorporation of the 2′-deoxycytidine analog 5-Aza-2′-deoxycytidine in the genome during replication, restricting its implementation to living cells that are undergoing active replication. Additionally, the accumulation of Dnmt-DNA adducts as a result of prolonged 5-Aza-2-dC treatment triggers base-excision DNA repair and cell apoptosis pathways. Therefore, treatment time and dosage must be optimized for every cell line according to doubling time. Another limitation of this technique is that 5-Aza-dC treatment could potentially affect cellular reactions to signaling pathways and alter their biological response. This is unlikely because 5-Aza-dC treatment should be optimized to be short and acute, in addition to the possibility of comparing the kinetics of transcriptional changes with that of an untreated control.

Taken together, TSCC-DIP is an adaptable tool that could be used together with other techniques that examine histone modifications, chromatin organization, and RNA expression to answer many open questions in the field. We are proposing this method as a novel approach to track the dynamic changes in DNA methylation by any Dnmt expressed during cell fate specification, disease state, and the specific activities during homeostasis.

3.7 Future directions

Given the low read numbers obtained from the Wide-Seq experiment, we are preparing libraries to be sequenced using the NovaSeq 6000 platform. Correlation and statistical studies can then be performed to analyze the sites actively methylated by Dnmt3a in the undifferentiated state and during differentiation.

CHAPTER 4. MISCELLANEOUS

4.1 The effect of N-Myc expression on DNA methylation levels in Vezf1 KO cells

4.1.1 Analysis of N-Myc regulation of Dnmt3b expression

Vascular endothelial zinc finger 1 (Vezf1) is a transcription factor implicated in angiogenesis and vascular development (287). Previous studies from our laboratory demonstrated a mechanism by which Vezf1 mediates the induction of endothelial markers post-ESC differentiation through the repression of a stem cell factor, Cbp/p300-interacting transactivator 2 (Cited2) (288). These conclusions were drawn from experiments performed using Vezf1 KO ESCs which, interestingly, exhibit genome-wide hypomethylation concomitant with reduction in the expression of Dnmt3b (277). Mechanism(s) illustrating how Dnmt3b expression is affected by Vezf1 loss are not fully understood.

By comparing previously published Microarray data from Vezf1 KO and WT ESCs (277), we noted an increase in the expression of N-Myc in the Vezf1 null cell line. Additionally, a tentative N-Myc binding site is located at Dnmt3b promoter. To test the direct regulation of Dnmt3b by N-Myc, we generated a doxycycline-inducible system for FLAG-N-Myc expression in ESCs. Experiments examining Dnmt3b expression in response to N-Myc induction could be performed. Anti-FLAG ChIP assays could further elucidate N-Myc-mediated regulation by its potential physical binding at Dnmt3b promoter.

The significance of Dnmt3b activity during early embryogenesis is supported by mouse studies demonstrating that a Dnmt3b KO is embryonic lethal (139, 289). Hence, understanding the mechanisms regulating the expression, which could reflect on the enzymatic activity, of this epigenetic modifier is not only vital to our increasing knowledge of developmental biology, but also to our interpretation of how these mechanisms are perturbed in the diseased state.

4.1.2 Tet-inducible system for the controlled expression of N-Myc

ESCs were transfected with a tetracycline-controlled transactivator (tTA) expressing plasmid. Clones were screened for the highest expression and induction by using a luciferase expressing plasmid under the control of a tetracycline-dependent promoter (Figure 4.1A). Clones with the highest induction were tested for pluripotency via Alkaline Phosphatase (AP) staining and

the expression of *Oct3/4* by RT-qPCR compared to WT ESCs (Figure 4.1B and C). The clone with the highest expression of the pioneer factor Oct3/4 was used for subsequent transfection with a FLAG-N-Myc expressing plasmid under the control of a tetracycline-dependent promoter. Clones were then screened for FLAG-N-Myc expression by drug induction. The clone with the highest expression of FLAG-N-Myc in response to doxycycline induction was expanded and stored for future experiments (Figure 4.1D).

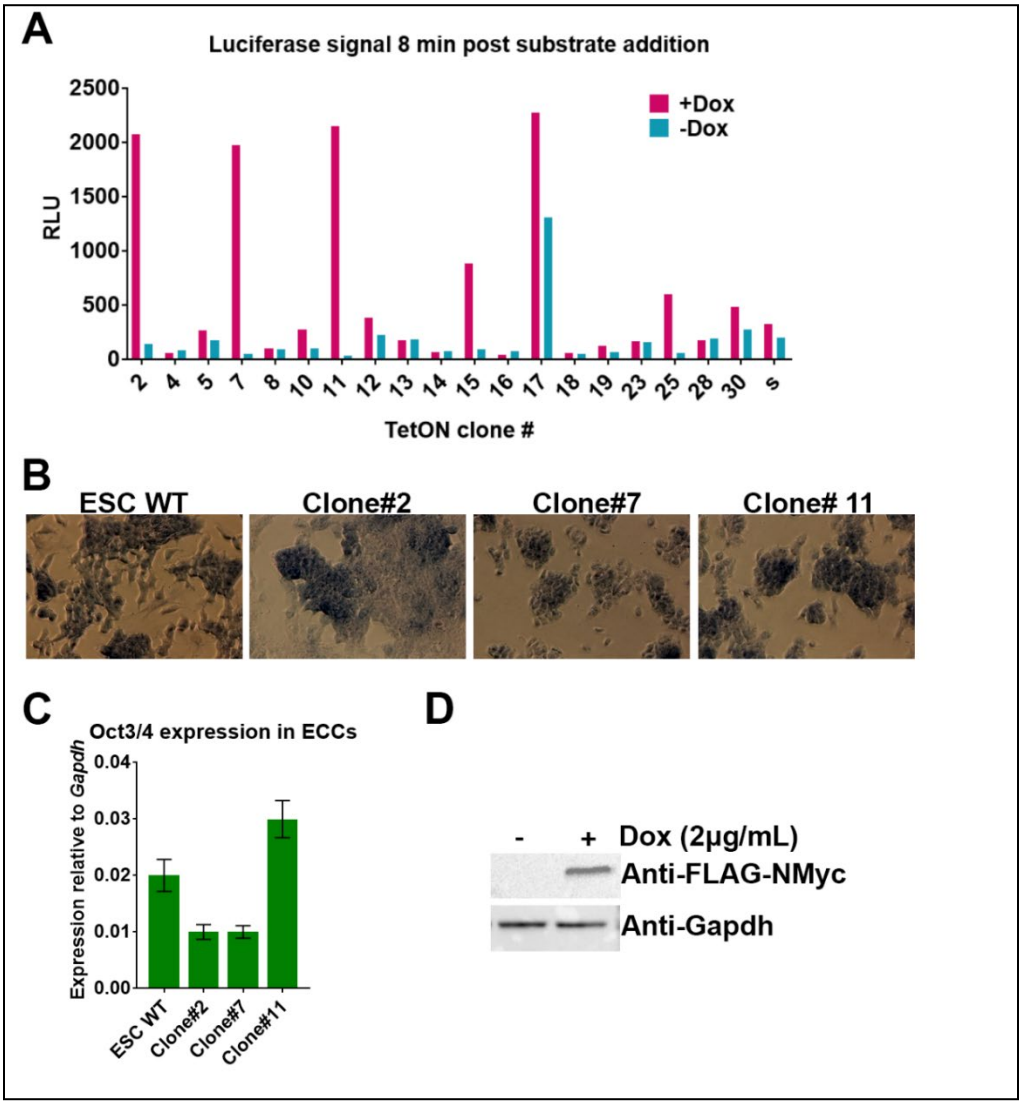

Figure 4.1 Development of inducible FLAG-N-Myc ESC cell line.

(A) Luciferase assay to screen for Tet-inducible expression of luciferase. Equal numbers of cells from each clone were plated as duplicates on a 96 well plate with one set treated with 2 µg/mL doxycycline while the other set was treated with H_2O solvent. Luciferase activity was recorded for each clone using a luminometer 8 min after the addition of the luciferin substrate. S is scramble cell line, which is a pool of multiple clones. RLU is relative light units. (B and C) Analysis of the transgenic cell lines for pluripotency by (B) Alkaline Phosphatase (AP) stain where blue signal indicates pluripotency, and (C) *Oct3*/4 expression by RT-qPCR. The C_t values for each gene were normalized to *Gapdh*. The clone with the highest expression of *Oct3*/4 (Clone# 11) was used for subsequent transfections. ESC WT is untransfected ESCs used as a control. (D) Western blot showing the induced expression of FLAG-N-Myc. Doxycycline uninduced cell lysate is the negative control and Gapdh is the loading control. Microscopy images are 10X magnification.

4.2 The effect of the dynamic changes of Dnmt3l expression on ESC differentiation

Dnmt3l is the catalytically inactive homologue of Dnmt3a and Dnmt3b in mammalian cells (252). Its biological function has been demonstrated by biochemical studies to enhance the activities of Dnmt3a and Dnmt3b by forming heterotetramers (270, 290). Cell culture based experiments showed that Dnmt3l is necessary for the stability of Dnmt3a in ESCs (291). Loss of function assays showed that although Dnmt3l KO mice are viable, they are sterile. Further analysis showed that Dnmt3l is essential for the methylation of imprinted regions by its functional interaction with the other catalytically competent Dnmt3 enzymes (292-294). Given the high sequence similarities between Dnmt3 proteins, in addition to the comparable loss of their expression post-ESC differentiation (295), the mechanism(s) dictating Dnmt3l-directed methylation of imprinted regions are not completely understood. Furthermore, it is unknown whether Dnmt3l plays a role in regulating Dnmt3a activity at PpGe in differentiating ESCs.

4.2.1 Analysis of Dnmt3l expression on gain of DNA methylation at PpGe

To test whether Dnmt3l plays a role in PpGe silencing during ESC differentiation, we induced the differentiation of Dnmt3l KO ESCs and rescue cell lines (291). Our preliminary data using bisulfite sequencing showed a disruption in DNA methylation gain at most PpGe post-differentiation of ESCs depleted of Dnmt3l compared to WT control. This defect was rescued at most enhancers when Dnmt3l was re-expressed, indicating that the presence of Dnmt3l is required for PpGe silencing (Figure 4.2A). Defect the DNA methylation gain post-differentiation were not observed at the Sall4 enhancer. This observation suggests that DNA methylation regulation is independent of Dnmt3l at this site. These conclusions were further supported by gain of function studies where we recombinantly maintained the expression of Dnmt3l in differentiating ESCs (Figure 4.2B). DNA methylation analysis using ESCs expressing Myc-Dnmt3l showed enhanced gain of DNA methylation at PpGe post-differentiation compared to the empty vector (EV) control (Figure 4.2C). Interestingly, the Lefty2 enhancer was not significantly affected by Dnmt3l depletion or overexpression, suggesting that it undergoes a Dnmt3l-independent regulation of DNA methylation post-ESC differentiation. It is still unclear whether the effect of Dnmt3l expression on PpGe is due to its regulation of Dnmt3a stability or activity, or via recruitment of the catalytically active enzyme to these sites. DNA methylation analysis on differentiating ESC

cell lines expressing Dnmt3l with defective regulatory PHD domain (Dnmt3l-D124A, -I141W, or C-terminal domain only (126, 296)) or with mutations that would impeded its interaction with Dnmt3a (Dnmt3l-F261A (296, 297)) can be performed to uncouple these mechanistic pathways.

4.2.2 Investigation of mechanisms dictating Dnmt3l regulation of DNA methylation at imprinted regions

In vivo studies have shown that Dnmt3l is required for the maintenance of DNA methylation at imprinted regions (292-294). However, the mechanisms governing Dnmt3l-mediated recruitment of other Dnmt3s to these sites are not fully understood. Our preliminary data show that, as expected, Dnmt3l KO ESCs exhibited hypomethylation of the H19 imprinted region. Surprisingly, restoration of Dnmt3l levels in these cells did not rescue the methylation status at the imprinted locus (Figure 4.2D). Overexpression of Dnmt3l in ESCs did not affect the levels of DNA methylation at these sites compared to the EV control (Figure 4.2E). These data suggest that the role of Dnmt3l in the methylation of imprinted regions is established early in development. The additional loss of DNA methylation at the H19 imprinted region in the Dnmt3l rescue cell line is potentially due to the expansion of the culture and the increase in cell divisions in the absence of Dnmt3l. This process could propagate the decline in DNA methylation levels via passive DNA demethylation, despite the increasing levels of Dnmt3l protein. An alternative hypothesis is that Dnmt3l is essential for the establishment, and not the maintenance, of DNA methylation at imprinted regions. This hypothesis can be tested by inducible Dnmt3l KD studies followed by DNA methylation analysis at imprinted loci. These studies would uncouple the effect of Dnmt3l depletion and cell passaging on loss of DNA methylation at imprinted regions.

Figure 4.2 Dnmt3l is required at PpGe in differentiating ESCs.

(A, C, D, and E) DNA methylation analysis by Bis-Seq probing (A and B) the enhancers of PpG and (C and D) the H19 imprinted region. (A) Dnmt3l KO and rescue cell lines together with WT control were differentiated to Day 3 (D3) and Day 5 (D5) post-retinoic acid addition. Differentiating Dnmt3l KO cells exhibited defects in gain of DNA methylation at PpGe, with the exception of Lefty2 and Sall4, when compared to WT and rescue cell lines. (B) Western blot showing expression of Myc-Dnmt3l in ESCs compared to Empty vector control (ESC+EV). Actin was used as a loading control. (C) In contrast to KO studies, ESCs overexpressing Myc-Dnmt3l showed enhanced methylation at PpGe, except for Lefty1, when compared to the EV control. (D) DNA methylation at the H19 imprinted region was reduced in Dnmt3l KO cells compared to WT control. Re-expression of Dnmt3l did not rescue DNA methylation levels. (E) Similar DNA methylation levels at the H19 locus in Dnmt3l overexpressing ESCs and EV control.

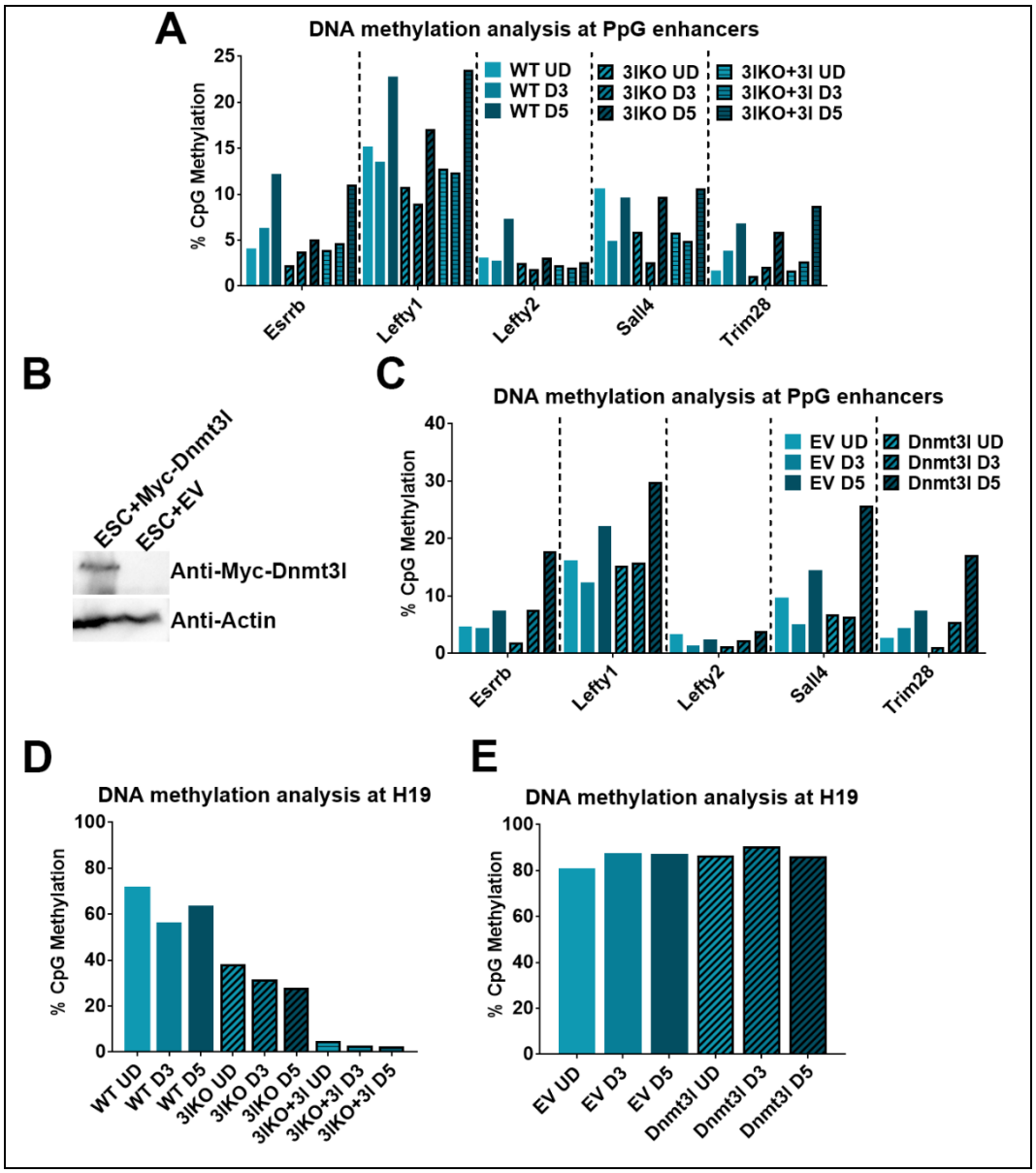
A
DNA methylation analysis at PpG enhancers
% CpG Methylation
WT UD
WT D3
WT D5
3IKO UD
3IKO D3
3IKO D5
3IKO+3I UD
3IKO+3I D3
3IKO+3I D5
Esrrb
Lefty1
Lefty2
Sall4
Trim28
B
ESC+Myc-Dnmt3l
ESC+EV
Anti-Myc-Dnmt3l
Anti-Actin
C
DNA methylation analysis at PpG enhancers
% CpG Methylation
EV UD
EV D3
EV D5
Dnmt3l UD
Dnmt3l D3
Dnmt3l D5
Esrrb
Lefty1
Lefty2
Sall4
Trim28
D
DNA methylation analysis at H19
% CpG Methylation
WT UD
WT D3
WT D5
3IKO UD
3IKO D3
3IKO D5
3IKO+3I UD
3IKO+3I D3
3IKO+3I D5
E
DNA methylation analysis at H19
% CpG Methylation
EV UD
EV D3
EV D5
Dnmt3l UD
Dnmt3l D3
Dnmt3l D5

CHAPTER 5. PERSPECTIVES

5.1 Outlook on the regulation of Lsd1 activity by transcription factors

5.1.1 Conclusions

The enzymatic activity of the histone demethylase Lsd1 is critical for PpGe silencing post-differentiation. Silencing occurs via the activation of Dnmt3a, which ensures stable gene repression (102). We demonstrated how the disruption of PpG repression leads to the emergence of primed enhancers in differentiating F9 ECCs that renders PpG vulnerable for re-expression upon binding of a coactivator. We predict that the activity of Lsd1 at the enhancers of PpG is governed by its interaction with Oct3/4 in the undifferentiated state. The repression of Oct3/4 post-differentiation leads to the loss of Lsd1-Oct3/4 interaction and the activation of Lsd1 enzyme. The timely demethylation of H3K4me1 by Lsd1 generates an unmethylated H3K4me0 tail which interacts with the ADD domain of Dnmt3a, relieving it from its autoinhibited state (102). This study provided a mechanism by which the regulation of Lsd1 activity by Oct3/4 influences the epigenetic state of regulatory elements and controls PpG expression in two ways: 1) Lsd1-Oct3/4 interaction at the enhancers of PpGs in the undifferentiated state curbs Lsd1 activity and maintains these enhancers as active, and 2) the dissociation of this interaction is critical for initiating the downstream epigenetic events necessary for stable gene repression by enhancer silencing. If this interaction were not disrupted, as is the case in differentiating F9 ECCs, these enhancers would switch to a primed state marked by H3K4me1 and lacking H3K27Ac and DNA methylation. Numerous studies speculate that enhancer priming aids in gene reactivation and the maintenance of an epigenetic memory of previous activations (298). Therefore, a primed enhancer is likely to be susceptible to aberrant activation in an anomalous cellular state. Moreover, retention of H3K4me1 blocks gain of DNA methylation at these regulatory elements. Several reports have highlighted the importance of DNA methylation in gene repression by showing that the targeted methylation of their respective promoters drives their transcriptional repression (155, 156, 299, 300), thus reinforcing the role of DNA methylation in silencing regulatory elements and the concomitant stable gene repression.

We used F9 ECCs as a cancer stem cell model to study the dysregulation of mechanisms that safeguard PpGe silencing during differentiation. The next step would be to determine if this

is also observed in caner stem cells isolated from tumors that exhibit anti-cancer drug and radiation therapy resistance. Further studies could investigate the broad effect of this mechanism by tracking the changes in DNA methylation and histone modifications at PpGe before and after cancer resurgence.

5.1.2 Mapping Lsd1-Oct3/4 interaction domains

As an epigenetic modifier with diverse catalytic functions, the fine-tuning of Lsd1 activity is achieved via a wide-range of mechanisms. Anomalous activity of Lsd1 could be attributed to its aberrant expression. For example, several studies reported high expression of Lsd1 in different cancers such as breast, prostate, bladder, neuroblastoma, and acute myeloid leukemia (301, 302). Lsd1 activity is regulated not only through transcript level regulation, but also through controlled protein degradation. Lsd1 levels are regulated by ubiquitination and deubiquitination which are critical for cell fate determination in ESCs (303, 304). Posttranslational modifications also influence the activity of the enzyme. SUMOlation by SUMO2 was reported to alter Lsd1 activity or localization, possibly by the generation of a new protein-protein interaction interface (305). Furthermore, Lsd1 catalytic activity or its localization to a genomic region can be mediated through binding with TFs or epigenetic modifiers (90-92, 306).

Our study answered a key question in the field regarding Lsd1 association with PpGe in the undifferentiated state despite the absence of its enzymatic activity (179). We showed that through its direct interaction with Oct3/4, Lsd1 activity was inhibited. Although this mechanism is employed by healthy cells to keep their PpGe in the active state and prevent spurious activity of Lsd1 at these sites, this mechanism can also be hijacked by cancer cells to mark PpGe as primed for activation. TF-mediated targeting or allosteric regulation of Lsd1 has also been previously reported (90-92, 306).

Given that our analysis of the Lsd1 interaction network in both ESCs and F9 ECCs includes a large number of TFs, we postulate that Lsd1 activity is also regulated by other zinc finger containing proteins. Preliminary studies using recombinant proteins showed that SP1 also inhibits Lsd1activity (Figure 5.1A). A screen for potential regulators of its demethylation activity, using an *in vitro* Lsd1 demethylation assay, would not only add to our understanding of how epigenetic modifiers are regulated, but also how these epigenetic events are chronologically and functionally linked. Epigenetic regulation is key for proper development and its dysregulation is evident in the

state of disease. Therefore, mapping regulators of epigenetic effectors and characterizing their functional and physical interactions are necessary for our interpretation of the dysregulated mechanisms that contribute to the emergence and progression of the disease state.

Additionally, identifying Lsd1 interactors will aid in determining protein-protein interaction domains. Both Oct3/4 and p53 interact with Lsd1 and inhibit its activity (91). Protein sequence ligament analysis showed that there is 31% sequence similarity between the two proteins (Figure 5.1B). The p53 C-terminal domain interaction with Lsd1 has been crystalized. Using the crystal structure as a reference, a computational modeling approach can be used to map the residues mediating Oct3/4 interaction with Lsd1. Given that Lsd1 is reported to interact with a substantial number of TFs, characterizing these interactions, and how they affect Lsd1 recruitment and enzymatic activity in different biological contexts, will aid in highlighting the broader spectrum of epigenetic regulation.

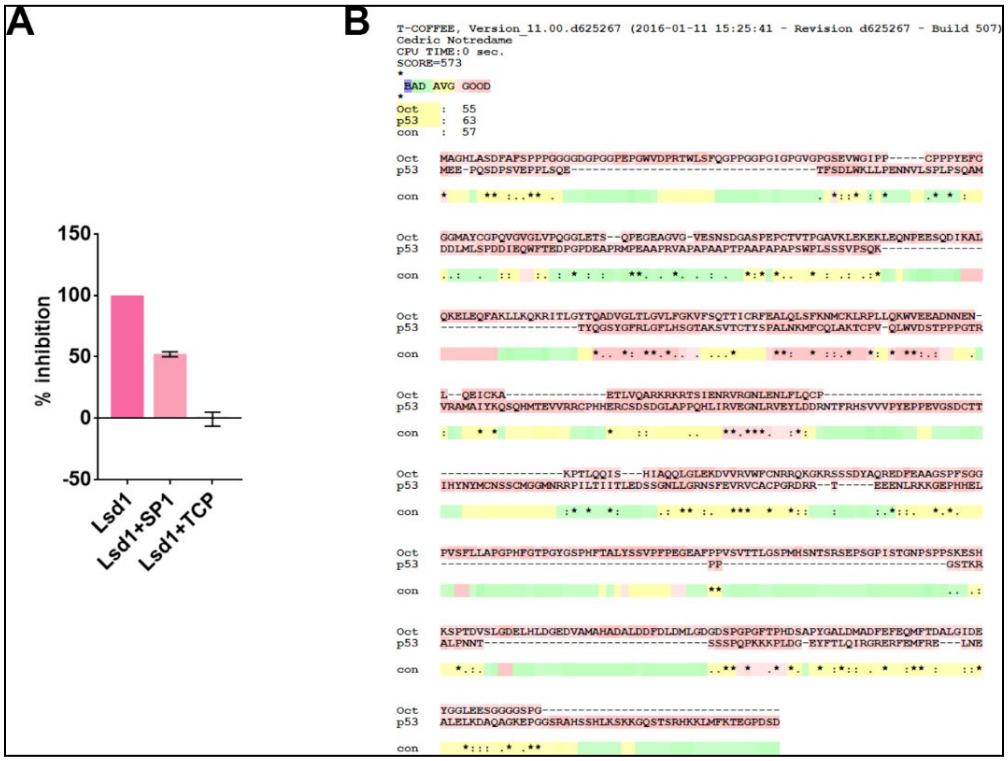

Figure 5.1 Transcription factors modulate Lsd1 activity.

(A) An Lsd1 demethylase assay was performed using 0.25 µM of Lsd1 and H3K4me2 peptide. Lsd1 activity was inhibited by the addition of TCP (tranylcypromine) (0.1 mM) to the reaction. To test whether SP1 inhibits Lsd1 activity, demethylation assays were performed in the presence of 0.5 µM SP1 at 1:2 (Lsd1:SP1) molar ratio. (B) Sequence alignments of human Oct3/4 (Oct) and human p53 proteins using T-COFFEE software (version 11.00.d625267). There is high sequence homology between the two proteins. "Good" alignment is generated between C-terminal domains of Oct3/4 and p53 where Lsd1 was shown to interact (91): (AQAGKEPGGSRAHSSHLKSKKGQSTSRHKKLMFKTEGPDSD)

5.1.3 Regulation of Oct3/4 expression in differentiating F9 ECCs

Our study demonstrated that the partial repression of Oct3/4 in differentiating F9 ECCs facilitated the generation of a primed enhancer state by inhibiting Lsd1 demethylase activity. At the onset of ESC differentiation, Oct3/4 is marked for proteosomal degradation, alleviating this inhibition. Because F9 ECCs is a testicular teratoma stem cell line, it is reasonable to argue that during differentiation, Oct3/4 expression is not completely repressed because of these cells germline heritage (201, 307, 308). Uncoupling the tumorigenic factors from primordial germline development is key to understand the pathology of these cells. Given that differentiating ESCs and the analogous cell line P19 ECCs undergoes silencing of Oct3/4 regulatory elements, this provides evidence that supports the tumorigenic properties of F9 ECCs. Experiments designed to interrogate Oct3/4 regulatory elements coupled with genome-wide expression analyses during F9 ECC differentiation, compared to that of P19 ECCs, are warranted to determine whether this dysregulation in expression is initiated by a perturbation of an epigenetic mechanism. Moreover, careful examination of the activation of cell signaling pathways during differentiation would shed light into the possibility of a disruption of a signaling event.

5.1.4 Differentiation-mediated drug development

Our study elucidated how Lsd1-Oct3/4 interaction post-differentiation prevents enhancer silencing. Instead, the abbreviated activity of Lsd1 leads to the development of primed enhancers. Given that enhancer silencing mediates PpG repression, which is critical for proper differentiation (102), we propose the disruption of Lsd1-Oct3/4 interaction as a target for the development of differentiation-inducing therapeutics. Small molecules that are able to interrupt this protein-protein interaction could be used in a screen with Lsd1 demethylase activity as a readout. The initial hits that could potentially alleviate the Oct3/4-Lsd1 inhibitory interaction could be further decorated to produce potent inhibitors. The directed decoration is achieved by solving the protein-protein interacting domains by crystallography and then identifying the amino acid residues critical for the interaction. The potential inhibitors can then be remodeled into the structure and altered to produce a better fit that would ensure the disruption of the interaction. In combination with other cytotoxic drugs, these differentiation-inducing drugs could help eradicate the cancer stem cell population.

5.2 Applications for TSCC-DIP

5.2.1 Conclusions

Conventional methods used to detect Dnmt occupancy in the genome are unable to discern if the Dnmts are actively methylating the DNA or are associated with protein complexes that are modifying the chromatin state. We repurposed the Dnmt inhibitor 5-Aza-deoxycitidine, which is able to form a covalent intermediate with Dnmts (163). Because Dnmts cannot methylate this 2′-deoxycytidine analogue, they become chemically cross-linked to DNA. By using a lysis buffer that preserves these Dnmt-DNA adducts, we were able to capture Dnmts by 5-Aza-dC treatment and demonstrated the accumulation these adducts as a function of time. We also showed that the Dnmt3a-DNA adducts can be stably immunoprecipitated and sequenced. This approach is less laborious than are conventional methods, and selectively captures Dnmts during their catalysis.

5.2.2 TSCC-DIP to examine the effect of mutations on Dnmt activities

Transition State Covalent Crosslinking followed by DNA Immunoprecipitation (TSCC-DIP) could be used to determine the effect of pathological mutations on Dnmt activities or recruitment to certain genomic loci. We have performed preliminary *in vitro* experiments, which showed that an acute myeloid leukemia (AML) prevalent point mutation that occurs in a Dnmt3a catalytic domain causes a change in the enzyme's substrate flanking sequence preference. This observation was further substantiated at some genomic regions by expressing this mutant in ESCs. Because of its selectivity, TSCC-DIP could be utilized to compare the changes in the substrate preference between WT and mutant Dnmt3a, and could shed light onto the enzymatic mechanism(s) of these enzymes in cellular context. Additionally, the consequence of functional interactions between Dnmts and other proteins could be established for each Dnmt under different physiological conditions.

5.2.3 Evaluation of Dnmts functions during ESC differentiation

Our study provided preliminary results indicating the feasibility of using 5-Aza-dC treatment to capture Dnmts in a dynamic system. We propose the use of TSCC-DIP to monitor systematically the changes in the DNA methylation landscape during cell fate commitment and under variable environmental stimuli. The role of DNA methylation in the regulation of gene expression is most evident during the early stages of development mimicked by ESC

differentiation (309). There are many genome-wide datasets investigating the patterns of DNA methylation and the functions of the different Dnmts during these fate-determining series of events (145, 310). Our study showed that TSCC-DIP could be a tool that uncouples the activities of these Dnmts at all the sites mapped. Because this approach relies on the capture of Dnmts during catalysis, determining the cause and effect of many transient epigenetic changes that occur at particular site is an integral function of this technique when coupled with histone modification analysis or chromatin organization assessment assays.

TSCC-DIP can also be used to establish which sites show true functional redundancy among the different Dnmts. Several reports showed that when Dnmt3a or Dnmt3b are depleted from cells, certain regions maintain their methylation levels due to compensatory activity of the homologous Dnmt3 (311). We propose the use of TSCC-DIP to investigate if these shared regions are equally occupied by both enzymes, or if the functional compensation is due to cellular stress brought about by the absence of the principal Dnmt3.

REFERENCES

1. Rossant J, Tam PPL. New Insights into Early Human Development: Lessons for Stem Cell Derivation and Differentiation. Cell Stem Cell. 2017;20(1):18-28. doi: 10.1016/j.stem.2016.12.004. PubMed PMID: 28061351.
2. Nowotschin S, Hadjantonakis AK. Cellular dynamics in the early mouse embryo: from axis formation to gastrulation. Curr Opin Genet Dev. 2010;20(4):420-7. doi: 10.1016/j.gde.2010.05.008. PubMed PMID: 20566281; PMCID: PMC2908213.
3. Takaoka K, Hamada H. Cell fate decisions and axis determination in the early mouse embryo. Development. 2012;139(1):3-14. doi: 10.1242/dev.060095. PubMed PMID: 22147950.
4. Rossant J, Tam PP. Blastocyst lineage formation, early embryonic asymmetries and axis patterning in the mouse. Development. 2009;136(5):701-13. doi: 10.1242/dev.017178. PubMed PMID: 19201946.
5. Bedzhov I, Graham SJ, Leung CY, Zernicka-Goetz M. Developmental plasticity, cell fate specification and morphogenesis in the early mouse embryo. Philos Trans R Soc Lond B Biol Sci. 2014;369(1657). doi: 10.1098/rstb.2013.0538. PubMed PMID: 25349447; PMCID: PMC4216461.
6. Nichols J, Smith A. Pluripotency in the embryo and in culture. Cold Spring Harb Perspect Biol. 2012;4(8):a008128. doi: 10.1101/cshperspect.a008128. PubMed PMID: 22855723; PMCID: PMC3405859.
7. Lawson KA, Meneses JJ, Pedersen RA. Clonal analysis of epiblast fate during germ layer formation in the mouse embryo. Development. 1991;113(3):891-911. PubMed PMID: 1821858.
8. Rizzino A, Crowley C. Growth and differentiation of embryonal carcinoma cell line F9 in defined media. Proc Natl Acad Sci U S A. 1980;77(1):457-61. doi: 10.1073/pnas.77.1.457. PubMed PMID: 6244561; PMCID: PMC348290.
9. Bryja V, Bonilla S, Cajanek L, Parish CL, Schwartz CM, Luo Y, Rao MS, Arenas E. An efficient method for the derivation of mouse embryonic stem cells. Stem Cells. 2006;24(4):844-9. doi: 10.1634/stemcells.2005-0444. PubMed PMID: 16339993.
10. Niakan KK, Schrode N, Cho LT, Hadjantonakis AK. Derivation of extraembryonic endoderm stem (XEN) cells from mouse embryos and embryonic stem cells. Nat Protoc. 2013;8(6):1028-41. doi: 10.1038/nprot.2013.049. PubMed PMID: 23640167; PMCID: PMC3927835.
11. Kleinsmith LJ, Pierce GB, Jr. Multipotentiality of Single Embryonal Carcinoma Cells. Cancer Res. 1964;24:1544-51. PubMed PMID: 14234000.
12. Evans M. Isolation and Maintenance of Murine Embryonic Stem Cells. Essentials of Stem Cell Biology, 2nd Edition. 2009:345-9. doi: Doi 10.1016/B978-0-12-374729-7.00039-1. PubMed PMID: WOS:000311099200044.
13. Stevens LC. The development of teratomas from intratesticular grafts of tubal mouse eggs. J Embryol Exp Morphol. 1968;20(3):329-41. PubMed PMID: 5728202.
14. Martin GR. Isolation of a pluripotent cell line from early mouse embryos cultured in medium conditioned by teratocarcinoma stem cells. Proc Natl Acad Sci U S A. 1981;78(12):7634-8. doi: 10.1073/pnas.78.12.7634. PubMed PMID: 6950406; PMCID: PMC349323.

15. Evans MJ, Kaufman MH. Establishment in culture of pluripotential cells from mouse embryos. Nature. 1981;292(5819):154-6. doi: 10.1038/292154a0. PubMed PMID: 7242681.
16. Belaoussoff M, Farrington SM, Baron MH. Hematopoietic induction and respecification of A-P identity by visceral endoderm signaling in the mouse embryo. Development. 1998;125(24):5009-18. PubMed PMID: 9811585.
17. Tam PP, Behringer RR. Mouse gastrulation: the formation of a mammalian body plan. Mech Dev. 1997;68(1-2):3-25. PubMed PMID: 9431800.
18. Goldie LC, Nix MK, Hirschi KK. Embryonic vasculogenesis and hematopoietic specification. Organogenesis. 2008;4(4):257-63. doi: 10.4161/org.4.4.7416. PubMed PMID: 19337406; PMCID: PMC2634331.
19. Risau W. Mechanisms of angiogenesis. Nature. 1997;386(6626):671-4. doi: 10.1038/386671a0. PubMed PMID: 9109485.
20. Marcelo KL, Goldie LC, Hirschi KK. Regulation of endothelial cell differentiation and specification. Circ Res. 2013;112(9):1272-87. doi: 10.1161/CIRCRESAHA.113.300506. PubMed PMID: 23620236; PMCID: PMC3768127.
21. Breier G, Clauss M, Risau W. Coordinate expression of vascular endothelial growth factor receptor-1 (flt-1) and its ligand suggests a paracrine regulation of murine vascular development. Dev Dyn. 1995;204(3):228-39. doi: 10.1002/aja.1002040303. PubMed PMID: 8573716.
22. Blancas AA, Lauer NE, McCloskey KE. Endothelial differentiation of embryonic stem cells. Curr Protoc Stem Cell Biol. 2008;Chapter 1:Unit 1F 5. doi: 10.1002/9780470151808.sc01f05s6. PubMed PMID: 18819086; PMCID: PMC2638496.
23. McCloskey KE, Stice SL, Nerem RM. In vitro derivation and expansion of endothelial cells from embryonic stem cells. Methods Mol Biol. 2006;330:287-301. doi: 10.1385/1-59745-036-7:287. PubMed PMID: 16846032.
24. Ramakrishnan V. Histone structure and the organization of the nucleosome. Annu Rev Biophys Biomol Struct. 1997;26:83-112. doi: 10.1146/annurev.biophys.26.1.83. PubMed PMID: 9241414.
25. Luger K, Mader AW, Richmond RK, Sargent DF, Richmond TJ. Crystal structure of the nucleosome core particle at 2.8 A resolution. Nature. 1997;389(6648):251-60. doi: 10.1038/38444. PubMed PMID: 9305837.
26. Allan J, Mitchell T, Harborne N, Bohm L, Crane-Robinson C. Roles of H1 domains in determining higher order chromatin structure and H1 location. J Mol Biol. 1986;187(4):591-601. PubMed PMID: 3458926.
27. Hansen JC. Conformational dynamics of the chromatin fiber in solution: determinants, mechanisms, and functions. Annu Rev Biophys Biomol Struct. 2002;31:361-92. Epub 2002/05/04. doi: 10.1146/annurev.biophys.31.101101.140858. PubMed PMID: 11988475.
28. Blackwood EM, Kadonaga JT. Going the distance: a current view of enhancer action. Science. 1998;281(5373):60-3. PubMed PMID: 9679020.
29. West AG, Gaszner M, Felsenfeld G. Insulators: many functions, many mechanisms. Genes Dev. 2002;16(3):271-88. doi: 10.1101/gad.954702. PubMed PMID: 11825869.
30. Palstra RJ, Grosveld F. Transcription factor binding at enhancers: shaping a genomic regulatory landscape in flux. Front Genet. 2012;3:195. doi: 10.3389/fgene.2012.00195. PubMed PMID: 23060900; PMCID: PMC3460357.

31. Boehm AK, Saunders A, Werner J, Lis JT. Transcription factor and polymerase recruitment, modification, and movement on dhsp70 in vivo in the minutes following heat shock. Mol Cell Biol. 2003;23(21):7628-37. doi: 10.1128/mcb.23.21.7628-7637.2003. PubMed PMID: 14560008; PMCID: PMC207607.
32. Phatnani HP, Greenleaf AL. Phosphorylation and functions of the RNA polymerase II CTD. Genes Dev. 2006;20(21):2922-36. doi: 10.1101/gad.1477006. PubMed PMID: 17079683.
33. Mohtat D, Susztak K. Fine tuning gene expression: the epigenome. Semin Nephrol. 2010;30(5):468-76. doi: 10.1016/j.semnephrol.2010.07.004. PubMed PMID: 21044758; PMCID: PMC3164355.
34. Lambert SA, Jolma A, Campitelli LF, Das PK, Yin Y, Albu M, Chen X, Taipale J, Hughes TR, Weirauch MT. The Human Transcription Factors. Cell. 2018;175(2):598-9. doi: 10.1016/j.cell.2018.09.045. PubMed PMID: 30290144.
35. Lee TI, Young RA. Transcriptional regulation and its misregulation in disease. Cell. 2013;152(6):1237-51. doi: 10.1016/j.cell.2013.02.014. PubMed PMID: 23498934; PMCID: PMC3640494.
36. Takahashi K, Yamanaka S. A decade of transcription factor-mediated reprogramming to pluripotency. Nat Rev Mol Cell Biol. 2016;17(3):183-93. doi: 10.1038/nrm.2016.8. PubMed PMID: 26883003.
37. Bejerano G, Pheasant M, Makunin I, Stephen S, Kent WJ, Mattick JS, Haussler D. Ultraconserved elements in the human genome. Science. 2004;304(5675):1321-5. doi: 10.1126/science.1098119. PubMed PMID: 15131266.
38. Carroll SB. Evo-devo and an expanding evolutionary synthesis: a genetic theory of morphological evolution. Cell. 2008;134(1):25-36. doi: 10.1016/j.cell.2008.06.030. PubMed PMID: 18614008.
39. Bradner JE, Hnisz D, Young RA. Transcriptional Addiction in Cancer. Cell. 2017;168(4):629-43. doi: 10.1016/j.cell.2016.12.013. PubMed PMID: 28187285; PMCID: PMC5308559.
40. Lambert M, Jambon S, Depauw S, David-Cordonnier MH. Targeting Transcription Factors for Cancer Treatment. Molecules. 2018;23(6). doi: 10.3390/molecules23061479. PubMed PMID: 29921764; PMCID: PMC6100431.
41. Ip YT. Transcriptional regulation. Converting an activator into a repressor. Curr Biol. 1995;5(1):1-3. PubMed PMID: 7697337.
42. Reynolds N, O'Shaughnessy A, Hendrich B. Transcriptional repressors: multifaceted regulators of gene expression. Development. 2013;140(3):505-12. doi: 10.1242/dev.083105. PubMed PMID: 23293282.
43. Ge K, Guermah M, Yuan CX, Ito M, Wallberg AE, Spiegelman BM, Roeder RG. Transcription coactivator TRAP220 is required for PPAR gamma 2-stimulated adipogenesis. Nature. 2002;417(6888):563-7. doi: 10.1038/417563a. PubMed PMID: 12037571.
44. Whyte WA, Orlando DA, Hnisz D, Abraham BJ, Lin CY, Kagey MH, Rahl PB, Lee TI, Young RA. Master transcription factors and mediator establish super-enhancers at key cell identity genes. Cell. 2013;153(2):307-19. doi: 10.1016/j.cell.2013.03.035. PubMed PMID: 23582322; PMCID: PMC3653129.

45. Yin JW, Wang G. The Mediator complex: a master coordinator of transcription and cell lineage development. Development. 2014;141(5):977-87. doi: 10.1242/dev.098392. PubMed PMID: 24550107.
46. Akerblom IE, Slater EP, Beato M, Baxter JD, Mellon PL. Negative regulation by glucocorticoids through interference with a cAMP responsive enhancer. Science. 1988;241(4863):350-3. PubMed PMID: 2838908.
47. Eichten SR, Schmitz RJ, Springer NM. Epigenetics: Beyond Chromatin Modifications and Complex Genetic Regulation. Plant Physiol. 2014;165(3):933-47. doi: 10.1104/pp.113.234211. PubMed PMID: 24872382; PMCID: PMC4081347.
48. Li S. Expression of Concern: The functional role of long non-coding RNAs and epigenetics. Biol Proced Online. 2016;18:12. doi: 10.1186/s12575-016-0042-1. PubMed PMID: 27293384; PMCID: PMC4901470.
49. Cao J. The functional role of long non-coding RNAs and epigenetics. Biol Proced Online. 2014;16:11. doi: 10.1186/1480-9222-16-11. PubMed PMID: 25276098; PMCID: PMC4177375.
50. Felsenfeld G, Boyes J, Chung J, Clark D, Studitsky V. Chromatin structure and gene expression. Proc Natl Acad Sci U S A. 1996;93(18):9384-8. doi: 10.1073/pnas.93.18.9384. PubMed PMID: 8790338; PMCID: PMC38436.
51. Bannister AJ, Kouzarides T. Regulation of chromatin by histone modifications. Cell Res. 2011;21(3):381-95. doi: 10.1038/cr.2011.22. PubMed PMID: 21321607; PMCID: PMC3193420.
52. Geiman TM, Robertson KD. Chromatin remodeling, histone modifications, and DNA methylation-how does it all fit together? J Cell Biochem. 2002;87(2):117-25. doi: 10.1002/jcb.10286. PubMed PMID: 12244565.
53. Smith ZD, Meissner A. DNA methylation: roles in mammalian development. Nature reviews Genetics. 2013;14(3):204-20. doi: 10.1038/nrg3354. PubMed PMID: 23400093.
54. Thurman RE, Rynes E, Humbert R, Vierstra J, Maurano MT, Haugen E, Sheffield NC, Stergachis AB, Wang H, Vernot B, Garg K, John S, Sandstrom R, Bates D, Boatman L, Canfield TK, Diegel M, Dunn D, Ebersol AK, Frum T, Giste E, Johnson AK, Johnson EM, Kutyavin T, Lajoie B, Lee BK, Lee K, London D, Lotakis D, Neph S, Neri F, Nguyen ED, Qu H, Reynolds AP, Roach V, Safi A, Sanchez ME, Sanyal A, Shafer A, Simon JM, Song L, Vong S, Weaver M, Yan Y, Zhang Z, Zhang Z, Lenhard B, Tewari M, Dorschner MO, Hansen RS, Navas PA, Stamatoyannopoulos G, Iyer VR, Lieb JD, Sunyaev SR, Akey JM, Sabo PJ, Kaul R, Furey TS, Dekker J, Crawford GE, Stamatoyannopoulos JA. The accessible chromatin landscape of the human genome. Nature. 2012;489(7414):75-82. doi: 10.1038/nature11232. PubMed PMID: 22955617; PMCID: PMC3721348.
55. Neph S, Stergachis AB, Reynolds A, Sandstrom R, Borenstein E, Stamatoyannopoulos JA. Circuitry and dynamics of human transcription factor regulatory networks. Cell. 2012;150(6):1274-86. doi: 10.1016/j.cell.2012.04.040. PubMed PMID: 22959076; PMCID: PMC3679407.
56. Maurano MT, Wang H, John S, Shafer A, Canfield T, Lee K, Stamatoyannopoulos JA. Role of DNA Methylation in Modulating Transcription Factor Occupancy. Cell Rep. 2015;12(7):1184-95. doi: 10.1016/j.celrep.2015.07.024. PubMed PMID: 26257180.

57. Stadler MB, Murr R, Burger L, Ivanek R, Lienert F, Scholer A, van Nimwegen E, Wirbelauer C, Oakeley EJ, Gaidatzis D, Tiwari VK, Schubeler D. DNA-binding factors shape the mouse methylome at distal regulatory regions. Nature. 2011;480(7378):490-5. doi: 10.1038/nature10716. PubMed PMID: 22170606.
58. Calo E, Wysocka J. Modification of enhancer chromatin: what, how, and why? Molecular cell. 2013;49(5):825-37. doi: 10.1016/j.molcel.2013.01.038. PubMed PMID: 23473601; PMCID: 3857148.
59. Bohmdorfer G, Wierzbicki AT. Control of Chromatin Structure by Long Noncoding RNA. Trends Cell Biol. 2015;25(10):623-32. doi: 10.1016/j.tcb.2015.07.002. PubMed PMID: 26410408; PMCID: PMC4584417.
60. Geisler S, Coller J. RNA in unexpected places: long non-coding RNA functions in diverse cellular contexts. Nat Rev Mol Cell Biol. 2013;14(11):699-712. doi: 10.1038/nrm3679. PubMed PMID: 24105322; PMCID: PMC4852478.
61. van Steensel B, Belmont AS. Lamina-Associated Domains: Links with Chromosome Architecture, Heterochromatin, and Gene Repression. Cell. 2017;169(5):780-91. doi: 10.1016/j.cell.2017.04.022. PubMed PMID: 28525751; PMCID: PMC5532494.
62. Ali T, Renkawitz R, Bartkuhn M. Insulators and domains of gene expression. Curr Opin Genet Dev. 2016;37:17-26. doi: 10.1016/j.gde.2015.11.009. PubMed PMID: 26802288.
63. Smallwood A, Ren B. Genome organization and long-range regulation of gene expression by enhancers. Curr Opin Cell Biol. 2013;25(3):387-94. doi: 10.1016/j.ceb.2013.02.005. PubMed PMID: 23465541; PMCID: PMC4180870.
64. Gonzalez-Sandoval A, Gasser SM. On TADs and LADs: Spatial Control Over Gene Expression. Trends Genet. 2016;32(8):485-95. doi: 10.1016/j.tig.2016.05.004. PubMed PMID: 27312344.
65. Clapier CR, Iwasa J, Cairns BR, Peterson CL. Mechanisms of action and regulation of ATP-dependent chromatin-remodelling complexes. Nat Rev Mol Cell Biol. 2017;18(7):407-22. doi: 10.1038/nrm.2017.26. PubMed PMID: 28512350.
66. Boeger H, Griesenbeck J, Strattan JS, Kornberg RD. Removal of promoter nucleosomes by disassembly rather than sliding in vivo. Molecular cell. 2004;14(5):667-73. doi: 10.1016/j.molcel.2004.05.013. PubMed PMID: 15175161.
67. Clapier CR, Cairns BR. The biology of chromatin remodeling complexes. Annu Rev Biochem. 2009;78:273-304. doi: 10.1146/annurev.biochem.77.062706.153223. PubMed PMID: 19355820.
68. Langst G, Manelyte L. Chromatin Remodelers: From Function to Dysfunction. Genes (Basel). 2015;6(2):299-324. doi: 10.3390/genes6020299. PubMed PMID: 26075616; PMCID: PMC4488666.
69. Lennartsson A, Ekwall K. Histone modification patterns and epigenetic codes. Biochim Biophys Acta. 2009;1790(9):863-8. doi: 10.1016/j.bbagen.2008.12.006. PubMed PMID: 19168116.
70. Albaugh BN, Arnold KM, Denu JM. KAT(ching) metabolism by the tail: insight into the links between lysine acetyltransferases and metabolism. Chembiochem. 2011;12(2):290-8. doi: 10.1002/cbic.201000438. PubMed PMID: 21243716; PMCID: PMC3327878.
71. Workman JL, Kingston RE. Alteration of nucleosome structure as a mechanism of transcriptional regulation. Annu Rev Biochem. 1998;67:545-79. doi: 10.1146/annurev.biochem.67.1.545. PubMed PMID: 9759497.

72. Brown CE, Lechner T, Howe L, Workman JL. The many HATs of transcription coactivators. Trends Biochem Sci. 2000;25(1):15-9. PubMed PMID: 10637607.
73. Delcuve GP, Khan DH, Davie JR. Roles of histone deacetylases in epigenetic regulation: emerging paradigms from studies with inhibitors. Clin Epigenetics. 2012;4(1):5. doi: 10.1186/1868-7083-4-5. PubMed PMID: 22414492; PMCID: PMC3320549.
74. Seto E, Yoshida M. Erasers of histone acetylation: the histone deacetylase enzymes. Cold Spring Harb Perspect Biol. 2014;6(4):a018713. doi: 10.1101/cshperspect.a018713. PubMed PMID: 24691964; PMCID: PMC3970420.
75. Eberharter A, Becker PB. Histone acetylation: a switch between repressive and permissive chromatin. Second in review series on chromatin dynamics. EMBO Rep. 2002;3(3):224-9. doi: 10.1093/embo-reports/kvf053. PubMed PMID: 11882541; PMCID: PMC1084017.
76. Seto E, Yoshida M. Erasers of Histone Acetylation: The Histone Deacetylase Enzymes. Csh Perspect Biol. 2014;6(4). doi: ARTN a018713 10.1101/cshperspect.a018713. PubMed PMID: WOS:000341575100006.
77. Fischle W, Wang YM, Allis CD. Histone and chromatin cross-talk. Current Opinion in Cell Biology. 2003;15(2):172-83. doi: 10.1016/S0955-0674(03)00013-9. PubMed PMID: WOS:000182183300008.
78. Caron C, Boyault C, Khochbin S. Regulatory cross-talk between lysine acetylation and ubiquitination: role in the control of protein stability. Bioessays. 2005;27(4):408-15. doi: 10.1002/bies.20210. PubMed PMID: WOS:000228041600008.
79. Shi YJ, Matson C, Lan F, Iwase S, Baba T, Shi Y. Regulation of LSD1 histone demethylase activity by its associated factors. Molecular cell. 2005;19(6):857-64. doi: 10.1016/j.molcel.2005.08.027. PubMed PMID: 16140033.
80. Segre CV, Chiocca S. Regulating the regulators: the post-translational code of class I HDAC1 and HDAC2. J Biomed Biotechnol. 2011;2011:690848. doi: 10.1155/2011/690848. PubMed PMID: 21197454; PMCID: PMC3004424.
81. Zhang X, Ozawa Y, Lee H, Wen YD, Tan TH, Wadzinski BE, Seto E. Histone deacetylase 3 (HDAC3) activity is regulated by interaction with protein serine/threonine phosphatase 4. Genes Dev. 2005;19(7):827-39. doi: 10.1101/gad.1286005. PubMed PMID: 15805470; PMCID: PMC1074320.
82. Black JC, Van Rechem C, Whetstine JR. Histone lysine methylation dynamics: establishment, regulation, and biological impact. Molecular cell. 2012;48(4):491-507. doi: 10.1016/j.molcel.2012.11.006. PubMed PMID: 23200123; PMCID: PMC3861058.
83. Lanouette S, Mongeon V, Figeys D, Couture JF. The functional diversity of protein lysine methylation. Mol Syst Biol. 2014;10:724. doi: 10.1002/msb.134974. PubMed PMID: 24714364; PMCID: PMC4023394.
84. Hyun K, Jeon J, Park K, Kim J. Writing, erasing and reading histone lysine methylations. Exp Mol Med. 2017;49(4):e324. doi: 10.1038/emm.2017.11. PubMed PMID: 28450737; PMCID: PMC6130214.
85. Rose NR, Klose RJ. Understanding the relationship between DNA methylation and histone lysine methylation. Biochim Biophys Acta. 2014;1839(12):1362-72. doi: 10.1016/j.bbagrm.2014.02.007. PubMed PMID: 24560929; PMCID: PMC4316174.
86. Di Lorenzo A, Bedford MT. Histone arginine methylation. FEBS Lett. 2011;585(13):2024-31. doi: 10.1016/j.febslet.2010.11.010. PubMed PMID: 21074527; PMCID: PMC3409563.

87. Cloos PA, Christensen J, Agger K, Helin K. Erasing the methyl mark: histone demethylases at the center of cellular differentiation and disease. Genes Dev. 2008;22(9):1115-40. doi: 10.1101/gad.1652908. PubMed PMID: 18451103; PMCID: PMC2732404.
88. Lin Y, Wu Y, Li J, Dong C, Ye X, Chi YI, Evers BM, Zhou BP. The SNAG domain of Snail1 functions as a molecular hook for recruiting lysine-specific demethylase 1. EMBO J. 2010;29(11):1803-16. doi: 10.1038/emboj.2010.63. PubMed PMID: 20389281; PMCID: PMC2885925.
89. Baron R, Binda C, Tortorici M, McCammon JA, Mattevi A. Molecular mimicry and ligand recognition in binding and catalysis by the histone demethylase LSD1-CoREST complex. Structure. 2011;19(2):212-20. doi: 10.1016/j.str.2011.01.001. PubMed PMID: 21300290; PMCID: PMC3059804.
90. Ahmed M, Streit A. Lsd1 interacts with cMyb to demethylate repressive histone marks and maintain inner ear progenitor identity. Development. 2018;145(4). doi: 10.1242/dev.160325. PubMed PMID: 29437831; PMCID: PMC5869009.
91. Speranzini V, Ciossani G, Marabelli C, Mattevi A. Probing the interaction of the p53 C-terminal domain to the histone demethylase LSD1. Arch Biochem Biophys. 2017;632:202-8. doi: 10.1016/j.abb.2017.07.021. PubMed PMID: 28784588.
92. McClellan D, Casey MJ, Bareyan D, Lucente H, Ours C, Velinder M, Singer J, Lone MD, Sun W, Coria Y, Mason C, Engel ME. Growth Factor Independence (GFI) 1B-mediated transcriptional repression and lineage allocation require Lysine Specific Demethylase (LSD)1-dependent recruitment of the BHC complex. Mol Cell Biol. 2019. Epub 2019/04/17. doi: 10.1128/mcb.00020-19. PubMed PMID: 30988160.
93. Moore LD, Le T, Fan G. DNA methylation and its basic function. Neuropsychopharmacology. 2013;38(1):23-38. doi: 10.1038/npp.2012.112. PubMed PMID: 22781841; PMCID: PMC3521964.
94. Lister R, Pelizzola M, Dowen RH, Hawkins RD, Hon G, Tonti-Filippini J, Nery JR, Lee L, Ye Z, Ngo QM, Edsall L, Antosiewicz-Bourget J, Stewart R, Ruotti V, Millar AH, Thomson JA, Ren B, Ecker JR. Human DNA methylomes at base resolution show widespread epigenomic differences. Nature. 2009;462(7271):315-22. doi: 10.1038/nature08514. PubMed PMID: 19829295; PMCID: PMC2857523.
95. Luo C, Hajkova P, Ecker JR. Dynamic DNA methylation: In the right place at the right time. Science. 2018;361(6409):1336-40. doi: 10.1126/science.aat6806. PubMed PMID: 30262495; PMCID: PMC6197482.
96. Jones PA. Functions of DNA methylation: islands, start sites, gene bodies and beyond. Nature reviews Genetics. 2012;13(7):484-92. doi: 10.1038/nrg3230. PubMed PMID: 22641018.
97. Edwards JR, Yarychkivska O, Boulard M, Bestor TH. DNA methylation and DNA methyltransferases. Epigenetics Chromatin. 2017;10:23. doi: 10.1186/s13072-017-0130-8. PubMed PMID: 28503201; PMCID: PMC5422929.
98. Ziller MJ, Gu H, Muller F, Donaghey J, Tsai LT, Kohlbacher O, De Jager PL, Rosen ED, Bennett DA, Bernstein BE, Gnirke A, Meissner A. Charting a dynamic DNA methylation landscape of the human genome. Nature. 2013;500(7463):477-81. doi: 10.1038/nature12433. PubMed PMID: 23925113; PMCID: PMC3821869.

99. Schultz MD, He Y, Whitaker JW, Hariharan M, Mukamel EA, Leung D, Rajagopal N, Nery JR, Urich MA, Chen H, Lin S, Lin Y, Jung I, Schmitt AD, Selvaraj S, Ren B, Sejnowski TJ, Wang W, Ecker JR. Corrigendum: Human body epigenome maps reveal noncanonical DNA methylation variation. Nature. 2016;530(7589):242. doi: 10.1038/nature16179. PubMed PMID: 26605523.
100. Luo C, Keown CL, Kurihara L, Zhou J, He Y, Li J, Castanon R, Lucero J, Nery JR, Sandoval JP, Bui B, Sejnowski TJ, Harkins TT, Mukamel EA, Behrens MM, Ecker JR. Single-cell methylomes identify neuronal subtypes and regulatory elements in mammalian cortex. Science. 2017;357(6351):600-4. doi: 10.1126/science.aan3351. PubMed PMID: 28798132; PMCID: PMC5570439.
101. Guo X, Wang L, Li J, Ding Z, Xiao J, Yin X, He S, Shi P, Dong L, Li G, Tian C, Wang J, Cong Y, Xu Y. Structural insight into autoinhibition and histone H3-induced activation of DNMT3A. Nature. 2015;517(7536):640-4. doi: 10.1038/nature13899. PubMed PMID: 25383530.
102. Petell CJ, Alabdi L, He M, San Miguel P, Rose R, Gowher H. An epigenetic switch regulates de novo DNA methylation at a subset of pluripotency gene enhancers during embryonic stem cell differentiation. Nucleic acids research. 2016;44(16):7605-17. doi: 10.1093/nar/gkw426. PubMed PMID: 27179026; PMCID: 5027477.
103. Wapinski OL, Vierbuchen T, Qu K, Lee QY, Chanda S, Fuentes DR, Giresi PG, Ng YH, Marro S, Neff NF, Drechsel D, Martynoga B, Castro DS, Webb AE, Sudhof TC, Brunet A, Guillemot F, Chang HY, Wernig M. Hierarchical mechanisms for direct reprogramming of fibroblasts to neurons. Cell. 2013;155(3):621-35. doi: 10.1016/j.cell.2013.09.028. PubMed PMID: 24243019; PMCID: PMC3871197.
104. Baubec T, Colombo DF, Wirbelauer C, Schmidt J, Burger L, Krebs AR, Akalin A, Schubeler D. Genomic profiling of DNA methyltransferases reveals a role for DNMT3B in genic methylation. Nature. 2015;520(7546):243-7. doi: 10.1038/nature14176. PubMed PMID: 25607372.
105. Morselli M, Pastor WA, Montanini B, Nee K, Ferrari R, Fu K, Bonora G, Rubbi L, Clark AT, Ottonello S, Jacobsen SE, Pellegrini M. In vivo targeting of de novo DNA methylation by histone modifications in yeast and mouse. Elife. 2015;4:e06205. doi: 10.7554/eLife.06205. PubMed PMID: 25848745; PMCID: PMC4412109.
106. Wolf SF, Jolly DJ, Lunnen KD, Friedmann T, Migeon BR. Methylation of the hypoxanthine phosphoribosyltransferase locus on the human X chromosome: implications for X-chromosome inactivation. Proc Natl Acad Sci U S A. 1984;81(9):2806-10. doi: 10.1073/pnas.81.9.2806. PubMed PMID: 6585829; PMCID: PMC345159.
107. Wu H, Coskun V, Tao J, Xie W, Ge W, Yoshikawa K, Li E, Zhang Y, Sun YE. Dnmt3a-dependent nonpromoter DNA methylation facilitates transcription of neurogenic genes. Science. 2010;329(5990):444-8. doi: 10.1126/science.1190485. PubMed PMID: 20651149; PMCID: PMC3539760.
108. Neri F, Rapelli S, Krepelova A, Incarnato D, Parlato C, Basile G, Maldotti M, Anselmi F, Oliviero S. Intragenic DNA methylation prevents spurious transcription initiation. Nature. 2017;543(7643):72-7. doi: 10.1038/nature21373. PubMed PMID: 28225755.
109. Teissandier A, Bourc'his D. Gene body DNA methylation conspires with H3K36me3 to preclude aberrant transcription. EMBO J. 2017;36(11):1471-3. doi: 10.15252/embj.201796812. PubMed PMID: 28442531; PMCID: PMC5452023.

110. Hermann A, Goyal R, Jeltsch A. The Dnmt1 DNA-(cytosine-C5)-methyltransferase methylates DNA processively with high preference for hemimethylated target sites. J Biol Chem. 2004;279(46):48350-9. doi: 10.1074/jbc.M403427200. PubMed PMID: 15339928.
111. Pradhan S, Bacolla A, Wells RD, Roberts RJ. Recombinant human DNA (cytosine-5) methyltransferase. I. Expression, purification, and comparison of de novo and maintenance methylation. J Biol Chem. 1999;274(46):33002-10. doi: 10.1074/jbc.274.46.33002. PubMed PMID: 10551868.
112. Hervouet E, Peixoto P, Delage-Mourroux R, Boyer-Guittaut M, Cartron PF. Specific or not specific recruitment of DNMTs for DNA methylation, an epigenetic dilemma. Clin Epigenetics. 2018;10:17. doi: 10.1186/s13148-018-0450-y. PubMed PMID: 29449903; PMCID: PMC5807744.
113. Vertino PM, Sekowski JA, Coll JM, Applegren N, Han S, Hickey RJ, Malkas LH. DNMT1 is a component of a multiprotein DNA replication complex. Cell Cycle. 2002;1(6):416-23. doi: 10.4161/cc.1.6.270. PubMed PMID: 12548018.
114. Jones PA, Liang G. Rethinking how DNA methylation patterns are maintained. Nature reviews Genetics. 2009;10(11):805-11. doi: 10.1038/nrg2651. PubMed PMID: 19789556; PMCID: PMC2848124.
115. Schubeler D. Function and information content of DNA methylation. Nature. 2015;517(7534):321-6. doi: 10.1038/nature14192. PubMed PMID: 25592537.
116. Monk M, Boubelik M, Lehnert S. Temporal and regional changes in DNA methylation in the embryonic, extraembryonic and germ cell lineages during mouse embryo development. Development. 1987;99(3):371-82. PubMed PMID: 3653008.
117. Kafri T, Ariel M, Brandeis M, Shemer R, Urven L, McCarrey J, Cedar H, Razin A. Developmental pattern of gene-specific DNA methylation in the mouse embryo and germ line. Genes Dev. 1992;6(5):705-14. doi: 10.1101/gad.6.5.705. PubMed PMID: 1577268.
118. Cedar H, Bergman Y. Programming of DNA methylation patterns. Annu Rev Biochem. 2012;81:97-117. doi: 10.1146/annurev-biochem-052610-091920. PubMed PMID: 22404632.
119. Chaillet JR, Vogt TF, Beier DR, Leder P. Parental-specific methylation of an imprinted transgene is established during gametogenesis and progressively changes during embryogenesis. Cell. 1991;66(1):77-83. PubMed PMID: 1649008.
120. Guo F, Li XL, Liang D, Li T, Zhu P, Guo HS, Wu XL, Wen L, Gu TP, Hu BQ, Walsh CP, Li JS, Tang FC, Xu GL. Active and Passive Demethylation of Male and Female Pronuclear DNA in the Mammalian Zygote. Cell Stem Cell. 2014;15(4):447-58. doi: 10.1016/j.stem.2014.08.003. PubMed PMID: WOS:000343235800011.
121. Wu H, Zhang Y. Reversing DNA methylation: mechanisms, genomics, and biological functions. Cell. 2014;156(1-2):45-68. doi: 10.1016/j.cell.2013.12.019. PubMed PMID: 24439369; PMCID: PMC3938284.
122. Feinberg AP, Tycko B. The history of cancer epigenetics. Nat Rev Cancer. 2004;4(2):143-53. doi: 10.1038/nrc1279. PubMed PMID: 14732866.
123. Wysocka J, Swigut T, Xiao H, Milne TA, Kwon SY, Landry J, Kauer M, Tackett AJ, Chait BT, Badenhorst P, Wu C, Allis CD. A PHD finger of NURF couples histone H3 lysine 4 trimethylation with chromatin remodelling. Nature. 2006;442(7098):86-90. doi: 10.1038/nature04815. PubMed PMID: 16728976.

124. Esteller M. Epigenetics in cancer. N Engl J Med. 2008;358(11):1148-59. doi: 10.1056/NEJMra072067. PubMed PMID: 18337604.
125. Muntean AG, Hess JL. Epigenetic dysregulation in cancer. Am J Pathol. 2009;175(4):1353-61. doi: 10.2353/ajpath.2009.081142. PubMed PMID: 19717641; PMCID: PMC2751531.
126. Ooi SK, Qiu C, Bernstein E, Li K, Jia D, Yang Z, Erdjument-Bromage H, Tempst P, Lin SP, Allis CD, Cheng X, Bestor TH. DNMT3L connects unmethylated lysine 4 of histone H3 to de novo methylation of DNA. Nature. 2007;448(7154):714-7. doi: 10.1038/nature05987. PubMed PMID: 17687327; PMCID: PMC2650820.
127. Kurdyukov S, Bullock M. DNA Methylation Analysis: Choosing the Right Method. Biology (Basel). 2016;5(1). doi: 10.3390/biology5010003. PubMed PMID: 26751487; PMCID: PMC4810160.
128. Karimi M, Johansson S, Stach D, Corcoran M, Grander D, Schalling M, Bakalkin G, Lyko F, Larsson C, Ekstrom TJ. LUMA (LUminometric Methylation Assay)--a high throughput method to the analysis of genomic DNA methylation. Exp Cell Res. 2006;312(11):1989-95. doi: 10.1016/j.yexcr.2006.03.006. PubMed PMID: 16624287.
129. Wang S, Lv J, Zhang L, Dou J, Sun Y, Li X, Fu X, Dou H, Mao J, Hu X, Bao Z. MethylRAD: a simple and scalable method for genome-wide DNA methylation profiling using methylation-dependent restriction enzymes. Open Biol. 2015;5(11). doi: 10.1098/rsob.150130. PubMed PMID: 26581575; PMCID: PMC4680569.
130. Song L, James SR, Kazim L, Karpf AR. Specific method for the determination of genomic DNA methylation by liquid chromatography-electrospray ionization tandem mass spectrometry. Anal Chem. 2005;77(2):504-10. doi: 10.1021/ac0489420. PubMed PMID: 15649046.
131. Kuo KC, McCune RA, Gehrke CW, Midgett R, Ehrlich M. Quantitative reversed-phase high performance liquid chromatographic determination of major and modified deoxyribonucleosides in DNA. Nucleic acids research. 1980;8(20):4763-76. doi: 10.1093/nar/8.20.4763. PubMed PMID: 7003544; PMCID: PMC324386.
132. Petell CJ, Loiseau G, Gandy R, Pradhan S, Gowher H. A refined DNA methylation detection method using MspJI coupled quantitative PCR. Anal Biochem. 2017;533:1-9. doi: 10.1016/j.ab.2017.06.006. PubMed PMID: 28624296; PMCID: PMC5972016.
133. Li P, Demirci F, Mahalingam G, Demirci C, Nakano M, Meyers BC. An integrated workflow for DNA methylation analysis. J Genet Genomics. 2013;40(5):249-60. doi: 10.1016/j.jgg.2013.03.010. PubMed PMID: 23706300.
134. Bhattacharjee R, Moriam S, Umer M, Nguyen NT, Shiddiky MJA. DNA methylation detection: recent developments in bisulfite free electrochemical and optical approaches. Analyst. 2018;143(20):4802-18. doi: 10.1039/c8an01348a. PubMed PMID: 30226502.
135. Poh WJ, Wee CP, Gao Z. DNA Methyltransferase Activity Assays: Advances and Challenges. Theranostics. 2016;6(3):369-91. doi: 10.7150/thno.13438. PubMed PMID: 26909112; PMCID: PMC4737724.
136. Kim SJ, Zhao H, Hardikar S, Singh AK, Goodell MA, Chen T. A DNMT3A mutation common in AML exhibits dominant-negative effects in murine ES cells. Blood. 2013;122(25):4086-9. doi: 10.1182/blood-2013-02-483487. PubMed PMID: 24167195; PMCID: 3952368.

137. Poh WJ, Wee CPP, Gao ZQ. DNA Methyltransferase Activity Assays: Advances and Challenges. Theranostics. 2016;6(3):369-91. doi: 10.7150/thno.13438. PubMed PMID: WOS:000377797200007.
138. Hemeon I, Gutierrez JA, Ho MC, Schramm VL. Characterizing DNA Methyltransferases With An Ultrasensitive Luciferase-Linked Continuous Assay. Analytical Chemistry. 2011;83(12):4996-5004. doi: 10.1021/ac200816m. PubMed PMID: WOS:000291499800056.
139. Okano M, Bell DW, Haber DA, Li E. DNA methyltransferases Dnmt3a and Dnmt3b are essential for de novo methylation and mammalian development. Cell. 1999;99(3):247-57. doi: Doi 10.1016/S0092-8674(00)81656-6. PubMed PMID: WOS:000083440600003.
140. Ueda Y, Okano M, Williams C, Chen TP, Georgopoulos K, Li E. Roles for Dnmt3b in mammalian development: a mouse model for the ICF syndrome. Development. 2006;133(6):1183-92. doi: 10.1242/dev.02293. PubMed PMID: WOS:000236676900019.
141. Kaneda M, Okano M, Hata K, Sado T, Tsujimoto N, Li E, Sasaki H. Essential role for de novo DNA methyltransferase Dnmt3a in paternal and maternal imprinting. Nature. 2004;429(6994):900-3. doi: 10.1038/nature02633. PubMed PMID: WOS:000222213000047.
142. Bogdanovic O, Lister R. Of Mice and Man: Differential DNMT Dependence in Mammalian ESCs. Cell Stem Cell. 2015;16(5):459-60. doi: 10.1016/j.stem.2015.04.009. PubMed PMID: WOS:000354188600006.
143. Takebayashi S, Tamura T, Matsuoka C, Okano M. Major and essential role for the DNA methylation mark in mouse embryogenesis and stable association of DNMT1 with newly replicated regions. Molecular and Cellular Biology. 2007;27(23):8243-58. doi: 10.1128/Mcb.00899-07. PubMed PMID: WOS:000251527100018.
144. Li HW, Rauch T, Chen ZX, Szabo PE, Riggs AD, Pfeifer GP. The histone methyltransferase SETDB1 and the DNA methyltransferase DNMT3A interact directly and localize to promoters silenced in cancer cells. Journal of Biological Chemistry. 2006;281(28):19489-500. doi: 10.1074/jbc.M513249200. PubMed PMID: WOS:000238847000064.
145. Jin BL, Ernst J, Tiedemann RL, Xu HY, Sureshchandra S, Kellis M, Dalton S, Liu C, Choi JH, Robertson KD. Linking DNA Methyltransferases to Epigenetic Marks and Nucleosome Structure Genome-wide in Human Tumor Cells. Cell Reports. 2012;2(5):1411-24. doi: 10.1016/j.celrep.2012.10.017. PubMed PMID: WOS:000314457700034.
146. Zhu Q, Stoger R, Alberio R. A Lexicon of DNA Modifications: Their Roles in Embryo Development and the Germline. Front Cell Dev Biol. 2018;6:24. doi: 10.3389/fcell.2018.00024. PubMed PMID: 29637072; PMCID: PMC5880922.
147. Zeng Y, Chen T. DNA Methylation Reprogramming during Mammalian Development. Genes (Basel). 2019;10(4). doi: 10.3390/genes10040257. PubMed PMID: 30934924; PMCID: PMC6523607.
148. Auclair G, Guibert S, Bender A, Weber M. Ontogeny of CpG island methylation and specificity of DNMT3 methyltransferases during embryonic development in the mouse. Genome Biol. 2014;15(12):545. doi: 10.1186/s13059-014-0545-5. PubMed PMID: 25476147; PMCID: PMC4295324.

149. Kelsey G, Stegle O, Reik W. Single-cell epigenomics: Recording the past and predicting the future. Science. 2017;358(6359):69-75. doi: 10.1126/science.aan6826. PubMed PMID: 28983045.
150. Gu C, Liu S, Wu Q, Zhang L, Guo F. Integrative single-cell analysis of transcriptome, DNA methylome and chromatin accessibility in mouse oocytes. Cell Res. 2019;29(2):110-23. doi: 10.1038/s41422-018-0125-4. PubMed PMID: 30560925; PMCID: PMC6355938.
151. Clark SJ, Argelaguet R, Kapourani CA, Stubbs TM, Lee HJ, Alda-Catalinas C, Krueger F, Sanguinetti G, Kelsey G, Marioni JC, Stegle O, Reik W. scNMT-seq enables joint profiling of chromatin accessibility DNA methylation and transcription in single cells. Nat Commun. 2018;9(1):781. doi: 10.1038/s41467-018-03149-4. PubMed PMID: 29472610; PMCID: PMC5823944.
152. Luo C, Rivkin A, Zhou J, Sandoval JP, Kurihara L, Lucero J, Castanon R, Nery JR, Pinto-Duarte A, Bui B, Fitzpatrick C, O'Connor C, Ruga S, Van Eden ME, Davis DA, Mash DC, Behrens MM, Ecker JR. Robust single-cell DNA methylome profiling with snmC-seq2. Nat Commun. 2018;9(1):3824. doi: 10.1038/s41467-018-06355-2. PubMed PMID: 30237449; PMCID: PMC6147798.
153. Hui T, Cao Q, Wegrzyn-Woltosz J, O'Neill K, Hammond CA, Knapp D, Laks E, Moksa M, Aparicio S, Eaves CJ, Karsan A, Hirst M. High-Resolution Single-Cell DNA Methylation Measurements Reveal Epigenetically Distinct Hematopoietic Stem Cell Subpopulations. Stem Cell Reports. 2018;11(2):578-92. doi: 10.1016/j.stemcr.2018.07.003. PubMed PMID: 30078558; PMCID: PMC6093082.
154. Song Q, Decato B, Hong EE, Zhou M, Fang F, Qu J, Garvin T, Kessler M, Zhou J, Smith AD. A reference methylome database and analysis pipeline to facilitate integrative and comparative epigenomics. PLoS One. 2013;8(12):e81148. doi: 10.1371/journal.pone.0081148. PubMed PMID: 24324667; PMCID: PMC3855694.
155. Stepper P, Kungulovski G, Jurkowska RZ, Chandra T, Krueger F, Reinhardt R, Reik W, Jeltsch A, Jurkowski TP. Efficient targeted DNA methylation with chimeric dCas9-Dnmt3a-Dnmt3L methyltransferase. Nucleic acids research. 2017;45(4):1703-13. doi: 10.1093/nar/gkw1112. PubMed PMID: 27899645; PMCID: PMC5389507.
156. Bernstein DL, Le Lay JE, Ruano EG, Kaestner KH. TALE-mediated epigenetic suppression of CDKN2A increases replication in human fibroblasts. J Clin Invest. 2015;125(5):1998-2006. doi: 10.1172/JCI77321. PubMed PMID: 25866970; PMCID: PMC4463192.
157. Siddique AN, Nunna S, Rajavelu A, Zhang Y, Jurkowska RZ, Reinhardt R, Rots MG, Ragozin S, Jurkowski TP, Jeltsch A. Targeted methylation and gene silencing of VEGF-A in human cells by using a designed Dnmt3a-Dnmt3L single-chain fusion protein with increased DNA methylation activity. J Mol Biol. 2013;425(3):479-91. doi: 10.1016/j.jmb.2012.11.038. PubMed PMID: 23220192.
158. Galonska C, Charlton J, Mattei AL, Donaghey J, Clement K, Gu H, Mohammad AW, Stamenova EK, Cacchiarelli D, Klages S, Timmermann B, Cantz T, Scholer HR, Gnirke A, Ziller MJ, Meissner A. Genome-wide tracking of dCas9-methyltransferase footprints. Nat Commun. 2018;9(1):597. doi: 10.1038/s41467-017-02708-5. PubMed PMID: 29426832; PMCID: PMC5807365.

159. Xie N, Zhou Y, Sun Q, Tang B. Novel Epigenetic Techniques Provided by the CRISPR/Cas9 System. Stem Cells Int. 2018;2018:7834175. doi: 10.1155/2018/7834175. PubMed PMID: 30123293; PMCID: PMC6079388.
160. Pflueger C, Tan D, Swain T, Nguyen T, Pflueger J, Nefzger C, Polo JM, Ford E, Lister R. A modular dCas9-SunTag DNMT3A epigenome editing system overcomes pervasive off-target activity of direct fusion dCas9-DNMT3A constructs. Genome Res. 2018;28(8):1193-206. doi: 10.1101/gr.233049.117. PubMed PMID: 29907613; PMCID: PMC6071642.
161. van den Berg DL, Snoek T, Mullin NP, Yates A, Bezstarosti K, Demmers J, Chambers I, Poot RA. An Oct4-centered protein interaction network in embryonic stem cells. Cell Stem Cell. 2010;6(4):369-81. doi: 10.1016/j.stem.2010.02.014. PubMed PMID: 20362541; PMCID: PMC2860243.
162. Pardo M, Lang B, Yu L, Prosser H, Bradley A, Babu MM, Choudhary J. An expanded Oct4 interaction network: implications for stem cell biology, development, and disease. Cell Stem Cell. 2010;6(4):382-95. doi: 10.1016/j.stem.2010.03.004. PubMed PMID: 20362542; PMCID: PMC2860244.
163. Gowher H, Jeltsch A. Mechanism of inhibition of DNA methyltransferases by cytidine analogs in cancer therapy. Cancer biology & therapy. 2004;3(11):1062-8. Epub 2004/11/13. PubMed PMID: 15539938.
164. Wongpaiboonwattana W, Stavridis MP. Neural differentiation of mouse embryonic stem cells in serum-free monolayer culture. J Vis Exp. 2015(99):e52823. doi: 10.3791/52823. PubMed PMID: 26066640; PMCID: PMC4542683.
165. Iglesias JM, Gumuzio J, Martin AG. Linking Pluripotency Reprogramming and Cancer. Stem Cells Transl Med. 2017;6(2):335-9. doi: 10.5966/sctm.2015-0225. PubMed PMID: 28191771; PMCID: PMC5442824.
166. Andrews PW, Matin MM, Bahrami AR, Damjanov I, Gokhale P, Draper JS. Embryonic stem (ES) cells and embryonal carcinoma (EC) cells: Opposite sides of the same coin. Biochem Soc T. 2005;33:1526-30. doi: Doi 10.1042/Bst0331526. PubMed PMID: WOS:000233930800076.
167. Banerji J, Rusconi S, Schaffner W. Expression of a beta-globin gene is enhanced by remote SV40 DNA sequences. Cell. 1981;27(2 Pt 1):299-308. Epub 1981/12/01. PubMed PMID: 6277502.
168. Bulger M, Groudine M. Functional and mechanistic diversity of distal transcription enhancers. Cell. 2011;144(3):327-39.
169. Ong C-T, Corces VG. Enhancer function: new insights into the regulation of tissue-specific gene expression. Nature Reviews Genetics. 2011;12(4):283.
170. Plank JL, Dean A. Enhancer function: mechanistic and genome-wide insights come together. Molecular cell. 2014;55(1):5-14. Epub 2014/07/06. doi: 10.1016/j.molcel.2014.06.015. PubMed PMID: 24996062.
171. Heinz S, Romanoski CE, Benner C, Glass CK. The selection and function of cell type-specific enhancers. Nat Rev Mol Cell Biol. 2015;16(3):144-54. Epub 2015/02/05. doi: 10.1038/nrm3949. PubMed PMID: 25650801; PMCID: 4517609.
172. Ernst J, Kellis M. Discovery and characterization of chromatin states for systematic annotation of the human genome. Nat Biotechnol. 2010;28(8):817.

173. Ernst J, Kheradpour P, Mikkelsen TS, Shoresh N, Ward LD, Epstein CB, Zhang X, Wang L, Issner R, Coyne M. Mapping and analysis of chromatin state dynamics in nine human cell types. Nature. 2011;473(7345):43.
174. Heintzman ND, Stuart RK, Hon G, Fu Y, Ching CW, Hawkins RD, Barrera LO, Van Calcar S, Qu C, Ching KA. Distinct and predictive chromatin signatures of transcriptional promoters and enhancers in the human genome. Nat Genet. 2007;39(3):311.
175. Creyghton MP, Cheng AW, Welstead GG, Kooistra T, Carey BW, Steine EJ, Hanna J, Lodato MA, Frampton GM, Sharp PA. Histone H3K27ac separates active from poised enhancers and predicts developmental state. Proceedings of the National Academy of Sciences. 2010;107(50):21931-6.
176. Heinz S, Benner C, Spann N, Bertolino E, Lin YC, Laslo P, Cheng JX, Murre C, Singh H, Glass CK. Simple combinations of lineage-determining transcription factors prime cis-regulatory elements required for macrophage and B cell identities. Molecular cell. 2010;38(4):576-89.
177. Rada-Iglesias A, Bajpai R, Swigut T, Brugmann SA, Flynn RA, Wysocka J. A unique chromatin signature uncovers early developmental enhancers in humans. Nature. 2011;470(7333):279-83. doi: 10.1038/nature09692. PubMed PMID: 21160473; PMCID: PMC4445674.
178. Zentner GE, Tesar PJ, Scacheri PC. Epigenetic signatures distinguish multiple classes of enhancers with distinct cellular functions. Genome Res. 2011.
179. Whyte WA, Bilodeau S, Orlando DA, Hoke HA, Frampton GM, Foster CT, Cowley SM, Young RA. Enhancer decommissioning by LSD1 during embryonic stem cell differentiation. Nature. 2012;482(7384):221-5. doi: 10.1038/nature10805. PubMed PMID: WOS:000299994100039.
180. Mendenhall EM, Williamson KE, Reyon D, Zou JY, Ram O, Joung JK, Bernstein BE. Locus-specific editing of histone modifications at endogenous enhancers. Nat Biotechnol. 2013;31(12):1133-6. Epub 2013/09/10. doi: 10.1038/nbt.2701. PubMed PMID: 24013198; PMCID: 3858395.
181. Metzger E, Wissmann M, Yin N, Muller JM, Schneider R, Peters AH, Gunther T, Buettner R, Schule R. LSD1 demethylates repressive histone marks to promote androgen-receptor-dependent transcription. Nature. 2005;437(7057):436-9. doi: 10.1038/nature04020. PubMed PMID: 16079795.
182. Zibetti C, Adamo A, Binda C, Forneris F, Toffolo E, Verpelli C, Ginelli E, Mattevi A, Sala C, Battaglioli E. Alternative splicing of the histone demethylase LSD1/KDM1 contributes to the modulation of neurite morphogenesis in the mammalian nervous system. J Neurosci. 2010;30(7):2521-32. doi: 10.1523/JNEUROSCI.5500-09.2010. PubMed PMID: 20164337.
183. Laurent B, Ruitu L, Murn J, Hempel K, Ferrao R, Xiang Y, Liu S, Garcia BA, Wu H, Wu F, Steen H, Shi Y. A specific LSD1/KDM1A isoform regulates neuronal differentiation through H3K9 demethylation. Molecular cell. 2015;57(6):957-70. doi: 10.1016/j.molcel.2015.01.010. PubMed PMID: 25684206; PMCID: PMC4369399.

184. Wang J, Telese F, Tan Y, Li W, Jin C, He X, Basnet H, Ma Q, Merkurjev D, Zhu X, Liu Z, Zhang J, Ohgi K, Taylor H, White RR, Tazearslan C, Suh Y, Macfarlan TS, Pfaff SL, Rosenfeld MG. LSD1n is an H4K20 demethylase regulating memory formation via transcriptional elongation control. Nat Neurosci. 2015;18(9):1256-64. doi: 10.1038/nn.4069. PubMed PMID: 26214369; PMCID: PMC4625987.
185. Carnesecchi J, Forcet C, Zhang L, Tribollet V, Barenton B, Boudra R, Cerutti C, Billas IM, Serandour AA, Carroll JS, Beaudoin C, Vanacker JM. ERRalpha induces H3K9 demethylation by LSD1 to promote cell invasion. Proc Natl Acad Sci U S A. 2017;114(15):3909-14. doi: 10.1073/pnas.1614664114. PubMed PMID: 28348226; PMCID: PMC5393192.
186. Vinyard ME, Su C, Siegenfeld AP, Waterbury AL, Freedy AM, Gosavi PM, Park Y, Kwan EE, Senzer BD, Doench JG, Bauer DE, Pinello L, Liau BB. CRISPR-suppressor scanning reveals a nonenzymatic role of LSD1 in AML. Nature chemical biology. 2019;15(5):529-39. Epub 2019/04/18. doi: 10.1038/s41589-019-0263-0. PubMed PMID: 30992567.
187. Liu A, Yu X, Liu S. Pluripotency transcription factors and cancer stem cells: small genes make a big difference. Chinese journal of cancer. 2013;32(9):483-7. doi: 10.5732/cjc.012.10282. PubMed PMID: 23419197; PMCID: 3845564.
188. Zhang XM, Lu F, Wang J, Yin F, Xu ZS, Qi DD, Wu XH, Cao YW, Liang WH, Liu YQ, Sun H, Ye T, Zhang H. Pluripotent Stem Cell Protein Sox2 Confers Sensitivity to LSD1 Inhibition in Cancer Cells. Cell Reports. 2013;5(2):445-57. doi: 10.1016/j.celrep.2013.09.018. PubMed PMID: WOS:000328263000017.
189. Feske S. Calcium signalling in lymphocyte activation and disease. Nature reviews Immunology. 2007;7(9):690-702. Epub 2007/08/19. doi: 10.1038/nri2152. PubMed PMID: 17703229.
190. Ben-Porath I, Thomson MW, Carey VJ, Ge R, Bell GW, Regev A, Weinberg RA. An embryonic stem cell-like gene expression signature in poorly differentiated aggressive human tumors. Nat Genet. 2008;40(5):499-507. doi: 10.1038/ng.127. PubMed PMID: 18443585; PMCID: 2912221.
191. Linn DE, Yang X, Sun F, Xie Y, Chen H, Jiang R, Chumsri S, Burger AM, Qiu Y. A Role for OCT4 in Tumor Initiation of Drug-Resistant Prostate Cancer Cells. Genes & cancer. 2010;1(9):908-16. Epub 2011/07/23. doi: 10.1177/1947601910388271. PubMed PMID: 21779471; PMCID: 3092260.
192. Peng S, Maihle NJ, Huang Y. Pluripotency factors Lin28 and Oct4 identify a sub-population of stem cell-like cells in ovarian cancer. Oncogene. 2010;29(14):2153-9. Epub 2010/01/27. doi: 10.1038/onc.2009.500. PubMed PMID: 20101213.
193. Wen J, Park JY, Park KH, Chung HW, Bang S, Park SW, Song SY. Oct4 and Nanog expression is associated with early stages of pancreatic carcinogenesis. Pancreas. 2010;39(5):622-6. Epub 2010/02/23. doi: 10.1097/MPA.0b013e3181c75f5e. PubMed PMID: 20173672.
194. Jeter CR, Liu B, Liu X, Chen X, Liu C, Calhoun-Davis T, Repass J, Zaehres H, Shen JJ, Tang DG. NANOG promotes cancer stem cell characteristics and prostate cancer resistance to androgen deprivation. Oncogene. 2011;30(36):3833-45. Epub 2011/04/19. doi: 10.1038/onc.2011.114. PubMed PMID: 21499299; PMCID: 3140601.

195. Kumar SM, Liu S, Lu H, Zhang H, Zhang PJ, Gimotty PA, Guerra M, Guo W, Xu X. Acquired cancer stem cell phenotypes through Oct4-mediated dedifferentiation. Oncogene. 2012;31(47):4898-911. Epub 2012/01/31. doi: 10.1038/onc.2011.656. PubMed PMID: 22286766; PMCID: 3343184.
196. Mak VC, Siu MK, Wong OG, Chan KK, Ngan HY, Cheung AN. Dysregulated stemness-related genes in gynecological malignancies. Histology and histopathology. 2012;27(9):1121-30. Epub 2012/07/19. PubMed PMID: 22806899.
197. Wang YD, Cai N, Wu XL, Cao HZ, Xie LL, Zheng PS. OCT4 promotes tumorigenesis and inhibits apoptosis of cervical cancer cells by miR-125b/BAK1 pathway. Cell death & disease. 2013;4:e760. Epub 2013/08/10. doi: 10.1038/cddis.2013.272. PubMed PMID: 23928699; PMCID: 3763434.
198. Gwak JM, Kim M, Kim HJ, Jang MH, Park SY. Expression of embryonal stem cell transcription factors in breast cancer: Oct4 as an indicator for poor clinical outcome and tamoxifen resistance. Oncotarget. 2017;8(22):36305-18. doi: 10.18632/oncotarget.16750. PubMed PMID: 28422735; PMCID: PMC5482656.
199. Yang F, Zhang J, Yang H. OCT4, SOX2, and NANOG positive expression correlates with poor differentiation, advanced disease stages, and worse overall survival in HER2(+) breast cancer patients. Onco Targets Ther. 2018;11:7873-81. doi: 10.2147/OTT.S173522. PubMed PMID: 30464534; PMCID: PMC6228048.
200. de The H. Differentiation therapy revisited. Nat Rev Cancer. 2018;18(2):117-27. doi: 10.1038/nrc.2017.103. PubMed PMID: 29192213.
201. Alonso A, Breuer B, Steuer B, Fischer J. The F9-EC cell line as a model for the analysis of differentiation. Int J Dev Biol. 1991;35(4):389-97. PubMed PMID: 1666294.
202. Zhu B, Liu T, Hu X, Wang G. Developmental toxicity of 3,4-dichloroaniline on rare minnow (Gobiocypris rarus) embryos and larvae. Chemosphere. 2013;90(3):1132-9. Epub 2012/10/11. doi: 10.1016/j.chemosphere.2012.09.021. PubMed PMID: 23047119.
203. Han JW, Gurunathan S, Choi YJ, Kim JH. Dual functions of silver nanoparticles in F9 teratocarcinoma stem cells, a suitable model for evaluating cytotoxicity- and differentiation-mediated cancer therapy. Int J Nanomed. 2017;12:7529-49. doi: 10.2147/Ijn.S145147. PubMed PMID: WOS:000413034800003.
204. Maruyama M, Ichisaka T, Nakagawa M, Yamanaka S. Differential roles for Sox15 and Sox2 in transcriptional control in mouse embryonic stem cells. J Biol Chem. 2005;280(26):24371-9. doi: 10.1074/jbc.M501423200. PubMed PMID: 15863505.
205. Andrews S. FastQC: a quality control tool for high throughput sequence data.2010. Available from: http://www.bioinformatics.babraham.ac.uk/projects/fastqc.
206. Bolger AM, Lohse M, Usadel B. Trimmomatic: a flexible trimmer for Illumina sequence data. Bioinformatics. 2014;30(15):2114-20. doi: 10.1093/bioinformatics/btu170. PubMed PMID: 24695404; PMCID: PMC4103590.
207. Martin M. Cutadapt removes adapter sequences from high-throughput sequencing reads. 2011. 2011;17(1):3. Epub 2011-08-02. doi: 10.14806/ej.17.1.200.
208. Langmead B, Trapnell C, Pop M, Salzberg SL. Ultrafast and memory-efficient alignment of short DNA sequences to the human genome. Genome Biol. 2009;10(3):R25. doi: 10.1186/gb-2009-10-3-r25. PubMed PMID: 19261174; PMCID: PMC2690996.
209. Langmead B, Salzberg SL. Fast gapped-read alignment with Bowtie 2. Nat Methods. 2012;9(4):357-9. doi: 10.1038/nmeth.1923. PubMed PMID: 22388286; PMCID: PMC3322381.

210. Gao TS, He B, Liu S, Zhu H, Tan K, Qian J. EnhancerAtlas: a resource for enhancer annotation and analysis in 105 human cell/tissue types. Bioinformatics. 2016;32(23):3543-51. doi: 10.1093/bioinformatics/btw495. PubMed PMID: WOS:000392749500002.
211. Krueger F. Trim Galore: A wrapper tool around Cutadapt and FastQC to consistently apply quality and adapter trimming to FastQ files. 2012.
212. Stovner EB, Saetrom P. epic2 efficiently finds diffuse domains in ChIP-seq data. Bioinformatics. 2019. doi: 10.1093/bioinformatics/btz232. PubMed PMID: 30923821.
213. Yu G, Wang LG, He QY. ChIPseeker: an R/Bioconductor package for ChIP peak annotation, comparison and visualization. Bioinformatics. 2015;31(14):2382-3. doi: 10.1093/bioinformatics/btv145. PubMed PMID: 25765347.
214. Shi Y, Lan F, Matson C, Mulligan P, Whetstine JR, Cole PA, Casero RA, Shi Y. Histone demethylation mediated by the nuclear amine oxidase homolog LSD1. Cell. 2004;119(7):941-53. doi: 10.1016/j.cell.2004.12.012. PubMed PMID: 15620353.
215. Spiller CM, Feng CW, Jackson A, Gillis AJ, Rolland AD, Looijenga LH, Koopman P, Bowles J. Endogenous Nodal signaling regulates germ cell potency during mammalian testis development. Development. 2012;139(22):4123-32. doi: 10.1242/dev.083006. PubMed PMID: 23034635.
216. Gao XN, Yan F, Lin J, Gao L, Lu XL, Wei SC, Shen N, Pang JX, Ning QY, Komeno Y, Deng AL, Xu YH, Shi JL, Li YH, Zhang DE, Nervi C, Liu SJ, Yu L. AML1/ETO cooperates with HIF1alpha to promote leukemogenesis through DNMT3a transactivation. Leukemia. 2015;29(8):1730-40. doi: 10.1038/leu.2015.56. PubMed PMID: 25727291.
217. Yu Z, Xiao Q, Zhao L, Ren J, Bai X, Sun M, Wu H, Liu X, Song Z, Yan Y, Mi X, Wang E, Jin F, Wei M. DNA methyltransferase 1/3a overexpression in sporadic breast cancer is associated with reduced expression of estrogen receptor-alpha/breast cancer susceptibility gene 1 and poor prognosis. Mol Carcinog. 2015;54(9):707-19. doi: 10.1002/mc.22133. PubMed PMID: 24464625.
218. Jones PA, Issa J-PJ, Baylin S. Targeting the cancer epigenome for therapy. Nature Reviews Genetics. 2016;17(10):630.
219. Ma HS, Wang EL, Xu WF, Yamada S, Yoshimoto K, Qian ZR, Shi L, Liu LL, Li XH. Overexpression of DNA (Cytosine-5)-Methyltransferase 1 (DNMT1) And DNA (Cytosine-5)-Methyltransferase 3A (DNMT3A) Is Associated with Aggressive Behavior and Hypermethylation of Tumor Suppressor Genes in Human Pituitary Adenomas. Med Sci Monit. 2018;24:4841-50. doi: 10.12659/MSM.910608. PubMed PMID: 30002361; PMCID: PMC6069575.
220. Zheng Y, Cohen-Karni D, Xu D, Chin HG, Wilson G, Pradhan S, Roberts RJ. A unique family of Mrr-like modification-dependent restriction endonucleases. Nucleic acids research. 2010;38(16):5527-34. doi: 10.1093/nar/gkq327. PubMed PMID: 20444879; PMCID: PMC2938202.
221. Cohen-Karni D, Xu D, Apone L, Fomenkov A, Sun Z, Davis PJ, Kinney SR, Yamada-Mabuchi M, Xu SY, Davis T, Pradhan S, Roberts RJ, Zheng Y. The MspJI family of modification-dependent restriction endonucleases for epigenetic studies. Proc Natl Acad Sci U S A. 2011;108(27):11040-5. doi: 10.1073/pnas.1018448108. PubMed PMID: 21690366; PMCID: PMC3131316.

222. Barski A, Cuddapah S, Cui K, Roh TY, Schones DE, Wang Z, Wei G, Chepelev I, Zhao K. High-resolution profiling of histone methylations in the human genome. Cell. 2007;129(4):823-37. doi: 10.1016/j.cell.2007.05.009. PubMed PMID: 17512414.
223. Lindroth AM, Park YJ, McLean CM, Dokshin GA, Persson JM, Herman H, Pasini D, Miro X, Donohoe ME, Lee JT. Antagonism between DNA and H3K27 methylation at the imprinted Rasgrf1 locus. PLoS genetics. 2008;4(8):e1000145.
224. Wang Z, Zang C, Rosenfeld JA, Schones DE, Barski A, Cuddapah S, Cui K, Roh T-Y, Peng W, Zhang MQ. Combinatorial patterns of histone acetylations and methylations in the human genome. Nature genetics. 2008;40(7):897.
225. Yegnasubramanian S, Wu Z, Haffner MC, Esopi D, Aryee MJ, Badrinath R, He TL, Morgan JD, Carvalho B, Zheng Q. Chromosome-wide mapping of DNA methylation patterns in normal and malignant prostate cells reveals pervasive methylation of gene-associated and conserved intergenic sequences. BMC genomics. 2011;12(1):313.
226. Laursen KB, Mongan NP, Zhuang Y, Ng MM, Benoit YD, Gudas LJ. Polycomb recruitment attenuates retinoic acid-induced transcription of the bivalent NR2F1 gene. Nucleic acids research. 2013;41(13):6430-43. doi: 10.1093/nar/gkt367. PubMed PMID: 23666625; PMCID: PMC3905905.
227. Zhao H, Sun ZF, Wang J, Huang HJ, Kocher JP, Wang LG. CrossMap: a versatile tool for coordinate conversion between genome assemblies. Bioinformatics. 2014;30(7):1006-7. doi: 10.1093/bioinformatics/btt730. PubMed PMID: WOS:000334078300017.
228. Li JY, Pu MT, Hirasawa R, Li BZ, Huang YN, Zeng R, Jing NH, Chen T, Li E, Sasaki H, Xu GL. Synergistic function of DNA methyltransferases Dnmt3a and Dnmt3b in the methylation of Oct4 and Nanog. Mol Cell Biol. 2007;27(24):8748-59. doi: 10.1128/MCB.01380-07. PubMed PMID: 17938196; PMCID: PMC2169413.
229. Schoenhals M, Kassambara A, De Vos J, Hose D, Moreaux J, Klein B. Embryonic stem cell markers expression in cancers. Biochem Biophys Res Commun. 2009;383(2):157-62. doi: 10.1016/j.bbrc.2009.02.156. PubMed PMID: 19268426.
230. Wang Y, Zhang H, Chen Y, Sun Y, Yang F, Yu W, Liang J, Sun L, Yang X, Shi L, Li R, Li Y, Zhang Y, Li Q, Yi X, Shang Y. LSD1 is a subunit of the NuRD complex and targets the metastasis programs in breast cancer. Cell. 2009;138(4):660-72. doi: 10.1016/j.cell.2009.05.050. PubMed PMID: 19703393.
231. Wang XQ, Ongkeko WM, Chen L, Yang ZF, Lu P, Chen KK, Lopez JP, Poon RT, Fan ST. Octamer 4 (Oct4) mediates chemotherapeutic drug resistance in liver cancer cells through a potential Oct4-AKT-ATP-binding cassette G2 pathway. Hepatology. 2010;52(2):528-39. doi: 10.1002/hep.23692. PubMed PMID: 20683952.
232. Lv T, Yuan D, Miao X, Lv Y, Zhan P, Shen X, Song Y. Over-expression of LSD1 promotes proliferation, migration and invasion in non-small cell lung cancer. PLoS One. 2012;7(4):e35065. doi: 10.1371/journal.pone.0035065. PubMed PMID: 22493729; PMCID: PMC3320866.
233. Kashyap V, Ahmad S, Nilsson EM, Helczynski L, Kenna S, Persson JL, Gudas LJ, Mongan NP. The lysine specific demethylase-1 (LSD1/KDM1A) regulates VEGF-A expression in prostate cancer. Mol Oncol. 2013;7(3):555-66. doi: 10.1016/j.molonc.2013.01.003. PubMed PMID: 23384557; PMCID: PMC3661758.

234. Kim BW, Cho H, Choi CH, Ylaya K, Chung JY, Kim JH, Hewitt SM. Clinical significance of OCT4 and SOX2 protein expression in cervical cancer. BMC Cancer. 2015;15:1015. doi: 10.1186/s12885-015-2015-1. PubMed PMID: 26706028; PMCID: PMC4691290.
235. Hosseini A, Minucci S. A comprehensive review of lysine-specific demethylase 1 and its roles in cancer. Epigenomics. 2017;9(8):1123-42. doi: 10.2217/epi-2017-0022. PubMed PMID: 28699367.
236. Chapuy B, McKeown MR, Lin CY, Monti S, Roemer MG, Qi J, Rahl PB, Sun HH, Yeda KT, Doench JG, Reichert E, Kung AL, Rodig SJ, Young RA, Shipp MA, Bradner JE. Discovery and characterization of super-enhancer-associated dependencies in diffuse large B cell lymphoma. Cancer Cell. 2013;24(6):777-90. doi: 10.1016/j.ccr.2013.11.003. PubMed PMID: 24332044; PMCID: PMC4018722.
237. Loven J, Hoke HA, Lin CY, Lau A, Orlando DA, Vakoc CR, Bradner JE, Lee TI, Young RA. Selective inhibition of tumor oncogenes by disruption of super-enhancers. Cell. 2013;153(2):320-34. Epub 2013/04/16. doi: 10.1016/j.cell.2013.03.036. PubMed PMID: 23582323; PMCID: 3760967.
238. Groschel S, Sanders MA, Hoogenboezem R, de Wit E, Bouwman BA, Erpelinck C, van der Velden VH, Havermans M, Avellino R, van Lom K, Rombouts EJ, van Duin M, Dohner K, Beverloo HB, Bradner JE, Dohner H, Lowenberg B, Valk PJ, Bindels EM, de Laat W, Delwel R. A single oncogenic enhancer rearrangement causes concomitant EVI1 and GATA2 deregulation in leukemia. Cell. 2014;157(2):369-81. Epub 2014/04/08. doi: 10.1016/j.cell.2014.02.019. PubMed PMID: 24703711.
239. Mansour MR, Abraham BJ, Anders L, Berezovskaya A, Gutierrez A, Durbin AD, Etchin J, Lawton L, Sallan SE, Silverman LB, Loh ML, Hunger SP, Sanda T, Young RA, Look AT. Oncogene regulation. An oncogenic super-enhancer formed through somatic mutation of a noncoding intergenic element. Science. 2014;346(6215):1373-7. Epub 2014/11/15. doi: 10.1126/science.1259037. PubMed PMID: 25394790.
240. Hnisz D, Schuijers J, Lin CY, Weintraub AS, Abraham BJ, Lee TI, Bradner JE, Young RA. Convergence of developmental and oncogenic signaling pathways at transcriptional super-enhancers. Molecular cell. 2015;58(2):362-70. Epub 2015/03/25. doi: 10.1016/j.molcel.2015.02.014. PubMed PMID: 25801169; PMCID: 4402134.
241. Akhtar-Zaidi B, Cowper-Sal R, Corradin O, Saiakhova A, Bartels CF, Balasubramanian D, Myeroff L, Lutterbaugh J, Jarrar A, Kalady MF. Epigenomic enhancer profiling defines a signature of colon cancer. Science. 2012;336(6082):736-9.
242. Magnani L, Stoeck A, Zhang X, Lánczky A, Mirabella AC, Wang T-L, Gyorffy B, Lupien M. Genome-wide reprogramming of the chromatin landscape underlies endocrine therapy resistance in breast cancer. Proceedings of the National Academy of Sciences. 2013:201219992.
243. Knoechel B, Roderick JE, Williamson KE, Zhu J, Lohr JG, Cotton MJ, Gillespie SM, Fernandez D, Ku M, Wang H. An epigenetic mechanism of resistance to targeted therapy in T cell acute lymphoblastic leukemia. Nature genetics. 2014;46(4):364.
244. Aran D, Hellman A. DNA methylation of transcriptional enhancers and cancer predisposition. Cell. 2013;154(1):11-3.
245. Aran D, Sabato S, Hellman A. DNA methylation of distal regulatory sites characterizes dysregulation of cancer genes. Genome biology. 2013;14(3):R21.

246. Taberlay PC, Statham AL, Kelly TK, Clark SJ, Jones PA. Reconfiguration of nucleosome-depleted regions at distal regulatory elements accompanies DNA methylation of enhancers and insulators in cancer. Genome research. 2014:gr. 163485.113.
247. Zaret KS, Carroll JS. Pioneer transcription factors: establishing competence for gene expression. Genes Dev. 2011;25(21):2227-41. doi: 10.1101/gad.176826.111. PubMed PMID: 22056668; PMCID: PMC3219227.
248. Gordeeva O, Khaydukov S. Tumorigenic and Differentiation Potentials of Embryonic Stem Cells Depend on TGFβ Family Signaling: Lessons from Teratocarcinoma Cells Stimulated to Differentiate with Retinoic Acid. Stem cells international. 2017;2017.
249. Sampieri K, Fodde R. Cancer stem cells and metastasis. Seminars in cancer biology. 2012;22(3):187-93. PubMed PMID: 22774232.
250. Hermann A, Gowher H, Jeltsch A. Biochemistry and biology of mammalian DNA methyltransferases. Cellular and molecular life sciences : CMLS. 2004;61(19-20):2571-87. Epub 2004/11/05. doi: 10.1007/s00018-004-4201-1. PubMed PMID: 15526163.
251. Goll MG, Bestor TH. Eukaryotic cytosine methyltransferases. Annu Rev Biochem. 2005;74:481-514. doi: 10.1146/annurev.biochem.74.010904.153721. PubMed PMID: 15952895.
252. Jurkowska RZ, Jurkowski TP, Jeltsch A. Structure and function of mammalian DNA methyltransferases. Chembiochem. 2011;12(2):206-22. doi: 10.1002/cbic.201000195. PubMed PMID: 21243710.
253. Dhe-Paganon S, Syeda F, Park L. DNA methyl transferase 1: regulatory mechanisms and implications in health and disease. Int J Biochem Mol Biol. 2011;2(1):58-66. PubMed PMID: 21969122; PMCID: PMC3180029.
254. Jeltsch A, Jurkowska RZ. Allosteric control of mammalian DNA methyltransferases - a new regulatory paradigm. Nucleic acids research. 2016;44(18):8556-75. doi: 10.1093/nar/gkw723. PubMed PMID: 27521372; PMCID: PMC5062992.
255. Oka M, Rodic N, Graddy J, Chang LJ, Terada N. CpG sites preferentially methylated by Dnmt3a in vivo. J Biol Chem. 2006;281(15):9901-8. doi: 10.1074/jbc.M511100200. PubMed PMID: 16439359.
256. Denis H, Ndlovu MN, Fuks F. Regulation of mammalian DNA methyltransferases: a route to new mechanisms. EMBO Rep. 2011;12(7):647-56. doi: 10.1038/embor.2011.110. PubMed PMID: 21660058; PMCID: PMC3128952.
257. Di Croce L, Raker VA, Corsaro M, Fazi F, Fanelli M, Faretta M, Fuks F, Lo Coco F, Kouzarides T, Nervi C, Minucci S, Pelicci PG. Methyltransferase recruitment and DNA hypermethylation of target promoters by an oncogenic transcription factor. Science. 2002;295(5557):1079-82. doi: 10.1126/science.1065173. PubMed PMID: 11834837.
258. Brenner C, Deplus R, Didelot C, Loriot A, Vire E, De Smet C, Gutierrez A, Danovi D, Bernard D, Boon T, Pelicci PG, Amati B, Kouzarides T, de Launoit Y, Di Croce L, Fuks F. Myc represses transcription through recruitment of DNA methyltransferase corepressor. EMBO J. 2005;24(2):336-46. doi: 10.1038/sj.emboj.7600509. PubMed PMID: 15616584; PMCID: PMC545804.
259. Hervouet E, Vallette FM, Cartron PF. Dnmt3/transcription factor interactions as crucial players in targeted DNA methylation. Epigenetics. 2009;4(7):487-99. doi: 10.4161/epi.4.7.9883. PubMed PMID: 19786833.

260. Geiman TM, Sankpal UT, Robertson AK, Zhao Y, Zhao Y, Robertson KD. DNMT3B interacts with hSNF2H chromatin remodeling enzyme, HDACs 1 and 2, and components of the histone methylation system. Biochem Biophys Res Commun. 2004;318(2):544-55. doi: 10.1016/j.bbrc.2004.04.058. PubMed PMID: 15120635.
261. Ma P, de Waal E, Weaver JR, Bartolomei MS, Schultz RM. A DNMT3A2-HDAC2 Complex Is Essential for Genomic Imprinting and Genome Integrity in Mouse Oocytes. Cell Rep. 2015;13(8):1552-60. doi: 10.1016/j.celrep.2015.10.031. PubMed PMID: 26586441; PMCID: PMC4662907.
262. Fuks F, Hurd PJ, Deplus R, Kouzarides T. The DNA methyltransferases associate with HP1 and the SUV39H1 histone methyltransferase. Nucleic acids research. 2003;31(9):2305-12. doi: 10.1093/nar/gkg332. PubMed PMID: 12711675; PMCID: PMC154218.
263. Feldman N, Gerson A, Fang J, Li E, Zhang Y, Shinkai Y, Cedar H, Bergman Y. G9a-mediated irreversible epigenetic inactivation of Oct-3/4 during early embryogenesis. Nat Cell Biol. 2006;8(2):188-94. doi: 10.1038/ncb1353. PubMed PMID: 16415856.
264. Epsztejn-Litman S, Feldman N, Abu-Remaileh M, Shufaro Y, Gerson A, Ueda J, Deplus R, Fuks F, Shinkai Y, Cedar H, Bergman Y. De novo DNA methylation promoted by G9a prevents reprogramming of embryonically silenced genes. Nat Struct Mol Biol. 2008;15(11):1176-83. doi: 10.1038/nsmb.1476. PubMed PMID: 18953337; PMCID: PMC2581722.
265. Shinkai Y, Tachibana M. H3K9 methyltransferase G9a and the related molecule GLP. Genes Dev. 2011;25(8):781-8. doi: 10.1101/gad.2027411. PubMed PMID: 21498567; PMCID: PMC3078703.
266. Lehnertz B, Ueda Y, Derijck AA, Braunschweig U, Perez-Burgos L, Kubicek S, Chen T, Li E, Jenuwein T, Peters AH. Suv39h-mediated histone H3 lysine 9 methylation directs DNA methylation to major satellite repeats at pericentric heterochromatin. Curr Biol. 2003;13(14):1192-200. PubMed PMID: 12867029.
267. Li BZ, Huang Z, Cui QY, Song XH, Du L, Jeltsch A, Chen P, Li G, Li E, Xu GL. Histone tails regulate DNA methylation by allosterically activating de novo methyltransferase. Cell Res. 2011;21(8):1172-81. doi: 10.1038/cr.2011.92. PubMed PMID: 21606950; PMCID: PMC3193484.
268. Otani J, Nankumo T, Arita K, Inamoto S, Ariyoshi M, Shirakawa M. Structural basis for recognition of H3K4 methylation status by the DNA methyltransferase 3A ATRX-DNMT3-DNMT3L domain. EMBO Rep. 2009;10(11):1235-41. doi: 10.1038/embor.2009.218. PubMed PMID: 19834512; PMCID: PMC2775176.
269. Cheng X. Structural and functional coordination of DNA and histone methylation. Cold Spring Harb Perspect Biol. 2014;6(8). doi: 10.1101/cshperspect.a018747. PubMed PMID: 25085914; PMCID: PMC4107986.
270. Gowher H, Liebert K, Hermann A, Xu G, Jeltsch A. Mechanism of stimulation of catalytic activity of Dnmt3A and Dnmt3B DNA-(cytosine-C5)-methyltransferases by Dnmt3L. J Biol Chem. 2005;280(14):13341-8. Epub 2005/01/27. doi: 10.1074/jbc.M413412200. PubMed PMID: 15671018.
271. Collas P. The current state of chromatin immunoprecipitation. Mol Biotechnol. 2010;45(1):87-100. doi: 10.1007/s12033-009-9239-8. PubMed PMID: 20077036.

272. Park PJ. ChIP-seq: advantages and challenges of a maturing technology. Nature reviews Genetics. 2009;10(10):669-80. doi: 10.1038/nrg2641. PubMed PMID: 19736561; PMCID: PMC3191340.
273. Li Y, Tollefsbol TO. DNA methylation detection: bisulfite genomic sequencing analysis. Methods Mol Biol. 2011;791:11-21. doi: 10.1007/978-1-61779-316-5_2. PubMed PMID: 21913068; PMCID: PMC3233226.
274. Kiianitsa K, Maizels N. Ultrasensitive isolation, identification and quantification of DNA-protein adducts by ELISA-based RADAR assay. Nucleic acids research. 2014;42(13):e108. doi: 10.1093/nar/gku490. PubMed PMID: 24914050; PMCID: PMC4117749.
275. Christman JK. 5-Azacytidine and 5-aza-2'-deoxycytidine as inhibitors of DNA methylation: mechanistic studies and their implications for cancer therapy. Oncogene. 2002;21(35):5483-95. doi: 10.1038/sj.onc.1205699. PubMed PMID: 12154409.
276. Champion C, Guianvarc'h D, Senamaud-Beaufort C, Jurkowska RZ, Jeltsch A, Ponger L, Arimondo PB, Guieysse-Peugeot AL. Mechanistic insights on the inhibition of c5 DNA methyltransferases by zebularine. PLoS One. 2010;5(8):e12388. doi: 10.1371/journal.pone.0012388. PubMed PMID: 20808780; PMCID: PMC2927531.
277. Gowher H, Stuhlmann H, Felsenfeld G. Vezf1 regulates genomic DNA methylation through its effects on expression of DNA methyltransferase Dnmt3b. Genes Dev. 2008;22(15):2075-84. doi: 10.1101/gad.1658408. PubMed PMID: 18676812; PMCID: PMC2492749.
278. Bouchard J, Momparler RL. Incorporation of 5-Aza-2'-deoxycytidine-5'-triphosphate into DNA. Interactions with mammalian DNA polymerase alpha and DNA methylase. Mol Pharmacol. 1983;24(1):109-14. PubMed PMID: 6191192.
279. Bashtrykov P, Ragozin S, Jeltsch A. Mechanistic details of the DNA recognition by the Dnmt1 DNA methyltransferase. FEBS Lett. 2012;586(13):1821-3. doi: 10.1016/j.febslet.2012.05.026. PubMed PMID: 22641038.
280. Huang N, Banavali NK, MacKerell AD, Jr. Protein-facilitated base flipping in DNA by cytosine-5-methyltransferase. Proc Natl Acad Sci U S A. 2003;100(1):68-73. doi: 10.1073/pnas.0135427100. PubMed PMID: 12506195; PMCID: PMC140885.
281. Chen L, MacMillan AM, Chang W, Ezaz-Nikpay K, Lane WS, Verdine GL. Direct identification of the active-site nucleophile in a DNA (cytosine-5)-methyltransferase. Biochemistry. 1991;30(46):11018-25. doi: 10.1021/bi00110a002. PubMed PMID: 1932026.
282. Santi DV, Norment A, Garrett CE. Covalent bond formation between a DNA-cytosine methyltransferase and DNA containing 5-azacytosine. Proc Natl Acad Sci U S A. 1984;81(22):6993-7. doi: 10.1073/pnas.81.22.6993. PubMed PMID: 6209710; PMCID: PMC392062.
283. Stresemann C, Lyko F. Modes of action of the DNA methyltransferase inhibitors azacytidine and decitabine. Int J Cancer. 2008;123(1):8-13. doi: 10.1002/ijc.23607. PubMed PMID: 18425818.
284. Palii SS, Van Emburgh BO, Sankpal UT, Brown KD, Robertson KD. DNA methylation inhibitor 5-Aza-2'-deoxycytidine induces reversible genome-wide DNA damage that is distinctly influenced by DNA methyltransferases 1 and 3B. Mol Cell Biol. 2008;28(2):752-71. doi: 10.1128/MCB.01799-07. PubMed PMID: 17991895; PMCID: PMC2223421.

285. Gopalakrishnan S, Van Emburgh BO, Robertson KD. DNA methylation in development and human disease. Mutat Res. 2008;647(1-2):30-8. doi: 10.1016/j.mrfmmm.2008.08.006. PubMed PMID: 18778722; PMCID: PMC2647981.
286. Chen T, Ueda Y, Dodge JE, Wang Z, Li E. Establishment and maintenance of genomic methylation patterns in mouse embryonic stem cells by Dnmt3a and Dnmt3b. Mol Cell Biol. 2003;23(16):5594-605. doi: 10.1128/mcb.23.16.5594-5605.2003. PubMed PMID: 12897133; PMCID: PMC166327.
287. Miyashita H, Kanemura M, Yamazaki T, Abe M, Sato Y. Vascular endothelial zinc finger 1 is involved in the regulation of angiogenesis: Possible contribution of stathmin/OP18 as a downstream target gene. Arterioscl Throm Vas. 2004;24(5):878-84. doi: 10.1161/01.Atv.0000126373.52450.32. PubMed PMID: WOS:000221272700015.
288. AlAbdi L, He M, Yang Q, Norvil AB, Gowher H. The transcription factor Vezf1 represses the expression of the antiangiogenic factor Cited2 in endothelial cells. J Biol Chem. 2018;293(28):11109-18. doi: 10.1074/jbc.RA118.002911. PubMed PMID: 29794136; PMCID: PMC6052231.
289. Okano M, Li E. Genetic analyses of DNA methyltransferase genes in mouse model system. J Nutr. 2002;132(8):2462s-5s. PubMed PMID: WOS:000177398500027.
290. Suetake I, Shinozaki F, Miyagawa J, Takeshima H, Tajima S. DNMT3L stimulates the DNA methylation activity of Dnmt3a and Dnmt3b through a direct interaction. Journal of Biological Chemistry. 2004;279(26):27816-23. doi: 10.1074/jbc.M400181200. PubMed PMID: WOS:000222120400117.
291. Veland N, Lu Y, Hardikar S, Gaddis S, Zeng Y, Liu BG, Estecio MR, Takata Y, Lin K, Tomida MW, Shen JJ, Saha D, Gowher H, Zhao HB, Chen TP. DNMT3L facilitates DNA methylation partly by maintaining DNMT3A stability in mouse embryonic stem cells. Nucleic acids research. 2019;47(1):152-67. doi: 10.1093/nar/gky947. PubMed PMID: WOS:000462586700019.
292. Bourc'his D, Bestor TH. Meiotic catastrophe and retrotransposon reactivation in male germ cells lacking Dnmt3L. Nature. 2004;431(7004):96-9. doi: 10.1038/nature02886. PubMed PMID: WOS:000223641500049.
293. Hata K, Okano M, Lei H, Li E. Dnmt3L cooperates with the Dnmt3 family of de novo DNA methyltransferases to establish maternal imprints in mice. Development. 2002;129(8):1983-93. PubMed PMID: WOS:000175473800018.
294. Bourc'his D, Xu GL, Lin CS, Bollman B, Bestor TH. Dnmt3L and the establishment of maternal genomic imprints. Science. 2001;294(5551):2536-9. doi: 10.1126/science.1065848. PubMed PMID: WOS:000172927700055.
295. Neri F, Krepelova A, Incarnato D, Maldotti M, Parlato C, Galvagni F, Matarese F, Stunnenberg HG, Oliviero S. Dnmt3L Antagonizes DNA Methylation at Bivalent Promoters and Favors DNA Methylation at Gene Bodies in ESCs. Cell. 2013;155(1):121-34. doi: 10.1016/j.cell.2013.08.056. PubMed PMID: WOS:000324916700014.
296. Kao TH, Liao HF, Wolf D, Tai KY, Chuang CY, Lee HS, Kuo HC, Hata K, Zhang X, Cheng XD, Goff SP, Ooi SKT, Bestor TH, Lin SP. Ectopic DNMT3L Triggers Assembly of a Repressive Complex for Retroviral Silencing in Somatic Cells. J Virol. 2014;88(18):10680-95. doi: 10.1128/Jvi.01176-14. PubMed PMID: WOS:000341234900036.

297. Jia D, Jurkowska RZ, Zhang X, Jeltsch A, Cheng X. Structure of Dnmt3a bound to Dnmt3L suggests a model for de novo DNA methylation. Nature. 2007;449(7159):248-51. doi: 10.1038/nature06146. PubMed PMID: 17713477; PMCID: PMC2712830.
298. Bonifer C, Cockerill PN. Chromatin priming of genes in development: Concepts, mechanisms and consequences. Exp Hematol. 2017;49:1-8. doi: 10.1016/j.exphem.2017.01.003. PubMed PMID: 28185904.
299. Vojta A, Dobrinic P, Tadic V, Bockor L, Korac P, Julg B, Klasic M, Zoldos V. Repurposing the CRISPR-Cas9 system for targeted DNA methylation. Nucleic acids research. 2016;44(12):5615-28. doi: 10.1093/nar/gkw159. PubMed PMID: 26969735; PMCID: PMC4937303.
300. Liu XS, Wu H, Ji X, Stelzer Y, Wu X, Czauderna S, Shu J, Dadon D, Young RA, Jaenisch R. Editing DNA Methylation in the Mammalian Genome. Cell. 2016;167(1):233-47 e17. doi: 10.1016/j.cell.2016.08.056. PubMed PMID: 27662091; PMCID: PMC5062609.
301. Maiques-Diaz A, Somervaille TC. LSD1: biologic roles and therapeutic targeting. Epigenomics. 2016;8(8):1103-16. doi: 10.2217/epi-2016-0009. PubMed PMID: 27479862; PMCID: PMC5066116.
302. Lynch JT, Harris WJ, Somervaille TC. LSD1 inhibition: a therapeutic strategy in cancer? Expert Opin Ther Targets. 2012;16(12):1239-49. doi: 10.1517/14728222.2012.722206. PubMed PMID: 22957941.
303. Wu Y, Wang Y, Yang XH, Kang T, Zhao Y, Wang C, Evers BM, Zhou BP. The deubiquitinase USP28 stabilizes LSD1 and confers stem-cell-like traits to breast cancer cells. Cell Rep. 2013;5(1):224-36. doi: 10.1016/j.celrep.2013.08.030. PubMed PMID: 24075993; PMCID: PMC4004762.
304. Wu CY, Persaud SD, Wei LN. Retinoic Acid Induces Ubiquitination-Resistant RIP140/LSD1 Complex to Fine-Tune Pax6 Gene in Neuronal Differentiation. Stem Cells. 2016;34(1):114-23. doi: 10.1002/stem.2190. PubMed PMID: 26372689; PMCID: PMC5473615.
305. Ouyang J, Shi Y, Valin A, Xuan Y, Gill G. Direct binding of CoREST1 to SUMO-2/3 contributes to gene-specific repression by the LSD1/CoREST1/HDAC complex. Molecular cell. 2009;34(2):145-54. doi: 10.1016/j.molcel.2009.03.013. PubMed PMID: 19394292; PMCID: PMC2727917.
306. Hakimi MA, Bochar DA, Chenoweth J, Lane WS, Mandel G, Shiekhattar R. A core-BRAF35 complex containing histone deacetylase mediates repression of neuronal-specific genes. Proc Natl Acad Sci U S A. 2002;99(11):7420-5. doi: 10.1073/pnas.112008599. PubMed PMID: 12032298; PMCID: PMC124246.
307. Kwon JT, Jin S, Choi H, Kim J, Jeong J, Kim J, Kim Y, Cho BN, Cho C. Identification and Characterization of Germ Cell Genes Expressed in the F9 Testicular Teratoma Stem Cell Line. Plos One. 2014;9(8). doi: ARTN e103837 10.1371/journal.pone.0103837. PubMed PMID: WOS:000340952200009.
308. Evans M. Origin of Mouse Embryonal Carcinoma-Cells and the Possibility of Their Direct Isolation into Tissue-Culture. J Reprod Fertil. 1981;62(2):625-&. PubMed PMID: WOS:A1981LW86900041.
309. Geiman TM, Muegge K. DNA Methylation in Early Development. Mol Reprod Dev. 2010;77(2):105-13. doi: 10.1002/mrd.21118. PubMed PMID: WOS:000273518200004.

310. Manzo M, Ambrosi C, Baubec T. Genome-Wide Profiling of DNA Methyltransferases in Mammalian Cells. Methods Mol Biol. 2018;1766:157-74. doi: 10.1007/978-1-4939-7768-0_9. PubMed PMID: 29605852.
311. Challen GA, Sun DQ, Mayle A, Jeong M, Luo M, Rodriguez B, Mallaney C, Celik H, Yang LB, Xia Z, Cullen S, Berg J, Zheng YY, Darlington GJ, Li W, Goodell MA. Dnmt3a and Dnmt3b Have Overlapping and Distinct Functions in Hematopoietic Stem Cells. Cell Stem Cell. 2014;15(3):350-64. doi: 10.1016/j.stem.2014.06.018. PubMed PMID: WOS:000341441600014.

VITA

Lama A. AlAbdi
Department of Biochemistry
Purdue University
175 South University St, West Lafayette IN, 47907

Education

Purdue University	Ph.D.	Biochemistry	2014-2019	West Lafayette, IN
King Abdullah University of Science and Technology	M.S.	Bioscience	2010-2011	Thuwal, Saudi Arabia
King Saud University	B.S.	Biochemistry	2005-2009	Riyadh, Saudi Arabia

Professional Experience

2011 - Current	University Demonstrator, Zoology Department, King Saud University, College of Science.
2014-2019	Graduate Student, PULSe graduate program, Department of Biochemistry, Purdue University, West Lafayette, IN
2009-2010	Research Assistant (Developmental Genetics), King Faisal Specialist Hospital and Research Center (2009 - 2010).
2009	Research Intern (DNA repair & Apoptosis), King Faisal Specialist Hospital and Research Center (2009)

Publications

Norvil, A. B., Petell, C. J., **Alabdi, L.**, Wu, L. C., Rossie, S., and Gowher, H. (2018) Dnmt3b Methylates DNA by a Noncooperative Mechanism, and Its Activity Is Unaffected by Manipulations at the Predicted Dinner Interface. *Biochemistry*-Us 57, 4312-4324

***AlAbdi, L.**, *He, M., Yang, Q. Y., Norvil, A. B., and Gowher, H. (2018) The transcription factor Vezf1 represses the expression of the antiangiogenic factor Cited2 in endothelial cells. *J Biol Chem* 293, 11109-11118

Petell, C. J., **Alabdi, L.**, He, M., San Miguel, P., Rose, R., and Gowher, H. (2016) An epigenetic switch regulates de novo DNA methylation at a subset of pluripotency gene enhancers during embryonic stem cell differentiation. *Nucleic Acids Res* 44, 7605-7617

*Co-First Author

Research Summary

As a graduate student under the supervision of Dr. Humaira Gowher at Purdue University's Department of Biochemistry, I had the privilege of collaborating with talented members of Gowher lab and contributed many publications. My research involved the use of embryonic stem cells and embryonal carcinoma cell differentiation as model system to study how enhancers fail to be silenced in cancer stem cells. Further, in our manuscript submitted to *Molecular Cell*, we determined a mechanism by which these enhancers acquire a primed state prone to activation. These primed enhancers are what render these cells plastic under the many environmental conditions.

In order to decipher how DNA methyltransferases are recruited and targeted to specific sites and how this mechanism is disrupted in cancer, I refined a DNA methyltransferase capture method. By the use of a suicide inhibitor, we demonstrated that we could capture DNA methyltransferases as they exert their catalytic activity onto their DNA substrate. This novel method can be used to investigate dynamic changes of DNA methylation deposited by specific DNA methyltransferases during cellular differentiation.

Additionally, I am a co-author on a 2018 publication in *J. Biol. Chem.,* where we illustrated how the transcription factor Vezf1 is critical for endothelial lineage determination via regulating the expression of stem cell factor, Cbp/p300-interacting transactivator 2 (Cited2). We showed that Vezf1 depleted cells have higher expression of Cited2. Given Vezf1 reported role as an insulator protein, our data highlights a mechanism by which Vezf1 occupancy at Cited2 promoter prevents aberrant promoter activation by blocking inappropriate interactions of promoters with nearby enhancers.

Since becoming part of Dr. Gowher's laboratory in 2015, I have been able to co-author in two published manuscripts and one, which I am the first co-author. I also attended many national conferences such as the Midwest Chromatin and Epigenetics Meeting and American Society for Biochemistry and Molecular Biology Meeting to name a few. I also mentored seven ambitious and talented undergraduate students as well as several graduate students during their rotations periods in the lab. My experiences in research and training acquired in US will equip me to perform in my role in an academic position in Saudi Arabia.

Awards

2018	Graduate Student Travel Award, Purdue University Center for Cancer Research, Purdue University
2017	Bird Stair Research Fellowship, Department of Biochemistry, Purdue University

2016	Interdisciplinary Life Science-PULSe Excellence Award, Purdue University
2013-Current	King Saud University (KSU) and Saudi Arabian Cultural Mission (SACM) graduate fellowship

Conferences Attended

2019†	Hitchhiker's Guide to the Biomolecular Galaxy, West Lafayette, IN
2018*	FASEB: Biological Methylation: Fundamental Mechanisms in Human Health and Disease, Florence, Italy
2018†	Midwest Chromatin & Epigenetics Meeting. Purdue University, West Lafayette, IN
2018†	Purdue University Department of Biochemistry Annual Research Retreat, West Lafayette, IN
2017*	Biochemical Horizons Symposium. Purdue University, West Lafayette, IN
2017†	Interdisciplinary Life Science-PULSe 5min thesis competition, West Lafayette, IN
2017*	Purdue University Department of Biochemistry Annual Research Retreat, West Lafayette, IN
2017	American Society for Biochemistry and Molecular Biology- Experimental Biology. Chicago, IL
2016†	Interdisciplinary Life Science-PULSe 5min thesis competition, West Lafayette, IN
2016*	Interdisciplinary Life Science-PULSe Retreat, West Lafayette, IN
2016*	Midwest Chromatin and Epigenetics Meeting, Van Andel Research Institute, Grand Rapids, MI
2016	Hitchhiker's Guide to the Biomolecular Galaxy, West Lafayette, IN

2016*	Purdue University Department of Biochemistry Annual Research Retreat, West Lafayette, IN
2016*	Health and Disease: Science, Culture and Policy Research Poster Session, West Lafayette, IN
2016*	Purdue Cancer Center Retreat, West Lafayette, IN
2015*	Purdue University Department of Biochemistry Annual Research Retreat, West Lafayette, IN

* Poster Presentation
† Oral Presentation

Presentations

2019†	Hitchhiker's Guide to the Biomolecular Galaxy. *Oct3/4 inhibits Lsd1 activity and affects gain of DNA methylation at pluripotency enhancers.* **Lama AlAbdi**
2018*	FASEB: Biological Methylation: Fundamental Mechanisms in Human Health and Disease. *Regulation of pluripotency by DNA methylation in F9 Embryonal carcinoma cells*. **Lama AlAbdi**
2018†	Midwest Chromatin & Epigenetics Meeting. *Regulation of pluripotency by DNA methylation in F9 Embryonal carcinoma cells.* **Lama AlAbdi**
2018†	Purdue University Department of Biochemistry Annual Research Retreat. *Regulation of pluripotency by DNA methylation in F9 Embryonal carcinoma.* **Lama AlAbdi**
2017*	Biochemical Horizons Symposium. *Biological outcomes of the catalytic specialization of DNA methyltransferases.* **Lama AlAbdi,** Ming He, Allison B. Norvil, Christopher J. Petell, Stephen McCune, Richard Rose, Lanchen Wu, and Humaira Gowher
2017*	Purdue University Department of Biochemistry Annual Research Retreat. *Biological outcomes of the catalytic specialization of DNA methyltransferases.* **Lama AlAbdi,** Ming He, Allison B. Norvil, Christopher J. Petell, Stephen McCune, Richard Rose, Lanchen Wu, and Humaira Gowher
2017†	Interdisciplinary Life Science-PULSe 5min thesis competition. *Mechanism of Altered Repression of Pluripotency Genes in Embryonic Carcinoma.* **Lama AlAbdi**
2016*	Midwest Chromatin & Epigenetics Meeting. *Dominant effect of Lsd1 inhibition on Dnmt3a activity at the enhancers of pluripotency genes.* **Lama AlAbdi,** Christopher J. Petell, Ming He, Phillip San Miguel, Richard Rose, and Humaira Gowher

2016*	Purdue University Department of Biochemistry Annual Research Retreat. *Altered repression of pluripotency genes in testicular teratoma post-differentiation*. **Lama AlAbdi**, Christopher J. Petell, Ming He, Nikhil Gupta, and Humaira Gowher
2016†	Interdisciplinary Life Science-PULSe 5min thesis competition. *Basis of altered repression of pluripotency genes in testicular teratoma.* **Lama AlAbdi**
2016*	Health and Disease: Science, Culture and Policy Research Poster Session. *Altered repression of pluripotency genes in testicular teratoma post-differentiation.* **Lama AlAbdi**, Christopher J. Petell, Ming He, Nikhil Gupta, and Humaira Gowher
2016†	Interdisciplinary Life Science-PULSe Retreat. *Regulation of DNA methylation during differentiation and its perturbation in cancer.* **Lama AlAbdi**
2016*	Purdue Cancer Center Retreat. *Altered repression of pluripotency genes in testicular teratoma post-differentiation*. **Lama AlAbdi**, Christopher J. Petell, Ming He, Nikhil Gupta, and Humaira Gowher
2015*	Purdue University Department of Biochemistry Annual Research Retreat. *Dominant effect of Lsd1 inhibition on Dnmt3a activity at the enhancers of pluripotency genes.* **Lama AlAbdi,** Christopher J. Petell, Ming He, Phillip San Miguel, Richard Rose, and Humaira Gowher

* Poster Presentation
† Oral Presentation

Mentoring/Teaching experience

2015-2019	Mentoring junior graduate students, rotation students and undergraduates, Department of Biochemistry, Purdue University
2018	Teaching assistant to Dr. Steven Broyles, General Biochemistry I (BCHM 561), Fall semester, Department of Biochemistry, Purdue University
2018	Academic leadership workshop

LIST OF PUBLICATIONS

*** The transcription factor Vezf1 represses the expression of the antiangiogenic factor Cited2 in endothelial cells**

*Originally published in *J. Biol. Chem.*

†**AlAbdi, L**., †He, M., Yang, Q. Y., Norvil, A. B., and Gowher, H. (2018) The transcription factor Vezf1 represses the expression of the antiangiogenic factor Cited2 in endothelial cells. J Biol Chem 293, 11109-11118

†Co-first author

Declaration of collaborative work

Lama AlAbdi, Ming He, and Dr. Humaira Gowher wrote the manuscript.

Lama AlAbdi, Ming He, Qianyi Yang, Allison Norvil, and Dr. Humaira Gowher performed experiments.

Dr. Humaira Gowher performed the Microarray experiment.

Lama AlAbdi performed Vezf1 ChIP-qPCR experiments, Western blot, and RT-qPCRs.

Ming He performed the remaining ChIP-qPCRs, DNA methylation analysis, and endothelial lineage differentiation and RT-qPCR at increasing concentrations of VEGF1.

Qianyi Yang generated the Cited2 knockdown cell lines, Alkaline Phosphatase staining experiments, and endothelial lineage differentiation.

Ming He and Qianyi Yang performed tube formation assays.

Allison Norvil performed cloning, protein purifications and PCRs.

***Dnmt3b methylates DNA by a non-cooperative mechanism and its activity is unaffected by manipulations at the predicted dimer interface**

*Originally published in *Biochemistry*.

†Norvil, A. B., †Petell, C. J., **Alabdi, L.**, Wu, L. C., Rossie, S., and Gowher, H. (2018) Dnmt3b methylates DNA by a noncooperative mechanism, and its activity is unaffected by manipulations at the predicted dimer interface. *Biochemistry*-Us 57, 4312-4324

†Co-first author

Declaration of collaborative work

Allison Norvil, Dr. Sandra Rossie, Dr. Humaira Gowher, and Christopher Petell wrote the manuscript.

Allison Norvil and Dr. Humaira Gowher designed experiments.

Allison Norvil, Lanchen Wu, Lama AlAbdi, and Christopher Petell performed experiments.

Lanchen Wu purified wild type Dnmt3-C enzymes.

Lama AlAbdi purified Dnmt3b-C R829H and performed experiments using the 30- and 509-mer substrates with Dnmt3a-C R878H and Dnmt3b-C R829H Dnmt3b-C enzymes.

Christopher Petell performed the experiments using the pUC19 substrate and performed data analysis.

Allison Norvil performed the remaining experiments.

***An epigenetic switch regulates de novo DNA methylation at a subset of pluripotency gene enhancers during embryonic stem cell differentiation**

* Originally published in *Nucleic Acids Research*:

Petell, CJ, **Alabdi, L**, He, M, San Miguel, P, Rose, R, Gowher, H. (2016) An epigenetic switch regulates de novo DNA methylation at a subset of pluripotency gene enhancers during embryonic stem cell differentiation. *Nucleic Acids Research* 44 (16): 7605-7617.

Declaration of collaborative work

Dr. Humaira Gowher and Christopher Petell wrote the manuscript and designed experiments.

Lama AlAbdi, Ming He, Richard Rose, and Christopher Petell performed experiments.

Lama AlAbdi performed microscopy and cell staining, a biological replicate for ChIPs performed in C646 treated and untreated E14T cells, the long exposure for the ESC-LIF. ChIP-Western blot for Lsd1 and a replicate for MD-qPCR of TCP treated cells.

Ming He performed co-immunoprecipitation experiments and a biological replicate for the

Dnmt3a ChIP in undifferentiated E14T cells.

Richard Rose performed qPCR replicates for MD-qPCR experiments.

Dr. Phillip San Miguel performed sequencing of bisulfite converted DNA and analyzed the sequencing data for DNA methylation.

All other experiments were performed by Christopher Petell.

PUBLICATIONS

JBC ARTICLE

Author's Choice

The transcription factor Vezf1 represses the expression of the antiangiogenic factor Cited2 in endothelial cells

Received for publication, March 13, 2018, and in revised form, May 19, 2018 Published, Papers in Press, May 24, 2018, DOI 10.1074/jbc.RA118.002911

Lama AlAbdi[‡1], **Ming He**[‡1], **Qianyi Yang**[‡2], **Allison B. Norvil**[‡], **and Humaira Gowher**[‡§3]

From the [‡]*Department of Biochemistry and* [§]*Purdue University Center for Cancer Research, Purdue University, West Lafayette, Indiana 47907*

Edited by Joel Gottesfeld

Formation of the vasculature by angiogenesis is critical for proper development, but angiogenesis also contributes to the pathogenesis of various disorders, including cancer and cardiovascular diseases. Vascular endothelial zinc finger 1 (Vezf1), is a Krüppel-like zinc finger protein that plays a vital role in vascular development. However, the mechanism by which Vezf1 regulates this process is not fully understood. Here, we show that *Vezf1*$^{-/-}$ mouse embryonic stem cells (ESC) have significantly increased expression of a stem cell factor, Cbp/p300-interacting transactivator 2 (Cited2). Compared with WT ESCs, *Vezf1*$^{-/-}$ ESCs inefficiently differentiated into endothelial cells (ECs), which exhibited defects in the tube-formation assay. These defects were due to reduced activation of EC-specific genes concomitant with lower enrichment of histone 3 acetylation at Lys^{27} (H3K27) at their promoters. We hypothesized that overexpression of Cited2 in *Vezf1*$^{-/-}$ cells sequesters P300/CBP away from the promoters of proangiogenic genes and thereby contributes to defective angiogenesis in these cells. This idea was supported by the observation that shRNA-mediated depletion of Cited2 significantly reduces the angiogenic defects in the *Vezf1*$^{-/-}$ ECs. In contrast to previous studies that have focused on the role of Vezf1 as a transcriptional activator of proangiogenic genes, our findings have revealed a role for Vezf1 in modulating the expression of the antiangiogenic factor Cited2. Vezf1 previously has been characterized as an insulator protein, and our results now provide insights into the mechanism, indicating that Vezf1 can block inappropriate, nonspecific interactions of promoters with *cis*-located enhancers, preventing aberrant promoter activation.

Development of a proper vascular system is indispensable for embryogenesis. Accurate spatial and temporal control of gene expression is required in endothelial cells (ECs),[4] which are committed to the formation of the vasculature (1, 2). Angiogenesis involves migration, growth, and differentiation of ECs and takes place during development as well as in adulthood. Angiogenesis is regulated by an interplay between pro- and anti-angiogenic factors (3). Hif-1α is a major pro-angiogenic factor, which interacts with p300/CBP and activates the expression of a number of pro-angiogenic genes including *VEGF*, thus initiating new vessel formation. Treatment of cultured ECs with VEGF-A_{165} induces Hif-1α expression, suggesting a bidirectional stimulatory relationship between VEGF and Hif-1α (4). *In vivo*, *Hif-1α* can be induced by a variety of factors including hypoxic conditions, (5–7), and certain cytokines and growth factors under normoxic conditions (8–12). Among many known factors, Vezf1 (DB1/Bgp1) and Cited2 (Mrg1/p35srj) play important roles in regulation of angiogenesis during development and in adulthood.

Cited2 (Cbp/p300-interacting transactivator with Glu/Asp-rich carboxyl-terminal domain 2) also named Mrg1/p35srj is a ubiquitously expressed essential transcriptional regulator that binds strongly to the histone acetyltransferases p300 and CBP (cAMP-responsive element-binding protein). Cited2 plays a critical role in heart development, neurulation, and maintenance of fetal and adult hematopoietic stem cells. It is expressed throughout early embryogenesis and in embryonic stem cells (ESCs) (13–17, 19–21). Several studies have demonstrated that by competing with Hif-1α to bind CBP/P300, Cited2 prevents the activation of pro-angiogenic genes such as *VEGF*, and inhibits angiogenesis (22–24). For example, over-expression of Cited2 suppresses *VEGF* promoter activity, and siRNA knockdown of Cited2 increases *VEGF* promoter activity (25). The expression levels of Hif-1α responsive genes including VEGF is increased in Cited2$^{-/-}$ embryos (14). Another study showed that Cited2 is a negative regulator of fracture healing, and its expression is inversely related to the expression of genes involved in extracellular matrix remodeling and angiogenesis, such as matrix metalloprotease, VEGF, and Hif-1α (26). These studies suggest that the proper up-regulation of pro-angiogenic genes requires the levels of Cited2 to be tightly controlled espe-

This work was supported by American Heart Association (AHA) Scientist Development Award 17SDG33700153 (to H. G.) a Graduate Student Fellowship from the King Saud University (KSU) (to L. A.) and NCI, National Institutes of Health Grant P30 CA023168. The authors declare that they have no conflicts of interest with the contents of this article. The content is solely the responsibility of the authors and does not necessarily represent the official views of the National Institutes of Health.

This article contains Fig. S1 and Table S1.

[1] Both authors contributed equally to the results of this work.

[2] Present address: Dept. of Anesthesiology, Washington University School of Medicine, 660 S. Euclid Ave., St. Louis, MO 63110.

[3] To whom correspondence should be addressed. Tel.: 301-820-2794; E-mail: hgowher@purdue.edu.

[4] The abbreviations used are: EC, endothelial cell; VEGF, vascular endothelial growth factor; Cited2, Cbp/p300-interacting transactivator with Glu/Asp-rich carboxyl-terminal domain 2; CBP, cAMP-responsive element-binding protein; ESC, embryonic stem cell; Vezf1, vascular endothelial zinc finger 1; LIF, leukemia inhibitory factor; IN, input; IP, immunoprecipitated, qPCR, quantitative PCR; Gapdh, glyceraldehyde-3-phosphate dehydrogenase; D, days post-differentiation.

cially at the onset of angiogenesis. Because its aberrant high expression in a specific developmental window can inhibit Hif-1α activity, this regulation can potentially be critical for angiogenesis in both embryonic stages and adulthood.

Mammalian Vezf1 is an essential transcription factor, which is expressed in the anterior-most mesoderm at E7.5 during development. Its expression is later restricted in the vascular endothelium, an observation that revealed its role in regulation of angiogenesis. *Vezf1* null mice die at approximately E9.5 (27). *Vezf1*$^{-/-}$ ESCs grow slower and make smaller embryoid bodies, which have defects in vascularization and cease to grow a few days post-differentiation (28, 29). *Vezf1* is expressed in both adult and embryonic ECs. Blocking the activity of Vezf1 by small molecule inhibitor Vec6 inhibits wound healing suggesting its role in postnatal angiogenesis (30). Vezf1 contains six Cys_2/His_2-type zinc finger motifs and binds poly(dG) or poly(dC) sequences (31, 32). It carries a glutamine-rich stretch and a proline-rich region that are characteristic of transcriptional activation or repression domains (33). It is proposed to act as a transcriptional activator of pro-angiogeneic genes including *endothelin 1*, *microtubule turnover protein*, *stathmin/OP18*, and *metallothionein* 1 (*MT1*) (34–36). However, no change in the expression of pro-angiogenic genes was seen in *Vezf1*$^{-/-}$ embryos (28). Other studies suggested an indirect role of Vezf1 by interacting with RhoB that promotes expression of RhoB-regulated pro-angiogenesis genes (30, 37). Therefore, the mechanism by which Vezf1 regulates angiogenesis is unclear.

To study the specific role of Vezf1 in endothelial development and angiogenesis, we examined the differentiation of WT and *Vezf1*$^{-/-}$ ESCs to ECs by treatment with VEGF-A_{165} and tested their angiogenic potential by a *in vitro* tube-formation assay. Our findings suggest that Vezf1 controls activation of angiogenesis in ECs by restricting *Cited2* expression to basal levels, which allows Hif-1α–mediated activation of the pro-angiogenic genes. We observed a strong increase in the expression of *Cited2* in *Vezf1*$^{-/-}$ ESCs compared with WT cells. In addition, the elevated expression of *Cited2* in *Vezf1*$^{-/-}$ ESCs affected their efficiency of differentiation into ECs and attenuated the ability of *Vezf1*$^{-/-}$ ECs to form vascular structures in a tube-formation assay. Concomitant with this, there was reduced activation of endothelial/pro-angiogenic genes in differentiating Vezf1$^{-/-}$ ECs. Based on our data showing reduced levels of histone H3K27Ac at the promoters of angiogenesis-specific genes, we propose that high levels of Cited2 sequester the histone acetyltransferase p300 away from angiogenesis-specific gene promoters, thus reducing their activation and gene expression. Together these observations substantiate the critical role of Vezf1 in controlling the expression of developmental regulators such as Cited2. Given that the expression of *Cited2* in ESCs is not completely turned off, we suggest the role of Vezf1 in fine-tuning *Cited2* expression in ESCs. Our previous work using genome-wide ChIP-SEQ showed that binding sites for Vezf1 are mostly present in CpG-rich regions (38). We also showed that Vezf1 binds to the chicken β-globin insulator suggesting a role in regulating enhancer-mediated control of gene expression (32, 38). Based on these studies, we speculate that the insulator function of Vezf1 blocks inappropriate interactions of the *Cited2* promoter with nearby enhancer/s, thus modulating the magnitude and spatiotemporal regulation of its expression.

Results

Cited2 expression is high in Vezf1$^{-/-}$ *ESCs*

To elucidate the mechanism of Vezf1, we had previously analyzed changes in gene expression of Vezf1$^{-/-}$ ESCs compared with WT ESCs using a microarray analysis (Fig. S1) (39). We found *Cited2* among the top 20 genes that were up-regulated in *Vezf1*$^{-/-}$ ESCs by more than 5-fold. To confirm this observation, we measured the gene expression of *Cited2* quantitatively in WT and *Vezf1*$^{-/-}$ ESCs by qRT-PCR and protein levels by Western blotting. The data show a 4–5-fold higher transcript and protein levels of Cited2 in *Vezf1*$^{-/-}$ ESCs compared with WT ESCs (Fig. 1, *A* and *B*). We found these observations consistent with our previously published ChIP-SEQ of Ser^2 phosphorylated RNA Pol II (elongating form of RNA Pol II) in WT and *Vezf1*$^{-/-}$ ESCs (38). Data analysis of elongating RNA Pol II showed more than a 2-fold higher enrichment in the Cited2 gene body in *Vezf1*$^{-/-}$ ESCs compared with the WT ESCs (Fig. 1*C*). Based on the known function of Cited2 as an anti-angiogenic factor (22–24), we hypothesized that a presence of high Cited2 level in *Vezf1*$^{-/-}$ cells could interrupt or delay the differentiation of ECs, or reduce their angiogenic potential.

Vezf1$^{-/-}$ *ESCs are defective in EC differentiation*

Cited2 expression is critical for pluripotency and differentiation of ESCs; therefore, we tested if overexpression of Cited2 affected the pluripotency of *Vezf1*$^{-/-}$ ESCs. We quantified the expression of the pioneer transcription factor, Oct4, in *Vezf1*$^{-/-}$ ESCs compared with that in the WT ESCs and observed no significant difference in its expression (Fig. 2*A*). Additionally, both WT and Vezf1$^{-/-}$ ESCs showed positive alkaline phosphate staining suggesting that high expression of Cited2 had little if any effect on the pluripotency of *Vezf1*$^{-/-}$ ESCs (Fig. 2*B*). Previous studies showed a reduced growth of *Vezf1*$^{-/-}$ EBs and defects in their vascular structures, but reported little or no difference in the endothelial differentiation in 3D cultures (27). We performed *in vitro* differentiation of WT and *Vezf1*$^{-/-}$ ESCs to ECs on gelatinized plates in the presence of 10 ng/μl of VEGF-A_{165}. The differentiation of ESCs to ECs was monitored by microscopy. During differentiation, the WT ESCs showed an expected loss of ~5–10% of cells, and differentiated efficiently into ECs. Comparatively, during the first 3 days of differentiation, over 80% *Vezf1*$^{-/-}$ cells died, leading to a reduced efficiency of EC derivation from the *Vezf1*$^{-/-}$ ESCs. This was confirmed by positive alkaline phosphatase staining of the surviving *Vezf1*$^{-/-}$ cells at 10 days post-differentiation (Fig. 2*C*).

Given that the expression of the EC lineage is driven by VEGF-A in an autoregulatory loop (9, 40), we tested if increasing the concentration of VEGF-A_{165} in the medium could improve EC differentiation and survival of *Vezf1*$^{-/-}$ cells. EC differentiation was monitored by measurement of endothelial-specific gene expression including *VEGF-A*, *Flk1*, *Flt1*, *CD31*, and *Tie2* (41). WT and Vezf1$^{-/-}$ ESCs were differentiated using 20, 40, and 60 ng/μl of VEGF-A_{165}. Increasing the VEGF-

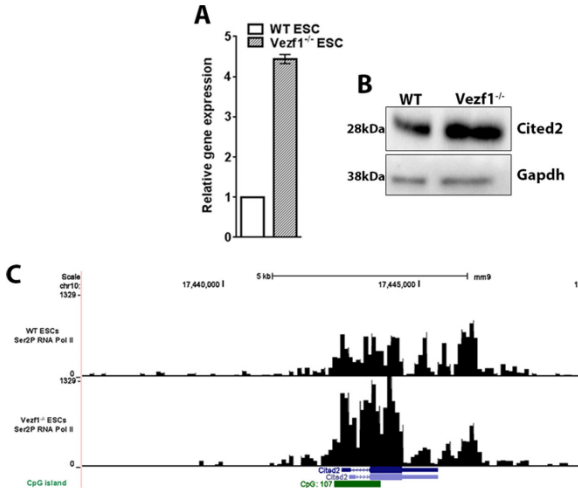

Figure 1. *A*, gene expression analysis of *Cited2* by RT-qPCR in WT and *Vezf1*$^{-/-}$ ESCs showed a 4–5-fold higher expression of *Cited2* in *Vezf1*$^{-/-}$ ESCs. Gene expression was normalized to Gapdh and represented relative to gene expression in WT ESC, set to 1. *B*, 50 μg of total cell extract were loaded from the WT and *Vezf1*$^{-/-}$ ESCs followed by Western blot analysis using anti-Cited2 antibody and anti-GAPDH antibody for loading control. *C*, screen shot from UCSC genome browser showing the occupancy of Ser^{5}-phosphorylated Pol II at the Cited2 locus in WT and *Vezf1*$^{-/-}$ ESCs. These data were obtained from the previously published publically available ChIP-SEQ data. *WT*, wildtype ESCs; *Vezf1*$^{-/-}$, Vezf1-knockout ESCs.

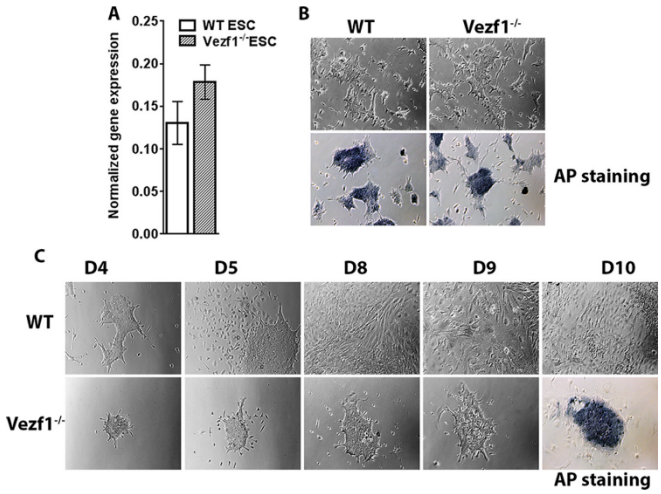

Figure 2. *A*, gene expression analysis by RT-qPCR of Oct4 in WT and *Vezf1*$^{-/-}$ ESCs. *B*, alkaline phosphatase (*AP*) staining for pluripotency in WT and *Vezf1*$^{-/-}$ ESCs; the presence of *dark blue* stain indicates positive for pluripotency. *C*, WT and *Vezf1*$^{-/-}$ ESCs were differentiated using 10 ng/μl of VEGF-A_{165} for 5, 6, 7, and 10 days and visualized using brightfield microscopy at ×10 magnification. Unlike the WT cells, the *Vezf1*$^{-/-}$ cells were unable to differentiate and most of the cells died. The field view is the representation of proliferation during differentiation and cell number. The panel for D10 shows alkaline phosphatase staining. A strong signal of *Vezf1*$^{-/-}$ cells indicates presence of undifferentiated stem cells. *WT*, wildtype ESCs; *Vezf1*$^{-/-}$, *Vezf1* knockout ESCs; *UD*, undifferentiated; D4–D10, days post-differentiation.

A_{165} to 20 ng/μl stimulated *Vezf1*$^{-/-}$ cells to differentiate to ECs with a higher efficiency (Fig. 3*A*). In both WT and *Vezf1*$^{-/-}$ ESCs, differentiation induced repression of the pluripotency gene, Oct4, and activation of endothelial-specific genes, *VEGF-A*, *Flk1*, *CD31*, and *Tie2*, albeit at lower levels in the *Vezf1*$^{-/-}$ cells (Fig. 3*B*). Reduced activation of *CD31* and *Tie2* in *Vezf1*$^{-/-}$ cells suggested a partial defect in EC differentiation. WT and *Vezf1*$^{-/-}$ ECs day (D) 6 and D8 post-differentiation treated with 20, 40, and 60 ng/μl of VEGF-A_{165} were collected for gene expression analysis by qRT-PCR. The data

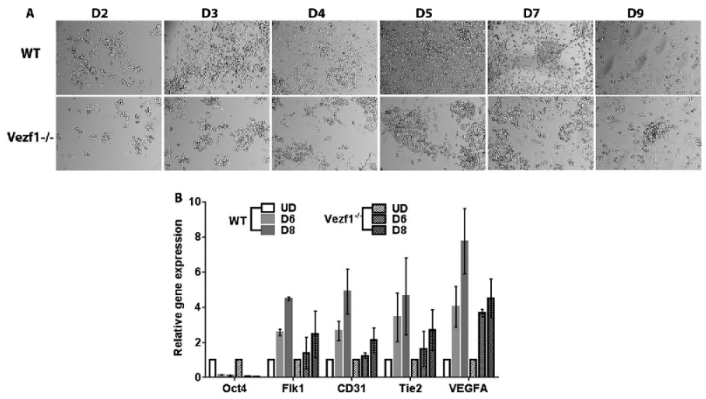

Figure 3. *A* and *B*, WT and *Vezf1*$^{-/-}$ ESCs were differentiated using 20 ng/μl of VEGF-A$_{165}$. *A*, differentiating WT and *Vezf1*$^{-/-}$ ECs were visualized using brightfield microscopy. Whereas most of the WT cells undergo distinct morphological changes, only a fraction acquire a similar morphology in *Vezf1*$^{-/-}$ cells. *B*, gene expression by RT-qPCR plotted as a relative change to the expression in UD where UD was set to 1. Endothelial specific genes, *Flk1*, *VEGF-A*, *CD31*, and *Tie2* show an expected increase in expression in differentiating WT ECs. Differentiating *Vezf1*$^{-/-}$ ECs, however, show significantly low expression of all tested endothelial-specific genes. A decrease in Oct4 expression is observed in both WT and *Vezf1*$^{-/-}$ ECs indicating loss of pluripotency. *WT*, wildtype; *Vezf1*$^{-/-}$, *Vezf1* knockout; *UD*, undifferentiated; *D2–D9*, days post-differentiation.

showed that at all three concentrations of VEGF-A$_{165}$, the expression of *VEGF-A* and its receptor, Flk1, was significantly higher in WT ECs compared with that in the *Vezf1*$^{-/-}$ ECs, indicating that gene expression is not further rescued by higher doses of VEGF-A$_{165}$ (Fig. 4). Previous studies have shown that *Hif-1*α expression can also be activated by treatment of ECs with VEGF-A$_{165}$ thus showing that VEGF regulates the expression of its own transcription factor (4). In WT and *Vezf1*$^{-/-}$ ECs, we checked the expression of *Hif-1*α and *Flt1*, which is the angiogenesis-specific VEGF receptor. Although no difference in the expression of *Hif-1*α was observed between WT and *Vezf1*$^{-/-}$ ECs, similar to *Flk1* and *VEGF-A*, *Flt1* expression was also comparatively lower in *Vezf1*$^{-/-}$ ECs at 20, 40, and 60 ng/μl of VEGF-A$_{165}$ in both D6 (Fig. 4, *A–D*) and D8 (Fig. 4, *E–H*) post-differentiation. These data show that in *Vezf1*$^{-/-}$ ECs, reduced expression of angiogenic genes including VEGF is not due to lower *Hif-1*α expression, but potentially due to its reduced activity.

Vezf1$^{-/-}$ *ECs are defective in forming vascular networks in 3D cultures*

We next tested the angiogenic potential of *Vezf1*$^{-/-}$ ECs by an *in vitro* tube-formation assay. We differentiated WT and *Vezf1*$^{-/-}$ ESCs to ECs for 8 days in the presence of VEGF-A$_{165}$ at 20 ng/μl. The ECs were collected and placed in Matrigel to form vascular networks or tubes in 3D culture. The mouse endothelial cell line, MSS31, was used as a positive control. Whereas WT ECs formed distinct tubes within 4–6 h in Matrigel, *Vezf1*$^{-/-}$ ECs showed significant defects in tube formation as indicated by the shorter tube length (Fig. 5, *A* and *B*).

Taken together, these data show that *Vezf1*$^{-/-}$ ESCs have reduced competence to differentiate into ECs and to form vascular structures in Matrigel. Given that Flt1 receptor function is required for tubulogenesis (42), the inability of *Vezf1*$^{-/-}$ ECs to form tubes in Matrigel could be the consequence of strongly reduced expression of *Flt1* in these cells. Because no change was observed in *Hif-1*α gene expression, we predict that the reduced expression of EC-specific genes is due to high *Cited2* expression in *Vezf1*$^{-/-}$ ESCs and ECs.

Induced repression of Cited2 partially rescues EC differentiation and vascular defects in Vezf1$^{-/-}$ *ECs*

We next tested the hypothesis that the defective vasculature formation by *Vezf1*$^{-/-}$ ECs is due to anomalous high expression of *Cited2*. We therefore asked if depletion of Cited2 in *Vezf1*$^{-/-}$ ESCs could rescue their ability to differentiate and make vascular networks. *Vezf1*$^{-/-}$ ESCs were transfected with *Cited2* shRNA, to generate stable transgenic ESCs lines, *Vezf1*$^{-/sh}$. Of the nine transgenic lines, some showed more than 10-fold reduction in Cited2 expression when compared with WT ESCs. Because Cited2 is known to be important for pluripotency (43), we chose to use the *Vezf1*$^{-/sh}$ cell line (7-2), in which Cited2 expression is reduced to levels similar to that of WT ESC (Fig. 6, *A* and *B*). The *Vezf1*$^{-/sh}$ ESCs were differentiated to ECs using 20, 40, and 60 ng/μl of VEGF-A$_{165}$. Compared with *Vezf1*$^{-/-}$ ESCs, *Vezf1*$^{-/sh}$ ESCs showed better survival and higher efficiency of EC differentiation at 20 ng/μl of VEGF-A$_{165}$, which was similar to the WT cells (Fig. 6*C*). The *Vezf1*$^{-/sh}$-derived ECs were collected on day 6 post-differentiation and RNA was extracted for gene-expression analysis. The data show that expression of VEGF-A was largely rescued, whereas Flt1 and Flk1 were partially rescued when compared with their expression in WT and *Vezf1*$^{-/-}$ ECs (Fig. 6*D*). Next, we tested if the derived ECs form vascular structures by a tube-formation assay. WT, *Vezf1*$^{-/-}$, and *Vezf1*$^{-/sh}$-derived ECs ((7-2) and (3-3)) were collected after 10 days and used to perform an *in vitro* tube-formation assay. *Vezf1*$^{-/sh}$ (3-3) ESCs have ~7-fold reduced expression of *Cited2* compared with WT ESCs. This cell line was therefore used to test the effect of Cited2 deficiency on EC differentiation and tube formation. The repression of

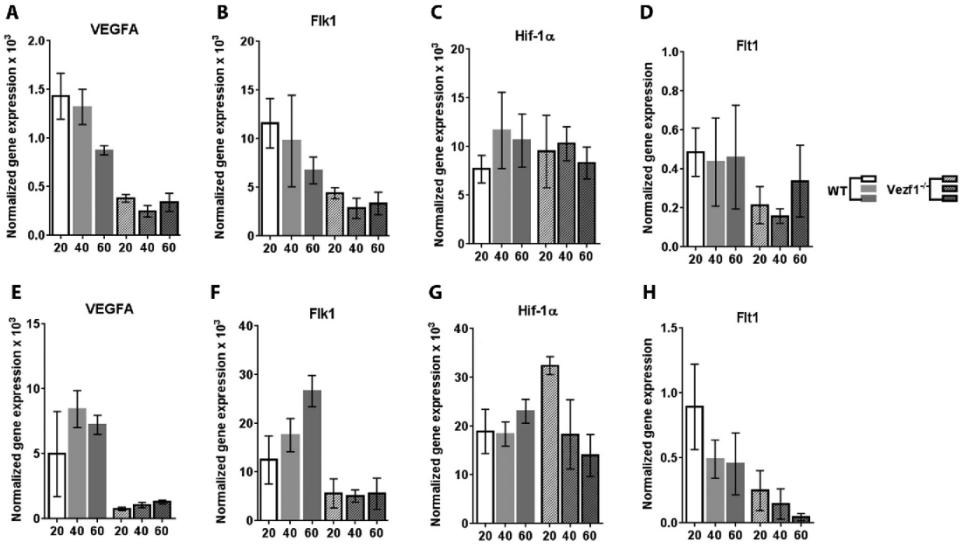

Figure 4. *A–D*, gene expression analysis in WT and *Vezf1*$^{-/-}$ D6 ECs, differentiated using 20, 40, and 60 ng/μl of VEGF-A$_{165}$. *E–H*, gene expression analysis in WT and *Vezf1*$^{-/-}$ D8 ECs differentiated using 20, 40 and 60 ng/μl of VEGF-A$_{165}$. The expression of all genes is increased in D8 compared with D6 post-differentiation. Higher doses of VEGF-A$_{165}$ have no further effect on expression of VEGF-A, Flk1, Hif-1α, and Flt1 in both WT or in *Vezf1*$^{-/-}$ cells. The data represents average and S.D. of 3 to 4 replicates. *WT*, wildtype; *Vezf1*$^{-/-}$, *Vezf1* knockout; *UD*, 20, 40, 60 ng/μl of VEGF-A$_{165}$ used for differentiation.

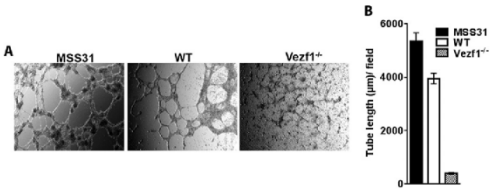

Figure 5. *A*, differentiated WT and *Vezf1*$^{-/-}$ EC plated in VEGF-supplemented Matrigel were incubated at 37 °C for 5–15 h. The formation of tube structures is visualized by brightfield microscopy. Mouse endothelial cell line MSS31 is used as a positive control. The images were taken at ×10 magnification at 12 h for MSS31, and 6 h for WT and *Vezf1*$^{-/-}$. *B*, measurement of tube length using ImageJ software. Compared with MSS31 and WT ECs, *Vezf1*$^{-/-}$ ECs were unable to make tube-like structures in Matrigel. *WT*, wildtype; *Vezf1*$^{-/-}$, *Vezf1* knockout.

Cited2 in *Vezf1*$^{-/sh}$ ECs largely rescued the defective tube formation on Matrigel, which was more prominent in *Vezf1*$^{-/sh}$ (7-2) compared with the (3-3) cell line (Fig. 7, *A* and *B*). This observation supports the known role of Cited2 in pluripotency and differentiation of ESCs and emphasizes the importance of the appropriate levels of developmental transcription factors for proper differentiation. These data directly support our hypothesis that an aberrant high expression of *Cited2* prevents the activation of EC-specific gene expression potentially by sequestering p300 from the promoters of angiogenesis-specific genes.

P300 activity is regulated by Cited2 at the VEGF-A promoter

In response to VEGF signaling, P300 acetyltransferase interacts with Hif-1α, which targets it to the HBS (HIF-1–binding element) of the promoters of angiogenesis-specific genes where it acetylates histone H3 at Lys^{27}. To test the impact of *Cited2* expression on the activity of P300 histone acetyltransferase at *VEGF* and *Flk-1* promoters, we performed a chromatin immunoprecipitation (ChIP) assay using anti-histone H3K27Ace antibody. We observed an expected increase in the fold-enrichment of H3K27Ace at VEGF and Flk-1 promoters in WT-differentiated ECs compared with the undifferentiated ESCs. However, this increase was markedly reduced in the differentiated *Vezf1*$^{-/-}$ ECs particularly at the *VEGF* promoter, which is a direct target of Hif-1α. As a control, we used the *Oct4* promoter where H3K27 acetylation is decreased post-differentiation in both the WT and *Vezf1*$^{-/-}$ ESCs (Fig. 8*A*). Although *Flk-1* has an HBS in its promoter, some studies indicate that it is targeted by both Hif-1α and HIF-1β (40). These data support our hypothesis that reduced P300 activity at angiogenesis-specific gene promoters inhibits their complete activation during *Vezf1*$^{-/-}$ EC differentiation.

Transcriptional regulation of Cited2 expression by Vezf1

Vezf1$^{-/-}$ ESCs show a genome-wide loss of DNA methylation at several CpG islands (CpGi's) flanking tissue-specific genes and a significant decrease in the expression of the DNA methyltransferase, Dnmt3b (39). Cited2 is encoded by a relatively small gene, which has a large CpGi at its promoter and exon 1 (Fig. 1*C*). We therefore asked if the increase in *Cited2* expression in *Vezf1*$^{-/-}$ ESCs could be due to loss of DNA methylation at its CpGi. To test the potential role of Dnmt3b in regulation of *Cited2* CpGi DNA methylation, genomic DNA from Dnmt3b$^{-/-}$ ESCs, *Vezf1*$^{-/-}$ ESCs, and WT ESCs was

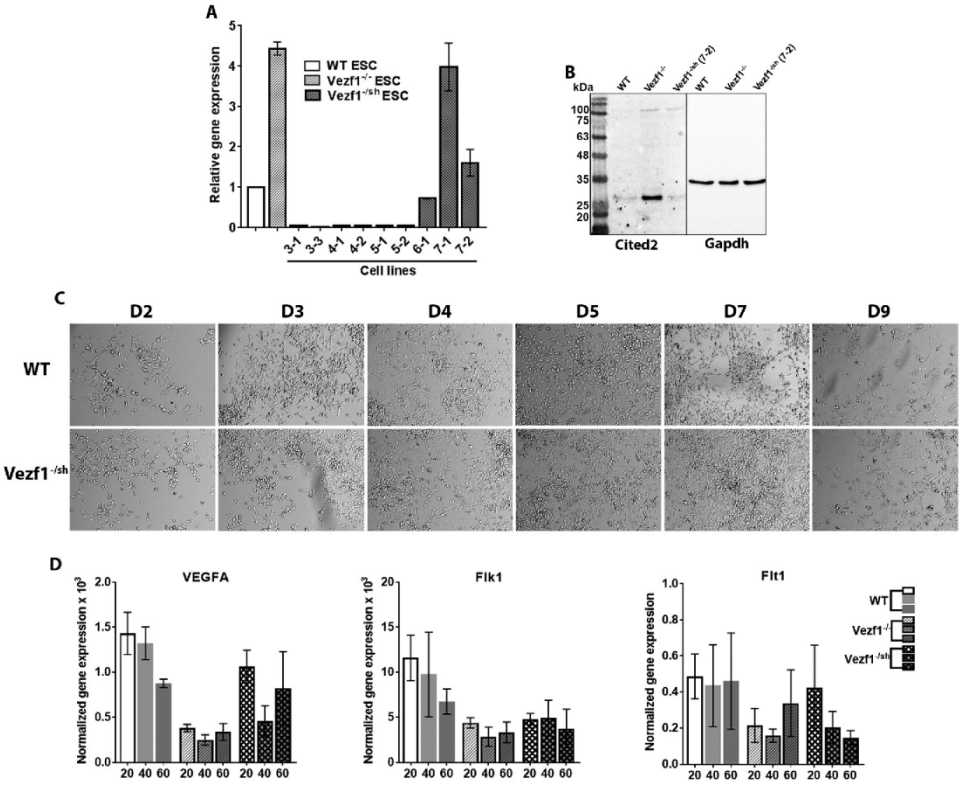

Figure 6. *A*, gene expression analysis of *Cited2* by RT-qPCR in *Vezf1*$^{-/sh}$ cell lines. Change in gene expression was plotted relative to that of WT ESCs, set to 1. Labels on the *x* axis represent various stable cell lines, of which the *Vezf1*$^{-/sh}$ cell line (7-2) has *Cited2* expression reduced to the levels similar to WT ESCs. *B*, Western blot analysis using 50 μg of total cell extract from the WT, *Vezf1*$^{-/-}$, and *Vezf1*$^{-/sh}$ (7-2) ESCs probed with anti-Cited2 antibody and anti-GAPDH. *C*, differentiation of WT, *Vezf1*$^{-/-}$, and *Vezf1*$^{-/sh}$ (7-2) ESCs was induced using 20 ng/μl of VEGF-A$_{165}$. D2–D6 are days post-differentiation. Compared with the differentiating WT cells, *Vezf1*$^{-/sh}$ (7-2) show similar morphology and cell number indicating at least a partial rescue of their ability to differentiate into ECs. *D*, gene expression analysis of *Vezf1*$^{-/sh}$ (7-2) ESCs, which were differentiated to ECs at 20, 40, and 60 ng/μl of VEGF-A$_{165}$. Expression of pro-angiogeneic genes *VEGF-A*, *Flk1*, and *Flt1* was measured. Compared with WT and *Vezf1*$^{-/-}$ cells, gene expression was largely rescued in *Vezf1*$^{-/sh}$ (7-2) ECs. The data represent the average and S.D. of 3 to 4 replicates. *WT*, wildtype ESCs; *Vezf1*$^{-/-}$, Vezf1 knockout ESCs; *Vezf1*$^{-/sh}$, stable transgenic *Vezf1*$^{-/-}$ ESCs expressing Cited2-shRNA; *20*, *40*, *60*, ng/μl of VEGF-A$_{165}$ used for differentiation.

extracted to quantify DNA methylation using bisulfite sequencing. Our data show very low CpG methylation at *Cited2* CpGi in WT ESCs that did not change in *Vezf1*$^{-/-}$ and Dnmt3b$^{-/-}$ ESCs (Fig. 8*B*). *Cited2* gene expression also showed no change in Dnmt3b$^{-/-}$ compared with that in WT ESCs (Fig. 8*C*). These data confirm that expression of *Cited2* is not regulated by Dnmt3b or changes in DNA methylation at its CpGi and support the direct role of Vezf1 in regulating *Cited2* expression. Therefore, we investigated the binding of Vezf1 near the *Cited2* promoter by ChIP assay using custom-made rabbit polyclonal anti-Vezf1 antibody, which was previously characterized and used in ChIP studies in ESCs (12, 34). We observed a high relative enrichment of Vezf1 at the *Cited2* promoter in WT ESCs (Fig. 8*D*). These data suggest a direct regulation of *Cited2* expression by Vezf1 through its binding at the promoter-associated CpGi.

Taken together our *in vitro* differentiation experiments show that the aberrant high expression of *Cited2* in *Vezf1*$^{-/-}$ ESCs suppresses their angiogenic potential by sequestering P300/CBP away from the pioneer transcription factor Hif-1α. This abbreviates the promoter activation of the downstream pro-angiogenic genes (Fig. 8*E*). These findings suggest that Vezf1 regulates angiogenesis by fine-tuning the level of anti-angiogenic factor Cited2.

Discussion

The transcription factor Vezf1 is highly expressed in vascular endothelium and its role in vascular development has been observed by several earlier studies (28, 34, 36, 44, 45). For example, recent studies have shown that a small molecule inhibitor of Vezf1, Vec6, prevents wound healing and angiogenesis (30). Although the function of Vezf1 has been suggested through its

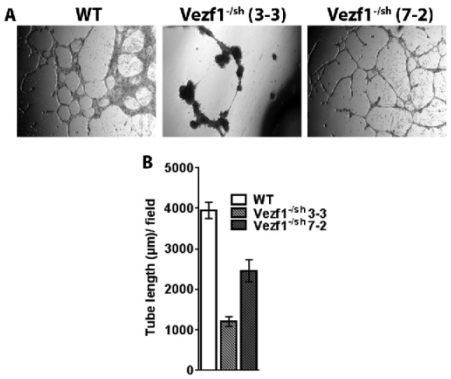

Figure 7. *A*, WT, *Vezf1*$^{-/sh}$ (7-2), and *Vezf1*$^{-/sh}$ (3-3) cells were differentiated for 10 days and used in a tube-formation assay. The *Vezf1*$^{-/sh}$ cell line (3-3) had about 7-fold lower Cited2 expression than WT. Compared with the WT cells, tube formation was rescued in *Vezf1*$^{-/sh}$ (7-2) ECs, which was absent in *Vezf1*$^{-/sh}$ (3-3) ECs. Images were taken at 12 h for *Vezf1*$^{-/sh}$ (3-3) and 6 h for WT and *Vezf1*$^{-/sh}$ (7-2). *B*, tube length was measured by ImageJ software and plotted.

role as a transcriptional activator of some genes that are known to promote angiogenesis, previous studies were performed using semi-quantitative RT-PCR to measure the expression of pro-angiogenic genes in *Vezf1*$^{-/-}$ embryos. These data showed no change in the expression of pro-angiogenic factors compared with WT embryos (28). Unlike the previous study (28), we used quantitative RT-PCR to measure gene expression changes and our data show about 2–3-fold lower expression of several pro-angiogenic genes, including *CD31*, *Tie2*, *VEGF-A*, and its receptors *Flk-1* and *Flt-1* in the *in vitro* derived *Vezf1*$^{-/-}$ ECs. The defective EC differentiation of *Vezf1*$^{-/-}$ ESCs was also supported by impaired morphological changes associated with EC differentiation. We further show that the expression of some of these genes can be largely rescued by down-regulating *Cited2*, which is aberrantly overexpressed in *Vezf1*$^{-/-}$ ESCs. Our data support the previously suggested role of Vezf1 in angiogenesis, however, through a different mechanism. In contrast to its previously predicted role as a transcriptional activator, our data show that Vezf1 restricts the expression of the anti-angiogenic gene *Cited2* to basal levels, ensuring a balanced gene expression during angiogenesis. Our data also emphasize that small but quantifiable changes in gene expression of developmental transcription factors and regulators can have profound effect on cell differentiation.

Cited2 (Mrg1/p35srj) belongs to a family of transactivators that lack direct DNA binding but contain glutamic acid/aspartic acid (ED)-rich tail, which interacts with P300/CBP acetyltransferase. Whereas, on one hand, Cited2 competes with Hif-1α to interact with P300/CBP, *Cited2* promoter has HIF1-binding sites and its expression is up-regulated in hypoxia by Hif-1α. Therefore, Cited2 participates in a negative-feedback loop with Hif-1α in which Cited2 accumulates during hypoxia. During restoration of normaxia, it will inhibit Hif-1α activity and prevent hypervascularization. An anomalous high expression of *Cited2* at the onset of angiogenesis could interfere with Hif-1α-mediated activation of pro-angiogenic genes, consequently the expression of *Cited2* must be tightly controlled. We propose that in undifferentiated ESCs, Vezf1 modulates the expression of *Cited2*, thus enabling Hif-1α–mediated gene activation during angiogenesis. This mechanism is supported by our data showing that overexpression of *Cited2* causes defective tube formation by *Vezf1*$^{-/-}$ ECs when there is no difference in Hif-1α expression between the WT and *Vezf1*$^{-/-}$ cells. *Cited2* is expressed throughout early embryogenesis and its expression in ESCs is critical for pluripotency, and appropriate differentiation (13, 43). Our data showing absence of rescue in a *Vezf1*$^{-/sh}$ (3-3) cell line, which has *Cited2* expression significantly lower than WT ESCs, supports the role of the basal expression of *Cited2* in maintenance of pluripotency and differentiation potential of ESCs. Vezf1-mediated regulation of *Cited2* expression is also potentially relevant during adult angiogenesis and wound healing where Vezf1 could down-regulate or maintain low *Cited2* expression in the ECs. This prediction is supported by our observation from a published microarray analysis of *Vezf1*-silenced BVEC's, listing *Cited2* among the up-regulated genes (30). This study also showed that loss of Vezf1 causes inhibition of wound healing and blood vessel formation (30).

Based on the previously characterized role of Vezf1 as an insulator binding protein, it is highly plausible that Vezf1 insulates its target promoters from interaction with nonspecific enhancers, and in the case of *Cited2* from the enhancers in the downstream gene, *β-taxilin* (*Txlnb*). The insulator function of Vezf1 is supported by our published ChIP-SEQ studies showing that a significant number of Vezf1-binding sites are adjacent to insulator protein, CTCF. Vezf1 shows widespread binding at CpGi's present in the regulatory elements of genes including promoters, enhancers, and insulators (32, 38). By using *in vitro* EC differentiation as a developmental model system, it will be important to explore the regulatory potential of Vezf1-mediated insulator function in modulating gene expression during development.

Experimental procedures

Embryonic stem cell culture

Undifferentiated WT, Dnmt3b$^{-/-}$, and *Vezf1*$^{-/-}$ ESCs were cultured in Dulbecco's modified Eagle's medium containing 15% ESC qualified fetal bovine serum (Millipore), supplemented with nonessential amino acids, glutamine, 1000 units/ml of leukemia inhibitory factor (LIF) (ESGRO; Chemicon International), and 50 μM β-mercaptoethanol. Cells were cultured on 0.1% gelatin for one passage before switching to differentiation conditions.

Endothelial lineage differentiation

ESCs were plated at a density of 3×10^3 cells/cm^2 on gelatinized plates in ESC medium with LIF and incubated overnight to attach. The next day the media was removed and cells were washed with PBS. Differentiation was induced by adding ESC medium without LIF and VEGF-A_{165} (R&D Systems) at 20 – 60 ng/μl. VEGF-A_{165} was supplemented to the culture every alternate day for 10 days to drive differentiation into endothelial lineage. Cell morphology was monitored using phase-contrast

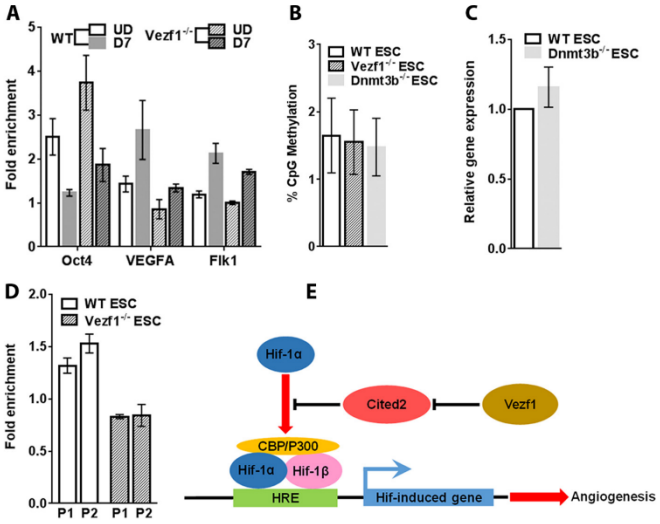

Figure 8. *A*, ChIP-qPCR of H3K27Ace showed an increase in the fold-enrichment of H3K27Ace at VEGF-A and Flk1 promoters in WT ECs that were reduced in *Vezf1*$^{-/-}$ ECs. At the Oct4 promoter, post-differentiation, deacetylation of H3K27 is accompanied by the loss of gene expression. Therefore, it serves as a negative control. *B*, DNA methylation was analyzed at *Cited2* CpGi using bisulfite sequencing in undifferentiated ESCs. The average percent methylation of 27 CpG sites in the CpGi was plotted. *C*, gene expression analysis of Cited2 in WT and Dnmt3b$^{-/-}$ ESCs. There was no significant difference in *Cited2* expression levels. *D*, ChIP-qPCR using anti-Vezf1 antibody showed an increase in the fold-enrichment at *Cited2* promoter in WT ESCs. Fold-enrichment below 1 in *Vezf1*$^{-/-}$ ESCs indicates absence of binding, and was used as negative control. The data in each *bar graph* represents average and S.D. of 3 to 4 replicates. *E*, model showing the effect of Cited2 on Hif-1α-mediated regulation of pro-angiogenic genes. Vezf1 regulates the expression of Cited2 at basal levels in ESCs before the induction of endothelial differentiation. This allows the interaction of Hif-1α and P300 that activate the pro-angiogenic genes. In the absence of Vezf1, high expression of Cited2 sequesters P300 away from Hif-1α, thus inhibiting the activation of pro-angiogenic genes. *WT*, wildtype; *Vezf1*$^{-/-}$, *Vezf1* knockout; *Dnmt3b*$^{-/-}$, Dnmt3b knockout; *UD*, undifferentiated; *D7*, days post-differentiation; *P1* and *P2*, two primer pairs in *Cited2* promoter used in ChIP-qPCR.

microscopy and pluripotency was monitored by alkaline phosphatase staining.

Tube-formation assay

The ECs on D10 post-differentiation were collected by trypsinization and counted using Bio-Rad Cell Counter. The tube-formation assay was performed by plating 2×10^5 ECs on a 24-well plate coated with VEGF supplemented Matrigel (BD Biosciences) according to the manufacturer's protocol (46, 47). The cells were incubated at 37 °C for 3–18 h. Tubing was scored using images from phase-contrast microscopy (29). The length of the tubes was measured by ImageJ software.

Transfection and generation of stable ESC lines

The lentivirus construct pLKO.1 carrying shRNA specific for Cited2 was purchased from Dharmacon. The recombinant lentivirus containing Cited2 shRNA was packaged using Vira Power (Fisher Thermo Scientific) in 293FT cells using the manufacturer's protocol. For shRNA-mediated depletion of Cited2, WT, and *Vezf1*$^{-/-}$ ESCs were transfected by lentivirus at a multiplicity of infection of 2 followed by selection of transgenic lines with stably integrated lentivirus construct using 3 μg/ml of puromycin.

Gene expression by quantitative RT-PCR and Western blotting

RNA from cells was purified using TRIzol (Invitrogen, 15596026) according to the manufacturer's protocol. Genomic DNA contamination was removed by DNase (Roche Applied Science, 04716728001) treatment at 37 °C overnight. Quantitative RT-PCR was performed for equal amounts of RNA by using Verso One-Step kit (Thermo Scientific, AB-4104A). The data were analyzed and gene expression was normalized to *Gapdh* expression. The change in expression is represented either as normalized gene expression or as relative gene expression that is changed relative to expression in the undifferentiated cells, set to 1. See Table S1 for primers used. Western blot analysis was performed using commercially available antibodies anti-Cited2 (ab108345, Abcam) and anti-Gapdh (sc47724, Santa Cruz) according to the manufacturers' recommendation.

DNA-methylation assay

DNA-methylation assay was performed by bisulfite sequencing (Bis-SEQ). Bisulfite sequencing was performed using the EpiTect Fast Bisulfite Conversion Kit (Qiagen, 59802). Genomic DNA was purified from WT, *Vezf1*$^{-/-}$, and Dnmt3b$^{-/-}$ ESCs. 1 μg of genomic DNA was used and bisulfite-converted DNA was amplified using nested primers and *Taq* polymerase (New England Biolabs, M0267L). Products from the inner PCR were used to generate a library for high throughput sequencing using Wide-SEQ. The primers used are listed in Table S1.

ChIP

ChIP was performed using cross-linked chromatin from WT and *Vezf1*$^{-/-}$ ESCs using a previously published protocol (18). Briefly, cells were cross-linked for 5 min with 1% formaldehyde in buffer (0.1 M NaCl, 1 mM EDTA, 0.5 mM EGTA, and 50 mM HEPES, pH 8). Nuclei were isolated and chromatin was sheared to 0.5–1-kb fragments using a Covaris E210 device, according to the manufacturer's protocols. Antibodies (8 μg) were immobilized on Protein A/G magnetic beads (Life Technologies, 10002D and 10004D) by overnight incubation. The magnetic beads were washed to remove unconjugated antibody and mixed with 8 μg of sonicated chromatin. After an overnight incubation, magnetic beads were washed, and bound DNA was purified. DNA was quantified using PicoGreen (Life Technologies, P11495) in a NanoDrop 3300 fluorospectrometer. Quantitative PCR was then performed using equal amounts of IN (input) and IP (immunoprecipitated sample) DNA. Fold-enrichment was calculated as follows: C_t(IN)−C_t(IP) and the fold-change was calculated by using $2\wedge(C_t(\text{IN})-C_t(\text{IP}))$. The fold-enrichment of 1 or less indicates no binding. See Table S1 for primers used. The H3K27Ace antibody used is commercially available (39133, Active Motif) and anti-Vezf1 antibody is a previously characterized custom-made polyclonal antibody.

Author contributions—L. A., M. H., Q. Y., and H. G. formal analysis; L. A., M. H., and A. B. N. validation; L. A., M. H., Q. Y., and A. B. N. investigation; L. A. and Q. Y. methodology; L. A., M. H., and H. G. writing-review and editing; M. H. visualization; M. H. and H. G. project administration; Q. Y. and H. G. writing-original draft; H. G. conceptualization; H. G. supervision; H. G. funding acquisition.

Acknowledgments—We thank Dr. Sandra Rossie for reading the manuscript, Dr. Taiping Chen for providing Dnmt3b$^{-/-}$ *ESCs, and Dr. Heidi Stuhlmann for Vezf1*$^{-/-}$ ESCs.

References

1. Carmeliet, P. (2000) Mechanisms of angiogenesis and arteriogenesis. *Nat. Med.* **6,** 389–395 CrossRef Medline
2. Risau, W. (1997) Mechanisms of angiogenesis. *Nature* **386,** 671–674 CrossRef Medline
3. Marcelo, K. L., Goldie, L. C., and Hirschi, K. K. (2013) Regulation of endothelial cell differentiation and specification. *Circ. Res.* **112,** 1272–1287 CrossRef Medline
4. Deudero, J. J., Caramelo, C., Castellanos, M. C., Neria, F., Fernández-Sánchez, R., Calabia, O., Peñnate, S., and González-Pacheco, F. R. (2008) Induction of hypoxia-inducible factor 1α gene expression by vascular endothelial growth factor. *J. Biol. Chem.* **283,** 11435–11444 CrossRef Medline
5. Imanirad, P., and Dzierzak, E. (2013) Hypoxia and HIFs in regulating the development of the hematopoietic system. *Blood Cells Mol. Dis.* **51,** 256–263CrossRef Medline
6. Semenza, G. L. (1999) Regulation of mammalian O2 homeostasis by hypoxia-inducible factor 1. *Annu. Rev. Cell Dev. Biol.* **15,** 551–578 CrossRef Medline
7. Semenza, G. L. (2001) Hypoxia-inducible factor 1: oxygen homeostasis and disease pathophysiology. *Trends Mol. Med.* **7,** 345–350 CrossRef Medline
8. Zelzer, E., Levy, Y., Kahana, C., Shilo, B. Z., Rubinstein, M., and Cohen, B. (1998) Insulin induces transcription of target genes through the hypoxia-inducible factor HIF-1alpha/ARNT. *EMBO J.* **17,** 5085–5094 CrossRef Medline
9. Hellwig-Bürgel, T., Rutkowski, K., Metzen, E., Fandrey, J., and Jelkmann, W. (1999) Interleukin-1β and tumor necrosis factor-α stimulate DNA binding of hypoxia-inducible factor-1. *Blood* **94,** 1561–1567 Medline
10. Görlach, A., Diebold, I., Schini-Kerth, V. B., Berchner-Pfannschmidt, U., Roth, U., Brandes, R. P., Kietzmann, T., and Busse, R. (2001) Thrombin activates the hypoxia-inducible factor-1 signaling pathway in vascular smooth muscle cells: role of the p22(phox)-containing NADPH oxidase. *Circ. Res.* **89,** 47–54 CrossRef Medline
11. Spinella, F., Rosanò, L., Di Castro, V., Natali, P. G., and Bagnato, A. (2002) Endothelin-1 induces vascular endothelial growth factor by increasing hypoxia-inducible factor-1α in ovarian carcinoma cells. *J. Biol. Chem.* **277,** 27850–27855 CrossRef Medline
12. Laughner, E., Taghavi, P., Chiles, K., Mahon, P. C., and Semenza, G. L. (2001) HER2 (neu) signaling increases the rate of hypoxia-inducible factor 1α (HIF-1α) synthesis: novel mechanism for HIF-1-mediated vascular endothelial growth factor expression. *Mol. Cell. Biol.* **21,** 3995–4004 CrossRef Medline
13. Pacheco-Leyva, I., Matias, A. C., Oliveira, D. V., Santos, J. M., Nascimento, R., Guerreiro, E., Michell, A. C., van De Vrugt, A. M., Machado-Oliveira, G., Ferreira, G., Domian, I., and Bragança, J. (2016) CITED2 cooperates with ISL1 and promotes cardiac differentiation of mouse embryonic stem cells. *Stem Cell Rep.* **7,** 1037–1049 CrossRef Medline
14. Yin, Z., Haynie, J., Yang, X., Han, B., Kiatchoosakun, S., Restivo, J., Yuan, S., Prabhakar, N. R., Herrup, K., Conlon, R. A., Hoit, B. D., Watanabe, M., and Yang, Y.-C. (2002) The essential role of Cited2, a negative regulator for HIF-1α, in heart development and neurulation. *Proc. Natl. Acad. Sci. U.S.A.* **99,** 10488–10493 CrossRef
15. Bamforth, S. D., Bragança, J., Eloranta, J. J., Murdoch, J. N., Marques, F. I., Kranc, K. R., Farza, H., Henderson, D. J., Hurst, H. C., and Bhattacharya, S. (2001) Cardiac malformations, adrenal agenesis, neural crest defects and exencephaly in mice lacking Cited2, a new Tfap2 co-activator. *Nat. Genet.* **29,** 469–474 CrossRef Medline
16. Bamforth, S. D., Bragança, J., Farthing, C. R., Schneider, J. E., Broadbent, C., Michell, A. C., Clarke, K., Neubauer, S., Norris, D., Brown, N. A., Anderson, R. H., and Bhattacharya, S. (2004) Cited2 controls left-right patterning and heart development through a Nodal-Pitx2c pathway. *Nat. Genet.* **36,** 1189–1196 CrossRef Medline
17. Qu, X., Lam, E., Doughman, Y. Q., Chen, Y., Chou, Y. T., Lam, M., Turakhia, M., Dunwoodie, S. L., Watanabe, M., Xu, B., Duncan, S. A., and Yang, Y. C. (2007) Cited2, a coactivator of HNF4α, is essential for liver development. *EMBO J.* **26,** 4445–4456 CrossRef Medline
18. Petell, C. J., Alabdi, L., He, M., San Miguel, P., Rose, R., and Gowher, H. (2016) An epigenetic switch regulates *de novo* DNA methylation at a subset of pluripotency gene enhancers during embryonic stem cell differentiation. *Nucleic Acids Res.* **44,** 7605–7617 CrossRef Medline
19. Du, J., and Yang, Y. C. (2013) Cited2 in hematopoietic stem cell function. *Curr. Opin. Hematol.* **20,** 301–307 CrossRef Medline
20. Du, J., and Yang, Y. C. (2012) HIF-1 and its antagonist Cited2: regulators of HSC quiescence. *Cell Cycle* **11,** 2413–2414 CrossRef Medline
21. Kranc, K. R., Schepers, H., Rodrigues, N. P., Bamforth, S., Villadsen, E., Ferry, H., Bouriez-Jones, T., Sigvardsson, M., Bhattacharya, S., Jacobsen, S. E., and Enver, T. (2009) Cited2 is an essential regulator of adult hematopoietic stem cells. *Cell Stem Cell* **5,** 659–665 CrossRef Medline
22. Bragança, J., Eloranta, J. J., Bamforth, S. D., Ibbitt, J. C., Hurst, H. C., and Bhattacharya, S. (2003) Physical and functional interactions among AP-2 transcription factors, p300/CREB-binding protein, and CITED2. *J. Biol. Chem.* **278,** 16021–16029 CrossRef Medline
23. Fox, S. B., Bragança, J., Turley, H., Campo, L., Han, C., Gatter, K. C., Bhattacharya, S., and Harris, A. L. (2004) CITED4 inhibits hypoxia-activated transcription in cancer cells, and its cytoplasmic location in breast cancer is associated with elevated expression of tumor cell hypoxia-inducible factor 1α. *Cancer Res.* **64,** 6075–6081 CrossRef Medline
24. Freedman, S. J., Sun, Z. Y., Kung, A. L., France, D. S., Wagner, G., and Eck, M. J. (2003) Structural basis for negative regulation of hypoxia-inducible factor-1α by CITED2. *Nat. Struct. Biol.* **10,** 504–512 CrossRef Medline
25. Agrawal, A., Gajghate, S., Smith, H., Anderson, D. G., Albert, T. J., Shapiro, I. M., and Risbud, M. V. (2008) Cited2 modulates hypoxia-inducible factor-dependent expression of vascular endothelial growth

factor in nucleus pulposus cells of the rat intervertebral disc. *Arthritis Rheum.* **58,** 3798–3808 CrossRef Medline
26. Lee, J. Y., Taub, P. J., Wang, L., Clark, A., Zhu, L. L., Maharam, E. R., Leong, D. J., Ramcharan, M., Li, Z., Liu, Z., Ma, Y. Z., Sun, L., Zaidi, M., Majeska, R. J., and Sun, H. B. (2009) Identification of CITED2 as a negative regulator of fracture healing. *Biochem. Biophys. Res. Commun.* **387,** 641–645 CrossRef Medline
27. Xiong, J. W., Leahy, A., Lee, H. H., and Stuhlmann, H. (1999) Vezf1: a Zn finger transcription factor restricted to endothelial cells and their precursors. *Dev. Biol.* **206,** 123–141 CrossRef Medline
28. Kuhnert, F., Campagnolo, L., Xiong, J. W., Lemons, D., Fitch, M. J., Zou, Z., Kiosses, W. B., Gardner, H., and Stuhlmann, H. (2005) Dosage-dependent requirement for mouse Vezf1 in vascular system development. *Dev. Biol.* **283,** 140–156 CrossRef Medline
29. Zou, Z., Ocaya, P. A., Sun, H., Kuhnert, F., and Stuhlmann, H. (2010) Targeted Vezf1-null mutation impairs vascular structure formation during embryonic stem cell differentiation. *Arterioscler. Thromb. Vasc. Biol.* **30,** 1378–1388 CrossRef
30. Gerald, D., Adini, I., Shechter, S., Perruzzi, C., Varnau, J., Hopkins, B., Kazerounian, S., Kurschat, P., Blachon, S., Khedkar, S., Bagchi, M., Sherris, D., Prendergast, G. C., Klagsbrun, M., Stuhlmann, H., Rigby, A. C., Nagy, J. A., and Benjamin, L. E. (2013) RhoB controls coordination of adult angiogenesis and lymphangiogenesis following injury by regulating VEZF1-mediated transcription. *Nat. Commun.* **4,** 2824 CrossRef Medline
31. Clark, S. P., Lewis, C. D., and Felsenfeld, G. (1990) Properties of BGP1, a poly(dG)-binding protein from chicken erythrocytes. *Nucleic Acids Res.* **18,** 5119–5126 CrossRef Medline
32. Dickson, J., Gowher, H., Strogantsev, R., Gaszner, M., Hair, A., Felsenfeld, G., and West, A. G. (2010) VEZF1 elements mediate protection from DNA methylation. *PLoS Genet.* **6,** e1000804 CrossRef Medline
33. Koyano-Nakagawa, N., Nishida, J., Baldwin, D., Arai, K., and Yokota, T. (1994) Molecular cloning of a novel human cDNA encoding a zinc finger protein that binds to the interleukin-3 promoter. *Mol. Cell. Biol.* **14,** 5099–5107 CrossRef Medline
34. Miyashita, H., and Sato, Y. (2005) Metallothionein 1 is a downstream target of vascular endothelial zinc finger 1 (VEZF1) in endothelial cells and participates in the regulation of angiogenesis. *Endothelium* **12,** 163–170 CrossRef Medline
35. Miyashita, H., Kanemura, M., Yamazaki, T., Abe, M., and Sato, Y. (2004) Vascular endothelial zinc finger 1 is involved in the regulation of angiogenesis: possible contribution of stathmin/OP18 as a downstream target gene. *Arterioscler. Thromb. Vasc. Biol.* **24,** 878–884 CrossRef
36. Aitsebaomo, J., Kingsley-Kallesen, M. L., Wu, Y., Quertermous, T., and Patterson, C. (2001) Vezf1/DB1 is an endothelial cell-specific transcription factor that regulates expression of the endothelin-1 promoter. *J. Biol. Chem.* **276,** 39197–39205 CrossRef Medline
37. Lebowitz, P. F., and Prendergast, G. C. (1998) Functional interaction between RhoB and the transcription factor DB1. *Cell Adhes. Commun.* **6,** 277–287 CrossRef Medline
38. Gowher, H., Brick, K., Camerini-Otero, R. D., and Felsenfeld, G. (2012) Vezf1 protein binding sites genome-wide are associated with pausing of elongating RNA polymerase II. *Proc. Natl. Acad. Sci. U.S.A.* **109,** 2370–2375 CrossRef
39. Gowher, H., Stuhlmann, H., and Felsenfeld, G. (2008) Vezf1 regulates genomic DNA methylation through its effects on expression of DNA methyltransferase Dnmt3b. *Genes Dev.* **22,** 2075–2084 CrossRef Medline
40. Hu, C.-J., Wang, L.-Y., Chodosh, L. A., Keith, B., and Simon, M. C. (2003) Differential roles of hypoxia-inducible factor 1α (HIF-1α) and HIF-2α in hypoxic gene regulation. *Mol. Cell. Biol.* **23,** 9361–9374 CrossRef Medline
41. Yamaguchi, T. P., Dumont, D. J., Conlon, R. A., Breitman, M. L., and Rossant, J. (1993) flk-1, an flt-related receptor tyrosine kinase is an early marker for endothelial cell precursors. *Development* **118,** 489–498 Medline
42. Yang, S., Xin, X., Zlot, C., Ingle, G., Fuh, G., Li, B., Moffat, B., de Vos, A. M., and Gerritsen, M. E. (2001) Vascular endothelial cell growth factor-driven endothelial tube formation is mediated by vascular endothelial cell growth factor receptor-2, a kinase insert domain-containing receptor. *Arterioscler. Thromb. Vasc. Biol.* **21,** 1934–1940 CrossRef
43. Kranc, K. R., Oliveira, D. V., Armesilla-Diaz, A., Pacheco-Leyva, I., Catarina Matias, A., Luisa Escapa, A., Subramani, C., Wheadon, H., Trindade, M., Nichols, J., Kaji, K., Enver, T., and Bragança, J. (2015) Acute loss of Cited2 impairs Nanog expression and decreases self-renewal of mouse embryonic stem cells. *Stem Cells* **33,** 699–712 Medline
44. Bruderer, M., Alini, M., and Stoddart, M. J. (2013) Role of HOXA9 and VEZF1 in endothelial biology. *J. Vasc. Res.* **50,** 265–278 CrossRef Medline
45. Yang, Z., and Li, J. C. (2008) Stimulation of endothelin-1 gene expression by insulin via phosphoinositide-3 kinase-glycogen synthase kinase-3β signaling in endothelial cells. *Life Sci.* **82,** 512–518 CrossRef Medline
46. Valster, A., Tran, N. L., Nakada, M., Berens, M. E., Chan, A. Y., and Symons, M. (2005) Cell migration and invasion assays. *Methods* **37,** 208–215 CrossRef Medline
47. Eccles, S. A., Box, C., and Court, W. (2005) Cell migration/invasion assays and their application in cancer drug discovery. *Biotechnol. Annu. Rev.* **11,** 391–421 CrossRef Medline

Biochemistry

Article

Cite This: *Biochemistry* 2018, 57, 4312−4324

pubs.acs.org/biochemistry

Dnmt3b Methylates DNA by a Noncooperative Mechanism, and Its Activity Is Unaffected by Manipulations at the Predicted Dimer Interface

Allison B. Norvil, Christopher J. Petell, Lama Alabdi, Lanchen Wu, Sandra Rossie, and Humaira Gowher*

Department of Biochemistry, Purdue University Center for Cancer Research, Purdue University, West Lafayette, Indiana 47907, United States

Supporting Information

ABSTRACT: The catalytic domains of the *de novo* DNA methyltransferases Dnmt3a-C and Dnmt3b-C are highly homologous. However, their unique biochemical properties could potentially contribute to differences in the substrate preferences or biological functions of these enzymes. Dnmt3a-C forms tetramers through interactions at the dimer interface, which also promote multimerization on DNA and cooperativity. Similar to the case for processive enzymes, cooperativity allows Dnmt3a-C to methylate multiple sites on the same DNA molecule; however, it is unclear whether Dnmt3b-C methylates DNA by a cooperative or processive mechanism. The importance of the tetramer structure and cooperative mechanism is emphasized by the observation that the R882H mutation in the dimer interface of DNMT3A is highly prevalent in acute myeloid leukemia and leads to a substantial loss of its activity. Under conditions that distinguish between cooperativity and processivity, we show that in contrast to that of Dnmt3a-C, the activity of Dnmt3b-C is not cooperative and confirm the processivity of Dnmt3b-C and the full length Dnmt3b enzyme. Whereas the R878H mutation (mouse homologue of R882H) led to the loss of cooperativity of Dnmt3a-C, the activity and processivity of the analogous Dnmt3b-C R829H variant were comparable to those of the wild-type enzyme. Additionally, buffer acidification that attenuates the dimer interface interactions of Dnmt3a-C had no effect on Dnmt3b-C activity. Taken together, these results demonstrate an important mechanistic difference between Dnmt3b and Dnmt3a and suggest that interactions at the dimer interface may play a limited role in regulating Dnmt3b-C activity. These new insights have potential implications for the distinct biological roles of Dnmt3a and Dnmt3b.

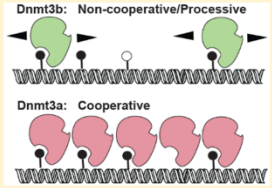

In mammals, DNA methylation at the C5 position of cytosine bases is catalyzed by three known DNA methyltransferases (Dnmts): Dnmt1, Dnmt3a, and Dnmt3b. Although mammalian Dnmts use a conserved catalytic mechanism that involves base flipping to methylate largely at CpG dinucleotides, these enzymes are structurally and functionally distinct.[1−4] Dnmt1 is primarily responsible for the postreplication maintenance of DNA methylation by copying it from the parent to daughter strand.[5] Dnmt3a and Dnmt3b, together with their catalytically inactive homologue, Dnmt3L, establish DNA methylation *de novo*.[2] Dnmt3a and Dnmt3b have different functions, supported by the distinct phenotypes of their respective murine knockouts,[6] their tissue specific expression patterns, and their unique roles in the development of cancer and other epigenetic disorders.[7−14] However, the distinct biochemical properties of Dnmt3a and Dnmt3b that potentially contribute to their unique roles *in vivo* have not been fully examined.

A common feature of all mammalian Dnmts is the presence of a C-terminal catalytic domain that contains 10 motifs conserved among prokaryotic and eukaryotic C5 DNA methyltransferases. The C-terminal catalytic domains of Dnmt3a and Dnmt3b (Dnmt3a-C and Dnmt3b-C, respectively) share approximately 85% sequence similarity and are active methyltransferases in the absence of their respective N-terminal regulatory domains.[15] Another member of the Dnmt3 family is Dnmt3L, in which the key catalytic residues required for binding of AdoMet and DNA are absent; Dnmt3L is therefore enzymatically inactive. Dnmt3L interacts with both Dnmt3a and Dnmt3b and allosterically stimulates their catalytic activity, therefore acting as a positive regulator of *de novo* DNA methylation.[16,17] The crystal structure of the Dnmt3a catalytic domain (Dnmt3a-C) alone and complexed with Dnmt3L exhibits a heterotetrameric structure of Dnmt3a-C/3L or a homodimer of Dnmt3a-C that can self-tetramerize through two interaction surfaces, the R−D dimer interface and the F−F tetramer interface.[18,19] The interactions at the dimer interface of Dnmt3a-C tetramers support its multimerization on DNA forming nucleoprotein filaments. This allows the enzyme to bind and methylate multiple CpG sites on DNA in a cooperative manner, thus increasing its activity.[20−22] Although controversial, some evidence also supports a processive mechanism for Dnmt3a.[15,23−25] Similar to the case for a processive enzyme, cooperative binding of multiple Dnmt3a molecules to DNA would allow it to methylate multiple sites on the same DNA molecule, complicating data analysis. However, the processivity of Dnmts is defined by their ability to diffuse along the DNA and methylate multiple sites before

Received: September 21, 2016
Published: October 21, 2016

DOI: 10.1021/acs.biochem.6b00964
Biochemistry 2018, 57, 4312−4324

Table 1. DNA Oligomers Used for DNA Methylation Analysis[a]

oligomer	sequence	no. of CpG sites
30-mer F	/5BiosG/GAAGCTGGGACTTCCGGGAGGAGAGTGCAA	1
30-mer R	TTGCACTCTCCTCCCGGAAGTCCCAGCTTC	1
32-mer F	/5BiosG/TGGGACTTCCGGGAGCTTCCGGGAGGAGAGTG	2
32-mer R	CACTCTCCTCCCGGAAGCTCCCGGAAGTCCCA	2
509-mer F	/5BiosG/AGATTAGGGAAGGGGGTGTG	58
509-mer R	AAGATCCTTTCAAGGCCTCAG	58
719-mer F	/5BiosG/CCCATGCGCCTGCGCCGGGTGCC	47
719-mer R	ATGCTCTAGACCTGCGATGTAGTTCGATC	47

[a]For the DNA binding experiments, the 30-mer oligomers used Cy5 5′ end labels in place of the biotin modification (/5BiosG/).

dissociation.[26,27] Therefore, it is important to use methods that differentiate processivity and cooperative activity of Dnmts. Previous studies have shown that Dnmt3a-C methylates DNA in a distributive manner. Supporting its cooperative mechanism, its activity was shown to increase exponentially with a 2-fold increase in enzyme concentration, however only with long DNA substrates.[24,28] The critical role of the tetramer formation and cooperative mechanism of Dnmt3a in its biological activity is apparent in acute myeloid leukemia (AML) cells that have a high frequency of mutation R882H present at the dimer interface of DNMT3A.[27] *In vitro* studies show that the R882H mutant protein has only ∼20% activity[29,30] and is suggested to cause genomewide hypomethylation in AML cells.[31,32]

Multiple-sequence alignment reveals that most residues in the dimer interface are conserved between Dnmt3a and Dnmt3b. However, the role of the dimer interface and that of cooperativity of Dnmt3b-C has not been evaluated. An earlier investigation using methylation-dependent restriction protection analysis of a 430-mer DNA showed that Dnmt3b-C methylates its substrate in a processive manner.[15] However, it is not clear from this study whether the activity of Dnmt3b-C was influenced by cooperativity in a manner similar to that reported for Dnmt3a-C. In the study presented here, we performed experiments that distinguish between cooperative and processive mechanisms. Our data show that in contrast to Dnmt3a-C, Dnmt3b-C methylates DNA in a noncooperative manner and by a processive mechanism on both unmethylated and hemimethylated substrates at physiological pH and ionic strength and confirms the processivity of the full length Dnmt3b enzyme. Experiments further characterizing the catalytic mechanism of Dnmt3b-C show that whereas preincubation of the enzyme with DNA reduces its activity, preincubation with AdoMet decreases its K_M by 10-fold, indicating that the cofactor AdoMet-bound form has an increased specificity for target sites. To further confirm the noncooperative mechanism of Dnmt3b-C, we tested the role of the R829 residue of Dnmt3b-C that is analogous to dimer interface residue R882 of Dnmt3a-C. Our data here show that whereas the reduced activity of the Dnmt3a-C R882H variant could be partially attributed to the loss of its cooperativity, mutation of the conserved analogous arginine R829 had no effect on the activity or processivity of Dnmt3b-C, thus supporting its noncooperative mechanism. Similarly, disruption of interactions at the dimer interface of Dnm3a-C, with a decrease in the pH of buffer, causes a 2−3-fold loss of Dnmt3a-C activity;[24,28] however, it has no effect on the DNA binding or catalytic activity of Dnmt3b-C. These data suggest that formation of tetramers may not be critical for the processive activity of Dnmt3b-C. Collectively, these data reveal important biochemical differences between Dnmt3a and Dnmt3b that can potentially impact their activity and function during development and in cancer cells.

EXPERIMENTAL PROCEDURES

Protein Purification. Mouse Dnmt3a-C, Dnmt3b-C, Dnmt3b-C E703A, Dnmt3a-C R878H, Dnmt3b-C R829H, and Dnmt3L cloned in pET28a with a six-His tag were expressed and purified using affinity chromatography as described previously.[25] Briefly, transformed BL21-DE3 cells were induced with 1 mM IPTG and grown for 2 h at 32 °C. Harvested cells were washed with STE buffer [10 mM Tris-HCl (pH 8.0), 0.1 mM EDTA, and 0.1 M NaCl] and resuspended in buffer A [20 mM potassium phosphate (pH 7.5), 0.5 M NaCl, 10% (v/v) glycerol, 1 mM EDTA, 0.1 mM DTT, and 80 mM imidazole]. Cells were disrupted by sonication, followed by removal of cell debris by centrifugation. The clarified lysate was incubated with 0.75 mL of Ni-NTA agarose for 3 h at 4 °C. The protein-bound slurry was packed in a 2 mL Bio-Rad column and washed with 50 mL of buffer A. Protein (5−10 μM) was eluted using 200 mM imidazole in buffer A at pH 7.5 and then stored in 20 mM HEPES (pH 7.5), 40 mM KCl, 0.2 mM DTT, 1 mM EDTA, and 20% glycerol at −80 °C. The purity and integrity of recombinant proteins were checked by SDS−PAGE and Western blot analysis using a mouse monoclonal anti-His antibody (Invitrogen, MA1-21315). M.SssI methyltransferase was obtained from New England Biolabs.

Enzyme Assays. Most methylation assays for determining kinetic parameters of recombinant enzymes were performed using ^{3}H-labeled *S*-adenosylmethionine (AdoMet) as a cofactor and biotinylated oligonucleotides of varying sizes bound on avidin-coated high-binding Elisa plates (Corning) as described previously.[33] The DNA methylation reaction was performed using either 250 nM 30-mer/32-mer DNA substrate or 150 nM 509-mer/719-mer DNA substrate in methylation buffer [20 mM HEPES (pH 7.5), 50 mM KCl, and 1 mM EDTA supplemented with 5 μg/mL BSA]. The methylation reaction included 0.76 μM [*methyl*-^{3}H]AdoMet (PerkinElmer Life Sciences). Storage buffer was added to compensate for the different enzyme volumes in all reaction mixtures. The substrates consisted of biotinylated oligonucleotides, including (1) a 30 bp oligonucleotide containing one CpG site, (2) a 32 bp oligonucleotide containing two CpG sites, (3) a 509-mer with 58 CpGs (amplified from the human SUHW1 gene promoter), or (4) a 719-mer DNA fragment with 46 CpGs (amplified from the mouse Aprt gene promoter). Primers used to amplify these substrates are listed in Table 1.

For steady state kinetic analysis, the larger amounts of the substrate could not be accommodated in the standard plate assay, which has a maximal binding capacity per well for DNA

DOI: 10.1021/acs.biochem.6b00964
Biochemistry 2018, 57, 4312−4324

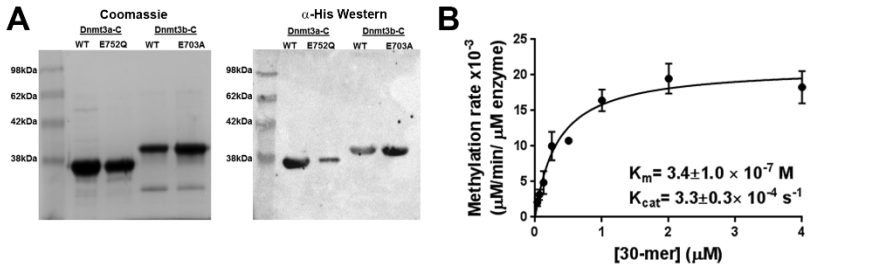

Figure 1. Expression of Dnmt3a-C, Dnmt3b-C, and their respective mutants. (A) Coomassie-stained SDS−PAGE gel and Western blot showing purified His-tagged WT Dnmt3a-C, inactive mutant Dnmt3a-C E752Q, WT Dnmt3b-C, and inactive mutant Dnmt3b-C E703A. The mouse monoclonal anti-His antibody was used to detect proteins on the Western blot. (B) Steady state kinetic analysis of Dnmt3b-C activity. Methylation reactions were performed for 10 min, and initial velocities were calculated as the number of methyl groups transferred per minute per micromolar enzyme for varying concentrations of 30-mer substrate ranging from 0.031 to 4 μM in the presence of 0.75 μM AdoMet. The reactions were started by addition of enzyme to the substrate cocktail. The data were fitted to the Michaelis−Menten equation to yield the kinetic parameters. The data are the average ± the standard error of the mean ($n \geq 3$ independent experiments).

substrate of 2 μM. These methylation assays were, therefore, performed using a filter binding assay.[10] Briefly, 10 μL of reaction mix was spotted on a 1.5 cm DE81 filter that was then washed three to five times in 0.2 M ammonium bicarbonate, followed by 100% ethanol, and air-dried. Incorporated radioactivity was quantified by scintillation counting.

Cooperativity Assay. To examine cooperativity, the following changes were made to the plate assay described above. Increasing concentrations of enzyme were preincubated with DNA substrate for 10 min at room temperature prior to the addition of AdoMet to start the reaction. AdoMet was a mixture of unlabeled and 0.76 μM ^{3}H-labeled AdoMet, which yielded a final concentration of 2 μM. Methylation assays were performed using 30-mer, 509-mer, and 719-mer DNA substrates. On the basis of the structural studies of Dnmt3a-C, it was estimated that the 30-mer substrate is too short to allow potential multimerization of the enzyme[18,21] and could therefore be used as a control. Additionally, cooperativity assays using 100 ng of the pUC19 plasmid as a substrate were performed using the filter binding assay described above. For these assays, unmethylated pUC19 was purified from the dam$^-$/dcm$^-$ *Escherichia coli* strain (C2925I, NEB).

Stimulation of Dnmt3b-C by the Inactive Mutant E703A. For assays aiming to investigate the ability of an inactive mutant to stimulate wild-type (WT) Dnmt3b-C activity, the activity of a 1:1 μM mixture of Dnmt3b-C E703A mutant and WT Dnmt3b-C was compared to the activity of WT Dnmt3b-C (1 or 2 μM), using two different DNA substrates, 1 μM 30-mer substrate with 1 CpG or 150 nM 509-mer substrate with 58 CpGs. Reactions were initiated by addition of enzyme. The WT and/or E703A enzymes were mixed together and incubated for 5 min at room temperature before addition to the reaction mix. A mixture of unlabeled and 0.76 μM ^{3}H-labeled AdoMet was used at a final concentration of 2 μM. Methylation rates were determined by using linear regression to analyze data. The fold change in methylation rate compared to that for 1 μM WT enzyme was plotted for each enzyme treatment.

Processivity Assay. Methylation kinetic analyses were performed using a range of enzyme concentrations and short oligonucleotide 30- and 32-mer substrates with one and two CpG sites, respectively. Low enzyme concentrations relative to DNA substrate concentrations were included to ensure that the reaction occurred under multiple-turnover conditions. Each DNA substrate was used at a concentration of 250 nM, and a 1:1 ratio of labeled and unlabeled AdoMet (final concentration of 1.5 μM) was used. To compare the identical CpG molarity, a parallel reaction using 500 nM 30-mer was also performed. Reactions were started by enzyme addition. M.SssI and Dnmt3a-C were used as positive and negative controls, respectively.

DNA Binding Assays. DNA binding of Dnmt3b-C was performed using Cy5-labeled 30-mer DNA containing one CpG site (Table 1) in nitrocellulose filter binding assays. Binding reactions were performed in 20 mM HEPES (pH 7.5), 100 mM KCl, 1 mM EDTA buffer, in the presence of 0.2 mM *S*-adenosylhomocysteine (AdoHcy) and 30 nM DNA, and increasing concentrations of Dnmt3b-C. Reaction mixtures were incubated at room temperature for 15 min prior to being spotted on the nitrocellulose membrane in a dot blot apparatus, followed by three washes with binding buffer. The enzyme-bound fraction of Cy5-DNA was quantified by fluorescence measurement (Typhoon).

Data Analysis. Data were analyzed using Prism software (GraphPad). For time-dependent kinetic measurements, values were fitted using linear regression of a nonlinear fit, which was weighted by $1/Y^2$. Each time point for methylation kinetics was an average and standard deviation of three to six experimental replicates. For secondary plots, a least-squares fitting method was used to plot the data, and the linear regression was not weighted. To determine the equilibrium binding constant, data were fitted to a one-site binding model with a Hill coefficient. Standard errors of the mean were calculated for three to six independent experiments, as described in the figure legends.

■ RESULTS

N-Terminally His-tagged Dnmt3b-C, Dnmt3b-C E703A, and Dnmt3L were overexpressed and purified on Ni-NTA agarose to 90−95% purity as estimated by the Coomassie-stained SDS gel (Figure 1A). The K_M and the turnover rate constant (K_{cat}) value for purified Dnmt3b-C were determined to be (3.4 ± 1) × 10^{-7} M and (3.3 ± 0.3) × 10^{-4} s^{-1}, respectively (Figure 1B), and catalytic efficiency $K_{cat}/K_M \sim 10^3$ M^{-1} s^{-1}. To confirm the catalytic robustness of the enzyme, we assessed the allosteric

DOI: 10.1021/acs.biochem.6b00964
Biochemistry 2018, 57, 4312−4324

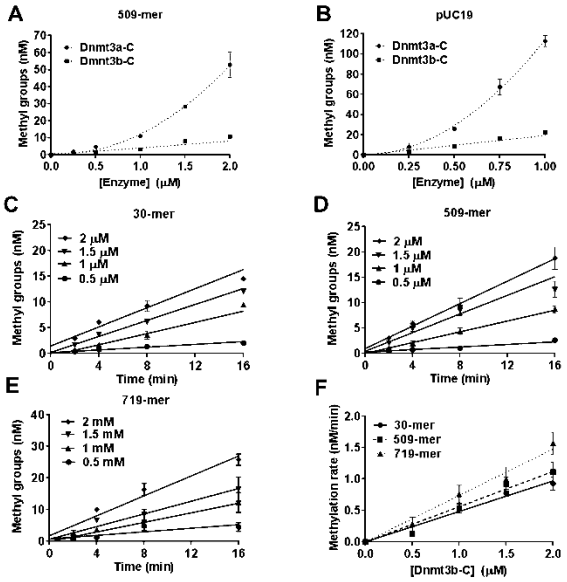

Figure 2. Catalytic mechanism of Dnmt3b-C. (A and B) Methylation activity of Dnmt3a-C and Dnmt3b-C enzymes measured for 10 min with the 509 bp and pUC19 substrates in the presence of 0.25−2 and 0.25−1 μM enzyme, respectively. The enzymes were preincubated with DNA for 10 min at room temperature, and the reaction was initiated by addition of AdoMet. Total methylation activity was plotted vs enzyme concentration using an average and standard deviation ($n \geq 3$ independent experiments). (C−E) Time course of DNA methylation with 30-mer, 509-mer, and 719-mer DNA substrates in the presence of 0.5, 1, 1.5, or 2 μM Dnmt3b-C enzyme that was preincubated with DNA for 10 min at room temperature. The reaction was initiated by addition of AdoMet. The data were fitted by linear regression, weighted by $1/Y^2$. (F) Methylation rates for all three DNA substrates plotted vs enzyme concentrations using linear regression without weighting. Averages ± the standard error of the mean are shown ($n \geq 3$ independent experiments).

activation of Dnmt3b-C by Dnmt3L.[16] Consistent with earlier observations, we observed ~6-fold activation of Dnmt3b activity in the presence of Dnmt3L[16] (SI Figure 1A). This Dnmt3b-C protein was next used to determine the catalytic mechanism.

Investigating the Cooperativity of Dnmt3b-C. Dnmt3a-C monomers interact with each other through two interfaces, the Dnmt3a−Dnmt3L interface (F−F interface) and the Dnmt3a−Dnmt3a dimer interface (R−D interface), to form tetramers.[18] Dnmt3a-C tetramers multimerize on DNA potentially through interactions along the dimer interface, which supports cooperativity of Dnmt3a.[24] Many amino acids known to be critical for the dimer and tetramer interface-mediated interactions of Dnmt3a are conserved in Dnmt3b.[18,19] However, the cooperativity of Dnmt3b has not been tested. The activity of a cooperative enzyme like Dnmt3a increases in a nonlinear manner at higher enzyme concentrations because of the allosteric effect of enzyme subunit interactions,[24] in contrast to a noncooperative enzyme for which the activity is expected to increase in a linear manner as a function of enzyme concentration. Previous studies showing cooperativity of Dnmt3a-C used a 509 bp DNA substrate to allow the binding of multiple protein molecules at higher enzyme concentrations.[24] To compare the cooperativity of Dnmt3a-C and Dnmt3b-C, DNA methylation analysis was performed using the same 509-mer DNA substrate. Increasing concentrations of the Dnmt3a-C and Dnmt3b-C enzymes ranging from 0 to 2 μM were preincubated with 509-mer DNA substrate for 10 min to allow the formation of nucleoprotein complexes. The methylation reaction was initiated by the addition of radiolabeled AdoMet and was monitored by incorporation of radioactivity into DNA for an additional 10 min. The methylation activity was plotted against Dnmt3a-C and Dnmt3b-C enzyme concentrations (Figure 2A). The data show that for Dnmt3a-C with an increase in concentration from 1 to 2 μM the activity increased ~5-fold, whereas for Dnmt3b-C, there was only ~2-fold increase in activity for every 2-fold increase in enzyme concentration. As shown previously,[24] this exponential increase in methylation activity of Dnmt3a-C was specific for only the long DNA substrate (509-mer) and was absent for a short 30-mer DNA substrate (SI Figure 1B). On the basis of the structural studies of Dnmt3a-C, the 30-mer DNA substrate is not expected to accommodate more than one or two tetramers and thus cannot support multimerization and cooperativity.[18,21,24] To test if Dnmt3b-C cooperativity could be supported on longer DNA substrates, we repeated the methylation assays using the pUC19 plasmid as a substrate. As shown in Figure 2B, whereas the activity of Dnmt3a-C was cooperative, the activity of Dnmt3b-C increased linearly with the increase in enzyme concentration similar to the data shown

DOI: 10.1021/acs.biochem.6b00964
Biochemistry 2018, 57, 4312−4324

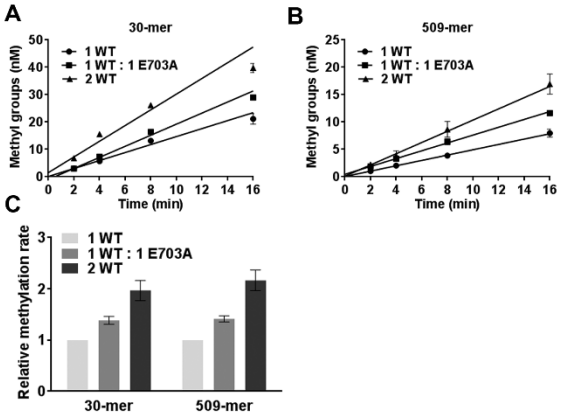

Figure 3. Dnmt3b-C is not cooperatively stimulated by addition of inactive Dnmt3b-C E703A. (A and B) Methylation kinetics of 30-mer and 509-mer substrates, respectively, by WT (Dnmt3b-C) and a mutant (catalytically inactive Dnmt3b-C E703A). Methylation was conducted using 1 μM WT, 1 μM WT and 1 μM E703A, and 2 μM WT with either 1 μM 30-mer or 150 nM 509-mer substrate. The reaction was initiated by addition of enzyme to the substrate mix, and data were fitted by linear regression, weighted by $1/Y^2$. (C) Methylation rates were measured from the slopes in panels A and B. The rate of methylation for each substrate was normalized to the rate for 1 μM enzyme and plotted in the bar graph with the normalized error. The average $\pm$ the standard error of the mean is shown ($n \geq 4$ independent experiments).

in Figure 2A. We also noticed that compared to the 509-mer, the plasmid substrate stimulated cooperativity of Dnmt3a-C at lower enzyme concentrations, suggesting cooperativity of Dnmt3a-C may be influenced by substrate length. To confirm the results for Dnmt3b-C, we performed a time course of DNA methylation to determine the initial rate of DNA methylation using three biotinylated substrates, a 30-mer with one CpG site at 250 nM, a 509 bp DNA substrate with 58 CpGs, and a 719 bp substrate with 46 CpG sites at concentrations of 150 nM each. Increasing concentrations of the Dnmt3b-C enzyme ranging from 0.5 to 2 μM were preincubated with the DNA, and the reaction was initiated via the addition of radiolabeled AdoMet and was monitored by the incorporation of radioactivity into the DNA (Figure 2C–E). Irrespective of the substrate length, the methylation rate increased linearly with the increase in Dnmt3b concentration (Figure 2F), with an ~2-fold increase in the rate of methylation for every 2-fold increase in enzyme concentration. We observed rates of methylation slightly lower than expected at the lowest enzyme concentration for all three substrates potentially because of the slow turnover under these conditions. At higher enzyme concentrations in which cooperative methylation was observed for Dnmt3a-C[24] (Figure 2A), the absence of an exponential or nonlinear increase in the methylation rate for Dnmt3b-C suggests that Dnmt3b methylates DNA by a noncooperative mechanism.

Dnmt3b-C Activity Is Not Stimulated by the Catalytically Inactive Mutant. Addition of a catalytically inactive mutant to WT Dnmt3a-C was shown to stimulate its catalytic activity because it contributes to the cooperativity of Dnmt3a on long DNA substrates, resulting in an allosteric effect.[24] This variant carries a mutation in conserved motif IV (ENV) that is required for catalysis, but this mutation does not affect the DNA binding activity of the methyltransferase enzymes.[24] The corresponding mutant Dnmt3b-C E703A has very low residual activity (SI Figure 2). As an additional test of cooperative stimulation, we tested the influence of the Dnmt3b-C E703A mutant on the activity of WT Dnmt3b-C. Methylation kinetic reactions were performed with two biotinylated substrates at near saturating concentrations: a 30 bp substrate with one CpG site at 1 μM and a 509 bp substrate at 150 nM using either 1 μM WT enzyme or 1 μM WT mixed with 1 μM inactive mutant (Figure 3A,B). The fold change in the rates of DNA methylation compared to that of 1 μM WT enzyme alone was then plotted (Figure 3C). A 2-fold increase in activity was observed when the enzyme concentration was increased from 1 to 2 μM for both substrates. The 1:1 WT/inactive mutant mixture yielded a small increase in activity, however, with both short (30-mer) and long (509-mer) DNA substrates. Because the short DNA substrate cannot bind multiple enzyme units,[18,21,24] this increase in activity is not likely due to cooperativity but may be due to interactions at the tetramer interface (F–F interface) as shown previously for Dnmt3a-C.[16,24] These data provide further support for the noncooperative mechanism of Dnmt3b activity.

Dnmt3b-C and Full Length Dnmt3b Methylate DNA in a Processive Manner. Unlike a previous method that used methylation-dependent restriction protection to test the processivity of Dnmt3b,[15] here we assayed the processivity using two DNA substrates of the same sequence, 30 and 32 bp in length, except that one substrate contained one CpG and the second contained two CpGs.[25] In a processive reaction, the second site on the two-site DNA substrate is expected to be methylated faster, so the methylation rate for the two-site substrate would be expected to be ~2-fold higher than that for the one-site substrate. This effect should be prominent at a low enzyme:DNA ratio, in which each DNA molecule is occupied by only one enzyme molecule, in other words, under multiple-turnover conditions. Therefore, methylation reactions were performed using a range of Dnmt3b-C enzyme concentrations

DOI: 10.1021/acs.biochem.6b00964
Biochemistry 2018, 57, 4312–4324

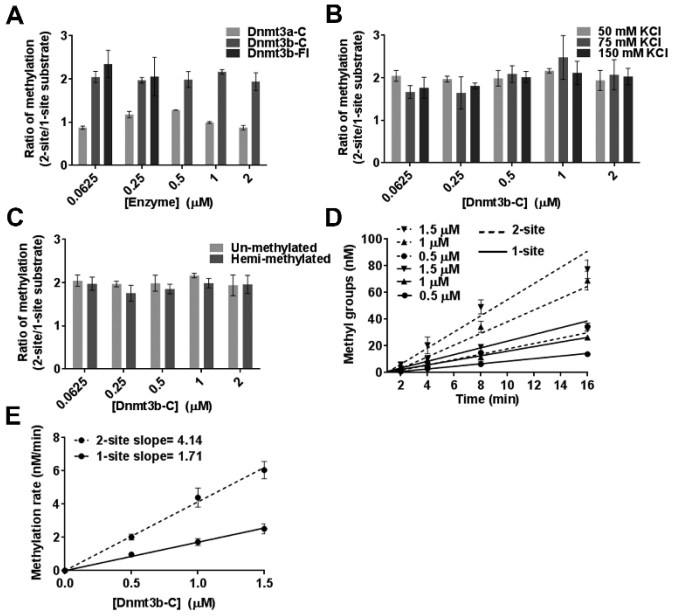

Figure 4. Dnmt3b-C exhibits processivity on a DNA substrate with two CpG sites. (A) Steady state DNA methylation levels were measured for 1 h at various concentrations of Dnmt3b-C, Dnmt3b-Fl, or Dnmt3a-C enzymes using 1.5 μM ^{3}H-labeled AdoMet (1:1 mixture of labeled and unlabeled) and 250 nM one-site or two-site substrate. For each enzyme concentration, the methylation of the two-site substrate was normalized to that of the one-site substrate to show the relative change in methylation level. (B and C) Relative DNA methylation as described in panel A at physiologically relevant salt concentrations with 250 nM hemimethylated one-site and two-site substrates. (D) Initial velocity of methylation measured at early time points (2, 4, 8, and 16 min) for one-site (—) and two-site (---) substrates. The concentration of Dnmt3b-C ranged from 0.5 to 1.5 μM, and the data were fitted to linear regression, weighted by $1/Y^2$. (E) DNA methylation rates measured in panel D were plotted vs enzyme concentration, and the slopes were determined from the linear regression without weighting. Data are the average ± the standard error of the mean ($n \geq 3$ independent experiments).

at near saturating substrate (DNA and AdoMet) concentrations. Unlike the cooperativity assays, the enzyme was not preincubated with DNA, and the methylation reactions were initiated by addition of enzyme to a buffer/substrate cocktail. This allowed the enzyme to bind to its preferred substrate first and catalysis to proceed at maximal efficiency. Short oligonucleotides were used as substrates to eliminate any potential cooperativity from occurring, because they cannot bind more than a few molecules of the enzyme. Assays of Dnmt3a-C and Dnmt3b-C (0.0625−2 μM) were performed with 0.25 μM one-site and two-site substrates (0.5 and 1 μM CpG sites). As previously reported, Dnmt3a-C methylated one- and two-site substrates to the same degree, indicating a distributive mechanism of DNA methylation.[15,24] In contrast, Dnmt3b-C methylated the two-site substrate with a 2-fold higher efficiency (Figure 4A). Because this effect was evident at the lowest concentration of enzyme assayed, the data indicate that the Dnmt3b enzyme methylates DNA in a processive fashion. We also demonstrated the processive activity of Dnmt3b by using the full length Dnmt3b enzyme (Dnmt3b-Fl) in the assays described above (Figure 4A and SI Figure 3A). Our data show that similar to the truncated Dnmt3b-C, at lower enzyme concentrations Dnmt3b-Fl methylates DNA in a processive manner. Because of its large size and tendency to precipitate, Dnmt3b-Fl could be purified at a maximal concentration of 0.5−1 μM; consequently, the assays at higher concentrations could not be performed. A similar effect was observed for the known processive methyltransferase M.SssI (SI Figure 3B). To determine if these results were influenced by the presence of a 2-fold higher CpG molarity of the two-site substrate, we performed a parallel reaction at an equal CpG molarity by comparing methylation of 0.5 μM one-site substrate and 0.25 μM two-site substrate. The ratio of DNA methylation at either 0.25 or 0.5 μM Dnmt3b-C remained at 2, confirming its processive mechanism of DNA methylation (SI Figure 3C). We next tested the effect of ionic strength on the processivity of the Dnmt3b-C enzyme. Figure 4B shows that increasing the ionic strength from 50 to 150 mM KCl had no effect on the degree of methylation of one- or two-site substrate, indicating that Dnmt3b can methylate DNA processively at a physiological ionic strength ranging from 100 to 150 mM. Salt concentrations of >250 mM disrupted enzyme activity. Dnmt3b has been shown to collaborate with Dnmt1 for the maintenance of DNA methylation.[34] We therefore tested the processivity of Dnmt3b-C on one- or two-site hemimethylated substrates. Similar to the unmethy-

DOI: 10.1021/acs.biochem.6b00964
Biochemistry 2018, 57, 4312−4324

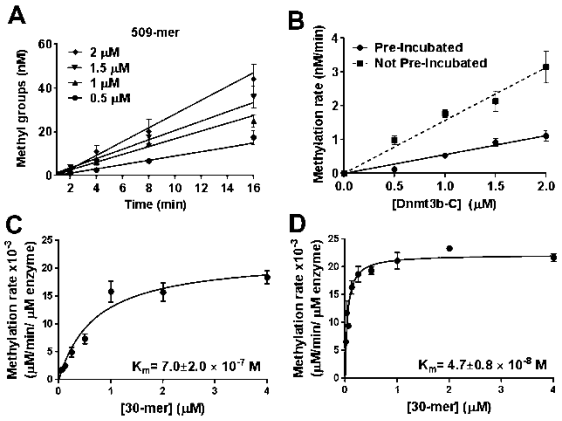

Figure 5. Preincubation with DNA decreases the methylation activity of Dnmt3b-C. (A) Methylation activity of Dnmt3b-C for the 509-mer was measured without preincubation with DNA for a range of enzyme concentrations. The reaction was initiated by addition of enzyme to the substrate cocktail. The data, which are the average ± the standard error of the mean ($n \geq 3$ independent experiments), were fitted to linear regression, weighted by $1/Y^2$. (B) Rates of DNA methylation calculated from panel A plotted vs enzyme concentration and compared to the rates obtained from assays with the preincubated enzyme from Figure 1D. (C and D) Steady state kinetic analysis of methylation by Dnmt3b-C. Methylation reactions were performed for 10 min, and initial velocities were calculated as the number of methyl groups transferred per minute per micromolar enzyme for varying concentrations of the 30-mer substrate ranging from 0.031 to 4 μM and 0.75 μM AdoMet. (C) The enzyme was preincubated with DNA for 15 min, and the reaction was started with AdoMet. (D) The enzyme was preincubated with Adomet for 15 min, and the reaction was initiated with DNA. The data, which are the average ± the standard error of the mean ($n \geq 3$ independent experiments), were fitted to the Michaelis–Menten equation, and the significance was estimated using a Student's paired t test yielding a p value of 0.014.

lated substrate, Dnmt3b methylated the two-site hemimethylated substrate with an efficiency 2-fold higher than that of the one-site substrate (Figure 4C).

Processivity of the Initial Phase of the Reaction. To confirm our conclusion from the steady state experiments described above, we next examined the processivity of Dnmt3b-C during the initial phase of the reaction. The initial rate of catalysis of a processive enzyme is also expected to be 2-fold higher with a two-site substrate than with a one-site substrate. DNA methylation using different enzyme concentrations was measured as a function of time, and initial rates were calculated from the slope after fitting the data by linear regression (Figure 4D). Methylation rates increased linearly with enzyme concentration, indicting multiple-turnover conditions. As shown in the secondary plot, DNA methylation rates for the two-site substrate were 2-fold higher than those for the one-site substrate, strongly suggesting that Dnmt3b-C operates in a processive fashion by methylating multiple CpGs on the same molecule of DNA before dissociation (Figure 4E).

Taken together, our data here confirm the processive mechanism of Dnmt3b and validate an important difference between the catalytic mechanism of Dnmt3a and Dnmt3b.

Effect of Preincubation with DNA on Catalytic Activity. Processivity is expected to increase the catalytic activity of a methyltransferase toward long DNA substrates with multiple target sites. However, for experiments in which Dnmt3b-C was preincubated with DNA, we did not observe a substantial increase in the methylation rate for long DNA substrates compared to that with the 30-mer (Figure 2E). Although preincubation with DNA may simply lead to a decrease in the active fraction of the enzyme, it is also possible that in the absence of AdoMet, nonspecific DNA binding by Dnmt3b-C keeps it in a nonproductive complex. This can potentially slow the methylation reaction and influence the processivity of the enzyme. To investigate the effect of preincubation with DNA on the processivity of Dnmt3b, the rate of DNA methylation for the 509 bp DNA substrate was compared under two conditions. The first condition, in which various concentrations of Dnmt3b-C were preincubated with DNA substrate and the methylation reaction was initiated with AdoMet, is represented in Figure 2D. For the second condition, no preincubation was performed and methylation was initiated by addition of enzyme to the substrate cocktail. Kinetics of DNA methylation at each enzyme concentration was performed, and the initial methylation rates were determined by linear regression (Figure 5A). At all the tested enzyme concentrations, methylation rates were significantly slower when DNA was preincubated with enzyme than when it was not (Figure 5B), confirming a negative effect of preincubation with DNA on the catalytic activity of Dnmt3b-C. This is not intuitive for a processive enzyme, because during multiple reactions the exchange of AdoHcy with AdoMet should not require the enzyme to be dislodged from the DNA. We speculate that in the absence of a cofactor (AdoMet or AdoHcy), the enzyme preincubated with DNA binds strongly to nonspecific sites, which slows catalysis suggesting that the enzyme prefers to bind AdoMet for the first turnover.

Order of Addition for Steady State Kinetic Analysis. To determine the effect of preincubation with the substrate and cofactor, we analyzed the steady state methylation activity of Dnmt3b-C. The avidin plate assay used for methylation assays has a maximal DNA binding capacity of 2 μM;[33] therefore, we used a filter binding assay for this experiment.[35] Using a 30-mer substrate with one CpG site and 0.5 μM enzyme, steady state

DOI: 10.1021/acs.biochem.6b00964
Biochemistry 2018, 57, 4312–4324

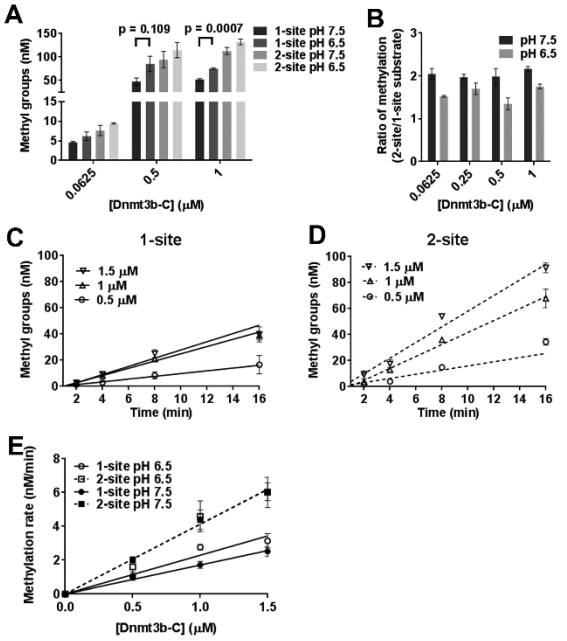

Figure 6. pH sensitivity of Dnmt3b-C processive catalysis. (A) Methylation at one- and two-site substrates by Dnmt3b-C was measured for 1 h at pH 6.5 or 7.5. (B) Ratio of the methylation levels calculated as the fold change at two-site vs one-site substrate. (C and D) Time course of DNA methylation by Dnmt3b-C at pH 6.5 for one- and two-site substrates. For each substrate, the time course of DNA methylation reaction was determined in the presence of 0.5−2 μM Dnmt3b-C. The reaction was started by the addition of enzyme, and the data were fitted by linear regression, which was weighted by $1/Y^2$. (E) The calculated methylation rates at pH 6.5 were plotted vs enzyme concentration and compared to those at pH 7.5. Data are the average ± the standard error of the mean ($n \geq 4$ independent experiments).

kinetic experiments were performed, and data were fitted to the Michaelis−Menten equation. Three different experimental conditions were used, one in which the enzyme was preincubated with DNA or AdoMet for 15 min before the reaction was started by addition of AdoMet or DNA, respectively, or the reaction was initiated by adding enzyme to a substrate/cofactor mix. All data sets fit well to the hyperbolic curve (Figures 1B and 5C,D). However, the data set for preincubation with DNA (Figure 5D) also fitted to a sigmoidal curve, indicating a slower reaction at lower substrate concentrations that recovers at higher enzyme concentrations. The comparison using Akaike's Information Criteria (AICc) or the extra sum of squares F-test suggests that the hyperbolic Michaelis−Menten model is a better fit with a 71.5% higher probability of being correct. The estimated V_{max} under all the conditions showed no significant change. Under these three conditions, the K_M value was estimated to be $(3.4 \pm 1) \times 10^{-7}$ M for the reaction with non-preincubated enzyme (Figure 1B) and $(7.0 \pm 2) \times 10^{-7}$ and $(4.7 \pm 0.8) \times 10^{-8}$ M when the enzyme was preincubated with DNA and AdoMet, respectively (Figure 5C,D). A 10-fold decrease in the K_M of the enzyme upon preincubation with AdoMet demonstrates that the cofactor-bound Dnmt3b-C enzyme exists in a conformation that favors catalysis, potentially by enhancing the specific interaction of Dnmt3b-C with DNA. On the basis of these results, we propose that the binding of Dnmt3b-C to DNA in the absence of AdoMet may lead to the formation of a nonspecific DNA−enzyme binary complex in a conformation that limits or restricts binding of the cofactor AdoMet, thus slowing the reaction. This may have a stronger influence on initial or pre-steady state rates, thus influencing the processivity of the enzyme at earlier time points as seen in Figure 5B. We propose that *in vivo* most enzyme exists in the AdoMet-bound state and that during processive DNA methylation, cofactor exchange takes place without dissociation of the enzyme from the DNA.

Activity and Processivity of Dnmt3b-C Are Not Affected by pH. Under various physiological conditions, changes in the intracellular pH can influence protein−protein and protein−DNA interactions.[36] Previous studies have shown that the interaction of Dnmt3a through its dimer interface can be disrupted by a change in pH from 7.5 to 6.5, which results in a decrease in its activity and cooperativity.[28] Our data showing that Dnmt3b methylates DNA in a noncooperative manner suggest that the activity of Dnmt3b may not be strongly dependent on interactions involving the dimer interface. We tested this by assessing the effect of pH on the processivity of Dnmt3b-C. Methylation assays were performed at pH 7.5 and

DOI: 10.1021/acs.biochem.6b00964
Biochemistry 2018, 57, 4312−4324

6.5 for one- and two-CpG site substrates for 60 min with varying concentrations of enzyme. As shown in Figure 6A, the steady state level of DNA methylation using a one-site substrate was slightly higher at pH 6.5 than at pH 7.5. As a consequence, the ratios of methylation between one- and two-site substrates were reduced to <2 (Figure 6B). We checked whether this difference in methylation activity was due to the impact of pH on the initial rate of DNA methylation. Methylation kinetics at various enzyme concentrations was performed with one- and two-site substrates at pH 6.5 and 7.5, and initial rates were measured (Figure 6C,D). The rates of DNA methylation for the one-site substrate at various enzyme concentrations were slightly higher at pH 6.5 compared to those at pH 7.5 (Figure 6E). We speculate that this higher methylation rate under pre-steady state conditions could be responsible for the difference observed at the steady state levels. However, the rates of methylation of the two-site substrate remained ~2-fold higher than those for the one-site substrate at all enzyme concentrations tested at pH 7.5 and 6.5, indicating that the activity and processivity of Dnmt3b-C are not affected by lower pH. This behavior is in contrast to that of Dnmt3a-C, for which lowering the pH to 6.5 decreased its methylation activity by disruption of the dimer interface.[28]

Influence of pH on the Dissociation Constant. To test the effect of lower pH on DNA binding by Dnmt3b-C, we performed DNA binding assays using Cy5-labeled 30-mer DNA with one CpG site. An increasing amount of Dnmt3b-C ranging from 0.5 to 2 μM was incubated with 30 nM DNA substrate, and the binding assay was performed using a dot blot assay. The binding was measured by trapping the protein−DNA complexes on a nitrocellulose membrane. The intensity of the spots was measured, and data were fitted to a one-site specific binding saturation curve. Binding curves were hyperbolic, and the data could also be fitted well with the Hill coefficient constrained to 1 (Figure 7A,B). The dissociation constants at pH 7.5 and 6.5 showed no significant difference, indicating that the binding of Dnmt3b-C to DNA is not sensitive to lower pH and there is potentially a limited contribution of the dimer interface to the activity of Dnmt3b-C.

The Processivity of Dnmt3b-C Is Not Affected by Mutation of the R829 Residue. The R882H mutation, which is close to the dimer interface of Dnmt3a, is highly prevalent in human AML cells. This mutation, as well as the equivalent R878H mutation in mouse, disrupts tetramer formation and leads to a significant decrease in enzymatic activity.[29,31,32] Although this residue is implicated in tetramer formation, its effect on the cooperativity of Dnmt3a has not been tested. We performed the cooperativity assays as described above using various concentrations of WT Dnmt3a-C and Dnmt3a-C R878H enzyme (SI Figure 4A). Methylation assays were performed using 32-mer, 509-mer, and pUC19 DNA as substrates of various lengths. Loss of 64% activity for the 32-mer substrate at two tested enzyme concentrations (0.5 and 1 μM) confirms the previous observation that the mutation affects tetramer formation and that the tetrameric form is the most catalytically active form of Dnmt3a-C[30,37](SI Figure 4B,C). Interestingly, on longer DNA substrates, although the activity was rescued at a lower enzyme concentration (0.5 μM) (SI Figure 4D), at a higher enzyme concentration, the enzymatic activity did not demonstrate an exponential increase that is expected because of cooperativity (Figure 8A,B). These data support our observation for the WT enzyme that the length of DNA positively affects the cooperative behavior of

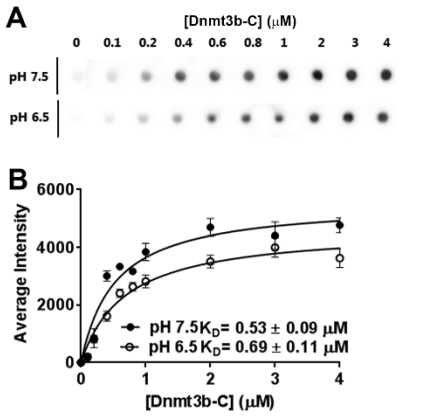

Figure 7. Effect of pH on DNA binding by Dnmt3b-C. For DNA binding analysis, the Dnmt3b-C enzyme was incubated with 30 nM Cy5-labeled 30-mer DNA in the presence of 0.2 mM AdoHcy (*S*-adenosylhomocysteine) in binding buffer at pH 6.5 or 7.5. (A) Representative blot for DNA binding. (B) The signal intensity on the blot was quantified using ImageQuant software, and data (average ± the standard error of the mean, $n \geq 3$ independent experiments) were fitted to a one-site binding saturation model and binding constants determined. The binding constants are within an error of <20%.

Dnmt3a. Destabilization of the tetramer structure due to the absence of R878 can be partially rescued by long DNA substrates, however not to the extent that it can restore cooperativity. Loss of cooperativity resulted in 78 and 63% losses of activity for 509-mer and pUC19, respectively, at higher enzyme concentrations. These data suggest that the human R882H mutation of Dnmt3a affects its cooperative mechanism at multiple CpG sites, which would have a substantial effect on its activity *in vivo*. We next tested the effect of the analogous mutation of the conserved R829 in Dnmt3b-C. On the basis of our data showing that the noncooperative and processive mechanism of Dnmt3b-C is not affected by acidification, we predicted that the mutation of R829 will not affect the processivity of Dnmt3b-C. Our data in Figure 8C−E demonstrate that the variant enzyme R829H has activity and processivity comparable to those of the WT enzyme.

Taken together, these data show that Dnmt3b-C methylates DNA in a noncooperative and processive manner and suggest that Dnmt3b-C may not require the interaction of Dnmt3b monomers or dimers along the dimer interface for optimal activity.

■ DISCUSSION

DNA methylation together with specific histone modifications plays an important role in regulating chromatin structure and thereby controlling gene expression. DNA methylation has a major role in regulation of epigenetic processes, including genomic imprinting, X-chromosome inactivation, nuclear reprogramming, and carcinogenesis.[7,38] Recent studies of the functions of the mammalian *de novo* methyltransferases Dnmt3a and Dnmt3b reveal both redundant and specific functions, highlighting the importance of differentiating their individual contributions to normal and diseased epigenomes.[39]

DOI: 10.1021/acs.biochem.6b00964
Biochemistry 2018, 57, 4312−4324

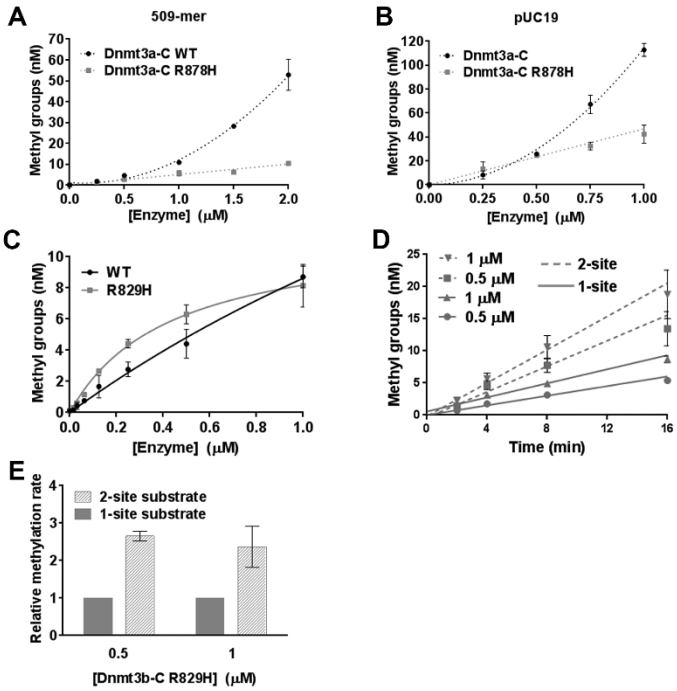

Figure 8. R829H mutation of Dnmt3b-C that does not reduce its activity and processivity. (A and B) Methylation activity of the WT and R878H mutant Dnmt3a-C enzymes was measured for 10 min with the 509 bp or pUC19 substrate in the presence of 0.25−2 and 0.25−1 μM enzyme, respectively. Enzymes were preincubated with DNA for 10 min at room temperature, and the reaction was initiated by addition of AdoMet. The total methylation activity was plotted vs enzyme concentration using an average and standard deviation ($n \geq 3$ independent experiments). (C) Methylation activity was measured for 10 min with the 30-mer substrate at enzyme concentrations ranging from 0.015 to 1 μM for the WT and mutant R829H Dnmt3b-C enzymes. (D) The initial velocity of methylation was measured for one-site (—) and two-site (---) substrates, in the presence of 0.5 and 1 μM Dnmt3b-C R829H mutant enzyme. The data were fitted to linear regression, weighted by $1/Y^2$. (E) Methylation rates for the one-site substrate were normalized to 1, and the relative change in the rate of methylation for the two-site substrate at different enzyme concentrations was plotted with a normalized error. For all the experiments, the average ± the standard error of the mean was derived ($n \geq 4$ independent experiments).

Whereas several biochemical studies have elucidated the structure−function relationship of Dnmt3a, less is known about the biochemical properties of Dnmt3b. Studies characterizing the enzymatic properties of Dnmt3a-C have provided critical information that facilitates our understanding of the biochemical basis of Dnmt3a function *in vivo*. This is underscored by the recent finding that ~20% of acute myeloid leukemia (AML) patients have mutations in Dnmt3a of which many are present in the dimer or tetramer interface of the enzyme.[30,31,37,40,41] These mutations were shown to disrupt oligomerization of Dnmt3a and alter its catalytic properties *in vitro* and *in vivo*. Likewise, a high frequency of Dnmt3b mutations is found in ICF syndrome, which is a rare genetic disease causing immunodeficiency, centromeric instabilities, and facial abnormalities. Many of these mutations are present in the Dnmt3b catalytic domain and result in reduced catalytic activity *in vitro*, potentially linking the mutations to hypomethylation of DNA in the diseased state.[6,15,42−45] Some of these mutations are present in the potential DNA binding region of Dnmt3b, and these residues are conserved in the dimer interface of Dnmt3a. In the absence of a Dnmt3b-C crystal structure, the detailed characterization of the catalytic mechanism of Dnmt3b-C here provides important insights into the impact of these mutations on the catalytic mechanism of Dnmt3b compared to that of Dnmt3a and highlights its properties that are distinct from those of Dnmt3a. Our findings suggest that the reduced activity of Dnmt3b mutants in ICF syndrome may not be because of the dimer-interface disruption.

Processivity of Dnmt3b-C has been reported previously; however, it was not clear whether the results reflected cooperative methylation of multiple sites by a multimerized enzyme or one enzyme unit processively methylating multiple sites.[15] By using DNA substrates of various lengths, our assays in this study distinguish processivity from cooperativity and show that Dnmt3b-C methylates DNA by a processive

DOI: 10.1021/acs.biochem.6b00964
Biochemistry 2018, 57, 4312−4324

mechanism in a noncooperative manner. We also show that Dnmt3b can methylate both unmethylated and hemimethylated sites processively, consistent with its collaborative function with Dnmt1 during the maintenance of DNA methylation. The noncooperative mechanism is further supported by our data showing that on the longer DNA substrates, the catalytic activity of Dnmt3b is not enhanced by the addition of its inactive mutant. Surprisingly, in our assays using DNA substrates of various lengths to examine the cooperativity of Dnmt3b-C, the methylation rate was not higher for the long DNA, which would be expected from a processive enzyme. Because these experiments were performed by preincubating the enzyme with DNA, this could be explained if the enzyme prefers binding AdoMet before binding to DNA. Our data demonstrating a 10-fold decrease in the K_M of Dnmt3b-C when it is preincubated with AdoMet support this conclusion. Our data are consistent with the model in which the binding of the enzyme to specific sites on DNA is favored by AdoMet binding, and during the processive catalysis, Dnmt3b is capable of cofactor exchange without dissociating from DNA.

Perturbations in the intracellular microenvironment including pH has a regulatory effect in several DNA binding proteins and enzymes. These regulatory mechanisms are expected to be prominent during tumor progression and also during development. Acidification has been shown to disrupt cooperativity and reduce the catalytic activity of Dnmt3a. Interestingly, again in contrast to that of Dnmt3a, the catalytic activity of Dnmt3b was not significantly affected at pH 6.5 and instead showed a slight increase in activity for a one-site substrate. We speculate that this may be because Dnmt3b-C has a slightly higher K_D value at pH 6.5. This difference between Dnmt3a and Dnmt3b mechanisms could be explained by the differences in their amino acid sequences, especially in the DNA binding region and the dimer interface. The interaction of several DNA binding proteins involves either water-mediated or direct H-bond interactions between the Arg and His residues and the DNA backbone. The protonation of His residues is pH-sensitive, which can alter its interaction with DNA and affect the activity of the protein. The activity of Dnmt3a decreases at lower pH because of the disruption of its dimer interface involving H821 and/or H873.[28] However, in Dnmt3b, the residues at the equivalent positions are replaced by Y821 and L847, respectively, both of which are also a part of DNA binding loop L2[18,19] (SI Figure 5). Compared to Dnmt3a, this makes the enzymatic activity of Dnmt3b potentially less dependent on protein−protein interaction at the dimer interface and less sensitive to changes in pH. A high level of expression of Dnmt3b has been implicated in the initiation and progression of several cancers and in some cases contributes to CpG island promoter methylation.[11] Its ability to function under low-pH conditions can be exploited by cancer cells in which the intracellular environment is typically more acidic than that of normal cells.

Further supporting a noncooperative mechanism, our data here show for the first time that the Dnmt3a R878H mutation disrupts the cooperativity of the enzyme whereas the analogous R829H mutation in Dnmt3b-C has no effect on its processivity. Although the SNP causing the R to H mutation in human DNMT3A was shown to be present at a very high frequency in AML cells,[46] the analogous mutation is not reported for DNMT3B in any epigenetic diseases. Therefore, we speculate that a smaller contribution of the dimer interface would promote the processivity of Dnmt3b, which may work efficiently for enzymes that do not form oligomers on DNA. These observations also emphasize that the minor difference in the amino acid sequence of Dnmt3a and Dnmt3b catalytic domains dictates a processive versus a cooperative mechanism.

■ ASSOCIATED CONTENT

Supporting Information

The Supporting Information is available free of charge on the ACS Publications website at DOI: 10.1021/acs.biochem.6b00964.

Five figures showing data that further supports the mechanism proposed herein (PDF)

■ AUTHOR INFORMATION

Corresponding Author

*Department of Biochemistry, Purdue University Center for Cancer Research, Purdue University, West Lafayette, IN 47907. E-mail: hgowher@purdue.edu.

Author Contributions

A.B.N. and C.J.P. contributed equally to this work. A.B.N., L.W., C.J.P., and L.A. performed the experiments. A.N., C.P., S.R., and H.G. performed data analysis and wrote the manuscript.

Funding

This work was supported by the Institutional Start up Fund of the Department of Biochemistry and Small Grants Program from the Purdue University Center for Cancer Research (P30 CA023168) and Purdue Showalter Trust Grant. A graduate research fellowship for L.A. is provided by the Saudi Arabian Cultural Mission.

Notes

The authors declare no competing financial interest.

■ ACKNOWLEDGMENTS

We thank Dr. Albert Jeltsch for providing Dnmt3a and Dnmt3b variants and Gowher lab members for their contributions via discussion.

■ ABBREVIATIONS

AdoMet, *S*-adenosylmethionine, also known as SAM; AdoHcy, *S*-adenosylhomocysteine, also known as SAH; Aprt, adenine phosphoribosyltransferase; CpG, dinucleotide of cytosine followed by guanine; Dnmt, DNA methyltransferase; DDT, dithiothreitol; EDTA, ethylenediaminetetraacetic acid; ENV, three amino acids in conserved motif IV, involved in AdoMet binding; HEPES, 4-(2-hydroxyethyl)-1-piperazineethanesulfonic acid; IPTG, isopropyl β-D-1-thiogalactopyranoside; MT, mutant enzyme; Ni-NTA, nickel-charged affinity resin; SDS−PAGE, sodium dodecyl sulfate−polyacrylamide gel electrophoresis; SUHW1, zinc finger protein 280A; WT, wild type.

■ REFERENCES

(1) Goll, M. G., and Bestor, T. H. (2005) Eukaryotic cytosine methyltransferases. *Annu. Rev. Biochem. 74*, 481−514.

(2) Jurkowska, R. Z., Jurkowski, T. P., and Jeltsch, A. (2011) Structure and function of mammalian DNA methyltransferases. *ChemBioChem 12*, 206−222.

(3) Cedar, H., and Bergman, Y. (2012) Programming of DNA methylation patterns. *Annu. Rev. Biochem. 81*, 97−117.

(4) Hermann, A., Gowher, H., and Jeltsch, A. (2004) Biochemistry and biology of mammalian DNA methyltransferases. *Cell. Mol. Life Sci. 61*, 2571−2587.

DOI: 10.1021/acs.biochem.6b00964
Biochemistry 2018, 57, 4312−4324

(5) Nishiyama, A., Yamaguchi, L., and Nakanishi, M. (2016) Regulation of maintenance DNA methylation via histone ubiquitylation. *J. Biochem. 159*, 9−15.
(6) Okano, M., Bell, D. W., Haber, D. A., and Li, E. (1999) DNA methyltransferases Dnmt3a and Dnmt3b are essential for de novo methylation and mammalian development. *Cell 99*, 247−257.
(7) Schubeler, D. (2015) Function and information content of DNA methylation. *Nature 517*, 321−326.
(8) Chen, B. F., and Chan, W. Y. (2014) The de novo DNA methyltransferase DNMT3A in development and cancer. *Epigenetics 9*, 669−677.
(9) Yang, L., Rau, R., and Goodell, M. A. (2015) DNMT3A in haematological malignancies. *Nat. Rev. Cancer 15*, 152−165.
(10) Jeong, M., and Goodell, M. A. (2014) New answers to old questions from genome-wide maps of DNA methylation in hematopoietic cells. *Exp. Hematol. 42*, 609−617.
(11) Walton, E. L., Francastel, C., and Velasco, G. (2014) Dnmt3b Prefers Germ Line Genes and Centromeric Regions: Lessons from the ICF Syndrome and Cancer and Implications for Diseases. *Biology 3*, 578−605.
(12) Duan, F., Cui, S., Song, C., Dai, L., Zhao, X., and Zhang, X. (2015) Systematic evaluation of cancer risk associated with DNMT3B polymorphisms. *J. Cancer Res. Clin. Oncol. 141*, 1205−1220.
(13) Jones, P. A. (2012) Functions of DNA methylation: islands, start sites, gene bodies and beyond. *Nat. Rev. Genet. 13*, 484−492.
(14) Challen, G. A., Sun, D., Mayle, A., Jeong, M., Luo, M., Rodriguez, B., Mallaney, C., Celik, H., Yang, L., Xia, Z., Cullen, S., Berg, J., Zheng, Y., Darlington, G. J., Li, W., and Goodell, M. A. (2014) Dnmt3a and Dnmt3b have overlapping and distinct functions in hematopoietic stem cells. *Cell stem cell 15*, 350−364.
(15) Gowher, H., and Jeltsch, A. (2002) Molecular enzymology of the catalytic domains of the Dnmt3a and Dnmt3b DNA methyltransferases. *J. Biol. Chem. 277*, 20409−20414.
(16) Gowher, H., Liebert, K., Hermann, A., Xu, G., and Jeltsch, A. (2005) Mechanism of stimulation of catalytic activity of Dnmt3A and Dnmt3B DNA-(cytosine-C5)-methyltransferases by Dnmt3L. *J. Biol. Chem. 280*, 13341−13348.
(17) Kareta, M. S., Botello, Z. M., Ennis, J. J., Chou, C., and Chedin, F. (2006) Reconstitution and mechanism of the stimulation of de novo methylation by human DNMT3L. *J. Biol. Chem. 281*, 25893−25902.
(18) Jia, D., Jurkowska, R. Z., Zhang, X., Jeltsch, A., and Cheng, X. (2007) Structure of Dnmt3a bound to Dnmt3L suggests a model for de novo DNA methylation. *Nature 449*, 248−251.
(19) Guo, X., Wang, L., Li, J., Ding, Z., Xiao, J., Yin, X., He, S., Shi, P., Dong, L., Li, G., Tian, C., Wang, J., Cong, Y., and Xu, Y. (2014) Structural insight into autoinhibition and histone H3-induced activation of DNMT3A. *Nature 517*, 640−644.
(20) Jurkowska, R. Z., Rajavelu, A., Anspach, N., Urbanke, C., Jankevicius, G., Ragozin, S., Nellen, W., and Jeltsch, A. (2011) Oligomerization and binding of the Dnmt3a DNA methyltransferase to parallel DNA molecules: heterochromatic localization and role of Dnmt3L. *J. Biol. Chem. 286*, 24200−24207.
(21) Jurkowska, R. Z., Anspach, N., Urbanke, C., Jia, D., Reinhardt, R., Nellen, W., Cheng, X., and Jeltsch, A. (2008) Formation of nucleoprotein filaments by mammalian DNA methyltransferase Dnmt3a in complex with regulator Dnmt3L. *Nucleic Acids Res. 36*, 6656−6663.
(22) Holz-Schietinger, C., Matje, D. M., Harrison, M. F., and Reich, N. O. (2011) Oligomerization of DNMT3A controls the mechanism of de novo DNA methylation. *J. Biol. Chem. 286*, 41479−41488.
(23) Holz-Schietinger, C., and Reich, N. O. (2010) The inherent processivity of the human de novo methyltransferase 3A (DNMT3A) is enhanced by DNMT3L. *J. Biol. Chem. 285*, 29091−29100.
(24) Emperle, M., Rajavelu, A., Reinhardt, R., Jurkowska, R. Z., and Jeltsch, A. (2014) Cooperative DNA binding and protein/DNA fiber formation increases the activity of the Dnmt3a DNA methyltransferase. *J. Biol. Chem. 289*, 29602−29613.
(25) Gowher, H., and Jeltsch, A. (2001) Enzymatic properties of recombinant Dnmt3a DNA methyltransferase from mouse: the enzyme modifies DNA in a non-processive manner and also methylates non-CpG [correction of non-CpA] sites. *J. Mol. Biol. 309*, 1201−1208.
(26) Renbaum, P., and Razin, A. (1992) Mode of action of the Spiroplasma CpG methylase M.SssI. *FEBS Lett. 313*, 243−247.
(27) Vilkaitis, G., Suetake, I., Klimasauskas, S., and Tajima, S. (2005) Processive methylation of hemimethylated CpG sites by mouse Dnmt1 DNA methyltransferase. *J. Biol. Chem. 280*, 64−72.
(28) Holz-Schietinger, C., and Reich, N. O. (2015) De novo DNA methyltransferase DNMT3A: Regulation of oligomeric state and mechanism of action in response to pH changes. *Biochim. Biophys. Acta, Gen. Subj. 1850*, 1131−1139.
(29) Gowher, H., Loutchanwoot, P., Vorobjeva, O., Handa, V., Jurkowska, R. Z., Jurkowski, T. P., and Jeltsch, A. (2006) Mutational analysis of the catalytic domain of the murine Dnmt3a DNA-(cytosine C5)-methyltransferase. *J. Mol. Biol. 357*, 928−941.
(30) Russler-Germain, D. A., Spencer, D. H., Young, M. A., Lamprecht, T. L., Miller, C. A., Fulton, R., Meyer, M. R., Erdmann-Gilmore, P., Townsend, R. R., Wilson, R. K., and Ley, T. J. (2014) The R882H DNMT3A mutation associated with AML dominantly inhibits wild-type DNMT3A by blocking its ability to form active tetramers. *Cancer Cell 25*, 442−454.
(31) Ley, T. J., Ding, L., Walter, M. J., McLellan, M. D., Lamprecht, T., Larson, D. E., Kandoth, C., Payton, J. E., Baty, J., Welch, J., Harris, C. C., Lichti, C. F., Townsend, R. R., Fulton, R. S., Dooling, D. J., Koboldt, D. C., Schmidt, H., Zhang, Q., Osborne, J. R., Lin, L., O'Laughlin, M., McMichael, J. F., Delehaunty, K. D., McGrath, S. D., Fulton, L. A., Magrini, V. J., Vickery, T. L., Hundal, J., Cook, L. L., Conyers, J. J., Swift, G. W., Reed, J. P., Alldredge, P. A., Wylie, T., Walker, J., Kalicki, J., Watson, M. A., Heath, S., Shannon, W. D., Varghese, N., Nagarajan, R., Westervelt, P., Tomasson, M. H., Link, D. C., Graubert, T. A., DiPersio, J. F., Mardis, E. R., and Wilson, R. K. (2010) DNMT3A mutations in acute myeloid leukemia. *N. Engl. J. Med. 363*, 2424−2433.
(32) Kim, S. J., Zhao, H., Hardikar, S., Singh, A. K., Goodell, M. A., and Chen, T. (2013) A DNMT3A mutation common in AML exhibits dominant-negative effects in murine ES cells. *Blood 122*, 4086−4089.
(33) Roth, M., and Jeltsch, A. (2000) Biotin-avidin microplate assay for the quantitative analysis of enzymatic methylation of DNA by DNA methyltransferases. *Biol. Chem. 381*, 269−272.
(34) Rhee, I., Bachman, K. E., Park, B. H., Jair, K. W., Yen, R. W., Schuebel, K. E., Cui, H., Feinberg, A. P., Lengauer, C., Kinzler, K. W., Baylin, S. B., and Vogelstein, B. (2002) DNMT1 and DNMT3b cooperate to silence genes in human cancer cells. *Nature 416*, 552−556.
(35) Rubin, R. A., and Modrich, P. (1977) EcoRI methylase. Physical and catalytic properties of the homogeneous enzyme. *J. Biol. Chem. 252*, 7265−7272.
(36) Smallbone, K., Gavaghan, D. J., Gatenby, R. A., and Maini, P. K. (2005) The role of acidity in solid tumour growth and invasion. *J. Theor. Biol. 235*, 476−484.
(37) Holz-Schietinger, C., Matje, D. M., and Reich, N. O. (2012) Mutations in DNA methyltransferase (DNMT3A) observed in acute myeloid leukemia patients disrupt processive methylation. *J. Biol. Chem. 287*, 30941−30951.
(38) Du, J., Johnson, L. M., Jacobsen, S. E., and Patel, D. J. (2015) DNA methylation pathways and their crosstalk with histone methylation. *Nat. Rev. Mol. Cell Biol. 16*, 519−532.
(39) Tiedemann, R. L., Putiri, E. L., Lee, J. H., Hlady, R. A., Kashiwagi, K., Ordog, T., Zhang, Z., Liu, C., Choi, J. H., and Robertson, K. D. (2014) Acute depletion redefines the division of labor among DNA methyltransferases in methylating the human genome. *Cell Rep. 9*, 1554−1566.
(40) Shih, A. H., Abdel-Wahab, O., Patel, J. P., and Levine, R. L. (2012) The role of mutations in epigenetic regulators in myeloid malignancies. *Nat. Rev. Cancer 12*, 599−612.
(41) Walter, M. J., Ding, L., Shen, D., Shao, J., Grillot, M., McLellan, M., Fulton, R., Schmidt, H., Kalicki-Veizer, J., O'Laughlin, M., Kandoth, C., Baty, J., Westervelt, P., DiPersio, J. F., Mardis, E. R.,

DOI: 10.1021/acs.biochem.6b00964
Biochemistry 2018, 57, 4312−4324

Wilson, R. K., Ley, T. J., and Graubert, T. A. (2011) Recurrent DNMT3A mutations in patients with myelodysplastic syndromes. *Leukemia 25*, 1153−1158.
(42) Xu, G. L., Bestor, T. H., Bourc'his, D., Hsieh, C. L., Tommerup, N., Bugge, M., Hulten, M., Qu, X., Russo, J. J., and Viegas-Pequignot, E. (1999) Chromosome instability and immunodeficiency syndrome caused by mutations in a DNA methyltransferase gene. *Nature 402*, 187−191.
(43) Hansen, R. S., Wijmenga, C., Luo, P., Stanek, A. M., Canfield, T. K., Weemaes, C. M., and Gartler, S. M. (1999) The DNMT3B DNA methyltransferase gene is mutated in the ICF immunodeficiency syndrome. *Proc. Natl. Acad. Sci. U. S. A. 96*, 14412−14417.
(44) Ehrlich, M., Buchanan, K. L., Tsien, F., Jiang, G., Sun, B., Uicker, W., Weemaes, C. M., Smeets, D., Sperling, K., Belohradsky, B. H., Tommerup, N., Misek, D. E., Rouillard, J. M., Kuick, R., and Hanash, S. M. (2001) DNA methyltransferase 3B mutations linked to the ICF syndrome cause dysregulation of lymphogenesis genes. *Hum. Mol. Genet. 10*, 2917−2931.
(45) Hamidi, T., Singh, A. K., and Chen, T. (2015) Genetic alterations of DNA methylation machinery in human diseases. *Epigenomics 7*, 247−265.
(46) Miller, C. A., Wilson, R. K., and Ley, T. J. (2013) Genomic landscapes and clonality of de novo AML. *N. Engl. J. Med. 369*, 1473.

DOI: 10.1021/acs.biochem.6b00964
Biochemistry 2018, 57, 4312−4324

tory role of the interaction of Dnmt3-ADD domain with demethylated histone tails in site-specific DNA methylation during ESC differentiation.

In response to signals of differentiation, ESCs initiate global changes in gene expression that are forged by alterations in the epigenetic state of the regulatory elements of various cohorts of genes. Among these, pluripotency genes (PpGs) are downregulated and at their promoters and enhancers acquire a repressed chromatin state that includes loss of histone H3K4 methylation and gain of DNA methylation. The interaction of Dnmt3a with the G9A histone methyltransferase has been shown to promote DNA methylation at the PpG promoters post differentiation of ESCs (9,10). However, little is known about how DNA methylation is regulated at PpG enhancers. Histone H3K4me1 (monomethylation) and H3K27Ac (acetylation) are prototypical epigenetic modifications for active enhancers (27). Compared to demethylation of histone H3K4me3 at promoters, which is proposed to require the combined activity of Kdm5/Jarid family and Lsd1 demethylases, demethylation of H3K4me1 at enhancers only requires Lsd1 activity (28–31). During differentiation of ESCs, Lsd1 associates with the Mi2/NuRD deacetylase complex specifically at PpG enhancers. The activity of this repressive complex is triggered by dissociation of the OSN (Oct4/Sox2/Nanog/HATp300) coactivator complex resulting in enhancer repression by histone deacetylation and demethylation, which is critical for PpG repression (31). Based on these observations we speculated that deacetylated and demethylated H3K4 histone tails at PpG enhancers may locally activate Dnmt3 enzymes via an interaction with their ADD domains, thus conferring a unique regulatory potential to this series of epigenetic events. Our studies here provide evidence for the timing, location and role of the interaction of the Dnmt3 ADD domain with demethylated histone tails in regulating site-specific DNA methylation at a subset of PpG enhancers during ESC differentiation.

MATERIALS AND METHODS

ESC culture and differentiation method

E14Tg2A (WT) ESCs were maintained in media containing LIF and induced to differentiate by LIF withdrawal and followed by retinoic acid addition (32). ZHBTc4 cells were maintained in media with LIF and induced to differentiate by simultaneous withdrawal of LIF and addition of doxycycline (31). Treatment of the Lsd1 inhibitors pargyline (3 mM) (Sigma, P8013), tranylcypromine TCP (1 mM) (Millipore, 616431) and the p300 inhibitor C646 (400 nM) (Sigma, SML0002) were performed as described (31). Low passage Dnmt3KO ESC were obtained from Dr Taiping Chen, MD Anderson and ZHBTc4 were obtained from Dr Dana Levasseur, University of Iowa. Single (KO) and double knockout (DKO) cells for Dnmt3a and/or Dnmt3b, as well as the transgenic Myc-ADD and Myc-Vector expressing cell lines were grown and induced to differentiate similar to E14Tg2A ESCs. For all experiments, ESC (all lines) were expanded by passaging twice after which differentiation was induced. At various time points post induction, a third of cells were harvested for preparation of DNA and RNA and rest were crosslinked to prepare chromatin. For all experiments this procedure was repeated at least 2 times for sample collection.

Chromatin immunoprecipitation

Chromatin immunoprecipitation (ChIP) was performed using crosslinked chromatin from ESCs and embryoid bodies. Cells were crosslinked with 1% formaldehyde in Crosslinking buffer (0.1 M NaCl, 1 mM EDTA, 0.5 mM EGTA and 50 mM HEPES pH 8) for 5 min, then quenched by adding glycine to 150 mM. The nuclei were isolated and chromatin was sheared using a Covaris E210 device, according to manufacturer's protocols. Eight micrograms of sonicated chromatin was added to protein A and protein G magnetic beads (Life Technologies, 10002D, 10004D) conjugated with desired antibody overnight. After washing the beads, bound chromatin was eluted and purified DNA was used for quantitative PCR (qPCR). DNA samples were quantified using a NanoDrop 3300 fluorospectrometer. qPCR was then performed using equal amounts of IN (input) and IP (immunoprecipitated sample) DNA. Percent input was calculated as follows: 2^(Cq(IN)-Cq(IP))X100. Cq is the quantification cycle as calculated by the Biorad CFX Manager 3.1 based on the MIQE guidelines (33). Standard deviations represent at least 2 technical and 2 biological replicates. For the all the experiments, the significance of the average change in the enrichment across all loci was calculated by Wilcoxon matched pairs signed rank test using GraphPad Prism and *P*-values were $\leq$0.035. For Myc-ADD ChIP, the percent enrichment for the ADD domain was determined by subtracting the percent enrichment obtained for the vector control. Additional information is available in the Supplementary Methods section for ChIP. See Supplementary Table S4 for primers used. A detailed ChIP protocol is in Supplementary Materials.

DNA methylation-dependent qPCR assay (MD-qPCR)

Genomic DNA was harvested using a standard phenol:chloroform isolation, followed by ethanol precipitation. DNA from various samples was digested initially with CviQI (NEB, R0639L) overnight at 25°C. Purified samples were subjected to digestion by MspJI (NEB, R0166L) overnight at 37°C. Digested DNA was purified and quantified by PicoGreen according to manufacturer's protocol (Life Technologies, P11495) using the NanoDrop 3300 fluorospectrometer. Quantitative PCR was performed by using equal amount of DNA for each sample. Change in DNA methylation is represented by relative fold change in the Cq values as follows: 2^[Cq(U)-Cq(I)], where Cq(U) is the Cq for the undifferentiated (ESC) sample, and Cq(I) represents a sample from a given time point post differentiation. Cq is the quantification cycle as calculated by the Biorad CFX Manager 3.1 based on the MIQE guidelines (Minimum Information for publication of Quantitative Real-Time PCR Experiments) (33). The primers used for DNA methylation-dependent qPCR analysis were the same as used for ChIP. Standard deviations represent at least 2 technical and 2 biological replicates.

Quantitative RT-PCR

RNA was isolated by using TRIzol (Invitrogen, 15596026) according to manufacturer's protocol, and purified after DNAse treatment (Roche, 04716728001). RT-qPCR (Real-Time quantitaive PCR) was performed by using Verso One-Step RT-qPCR kits (Thermo Scientific, AB-4104A). The data analysis was performed by calculating delta Cq normalized to Gapdh expression and represented as change relative to undifferentiated (ESC) expression, which was set to 0. Cq is the quantification cycle as calculated by the Bio-rad CFX Manager 3.1 based on the MIQE guidelines (33). Change in expression is reported in a $\log_2$ scale and the average data is calculated for 8 PpG. Standard deviations represent at least 2 technical and 2 biological replicates. The variance in average data is represented by SEM (standard error of the mean) with n = 8. The SD (standard deviation), SEM determination and *P*-value were calculated using GraphPad Prism using Student's paired *t*-test. See Supplementary Table S4 for primers used.

Microscopy

Alkaline phosphatase staining was performed using a kit (Sigma, AB0300) according to the manufacturers protocol. Cells were imaged under a Zeiss microscope at 20X objective. Immunofluorescence experiments were performed according to Whyte *et al.*, 2012 (31). Antibodies used for immunofluorescence include: SSEA-1 (Millipore, MAB430) 1:2000 and AlexaFluor 555 nm (Life Technologies, A21422) 1:1000. Brightfield imaging was done with a Nikon Ts microscope with a 20X objective.

Bisulfite sequencing

Bisulfite sequencing was performed by using the EpiTect Fast Bisulfite Conversion Kit (Qiagen, 59802) according to the manufacturer's protocol. Bisulfite-converted DNA was amplified using nested primers according to the published methods (34). Products from the inner PCR were gel purified (Qiagen, 28704) and used to generate a barcoded library for Mi-Seq. Barcoded amplicons for each region were purified and pooled to a final concentration of 8 pM. Illumina MiSeq 500 cycle run generated paired-end 250 base reads. The reads were then mapped by Bowtie2 and analyzed by Bismark for DNA methylation. Instances of methylated and unmethylated CpG were quantified and summed to an overall percent methylation for each enhancer region with standard deviations. An average percent methylation for all the enhancers was computed and the variance is represented by SEM with n = 6. See Supplementary Table S2 for number of reads for each sample and site, and Supplementary Table S3 for the percent CpG methylation by region for each sample. See Supplementary Table S4 for primers used for bisulfite sequencing.

ChIP-Western and co-immunoprecipitation

For the ChIP-Western, crosslinked chromatin was processed as described in the ChIP protocol. For the detection of proteins in ChIP samples, elution was performed with Laemmli's loading buffer. For co-immunoprecipitation (Co-IP), the nuclear extract was prepared according to manufacturer's protocol (Active Motif, 40010) except that DNase was added for the release of chromatin-associated proteins. The Co-IP was performed using Dynabead M280 (Life Technologies, 11201D) conjugated with 5 μg antibody and with 50 μg of nuclear extract according to the manufacturer's protocol. Antibodies used include: anti-Dnmt3a (Active Motif, 39206), anti-Chd4 (Abcam, ab72418), anti-Hdac1 (Abcam, ab 7028), anti-Lsd1 (Abcam, ab17721).

RESULTS

Dnmt3a methylates a subset of PpG enhancers

Dnmt3a and 3b have been previously reported to methylate PpG promoters (35) but their role in methylating PpG enhancers has not been fully defined. We tested the role of Dnmt3 enzymes in the methylation of the known enhancers of six commonly studied key PpGs; *Lefty1, Lefty2, Esrrb, Sall4, Sox2, Trim28* during ESC differentiation (36). We differentiated WT and Dnmt3a$^{-/-}$ 3b$^{-/-}$ DKO cells (Supplementary Figures S1 and S2A) and compared DNA methylation levels at these PpG enhancers (37). We used a methylation-dependent restriction method (MD-qPCR) in which the restriction enzyme MspJI cleaves methylated DNA (Supplementary Figure S2B) (38). A single methylation event will result in digestion by MspJI and loss of PCR amplification (39). The qPCR analysis showed an increase in Cq value representing an increase in the DNA methylation at PpG enhancers during differentiation of WT cells, which was completely absent in the DKOs (Supplementary Figure S2C). We further analyzed the DNA methylation at these PpG enhancers by bisulfite sequencing (Bis-seq) (Supplementary Tables S1 and S2) which confirmed the results obtained by MD-qPCR (Figure 1B and Supplementary Table S3). These data support the function of Dnmt3 enzymes in methylating these sites *de novo* during differentiation. Dnmt3a and 3b have distinct as well as redundant targets during early development (37). To determine whether both enzymes are involved in methylation of these PpG enhancers, we used Dnmt3a$^{-/-}$ and Dnmt3b$^{-/-}$ ESCs (3aKO, 3bKO) (Supplementary Figure S1), and induced them to differentiate as illustrated in Supplementary Figure S2A. Analysis using MD-qPCR and Bis-seq showed that DNA methylation at PpG enhancers in differentiating 3aKO cells was comparable to that in DKO cells, whereas in differentiating 3bKO cells, DNA methylation gradually increased to more than 50% of WT (Figure 1A and B). These data argue for a primary role of Dnmt3a in establishing DNA methylation at these PpG enhancers. The delayed and lower methylation in 3bKO cells suggests that either the activity of Dnmt3a is not fully operational in the absence of Dnmt3b or the propagation and/or maintenance of DNA methylation established by Dnmt3a requires Dnmt3b activity suggesting that combined activity of Dnmt3a and 3b is required to complete DNA methylation at these sites (37,40,41).

Next we compared the changes in the expression of these PpGs in WT and Dnmt3 KO cells post induction of differentiation. Relative to gene expression changes post induction of differentiation in WT, we observed that more PpGs showed a partial gene repression in 3aKO and DKO cells compared to 3bKO cells (Figure 1C, Supplementary

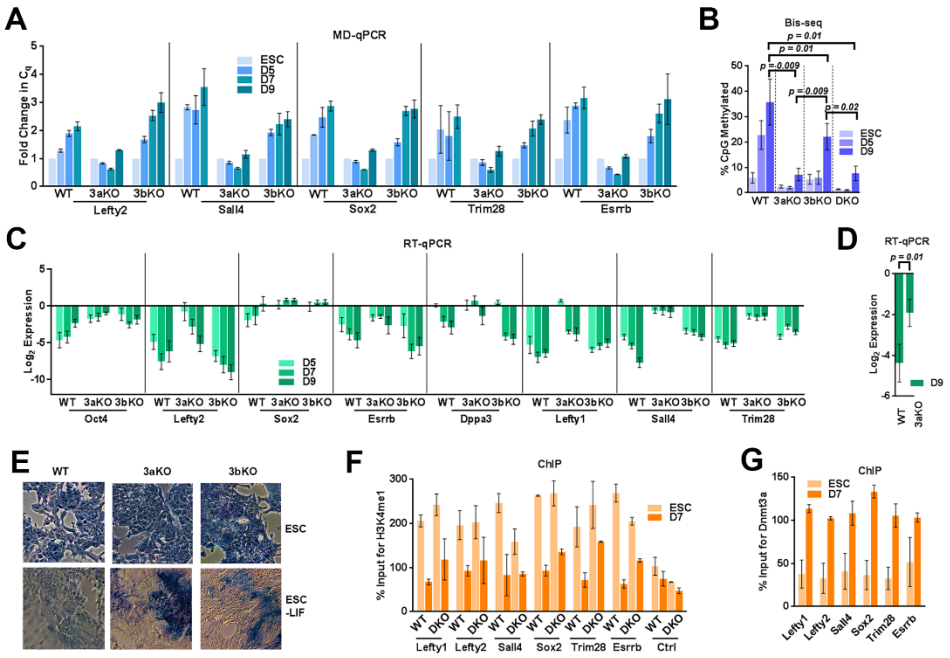

Figure 1. Dnmt3a is the principal methyltransferase for PpG enhancer methylation. ESC: undifferentiated embryonic stem cells and D3–D9: Days post-induction of differentiation WT: Wild Type, 3aKO: Dnmt3a$^{-/-}$, 3bKO: Dnmt3b$^{-/-}$, DKO: Dnmt3a$^{-/-}$ Dnmt3b$^{-/-}$. DNA methylation analysis of the PpG enhancers by (**A**) MD-qPCR and by (**B**) bisulfite sequencing (Bis-seq). For MD-qPCR, genomic DNA was digested with the restriction enzyme MspJI that cuts methylated DNA, followed by qPCR at PpG enhancers (illustration in Supplementary Figure S2B). An increase in the Cq (quantification cycle) represents the gain in DNA methylation. For Bis-seq (B) bisulfite-treated gDNA was used to determine the extent of CpG methylation at the PpG enhancers shown in A on a high throughput sequencing platform (MiSeq) and the data were analyzed using Bismark software. The number of CpGs, reads analyzed for each enhancer and percent CpG methylation by site in all cell lines and treatments are given in Supplementary Tables S1, S2, S3 and Materials and Methods. (**C**) Gene expression analysis of PpGs by RT-qPCR in WT and Dnmt3 KO cells; undifferentiated and post induction of differentiation. Gene expression is normalized to *Gapdh* and represented as a relative change to gene expression in ESC. (**D**) Average gene expression change across all 8 PpGs D9 post differentiation in Dnmt3aKO compared to WT. *P*-values are derived from Student's paired *t*-test (**E**) Alkaline phosphatase staining (blue) for pluripotency in ESCs and differentiated cells D9 post-induction, where the presence of stain indicates pluripotency. (F and G) ChIP-qPCR was used to determine percent enrichment of (**F**)H3K4me1 in WT and DKO cells (**G**) Dnmt3a in WT cells at PpG enhancers pre- and post-induction of differentiation. For A, C, F and G average and SD are shown for each gene.

Figure S2D). The average effect on the repression of all the PpGs post differentiation in Dnmt3aKO was significant when compared to the WT (Figure 1D). This suggests a common role of Dnmt3a in the repression of these PpG during differentiation. Both Dnmt3a and 3b KO ESC differentiated into embryoid bodies (EBs), however, we noticed they had aberrant size and morphology (Supplementary Figure S2E). Compared to WT and 3bKO cells, the 3aKO cells also maintained a higher level of alkaline phosphatase (AP) expression post differentiation, a marker of pluripotency (Figure 1E). However, the germ layer specific genes were activated in both 3aKO and 3bKO cells post induction of differentiation (Supplementary Figure S2F, S2G), indicating only a partial defect in their differentiation potential.

Although we cannot exclude the possibility that in the 3aKO cells, the absence of DNA methylation at other Dnmt3a targets could affect the PpG repression, this observation resembles the published effects of Lsd1 inhibition on PpG repression. During ESC differentiation, Lsd1-Mi2/NuRD removes histone H3K4me1 and H3K27Ac from PpG enhancers and the demethylation activity of Lsd1 was shown to be critical for complete repression of PpGs (31). Therefore, we tested the Lsd1 activity at the PpG enhancers in DKO cells post induction of differentiation by ChIP of histone H3K4me1. Comparable levels of H3K4me1 were observed in DKO and WT cells, which were similarly reduced post induction, showing that Lsd1 activity is unaltered at PpG enhancers in DKO cells (Figure 1F). These results suggest Dnmt3a may be a potential downstream epigenetic effector of Lsd1-Mi2/NuRD activity and could contribute to the complete repression of these PpGs. We propose that during ESC differentiation, deacety-

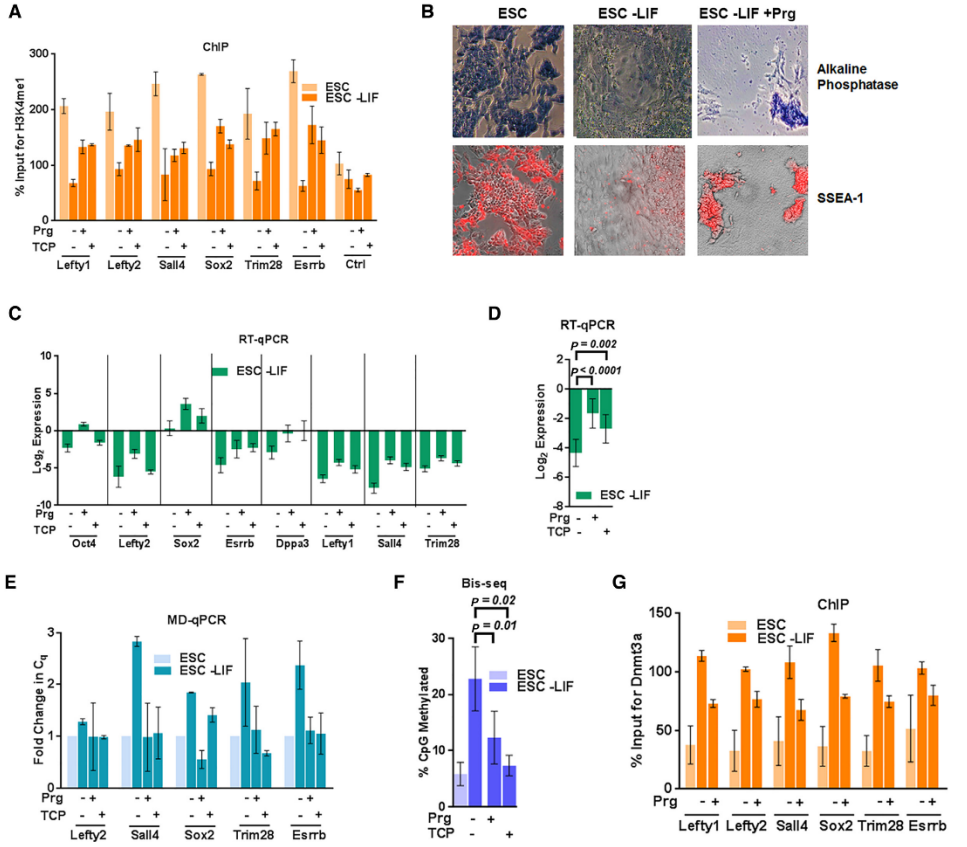

Figure 2. Lsd1 inhibition restricts establishment of DNA methylation at PpG enhancers by Dnmt3a. ESC: undifferentiated embryonic stem cells, and ESC-LIF: Cells induced to differentiate. (**A**) ChIP-qPCR was used to determine the percent enrichments of H3K4me1 at the PpG enhancers in ESC and cells 7 days post- induction of differentiation in absence and presence of Lsd1 inhibitors, Prg: Pargyline, TCP: Tranylcypromine. (**B**) Alkaline phosphatase staining (blue) and SSEA-1 immunofluorescence (red) in ESCs and cells 9 days post induction of differentiation in absence and presence of pargyline, where positive staining indicates pluripotency. (**C**) Gene expression analysis of PpGs using R1-qPCR in ESCs and cells 9 days post induction of differentiation in absence and presence of Lsd1 inhibitors. Gene expression is normalized to *Gapdh* and represented relative to ESC. (**D**) Average expression change with SEM across all loci shown in C; (**E**) DNA methylation analysis of the PpG enhancers in ESCs and cells 5 days post induction of differentiation in absence and presence of pargyline and TCP was assayed by MD-qPCR as in Figure 1A. (**F**) Bis-seq was used to determine the extent of CpG methylation (details same as Figure 1B) and the data are the average and SEM of 6 PpG enhancers shown in E. (**G**) Percent enrichment of Dnmt3a using ChIP-qPCR at PpG enhancers in ESC and cells 7 days post-induction of differentiation in absence and presence of Lsd1 inhibitors. For D and F, *P*-values are derived from Student's paired *t*-test using GraphPad Prism. For A, C, E and G average and SD are shown for each gene.

lation and demethylation by the Lsd1-Mi2/NuRD complex primes the histone tails to interact with the Dnmt3a-ADD domain. This hypothesis is further supported by ChIP analysis showing an increased enrichment of Dnmt3a at PpG enhancers in differentiated cells (Figure 1G).

Given that several studies have described the relationship between histone deacetylation and DNA methylation (16), we investigated the contribution of Lsd1 activity in regulating DNA methylation by Dnmt3a at PpG enhancers during ESC differentiation.

Lsd1-mediated demethylation triggers Dnmt3a activity at PpG enhancers

In contrast to other histone demethylases, Lsd1 uniquely catalyzes an FAD-dependent oxidation reaction to remove H3K4me1. It is specifically inhibited by the monoamine

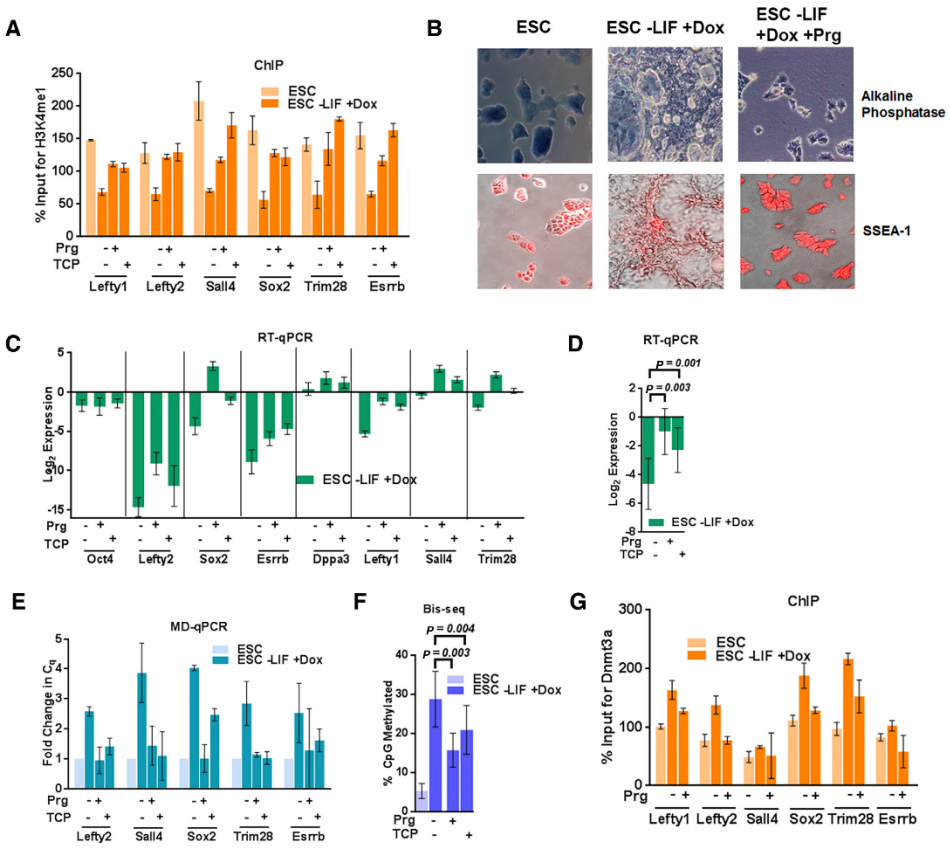

Figure 3. Lsd1 inhibition affects DNA methylation at PpG enhancers in absence of Oct4 expression. ESC: undifferentiated embryonic stem cells, and ESC -LIF +Dox: Cells induced to differentiate by Doxycycline treatment. (**A**) Percent enrichments of H3K4me1 using ChIP-qPCR at the PpG enhancers in ESC and cells 4 days post-induction of differentiation normalized to a negative control region in absence and presence of Lsd1 inhibitors, Prg: Pargyline, TCP: Tranylcypromine. (**B**) Alkaline phosphatase (blue stain) and SSEA-1 immunofluorescence staining (red stain) for pluripotency in ESCs and cells 8 days post-induction of differentiation in absence and presence of Prg, where positive staining indicates pluripotency. (**C**) Gene expression of PpGs by R1-qPCR in ZHTBTc4 cells untreated and treated with Lsd1 inhibitors for 8 days post induction of differentiation. Gene expression is normalized to *Gapdh* and represented relative to ESC. (**D**) Average expression change with SEM across all loci shown in C; (**E**) DNA methylation analysis of the PpG enhancers in ESCs and cells 4 days post-induction of differentiation in absence and presence of pargyline and TCP was assayed by MD-qPCR as in Figure 1A. (**F**) Bis-seq was used to determine the extent of CpG methylation (details same as Figure 1B) and the data are the average and SEM of 6 PpG enhancers shown in E. (**G**) Percent enrichment of Dnmt3a using ChIP-qPCR at PpG enhancers from cells pre- and 4 days post-induction of differentiation in presence and absence of prg. *P*-values are derived from Student's paired *t*-test using GraphPad Prism. For A, C, E and G average and SD are shown for each gene.

oxidase inhibitors pargyline (Prg) and tranylcypromine (TCP). Both of these inhibitors have been earlier demonstrated to inhibit Lsd1 activity and PpG repression during ESC differentiation (31,42,43). With the use of these inhibitors, we asked whether Dnmt3a activity is regulated by Lsd1-mediated histone demethylation at the examined PpG enhancers. The speculation that the Lsd1 inhibition will suppress Dnmt3a activity is supported by fluorescence polarization and isothermal titration calorimetry experiments, which show that H3K4me1 decreases the interaction of Dnmt3-ADD with H3 tails by 18- and 2-fold, respectively (21,26). Compared to H3K4me3, although H3K4me1 partially blocked this interaction *in vitro*, we anticipated the possibility of a significant effect *in vivo*. To test our hypothesis, ESC differentiation was induced in the presence of Prg or TCP (Supplementary Figure S3A). ChIP of H3K4me1

at a subset of the enhancers of PpGs confirmed the suppression of Lsd1 activity in inhibitor-treated, induced cells (Figure 2A). Consistent with earlier studies, treatment of Lsd1 inhibitors during differentiation lead to cell death (31,44), but the surviving cells retain pluripotency as shown by SSEA-1 and AP staining (Figure 2B). We also observed weak PpG repression and no significant change in the activation of germ layer-specific genes in Lsd1 inhibitor-treated induced cells (Figure 2C, D, Supplementary Figure S3B and S3C) confirming the previously known role of Lsd1 in regulation of PpG repression during ESC differentiation. Since the measurable increase in DNA methylation takes places 4–5d post differentiation in untreated WT cells (Figure 1A and B), we determined the effect of Lsd1 inhibition on the establishment of DNA methylation by analyzing these early time points using MD-qPCR and Bis-seq. Gain of DNA methylation at these PpG enhancers during differentiation was restricted in cells treated with Lsd1 inhibitors, suggesting a link between Lsd1 activity and DNA methylation at these PpG enhancers (Figure 2E and F). Consistent with these results, ChIP analysis showed that the enrichment of Dnmt3a at the PpG enhancers is reduced in Prg-treated induced cells (Figure 2G).

Effect of the master regulator Oct4 on gain of DNA methylation at PpG enhancers

Because Lsd1 inhibitors block differentiation of ESCs, the gain of DNA methylation at PpG enhancers may be affected by other protective mechanisms that include binding of the master transcriptional regulator of PpGs, Oct4 to these PpG enhancers. Gene expression analysis of the Prg-treated and induced cells showed a higher expression of Oct4 (Figure 2C). We reasoned that in these conditions, high Oct4 expression may result in its continued binding to PpG regulatory elements, thus overriding the effect of epigenetic regulators in the repression pathway. To uncouple the effect of Oct4-reinforced transcriptional activation from Lsd1 regulation of DNA methylation, we used the transgenic ESC line, ZHBTc4 (Z), in which doxycycline treatment induces Oct4 repression and consequent cell differentiation into trophectoderm as shown by an increase in the expression of *Cdx2* gene (Supplementary Figure S3D and S3E) (45). Similar to their effect in WT ESCs, in Z cells Lsd1 inhibitors prevented complete histone H3K4me1 demethylation (Figure 3A), impeded differentiation (Figure 3B) and caused incomplete repression of PpGs (Figure 3C, D and Supplementary Figure S3F). Further, compared to control differentiating Z cells, DNA methylation in treated cells was significantly reduced (Figure 3E–F) demonstrating that in the absence of Oct4 expression, inhibition of Lsd1 activity is sufficient to impede DNA methylation by Dnmt3a at PpG enhancers post induction of differentiation. ChIP analysis showed that similar to E14T cells, the enrichment of Dnmt3a at the PpG enhancers is reduced in Prg-treated induced cells (Figure 3G). The effect of Lsd1 inhibition on DNA methylation was not due to reduced expression of Lsd1, Dnmt3a, 3b or Dnmt1 (Supplementary Figure S4A–S4B) and did not affect global DNA methylation levels as evidenced by the integrity of genomic methylation at the repetitive elements, which is comparable to untreated differentiating ESCs (Supplementary Figure S4C). Taken together, our results support a functional interaction between the Lsd1-dependent histone H3K4 demethylation and Dnmt3a-catalyzed DNA methylation at these examined PpG enhancers.

Histone deacetylation by Mi2/NuRD and DNA methylation at PpG enhancers

Previous studies have shown that in ESCs, Lsd1 is part of the Mi2/NuRD complex (31,46–48). During ESC differentiation, dissociation of the OSN coactivator complex (Oct4/Sox2/Nanog-HATp300) from the PpG enhancers triggers the histone deacetylase activity of the Mi2/NuRD complex, which is critical for Lsd1-mediated histone demethylation. Since the acetylation of histones is known to inhibit the interaction of unmethylated histone tails with the Dnmt3a-ADD domain (22,49), we asked if Dnmt3a activity at PpG enhancers was blocked by the disruption of the histone deacetylase activity of the Mi2/NuRD complex in Lsd1 inhibitor treated cells. We first verified histone deacetylation during differentiation at a subset of PpG enhancers by ChIP of histone H3K27Ac. Surprisingly, deacetylation was partially inhibited in Prg-treated cells (Figure 4A) (27,50), which may be a consequence of the recursive nature of epigenetic processes (51–55). Therefore, to distinguish the potential effect of remnant histone acetylation from that of histone methylation on Dnmt3a activity in Prg-treated cells, we induced differentiation of ESCs in the presence of the p300 HAT inhibitor C646, in addition to the treatment with Prg (Supplementary Figure S5A) (56). Treatment of cells with C646 did not affect the differentiation, however, treatment with Prg together with C646 impeded differentiation as shown by AP and SSEA-1 staining (Figure 4B). The decrease of histone acetylation at PpG enhancers in C646-treated differentiated cells (Figure 4A) is expected to be permissive for Lsd1 activity and DNA methylation by Dnmt3a. Consistent with this, we observed a decrease in H3K4 methylation and an increase in DNA methylation in C646 treated cells (Figure 4C, D and E). Simultaneous treatment with Prg and C646 can therefore be used to determine the direct impact of histone demethylation on Dnmt3a activity (Figure 4C). When ESCs were induced to differentiate in the presence of both C646 and Prg, gain of DNA methylation at these PpG enhancers was strongly inhibited (Figure 4D and E), even though the histone acetylation was similarly reduced in C646 treated cells with and without Prg (Figure 4A).

A similar effect on the gain of DNA methylation at the PpG enhancers was seen in Z cells when they were induced to differentiate by doxycycline treatment in the presence of Prg and/or C646 (Figure 4F). Use of Z cells in these experiments uncouples the protective effects of both Oct4 and histone acetylation from the regulatory role of Lsd1-mediated histone demethylation on Dnmt3a-catalyzed DNA methylation at PpG enhancers. Although Dnmt3a could have other targets during differentiation, its coordinated activity with Lsd1 is likely to be specific to PpG enhancers, since the Lsd1 activity was shown to be largely recruited at the PpG enhancers during ESC differentiation (31). Taken together, these data establish a dominant effect of Lsd1 inhi-

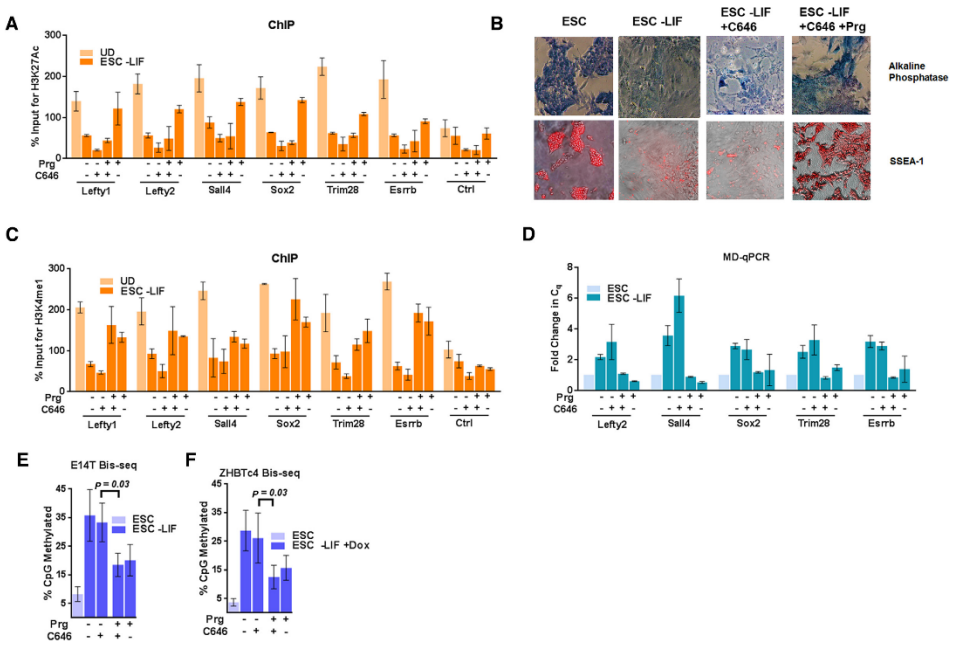

Figure 4. Effect of histone deacetylation on DNA methylation at PpG enhancers. ESC: undifferentiated embryonic stem cells, and ESC -LIF: E14T cells induced to differentiate, ESC -LIF+Dox: ZHBTc4 cells induced to differentiate. (**A**) ChIP-qPCR was used to determine the percent enrichments of H3K27ac at the PpG enhancers in ESC and cells 7 days post-induction of differentiation in absence and presence of Prg and/or C646, Prg: Pargyline, C646: p300 Histone acetyltransferase inhibitor. (**B**) Alkaline phosphatase staining (blue) and SSEA-1 immunofluorescence (red) in ESCs and cells 9 days post induction of differentiation in absence and presence of C646 and C646 with pargyline, where positive staining indicates pluripotency. (**C**) ChIP-qPCR was used to determine the percent enrichments of H3K4me1 at the PpG enhancers in ESC and cells 7 days post-induction of differentiation in absence and presence of Prg and/or C646. (**D**) DNA methylation analysis of the PpG enhancers in ESCs and cells post induction of differentiation in absence and presence of Prg and/or C646 was assayed by MD-qPCR as in Figure 1A. (E and F) Bis-seq was used to determine the extent of CpG methylation at these enhancers in (**E**) E14T cells or (**F**) ZHBTc4 cells and the data were analyzed using Bismark software (details same as Figure 1B) and the data are the average and SEM of 6 PpG enhancers shown in D. *P*-values are derived from Student's paired *t*-test. For A, C and D average and SD are shown for each gene.

bition on the mechanism that regulates the establishment of DNA methylation at a subset of PpG enhancers during ESC differentiation and suggest a functional link between Lsd1 activity and DNA methylation by Dnmt3a.

Interaction of Dnmt3a with Lsd1-Mi2/NuRD complex

Previous studies have shown that Lsd1 and Mi2/NuRD form a complex in undifferentiated ESCs and associate with PpG enhancers while they are in the active state. The enzymatic activity of the Lsd1-Mi2/NuRD complex is, however, only triggered upon dissociation of the OSN complex during ESC differentiation (31,47). Therefore, we tested the interaction of Dnmt3a with the Lsd1-Mi2/NuRD complex both in the undifferentiated ESCs and in differentiated cells. Reciprocal Co-IP from ESC nuclear extracts and from crosslinked chromatin using Lsd1 or Dnmt3a antibodies revealed the presence of Dnmt3a along with known components of the Lsd1-Mi2/NuRD complex (Figure 5A and B). Similar Co-IP experiments to determine the presence of Dnmt3b in Lsd1-Mi2/NuRD complex showed no specific interaction, which may also be due to low specificity of the available antibodies. Compared to that in undifferentiated ESCs, a weaker or no interaction of Dnmt3a with the Lsd1 complex was observed in crosslinked chromatin from differentiated cells (Supplementary Figure S5B). This suggests that post differentiation, Lsd1-Mi2/NuRD activity allows the subsequent interaction of Dnmt3a-ADD with histone tails, after which the interaction of Dnmt3a with the Lsd1-Mi2/NuRD complex may not persist and may not be required. Lsd1-facilitated interaction of Dnmt3a with histone tails is supported by the results from Dnmt3a ChIP (Figure 1G) that showed a higher enrichment of Dnmt3a at these PpG enhancers post differentiation, which is reduced by Lsd1 inhibitor treatment (Figures 2G and 3G). This higher enrichment of Dnmt3a post differentiation is because its interaction with demethylated histone tails could facilitate its

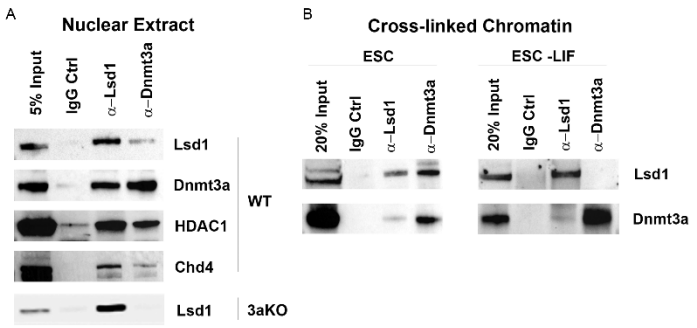

Figure 5. Dnmt3a is associated with the Lsd1-Mi2/NuRD complex. ESC: undifferentiated embryonic stem cells, ESC-LIF: Days post induction of differentiation. 3aKO: Dnmt3a knockout. (**A**) Nuclear extract was prepared from WT and 3aKO ESCs and used in Co-IP (co-immunoprecipitation) performed with anti-Dnmt3a or anti-Lsd1 antibody and control IgG. The immune complexes and input (5% of nuclear extract used in CoIP) were blotted to probe for Lsd1-Mi2/NuRD subunits (Lsd1, Hdac1 and Chd4) and Dnmt3a (shown in the right). Co-IP using 3aKO nuclear extract serves as a control. (**B**) Crosslinked chromatin from ESC and cells 7 days post differentiation was used for a ChIP-Western performed with anti-Dnmt3a or anti-Lsd1. The immune complexes and the input (20%) was blotted to probe for Lsd1 and Dnmt3a.

crosslinking to chromatin. Together, these data suggest a model in which the active enhancers of PpGs are poised for repression by the presence of a proximally located repressive Lsd1-Mi2/NuRD/Dnmt3a complex, which is activated as cells begin to differentiate (Figure 6C).

ADD domain–histone interaction guides PpG enhancer DNA methylation

Our data suggest that during ESC differentiation Lsd1-Mi2/NuRD activity at a subset of PpG enhancers induces a local interaction between histone H3K4me0 and the Dnmt3a-ADD domain, thus facilitating *de novo* DNA methylation at these sites. To investigate the role of the interaction of the Dnmt3-ADD domain with H3K4me0 histone tails in PpG enhancer DNA methylation, we created transgenic ESCs overexpressing the Myc-epitope tagged-ADD domain of Dnmt3a (Supplementary Figure S5C). We confirmed the pluripotency of these lines by SSEA and AP staining (Supplementary Figure S5D) and induced them to differentiate. We reasoned that overexpression of this domain can potentially compete with endogenous Dnmt3a to interact with the demethylated histone tails at the examined PpG enhancers, thereby affecting enhancer DNA methylation during differentiation. ChIP analysis showed the binding of the recombinant Myc-ADD domain at these PpG enhancers post differentiation (Figure 6A). Indeed, accumulation of DNA methylation at these PpG enhancers in the Myc-ADD expressing cells was significantly reduced both at D5 and D9 post differentiation compared to the control cells (Figure 6B). We noticed a more substantial difference in DNA methylation at D5 post induction that narrowed as differentiation proceeded. This is because the Myc-ADD competes with the binding and not the activity of endogenous Dnmt3a; therefore, the DNA methylation deposited for every Dnmt3a binding event could be further propagated by an Lsd1 independent mechanism of Dnmt1 or by Dnmt3b. A partial gain in DNA methylation at these PpG enhancers in 3bKO cells supports this premise (Figure 1A and B). We further examined the potential effect of Myc-ADD on global DNA methylation which showed no change in DNA methylation at Line1 elements and minor satellite repeats (Supplementary Figure S5E). A significant inhibition of PpG enhancer DNA methylation by Myc-ADD is consistent with the model that the interaction of the Dnmt3a-ADD domain with demethylated histone tails at PpG enhancers regulates the establishment of *de novo* DNA methylation during the early phase of differentiation.

Taken together our data suggest that the histone editing activity of the Lsd1-Mi2/NuRD complex at a subset of PpG enhancers regulates the epigenetic switch to locally activate Dnmt3a, leading to site specific DNA methylation and enhancer repression (Figure 6C).

DISCUSSION

Current investigations have advanced our understanding of the contribution of epigenetic mechanisms in the regulation of pluripotency and cellular differentiation in normal and diseased states. However, the mechanisms that regulate the interplay between the readers and writers of epigenetic marks and their subsequent impact on gene expression have not been fully elucidated. In this study, we identified a functional role for Dnmt3a as a reader and effector in a queue of epigenetic events, where local histone deacetylation and demethylation by Lsd1-Mi2/NuRD complex allows the interaction and specific activation of Dnmt3a at a subset of PpG enhancers.

Earlier investigations on the regulation of DNA methylation at PpG regulatory elements have shown that both Dnmt3a and 3b are required for *de novo* methylation of the promoters of *Oct4* and *Nanog* (35) and the interaction between G9a histone methyltransferase and Dnmt3a is required for DNA methylation at the *Oct4* promoter (9,10,57,58). Other studies have shown that G9a may not be required for DNA methylation at the *Oct4* enhancer

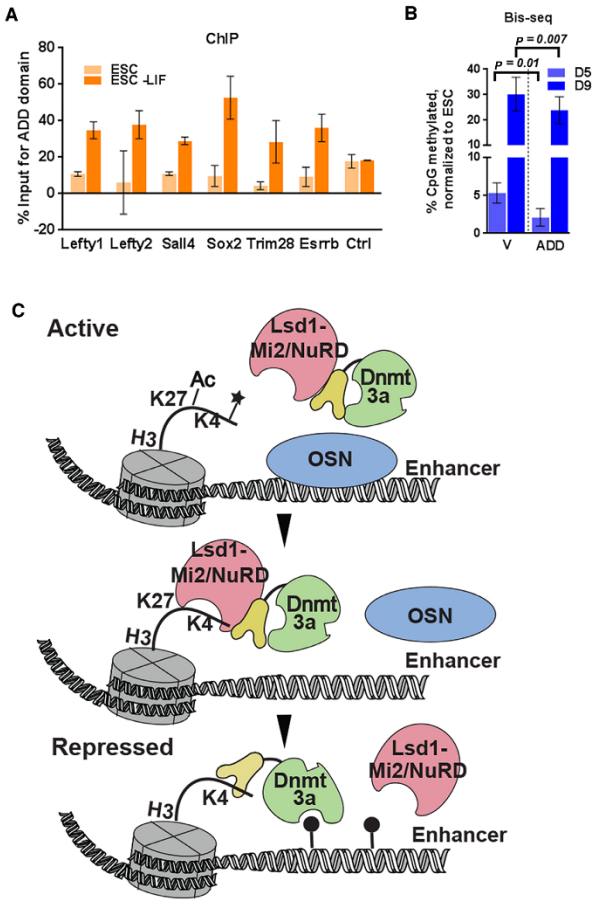

Figure 6. DNA methylation at PpG enhancers is facilitated by histone H3 and Dnmt3a-ADD interaction. ESC: undifferentiated embryonic stem cells, ESC-LIF: Cells induced to differentiate, D5, D9: Days post-induction of differentiation, V: empty Myc vector control and ADD: Myc-3a ADD expressing cells. (**A**) ChIP-qPCR was used to determine the percent enrichments of Myc-Dnmt3a ADD at the PpG enhancers in transgenic ESC lines expressing Myc Dnmt3a-ADD domain pre- and 9 days post-induction of differentiation; the percent enrichment is normalized by subtracting the percent enrichment of the empty vector control from the percent enrichment of ADD expressing cells. Average and SD is shown for each gene. (**B**) DNA methylation at PpG enhancers shown in A in transgenic ESC lines expressing Myc empty vector or Myc Dnmt3a-ADD domain 5 and 9 days post induction of differentiation was assayed by Bis-seq (details same as Figure 1B). The percent methylation for each cell line was were normalized to that in the respective ESC state. *P*-values are derived from Student's paired *t*-test. (**C**) Model illustrating the epigenetic switch at PpG enhancers that activates Dnmt3a through histone-ADD interaction. In their active state, PpGs enhancers are bound by the OSN coactivator complex and the chromatin is acetylated and methylated. Upon differentiation, dissociation of the coactivator complex triggers the activity of the Lsd1-Mi2/NuRD complex, which removes H3K27Ac and H3K4me1 at PpG enhancers. This in turn activates Dnmt3a through the interaction of its ADD domain with the newly generated H3K4me0 histone tails permitting site-specific DNA methylation. Ac: Acetylation; *: histone methylation; closed circle: DNA methylation.

(32,59). Our experiments using ESCs with targeted deletions of Dnmt3a and 3b (37) together with ChIP experiments first identify Dnmt3a as the primary MTase required for methylation of a subset of PpG enhancers. A supporting role of Dnmt3b in this process is suggested by delayed and partial gain of DNA methylation post differentiation in Dnmt3bKO ESCs. Further, our data suggest that DNA methylation at these PpG enhancers may contribute to the stable repression of PpGs during differentiation. Compared to WT cells, repression of some PpGs in Dnmt3aKO cells was partially affected suggesting that Dnmt3a-mediated DNA methylation is one of several processes that together promote complete repression of PpGs (Figure 1C). Additionally, in Dnmt3aKO cells, there was little or no effect on the activation of lineage specific genes during differentiation (Supplementary Figure S2F). Since a combination of PpG repression and lineage-specific gene activation is required to drive differentiation, these deficiencies may be insufficient to block development *in utero* thus explaining the ability of the Dnmt3a KO mice to reach term although they are born runted and die in less than 4 weeks after birth (37). Consistent with this argument we observed that 3aKO ESCs make embryoid bodies, albeit small (Supplementary Figure S2E), indicating that they can differentiate even though the PpG are not fully repressed.

Our data suggest that the activity of Dnmt3a at these PpG enhancers is regulated by the upstream Lsd1-Mi2/NuRD activity, which facilitates the binding of Dnmt3a-ADD domain to histone tails post differentiation. The inhibitory effect of the recombinant Myc-ADD domain on DNA methylation of these PpG enhancers confirms the mechanistic role of the interaction between the Dnmt3a-ADD domain and demethylated histone tails (H3K4me0) in regional specificity of Dnmt3a activity. Previous studies showing that Lsd1-Mi2/NuRD activity is localized at the PpG enhancers (31) suggest that this mechanism might specifically regulate the DNA methylation at these sites facilitated by the interaction of Dnmt3a with the Lsd1-Mi2/NuRD complex. Although the histone modification H3K4me0 is widely distributed in the mammalian genome, DNA methylation of these sites in ESCs and differentiated cells is largely maintained through mechanisms that are independent of Lsd1 activity and presence of the histone H3K4me0 modification (60–62) which is supported by our data showing no change in DNA methylation at the repetitive elements in Lsd1 inhibitor treated cells.

Previous studies have shown that continuous passage of Lsd1 KO ESCs leads to a progressive loss of DNA methylation at repetitive elements genome-wide due to loss of Dnmt1 protein (44). Under our experimental conditions, Lsd1 inhibition during induction of differentiation had no effect on Dnmt1 protein levels (Supplementary Figure S4B) or on global DNA methylation (Supplementary Figure S4C). In our studies, we exposed ESCs to Lsd1 inhibitors only 6 h prior to induction of differentiation and induced them for 8–9 days in the presence of these inhibitors. Therefore, most of the inhibitor treatment was post induction of differentiation in contrast to earlier studies where Lsd1 KO ESC were maintained and passaged in the pluripotent state, leading to reduced stability of Dnmt1 protein. This argues for the potential influence of the ESC state on the mechanism regulating Dnmt1 stability. Further, the near absence of DNA methylation in differentiated 3aKO cells suggests that the presence of Dnmt1 cannot compensate for the absence of Dnmt3a in establishing methylation at the PpG enhancers (Figure 1A and B). Taken together, our data suggest that inhibition of DNA methylation at PpG enhancers in Lsd1 inhibitor-treated cells is likely due to its effect on Dnmt3a activity rather than the loss of Dnmt1.

In this study, we also addressed the potential impact of the known protective mechanisms, which include the transcription factor Oct4 and histone acetylation, on gain of DNA methylation at these PpG enhancers in Lsd1 inhibitor treated cells. Use of Z cells allowed us to control the potential counteracting effects of the coactivator Oct4. Similar to E14T cells, although Lsd1 inhibition significantly impeded the gain of DNA methylation in Z cells, comparing Figure 2 to Figure 3, we indeed noticed that the effect on DNA methylation is less robust in Z cells. Use of C646 (a HAT inhibitor) and Prg during differentiation uncoupled the effect of histone acetylation and histone methylation on deposition of DNA methylation. We conclude that under these experimental conditions, deacetylation of histones is not sufficient to recruit Dnmt3a activity in the presence of H3K4me1 at PpG enhancers. However, this does not exclude the inhibitory effect of histone acetylation on the interaction of the Dnmt3a-ADD with histone tails when these enhancers are in the active state. We anticipate that in the ESC state, when PpG enhancers are active, histone acetylation together with histone methylation block the interaction of the Dnmt3a-ADD domain with histone H3 tails.

Recent structural studies have shown that the ADD domain of Dnmt3a autoinhibits its catalytic activity by sterically blocking its DNA binding domain and the interaction of the ADD domain with unmethylated histone tails relieves this autoinhibition (23). Our Co-IP and ChIP-Western experiments show that Dnmt3a associates with the Lsd1-Mi2/NuRD complex in undifferentiated ESCs. Based on these data, we speculate that in ESCs Dnmt3a associates with the Lsd1-Mi2/NuRD complex in its auto-inhibited state, poised to be activated during ESC differentiation. As differentiation proceeds, the Lsd1-Mi2/NuRD complex deacetylates H3K27 and demethylates H3K4 residues and the resulting 'edited' histone H3 tails interact with Dnmt3a-ADD domain and locally activate the enzyme.

These observations may also have potential implications for regulation of DNA methylation of other genomic elements with varying degrees of histone H3K4 methylation and histone acetylation, thus instructively creating tissue specific patterns of DNA methylation during differentiation. Therefore, it would be interesting to see if this represents a common mechanism for enhancer-mediated regulation of other genes controlling cell identity. For example, both Dnmt3a and Lsd1 are known to regulate hematopoietic stem cell (HSC) differentiation. Lsd1 mediated repression of the regulatory elements of hematopoietic stem and progenitor cell (HSPC) genes is required to fully silence these genes for proper hematopoietic maturation (63), and loss of Dnmt3a in HSCs results in the retention of multipotency gene expression during differentiation (64). It is possible that a similar epigenetic crosstalk mechanism may regulate enhancer repression and stable silencing of multipo-

tency genes, thus maintaining the fidelity of differentiation during hematopoiesis. Additionally, several recent studies have enumerated the role of enhancer-mediated regulation of oncogenes in various cancers (65). Thus, our studies may have implications for the mechanisms that contribute to aberrant gene expression in various human diseases.

SUPPLEMENTARY DATA

Supplementary Data are available at NAR Online.

ACKNOWLEDGEMENTS

The authors thank Dr. Joe Ogas for helpful discussions, Dr. Sandra Rossie for reading the manuscript, Dr. Taiping Chen for providing Dnmt3KO ESC's and Dr. Dana Levasseur for ZHBTc4 cells.
Contributions : C.J.P., L.A., M.H., R.R. and H.G. performed the experiments. P.S.M. analyzed the Bis-seq data. C.J.P. and H.G. wrote the manuscript.

FUNDING

Institutional Start up Fund from the College of Agriculture and the Department of Biochemistry, Purdue University. The authors gratefully acknowledge the DNA sequencing core facility and support from Purdue University Center for Cancer Research, NIH grant P30 CA023168, Graduate Research fellowship for LA supported by the Saudi Arabian Cultural Mission. Funding for open access charge: Institutional Start up Fund from College of Agriculture and the Department of Biochemistry, Purdue University.
Conflict of interest statement. None declared.

REFERENCES

1. Goll,M.G. and Bestor,T.H. (2005) Eukaryotic cytosine methyltransferases. *Annu. Rev. Biochem.*, **74**, 481–514.
2. Cedar,H. and Bergman,Y. (2012) Programming of DNA methylation patterns. *Annu. Rev. Biochem.*, **81**, 97–117.
3. Gowher,H. and Jeltsch,A. (2001) Enzymatic properties of recombinant Dnmt3a DNA methyltransferase from mouse: the enzyme modifies DNA in a non-processive manner and also methylates non-CpG [correction of non-CpA] sites. *J. Mol. Biol.*, **309**, 1201–1208.
4. Holz-Schietinger,C., Matje,D.M., Harrison,M.F. and Reich,N.O. (2011) Oligomerization of DNMT3A controls the mechanism of de novo DNA methylation. *J. Biol. Chem.*, **286**, 41479–41488.
5. Handa,V. and Jeltsch,A. (2005) Profound flanking sequence preference of Dnmt3a and Dnmt3b mammalian DNA methyltransferases shape the human epigenome. *J. Mol. Biol.*, **348**, 1103–1112.
6. Jia,D., Jurkowska,R.Z., Zhang,X., Jeltsch,A. and Cheng,X. (2007) Structure of Dnmt3a bound to Dnmt3L suggests a model for de novo DNA methylation. *Nature*, **449**, 248–251.
7. Gowher,H. and Jeltsch,A. (2002) Molecular enzymology of the catalytic domains of the Dnmt3a and Dnmt3b DNA methyltransferases. *J. Biol. Chem.*, **277**, 20409–20414.
8. Denis,H., Ndlovu,M.N. and Fuks,F. (2011) Regulation of mammalian DNA methyltransferases: a route to new mechanisms. *EMBO Rep.*, **12**, 647–656.
9. Epsztejn-Litman,S., Feldman,N., Abu-Remaileh,M., Shufaro,Y., Gerson,A., Ueda,J., Deplus,R., Fuks,F., Shinkai,Y., Cedar,H. *et al.* (2008) De novo DNA methylation promoted by G9a prevents reprogramming of embryonically silenced genes. *Nat. Struct. Mol. Biol.*, **15**, 1176–1183.
10. Feldman,N., Gerson,A., Fang,J., Li,E., Zhang,Y., Shinkai,Y., Cedar,H. and Bergman,Y. (2006) G9a-mediated irreversible epigenetic inactivation of Oct-3/4 during early embryogenesis. *Nat. Cell Biol.*, **8**, 188–194.
11. Dennis,K., Fan,T., Geiman,T., Yan,Q. and Muegge,K. (2001) Lsh, a member of the SNF2 family, is required for genome-wide methylation. *Genes Dev.*, **15**, 2940–2944.
12. Jones,P.L., Veenstra,G.J., Wade,P.A., Vermaak,D., Kass,S.U., Landsberger,N., Strouboulis,J. and Wolffe,A.P. (1998) Methylated DNA and MeCP2 recruit histone deacetylase to repress transcription. *Nat. Genet.*, **19**, 187–191.
13. Nan,X., Ng,H.H., Johnson,C.A., Laherty,C.D., Turner,B.M., Eisenman,R.N. and Bird,A. (1998) Transcriptional repression by the methyl-CpG-binding protein MeCP2 involves a histone deacetylase complex. *Nature*, **393**, 386–389.
14. Thomson,J.P., Skene,P.J., Selfridge,J., Clouaire,T., Guy,J., Webb,S., Kerr,A.R., Deaton,A., Andrews,R., James,K.D. *et al.* (2010) CpG islands influence chromatin structure via the CpG-binding protein Cfp1. *Nature*, **464**, 1082–1086.
15. Clouaire,T., Webb,S., Skene,P., Illingworth,R., Kerr,A., Andrews,R., Lee,J.H., Skalnik,D. and Bird,A. (2012) Cfp1 integrates both CpG content and gene activity for accurate H3K4me3 deposition in embryonic stem cells. *Genes Dev.*, **26**, 1714–1728.
16. Cedar,H. and Bergman,Y. (2009) Linking DNA methylation and histone modification: patterns and paradigms. *Nat. Rev. Genet.*, **10**, 295–304.
17. Lehnertz,B., Ueda,Y., Derijck,A.A., Braunschweig,U., Perez-Burgos,L., Kubicek,S., Chen,T., Li,E., Jenuwein,T. and Peters,A.H. (2003) Suv39h-mediated histone H3 lysine 9 methylation directs DNA methylation to major satellite repeats at pericentric heterochromatin. *Curr. Biol.*, **13**, 1192–1200.
18. Jackson,J.P., Lindroth,A.M., Cao,X. and Jacobsen,S.E. (2002) Control of CpNpG DNA methylation by the KRYPTONITE histone H3 methyltransferase. *Nature*, **416**, 556–560.
19. Tamaru,H. and Selker,E.U. (2001) A histone H3 methyltransferase controls DNA methylation in Neurospora crassa. *Nature*, **414**, 277–283.
20. Otani,J., Nankumo,T., Arita,K., Inamoto,S., Ariyoshi,M. and Shirakawa,M. (2009) Structural basis for recognition of H3K4 methylation status by the DNA methyltransferase 3A ATRX-DNMT3-DNMT3L domain. *EMBO Rep.*, **10**, 1235–1241.
21. Ooi,S.K., Qiu,C., Bernstein,E., Li,K., Jia,D., Yang,Z., Erdjument-Bromage,H., Tempst,P., Lin,S.P., Allis,C.D. *et al.* (2007) DNMT3L connects unmethylated lysine 4 of histone H3 to de novo methylation of DNA. *Nature*, **448**, 714–717.
22. Li,B.Z., Huang,Z., Cui,Q.Y., Song,X.H., Du,L., Jeltsch,A., Chen,P., Li,G., Li,E. and Xu,G.L. (2011) Histone tails regulate DNA methylation by allosterically activating de novo methyltransferase. *Cell Res.*, **21**, 1172–1181.
23. Guo,X., Wang,L., Li,J., Ding,Z., Xiao,J., Yin,X., He,S., Shi,P., Dong,L., Li,G. *et al.* (2015) Structural insight into autoinhibition and histone H3-induced activation of DNMT3A. *Nature*, **517**, 640–644.
24. Meissner,A., Mikkelsen,T.S., Gu,H., Wernig,M., Hanna,J., Sivachenko,A., Zhang,X., Bernstein,B.E., Nusbaum,C., Jaffe,D.B. *et al.* (2008) Genome-scale DNA methylation maps of pluripotent and differentiated cells. *Nature*, **454**, 766–770.
25. Weber,M., Hellmann,I., Stadler,M.B., Ramos,L., Paabo,S., Rebhan,M. and Schubeler,D. (2007) Distribution, silencing potential and evolutionary impact of promoter DNA methylation in the human genome. *Nat. Genet.*, **39**, 457–466.
26. Noh,K.M., Wang,H., Kim,H.R., Wenderski,W., Fang,F., Li,C.H., Dewell,S., Hughes,S.H., Melnick,A.M., Patel,D.J. *et al.* (2015) Engineering of a histone-recognition domain in Dnmt3a alters the epigenetic landscape and phenotypic features of mouse ESCs. *Mol. Cell*, **59**, 89–103.
27. Rada-Iglesias,A., Bajpai,R., Swigut,T., Brugmann,S.A., Flynn,R.A. and Wysocka,J. (2011) A unique chromatin signature uncovers early developmental enhancers in humans. *Nature*, **470**, 279–283.
28. Lopez-Bigas,N., Kisiel,T.A., Dewaal,D.C., Holmes,K.B., Volkert,T.L., Gupta,S., Love,J., Murray,H.L., Young,R.A. and Benevolenskaya,E.V. (2008) Genome-wide analysis of the H3K4 histone demethylase RBP2 reveals a transcriptional program controlling differentiation. *Mol. Cell*, **31**, 520–530.

29. Peng,J.C., Valouev,A., Swigut,T., Zhang,J., Zhao,Y., Sidow,A. and Wysocka,J. (2009) Jarid2/Jumonji coordinates control of PRC2 enzymatic activity and target gene occupancy in pluripotent cells. *Cell*, **139**, 1290–1302.
30. Schmitz,S.U., Albert,M., Malatesta,M., Morey,L., Johansen,J.V., Bak,M., Tommerup,N., Abarrategui,I. and Helin,K. (2011) Jarid1b targets genes regulating development and is involved in neural differentiation. *EMBO J.*, **30**, 4586–4600.
31. Whyte,W.A., Bilodeau,S., Orlando,D.A., Hoke,H.A., Frampton,G.M., Foster,C.T., Cowley,S.M. and Young,R.A. (2012) Enhancer decommissioning by LSD1 during embryonic stem cell differentiation. *Nature*, **482**, 221–225.
32. Athanasiadou,R., de Sousa,D., Myant,K., Merusi,C., Stancheva,I. and Bird,A. (2010) Targeting of de novo DNA methylation throughout the Oct-4 gene regulatory region in differentiating embryonic stem cells. *PloS One*, **5**, e9937.
33. Bustin,S.A., Benes,V., Garson,J.A., Hellemans,J., Huggett,J., Kubista,M., Mueller,R., Nolan,T., Pfaffl,M.W., Shipley,G.L. *et al.* (2009) The MIQE guidelines: minimum information for publication of quantitative real-time PCR experiments. *Clin. Chem.*, **55**, 611–622.
34. Tremblay,K.D., Duran,K.L. and Bartolomei,M.S. (1997) A 5′ 2-kilobase-pair region of the imprinted mouse H19 gene exhibits exclusive paternal methylation throughout development. *Mol. Cell. Biol.*, **17**, 4322–4329.
35. Li,J.Y., Pu,M.T., Hirasawa,R., Li,B.Z., Huang,Y.N., Zeng,R., Jing,N.H., Chen,T., Li,E., Sasaki,H. *et al.* (2007) Synergistic function of DNA methyltransferases Dnmt3a and Dnmt3b in the methylation of Oct4 and Nanog. *Mol. Cell. Biol.*, **27**, 8748–8759.
36. Young,R.A. (2011) Control of the embryonic stem cell state. *Cell*, **144**, 940–954.
37. Okano,M., Bell,D.W., Haber,D.A. and Li,E. (1999) DNA methyltransferases Dnmt3a and Dnmt3b are essential for de novo methylation and mammalian development. *Cell*, **99**, 247–257.
38. Cohen-Karni,D., Xu,D., Apone,L., Fomenkov,A., Sun,Z., Davis,P.J., Kinney,S.R., Yamada-Mabuchi,M., Xu,S.Y., Davis,T. *et al.* (2011) The MspJI family of modification-dependent restriction endonucleases for epigenetic studies. *Proc. Natl. Acad. Sci. U.S.A.*, **108**, 11040–11045.
39. Zheng,Y., Cohen-Karni,D., Xu,D., Chin,H.G., Wilson,G., Pradhan,S. and Roberts,R.J. (2010) A unique family of Mrr-like modification-dependent restriction endonucleases. *Nucleic Acids Res.*, **38**, 5527–5534.
40. Liang,G., Chan,M.F., Tomigahara,Y., Tsai,Y.C., Gonzales,F.A., Li,E., Laird,P.W. and Jones,P.A. (2002) Cooperativity between DNA methyltransferases in the maintenance methylation of repetitive elements. *Mol. Cell. Biol.*, **22**, 480–491.
41. Chen,T., Ueda,Y., Dodge,J.E., Wang,Z. and Li,E. (2003) Establishment and maintenance of genomic methylation patterns in mouse embryonic stem cells by Dnmt3a and Dnmt3b. *Mol. Cell. Biol.*, **23**, 5594–5605.
42. Shi,Y., Lan,F., Matson,C., Mulligan,P., Whetstine,J.R., Cole,P.A. and Casero,R.A. (2004) Histone demethylation mediated by the nuclear amine oxidase homolog LSD1. *Cell*, **119**, 941–953.
43. Sun,G., Alzayady,K., Stewart,R., Ye,P., Yang,S., Li,W. and Shi,Y. (2010) Histone demethylase LSD1 regulates neural stem cell proliferation. *Mol. Cell. Biol.*, **30**, 1997–2005.
44. Wang,J., Hevi,S., Kurash,J.K., Lei,H., Gay,F., Bajko,J., Su,H., Sun,W., Chang,H., Xu,G. *et al.* (2009) The lysine demethylase LSD1 (KDM1) is required for maintenance of global DNA methylation. *Nat. Genet.*, **41**, 125–129.
45. Niwa,H., Miyazaki,J. and Smith,A.G. (2000) Quantitative expression of Oct-3/4 defines differentiation, dedifferentiation or self-renewal of ES cells. *Nat. Genet.*, **24**, 372–376.
46. Amente,S., Lania,L. and Majello,B. (2013) The histone LSD1 demethylase in stemness and cancer transcription programs. *Biochim. et Biophys. Acta*, **1829**, 981–986.
47. Forneris,F., Binda,C., Vanoni,M.A., Battaglioli,E. and Mattevi,A. (2005) Human histone demethylase LSD1 reads the histone code. *J. Biol. Chem.*, **280**, 41360–41365.
48. Wang,Y., Zhang,H., Chen,Y., Sun,Y., Yang,F., Yu,W., Liang,J., Sun,L., Yang,X., Shi,L. *et al.* (2009) LSD1 is a subunit of the NuRD complex and targets the metastasis programs in breast cancer. *Cell*, **138**, 660–672.
49. Zhang,Y., Jurkowska,R., Soeroes,S., Rajavelu,A., Dhayalan,A., Bock,I., Rathert,P., Brandt,O., Reinhardt,R., Fischle,W. *et al.* (2010) Chromatin methylation activity of Dnmt3a and Dnmt3a/3L is guided by interaction of the ADD domain with the histone H3 tail. *Nucleic Acids Res.*, **38**, 4246–4253.
50. Karmodiya,K., Krebs,A.R., Oulad-Abdelghani,M., Kimura,H. and Tora,L. (2012) H3K9 and H3K14 acetylation co-occur at many gene regulatory elements, while H3K14ac marks a subset of inactive inducible promoters in mouse embryonic stem cells. *BMC Genomics*, **13**, 424–442.
51. Huang,P.H., Plass,C. and Chen,C.S. (2011) Effects of histone deacetylase inhibitors on modulating H3K4 methylation marks - a novel cross-talk mechanism between histone-modifying enzymes. *Mol. Cell. Pharmacol.*, **3**, 39–43.
52. Huang,Y., Vasilatos,S.N., Boric,L., Shaw,P.G. and Davidson,N.E. (2012) Inhibitors of histone demethylation and histone deacetylation cooperate in regulating gene expression and inhibiting growth in human breast cancer cells. *Breast Cancer Res. Treat.*, **131**, 777–789.
53. Vasilatos,S.N., Katz,T.A., Oesterreich,S., Wan,Y., Davidson,N.E. and Huang,Y. (2013) Crosstalk between lysine-specific demethylase 1 (LSD1) and histone deacetylases mediates antineoplastic efficacy of HDAC inhibitors in human breast cancer cells. *Carcinogenesis*, **34**, 1196–1207.
54. Yin,F., Lan,R., Zhang,X., Zhu,L., Chen,F., Xu,Z., Liu,Y., Ye,T., Sun,H., Lu,F. *et al.* (2014) LSD1 regulates pluripotency of embryonic stem/carcinoma cells through histone deacetylase 1-mediated deacetylation of histone H4 at lysine 16. *Mol. Cell. Biol.*, **34**, 158–179.
55. Lee,M.G., Wynder,C., Bochar,D.A., Hakimi,M.A., Cooch,N. and Shiekhattar,R. (2006) Functional interplay between histone demethylase and deacetylase enzymes. *Mol. Cell. Biol.*, **26**, 6395–6402.
56. Bowers,E.M., Yan,G., Mukherjee,C., Orry,A., Wang,L., Holbert,M.A., Crump,N.T., Hazzalin,C.A., Liszczak,G., Yuan,H. *et al.* (2010) Virtual ligand screening of the p300/CBP histone acetyltransferase: identification of a selective small molecule inhibitor. *Chem. Biol.*, **17**, 471–482.
57. Bittencourt,D., Lee,B.H., Gao,L., Gerke,D.S. and Stallcup,M.R. (2014) Role of distinct surfaces of the G9a ankyrin repeat domain in histone and DNA methylation during embryonic stem cell self-renewal and differentiation. *Epigenet. Chromatin*, **7**, 27–39.
58. Chang,Y., Sun,L., Kokura,K., Horton,J.R., Fukuda,M., Espejo,A., Izumi,V., Koomen,J.M., Bedford,M.T., Zhang,X. *et al.* (2011) MPP8 mediates the interactions between DNA methyltransferase Dnmt3a and H3K9 methyltransferase GLP/G9a. *Nat. Commun.*, **2**, 533–543.
59. Sharma,S., Gerke,D.S., Han,H.F., Jeong,S., Stallcup,M.R., Jones,P.A. and Liang,G. (2012) Lysine methyltransferase G9a is not required for DNMT3A/3B anchoring to methylated nucleosomes and maintenance of DNA methylation in somatic cells. *Epigenet. Chromatin*, **5**, 3–15.
60. Bostick,M., Kim,J.K., Esteve,P.O., Clark,A., Pradhan,S. and Jacobsen,S.E. (2007) UHRF1 plays a role in maintaining DNA methylation in mammalian cells. *Science*, **317**, 1760–1764.
61. Sharif,J., Muto,M., Takebayashi,S., Suetake,I., Iwamatsu,A., Endo,T.A., Shinga,J., Mizutani-Koseki,Y., Toyoda,T., Okamura,K. *et al.* (2007) The SRA protein Np95 mediates epigenetic inheritance by recruiting Dnmt1 to methylated DNA. *Nature*, **450**, 908–912.
62. Karagianni,P., Amazit,L., Qin,J. and Wong,J. (2008) ICBP90, a novel methyl K9 H3 binding protein linking protein ubiquitination with heterochromatin formation. *Mol. Cell. Biol.*, **28**, 705–717.
63. Kerenyi,M.A., Shao,Z., Hsu,Y.J., Guo,G., Luc,S., O'Brien,K., Fujiwara,Y., Peng,C., Nguyen,M. and Orkin,S.H. (2013) Histone demethylase Lsd1 represses hematopoietic stem and progenitor cell signatures during blood cell maturation. *eLife*, **2**, e00633.
64. Challen,G.A., Sun,D., Jeong,M., Luo,M., Jelinek,J., Berg,J.S., Bock,C., Vasanthakumar,A., Gu,H., Xi,Y. *et al.* (2012) Dnmt3a is essential for hematopoietic stem cell differentiation. *Nat. Genet.*, **44**, 23–31.
65. Kron,K.J., Bailey,S.D. and Lupien,M. (2014) Enhancer alterations in cancer: a source for a cell identity crisis. *Genome Med.*, **6**, 77–89.